Technische Universität München
TUM School of Life Sciences

The Metabolomic Signature of the RS6712203-C Risk Allele in Human Adipose Tissue

Sonia Erfanian

Vollständiger Abdruck der von der TUM School of Life Sciences der Technischen Universität München zur Erlangung des akademischen Grades einer

Doktorin der Naturwissenschaften

genehmigten Dissertation.

Vorsitz: Prof. Dr. Martin Klingenspor

Prüfende der Dissertation:

1. Prof. Dr. Johann J. Hauner
2. apl. Prof. Dr. Philippe Schmitt-Kopplin

Die Dissertation wurde am 21.02.2024 bei der Technischen Universität München eingereicht und durch die TUM School of Life Sciences am 08.08.2024 angenommen.

THE METABOLOMIC SIGNATURE OF THE RS6712203-C RISK ALLELE IN HUMAN ADIPOSE TISSUE

Sonia Erfanian

“Perhaps the most valuable result of all education is the ability to make yourself do the thing you have to do, when it ought to be done, whether you like it or not. It is the first lesson that ought to be learned and however early a man's training begins, it is probably the last lesson that he learns thoroughly.”

Thomas Huxley, Biologist

TABLE OF CONTENTS

ABSTRACT

Type 2 diabetes (T2D) is a chronic metabolic disease whose prevalence is steadily increasing at an alarming rate. Environmental risk factors such as diet and lifestyle play an important role in the development of T2D. Family and twin-based studies first suggested the heritability of T2D risk. Genome-wide association studies (GWAS) then provided additional evidence for the heritability of T2D and identified genetic variations associated with T2D risk. Most of these single nucleotide polymorphisms (SNPs) are located in non-coding regions of the genome, which makes their mechanistic or functional characterisation challenging. Recently, a study revealed that the non-coding rs6712203 variant is localized in an adipocyte-specific enhancer region and the C-to-T point mutation leads to a disrupted POU class 2 homeobox 2 (POU2F2) binding motif. Through *in vitro* knockdown studies, a possible mechanism for rs6712203-C risk allele carriers was suggested: the lack of POU2F2 binding at the enhancer leads to reduced cordon bleu like protein 1 (COBLL1) expression, which in turn leads to disturbed actin remodeling during adipogenesis, lower insulin-stimulated glucose uptake, triglyceride storage and response to lipolytic stimulation. Therefore, this thesis aimed to unravel which metabolic pathways are directly influenced by the COBLL1 rs6712203-C risk allele in adipocytes.

To address this question, pre-adipocyte cells (PACs) isolated from subcutaneous adipose tissue of six obese and female carriers of the rs6712203-C risk allele and five obese and female patients with the rs6712203-T non-risk allele, were *in vitro* differentiated. The microscopic analysis during standardized adipose differentiation did not show any remarkable changes between the two genotypes. Oil Red O lipid staining revealed the same amount of fat accumulation in adipocytes from rs6712203-C risk allele and rs6712203-T non-risk allele carriers.

To gain insight into the transcriptional changes following a decrease in COBLL1 in carriers of the rs6712203-C risk allele, expression analyses of selected lipid metabolism and obesity marker genes were performed. Adipocytes of rs6712203-C risk allele carriers revealed a similar expression pattern of *PPARG2 and IRS2* compared to adipocytes from rs6712203-T non-risk allele carriers. Whereas *PIK3CA* and *PLIN1* expression was upregulated in *in vitro* differentiating pre-adipocytes of carriers of the rs6712203-C risk allele, *ITGAM* expression was upregulated in pre-adipocytes of rs6712203-C risk allele carriers and *LEP* expression was decreased in *in vitro* differentiated adipocytes of carriers of the rs6712203-C risk allele.

To dissect the metabolic pathways which are affected by COBLL1, Direct injection Fourier-Transform Ion Cyclotron Resonance Mass Spectrometry (DI-FT-ICR/MS) measurement was performed of cell lysates of pre-adipocytes, differentiating pre-adipocytes and mature adipocytes from carriers of the rs6712203-C risk allele and rs6712203-T non-risk allele carriers. The data generated in this thesis

suggest that specific metabolic pathways such as nucleotide catabolism, metabolism of amino acids, glycolysis, fatty acyl-CoA biosynthesis and carnitine synthesis were upregulated in early adipogenesis of rs6712203-C risk allele carriers compared to rs6712203-T non-risk allele carriers. In late adipogenesis, fat and steroid metabolism was increased in adipocytes of carriers of the rs6712203-C risk allele compared to rs6712203-T non-risk allele carriers.

In conclusion, the results of this thesis provide unprecedented insight into the metabolic changes of adipocytes from rs6712203-C risk allele carriers.

ZUSAMMENFASSUNG

Typ-2-Diabetes (T2D) ist eine chronische Stoffwechselerkrankung, deren Prävalenz stetig und in alarmierendem Maße zunimmt. Umweltbedingte Risikofaktoren wie Ernährung und Lebensstil spielen eine wichtige Rolle bei der Entwicklung von T2D. Familien- und Zwillingsstudien wiesen erstmals auf die Vererbbarkeit des T2D-Risikos hin. Genomweite Assoziationsstudien (GWAS) lieferten dann zusätzliche Beweise für die Vererbbarkeit von T2D und identifizierten zahlreiche genetische Variationen, die mit dem T2D-Risiko in Verbindung stehen. Die meisten dieser Einzelnukleotid-Polymorphismen (SNPs) befinden sich in nicht kodierenden Regionen des Genoms, was ihre mechanistische oder funktionelle Charakterisierung schwierig macht. Kürzlich zeigte eine Studie, dass die nicht-kodierende Variante rs6712203 in einem adipozytenspezifischen Enhancer lokalisiert ist und die C-to-T-Punktmutation zu einem gestörten POU Klasse 2 Homeobox 2 (POU2F2) Bindungsmotiv führt. Durch *in vitro* Knockdown-Studien wurde ein möglicher Mechanismus für Träger des rs6712203-C-Risikoallels vorgeschlagen: Die gestörte POU2F2-Bindung am Enhancer führt zu einer verminderten Expression des Cordon Bleu Like Protein 1 (COBLL1), was wiederum zu einem gestörten Aktin-Remodeling während der Adipogenese, einer geringeren insulin-stimulierten Glukoseaufnahme, Triglyceridspeicherung und Reaktion auf lipolytische Stimulation führt. Ziel dieser Arbeit war es daher, herauszufinden, welche Stoffwechselwege direkt durch das COBLL1 Protein in Adipozyten mit dem Risikoallel rs6712203-C beeinflusst werden.

Um diese Frage zu klären, wurden Prä-Adipozyten (PACs), die aus dem subkutanen Fettgewebe von sechs fettleibigen weiblichen Trägern des Risiko-Allels rs6712203-C und fünf fettleibigen weiblichen Patienten mit dem Nicht-Risiko-Allel rs6712203-T isoliert wurden, *in vitro* differenziert. Die mikroskopische Analyse ergab keine nennenswerten Unterschiede zwischen den beiden Genotypen. Die Oil-Red-O-Lipid-Färbung zeigte, dass die Prä-Adipozyten von Trägern des Risiko-Allels rs6712203-C und Trägern des Nicht-Risiko-Allels rs6712203-T die gleiche Menge an Fett akkumulierten.

Um einen Einblick in die transkriptionellen Veränderungen nach einer Verminderung des COBLL1 Proteins bei Trägern des rs6712203-C-Risikoallels zu erhalten, wurden Expressionsanalysen ausgewählter Markergene des Lipidstoffwechsels und der Adipositas- durchgeführt. Adipozyten von Trägern des rs6712203-C-Risikoallels zeigten ein ähnliches Expressionsmuster von *PPARG2* und *IRS2* verglichen mit Adipozyten von Trägern des rs6712203-T-Nicht-Risikoallels. Während die Expression von *PIK3CA* und *PLIN1* in *in vitro* differenzierenden Prä-Adipozyten von Trägern des rs6712203-C-Risiko-Allels hochreguliert war, war die Expression von *ITGAM* in Prä-Adipozyten von Trägern des

rs6712203-C-Risiko-Allels hochreguliert und die Expression von *LEP* war in *in vitro* differenzierten Adipozyten von Trägern des rs6712203-C-Risiko-Allels vermindert.

Um die Stoffwechselwege, die von COBLL1 beeinflusst werden, zu entschlüsseln, wurde eine Direktinjektions-Fourier-Transformations-Ionenzyklotronresonanz-Massenspektrometrie (DI-FT-ICR/MS) Analyse von Zelllysaten von Präadipozyten, differenzierenden Präadipozyten und reifen Adipozyten von Trägern des rs6712203-C-Risikoallels und Trägern des rs6712203-T-Nicht-Risikoallels durchgeführt. Die in dieser Arbeit gewonnenen Daten deuten darauf hin, dass Stoffwechselwege wie Nukleotidkatabolismus, Aminosäurestoffwechsel, Glykolyse, Fettacyl-CoA-Biosynthese und Carnitinsynthese in der frühen Adipogenese von Trägern des rs6712203-C-Risikoallels im Vergleich zu Trägern des rs6712203-T-Nicht-Risikoallels hochreguliert sind. In der späten Adipogenese ist der Fett- und Steroidstoffwechsel in Adipozyten von Trägern des rs6712203-C-Risikoallels im Vergleich zu Trägern des rs6712203-T-Nicht-Risikoallels erhöht.

Insgesamt bieten die Ergebnisse dieser Untersuchungen einen neuen Einblick in die metabolischen Veränderungen von Adipozyten, die bei Trägern des rs6712203-C-Risikoallels auftreten und die Assoziation des Genotyps mit Typ 2 Diabetes weiter charakterisieren.

ABBREVIATIONS

General abbreviations

%	Percentage, percent
°C	Degree centigrade
3T3-L1	Mouse 3T3-L1 preadipocyte cell line
ABPs	Actin-binding proteins
Arp2/3	Actin-related protein 2/3
ATMs	Adipose tissue macrophages
BAT	Brown adipose tissue
BCA	Bicinchoninic acid
BMI	Body mass index
BMP	Bone morphogenetic protein
CD	Cluster of differentiation
cDNA	complementary DNA
CKD	Chronic kidney disease
CVD	Cardiovascular disease
Da	Dalton
Dcs	Dendritic cells
DI	Direct injection
DMAPP	dimethylallyldiphosphate
DMSO	Dimethyl sulfoxide
DNA	Deoxyribonucleic acid
ECM	Extracellular matrix
EDTA	Ethylenediaminetetraacetic acid
e.g.	Exempli gratia

EM	Endosome membrane
ESI	Electrospray ionisation
FA	Fatty acid
F-actin	Filamentous actin
FCS	Fetal calf serum
FT-ICR/MS	Fourier-Transform Ion Cyclotron Resonance Mass Spectrometry
G-actin	Globular monomeric actin
GPL	Glycerophospholipids
g/rcf	G force / relative centrifugal force
GWAS	Genome-wide association studies
hASC	Primary human adipose-derived stromal cells
HMDB	Human Metabolome Database
IBMX	3-Isobutyl-1-methylxanthine
ICR	Ion cyclotron resonance
IFG	Impaired fasting glycaemia
IGT	Impaired glucose tolerance
IPP	Isopentenyl diphosphate
ISO	International Standards Organization
LD	Linkage disequilibrium
MDEA	Mass difference enrichment analysis
MDiN	Mass difference network
MeOH	Methanol
MEP	Methylerythritol phosphate
MetS	Metabolic syndrome
mg	Milligram

min	Minute/minutes
miRNA	Micro ribonucleic acid
ml	Milliliter
mM	Millimolar
MOBB	Munich Obesity Biobank
mRNA	Messenger ribonucleic acid
MS	Mass spectrometry
MVA	Mevalonic acid
Mws	Megawords
m/z	Mass-to-charge ratio/mass over charge
NAFLD	Nonalcoholic fatty liver disease
NMR	Nuclear magnetic resonance
OD	Optical density
OGTT	Oral glucose tolerance test
PA	Phosphatidic acid
PAC	Pre-adipocyte cells
PBS	Phosphate-buffered saline
PC	Phosphatidylcholine
PCR	Polymerase-chain-reaction
PE	Phosphatidylethanolamine
PGE2	Prostaglandin E2
pH	Potentia hydrogenii
PH	Pleckstrin homology domain
PI	Phosphatidylinositol
PIP	Phosphatidylinositol phosphate

PIP2	Phosphatidylinositol 4,5-bisphosphate
PIP3	Phosphatidylinositol 3,4,5-trisphosphate
PL	Phospholipid
PLIS	Prediabetes Lifestyle Intervention Study
PM	Plasma membrane
PMCA	Phylogenetic module complexity analysis
PPE	Protein precipitation extraction
PR	Prenol lipids
PS	Phosphatidylserine
PTB	Phosphotyrosine binding domain
RF	Resonance frequency
rpm	Rotations per minute
RT	Room temperature
s	Seconds
SD	standard derivation
SGBS	Simpson–Golabi–Behmel syndrome cell line
S/N	Signal-to-noise ratio
SNPs	Single nucleotide polymorphisms
SPE	Solid phase extraction
T1D	Type 1 Diabetes
T2D	Type 2 Diabetes
TAG	Triacylglycerol
TCA	Tricarboxylic acid cycle
TF	Transcription factor
TSS	Transcriptional start site

TUM	Technical University Munich
TZDs	Thiazolidinediones
UV	Ultraviolet
VCA	verprolin homology, cofilin homology, and acidic region
WAT	White adipose tissue
WH2	WASP (Wiskott–Aldrich syndrome protein)-homology 2
WHO	World Health Organization
WHR	Waist-to-hip-ratio
µg	Microgram
µl	Microliter

Gene abbreviations

Arp2/3	Actin related protein 2/3 complex subunit 2 and 3
ATGL/ PNPLA2	Adipose triglyceride lipase/Patatin-like phospholipase domain containing 2
C/EBPα	CAAT/enhancer-binding protein alpha
C/EBPβ	CCAAT/enhancer-binding protein beta
C/EBPδ	CAAT/enhancer-binding protein delta
CGI-58	Comparative Gene Identification-58
COBL	Cordon-bleu protein
COBLL1	Cordon bleu like protein 1
EGFR	Epidermal growth factor receptor
FGFR	Fibroblast growth factor receptor
FOSL2	FOS like 2, AP-1 transcription factor subunit
GAPDH	Glyceraldehyde-3-phosphate dehydrogenase
GLUT4	Solute carrier family 2, facilitated glucose transporter member 4

GAPDH	Glyceraldehyde-3-phosphate dehydrogenase
GRB14	Growth factor receptor-bound protein 14
HSL/LIPE	Lipase E, hormone-sensitive
ILK	Integrin-linked kinase
IGF1R	Insulin-like growth factor-1 receptor
IPO8	Importin 8
IR	Insulin receptor
IRS2	Insulin receptor substrate 2
ITGAM	Integrin subunit alpha M
LEP	Leptin
LPL	Lipoprotein lipase
N-WASP	Neural Wiskott-Aldrich syndrome
PDGFR	Platelet-derived growth factor receptor
PIK3CA	Phosphatidylinositol-4-phosphate 3-kinase, catalytic subunit alpha
PDGFRα	Platelet-derived growth factor receptor alpha
PDGFRβ	Platelet-derived growth factor receptor beta
PLIN1	Perilipin 1
POU2F2	Pou domain, class 2, transcription factor 2
PPARG/PPARγ	Peroxisome proliferator activated receptor gamma
SOCS3	Suppressor of cytokine signaling 3
SQLE	Squalene epoxidase
TCF7L2	Transcription factor 7 like 2
Tek/Tie2	Tunica endothelial kinase
UCP1	Uncoupling protein 1
ZNF423	Zinc finger protein 423

INDEX OF TABLES

INDEX OF FIGURES

1 INTRODUCTION

1.1 Adipose tissue in energy homeostasis and metabolic disorders

1.1.1 Classification of adipose tissues

Adipose tissues can be considered as an organ where the body's energy is stored. There are two main types of adipose tissue with distinct functions: brown adipose tissue (BAT) and white adipose tissue (WAT) (Frontini and Cinti, 2010; Rosen and Spiegelman, 2014).

1.1.1.1 Brown adipose tissue (BAT)

The main function of brown adipocytes is to burn stored energy through thermogenesis (Cypess and Kahn, 2010). Brown adipocytes are characterised by an increased number of mitochondria and multilocular lipid droplets (Harms and Seale, 2013). They also express high levels of uncoupling protein 1 (UCP1), which is considered to be the main driver of the thermogenesis programme (Ricquier 2012). BAT develops embryonically from the mesoderm. In addition to BAT, the Myf5- and Pax7-expressing progenitor cells give also rise to skeletal muscle cells and UCP1-expressing adipocytes (Lepper and Fan, 2010; Sanchez-Gurm-aches et al., 2012; Seale et al., 2008; Wang and Seale, 2016). There are also clusters of UCP1-expressing adipocytes in WAT. These cells are termed beige adipocytes. They express UCP1 and reveal the capacity to perform thermogenesis in response to various stumuli (Vitali, A. et al. 2012). Previously, BAT in humans was thought to be found only in the interscapular region in infants and adults chronically exposed to extreme cold (Heaton, 1972; Lidell et al. 2013). Recent findings have shown that brown and beige adipocytes may be more widespread in adults than previously thought (Nedergaard, Bengtsson and Cannon, 2007; Saito et al., 2009; van Marken Lichtenbelt et al. 2009; Virtanen et al. 2009). This is especially interesting, since the activities of brown and beige fat cells reduce metabolic disease, including obesity, in mice and correlate with leanness in humans (Wang and Seale, 2016).

1.1.1.2 White adipose tissue (WAT)

The primary function of WAT is to store excess energy in the form of triglycerides (Rosen and MacDougald, 2006). Mature white adipocytes are unilocular and contain one large lipid droplet which makes up the majority of the cell (Greenberg et al. 2011). As a result, the white fat cells have a rounded cell shape (Orlicky et al. 2013; Smas and Sul 1995). White fat cells contain significantly fewer mitochondria than brown adipocytes. Based on its location in the body, WAT is further classified into two categories: subcutaneous WAT and visceral WAT. Furthermore, visceral and subcutaneous WAT show intrinsically different metabolic functions, including lipolysis rates, thermogenic potential and

the secretion of adipokines and inflammatory cytokines (Ghaben and Scherer, 2019). The visceral WAT can be found in different depots throughout the body including omental, mesenteric, retroperitoneal, gonadal, and pericardial WAT (Wajchenberg, 2000). The omental depot, one of the most studied visceral depots, is located inside the peritoneum, starts near the stomach and spleen and extends deep into the abdomen. The visceral WAT is often associated with metabolic disorders such as diabetes and cardiovascular disease (Shuster et al., 2012). The depots of subcutaneous WAT are located in several locations under the skin in upper (deep and superficial abdomen) and lower (gluteofemoral) body regions (Kwok et al. 2016). The gluteofemoral depot is anatomically located subcutaneously, along the hips, buttocks and thighs.

1.1.2 Adipogenesis of WAT

Adipogenesis refers to the process by which fibroblast-like progenitor cells express their potential to the adipogenic lineage, accumulate lipids and become mature round-shaped adipocytes filled with triglycerides (Kawaguchi et al. 2003). This process is divided into two steps, which are well characterised (Cristancho and Lazar, 2011). In the commitment step, a pluripotent fibroblast-like cell commits itself to the adipocyte lineage and forms a pre-adipocyte (Fig. 1). Mesenchymal precursor cells for instance are fibroblast-like cells which are characterized by the expression of platelet-derived growth factor receptor-α (PDGFRα) and/or PDGFRβ. The commitment step occurs without any morphological changes. Pre-adipocytes are located in the adipose vasculature (Tang et al. 2008; Gupta et al. 2012). After the commitment step, the terminal differentiation takes place. Here, specified pre-adipocytes undergo growth arrest, accumulate lipids and form insulin-responsive mature adipocytes (Fig. 1).

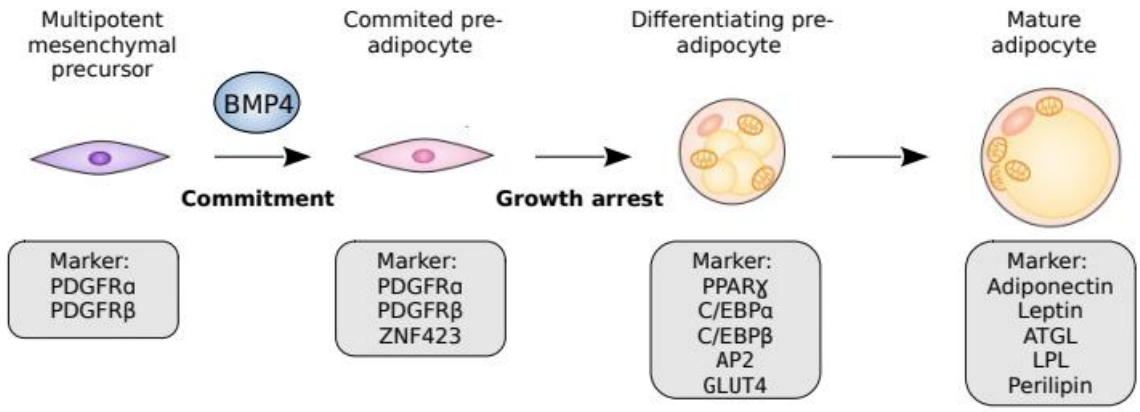

Figure 1 - Overview of molecular mechanisms of adipogenesis.
Bone morphogenetic protein (BMP) signalling restricts multipotent, fibroblast-like mesenchymal precursors marked by platelet-derived growth factor receptors (PDGFRα and/or PDGFRβ) to the adipocyte lineage as part of a process known as 'commitment'. Committed pre-adipocytes still reveal a morphologically fibroblast-like shape and express the transcription factor ZNF423. When the committed pre-adipocyte arrests its growth, it activates the master regulator of adipogenesis peroxisome proliferator-activated receptor-γ (PPARγ) and transcription co-activators CCAAT/enhancer-binding protein α and β (C/EBPα and C/EBPβ). Lipid accumulation is induced by the expression of the adipocyte fatty-acid binding protein (AP2) and the insulin-sensitive transporter GLUT4, marking adipocytes in early stages of differentiation. At the completion of differentiation, mature adipocytes express all the markers of early adipocyte differentiation as well as the peptide hormones adiponectin and leptin; the lipases adipose triglyceride lipase (ATGL) and lipoprotein lipase (LPL); and high levels of the lipid-droplet-associated protein perilipin 1. Adapted from: Ghaben and Scherer, 2019

The processes of adipogenesis are controlled by a transcriptional cascade (Farmer 2006; Rosen, Walkey, Puigserver and Spiegelman 2000) initiated by the opening of chromatin by the transcription factor (TF) CCAAT/enhancer-binding protein-β (C/EBPβ) (Steger et al. 2010; Siersbaek et al. 2011). *In vitro* studies have shown that C/EBPβ and C/EBPδ are expressed in the early stage of adipogenesis (Cao, Umek and McKnight 1991) and induce the expression of the nuclear hormone receptor peroxisome proliferator-activated receptor-γ (PPARγ) and C/EBPα (Wu et al. 1996). Cell culture studies with fibroblasts showed that the bone morphogenetic protein 2 (BMP2) and BMP4 are sufficient to drive adipocyte commitment and are required for *in vitro* adipogenic differentiation (Wang, Israel, Kelly and Luxenberg, 1993; Huang et al. 2009; Bowers, Kim, Otto, and Lane, 2006). BMPs bind and signal through BMP receptors to activate SMAD4 (Huang et al. 2009). Activated SMAD4 stimulates the transcription factor PPARγ. PPARγ is considered to be the master regulator of adipogenesis, as it is indispensable for adipocyte differentiation both *in vitro* and *in vivo* (Tontonoz, Hu and Spiegelman, 1994; Barak et al. 1999; Rosen et al. 1999; Wang, Mullican, DiSpirito, Peed and Lazar, 2013). PPARγ controls terminal differentiation of adipocytes (Rosen &MacDougald 2006; Farmer 2006; Lee and Ge 2014; Lefterova, Haakonsson, Lazar and Mandrup 2014.; Siersbaek and Mandrup 2011) and is required for maintaining their differentiated state (Tamori et al. 2002; Imai et al. 2004). Another important function of PPARγ is the activation of the transcription factor C/EBPα which acts in concert with PPARγ to establish the phenotype of mature adipocytes (Wu et al. 1999; Nielsen et al 2008; Lefterova et al. 2008). It hast been shown *in vitro*, that overexpression of C/EBPα in fibroblasts is

sufficient to drive adipocyte differentiation (Freytag, Paielli and Gilbert, 1994). Another key commitment factor of the white adipocyte lineage is the zinc-finger protein 423 (ZNF423) (Gupta, R. K. et al. 2010). ZNF423 is required for fetal development of subcutaneous adipose tissue (Shao, M. et al. 2017). In adipogenic fibroblasts ZNF423 sensitizes to pro-adipogenic BMP signalling.

1.1.3 The role of adipocytes in the development of obesity

The World Health Organization (WHO) defines overweight and obesity as abnormal or excessive fat accumulation that may impair health. The body mass index (BMI) is a commonly used measure for classifying overweight and obesity in adults. It is calculated by dividing a person's weight in kilogram by the square of its height in meter. According to the WHO Report on Obesity a person with a BMI of 25 to 29.9 is classified as overweight; a BMI of 30 or more is defined as obesity (WHO Consultation on Obesity, 1999). Since 1980, the global prevalence of excessive weight gain has at least doubled (Ataey et al. 2020). According to the WHO, more than 1.9 billion adults were overweight and 650 million obese in 2016 (WHO, 2016). Frighteningly, in some countries such as the USA 30 to 40 percent of the adults are obese, although the percentages are also quite high in European countries (Fig. 2). What is even more alarming is that rates of overweight and obesity continue to grow in children. From 1975 to 2016, the prevalence of overweight or obese children and adolescents aged 5–19 years increased more than four-fold from 4% to 18% globally (WHO (obesity), 2023).

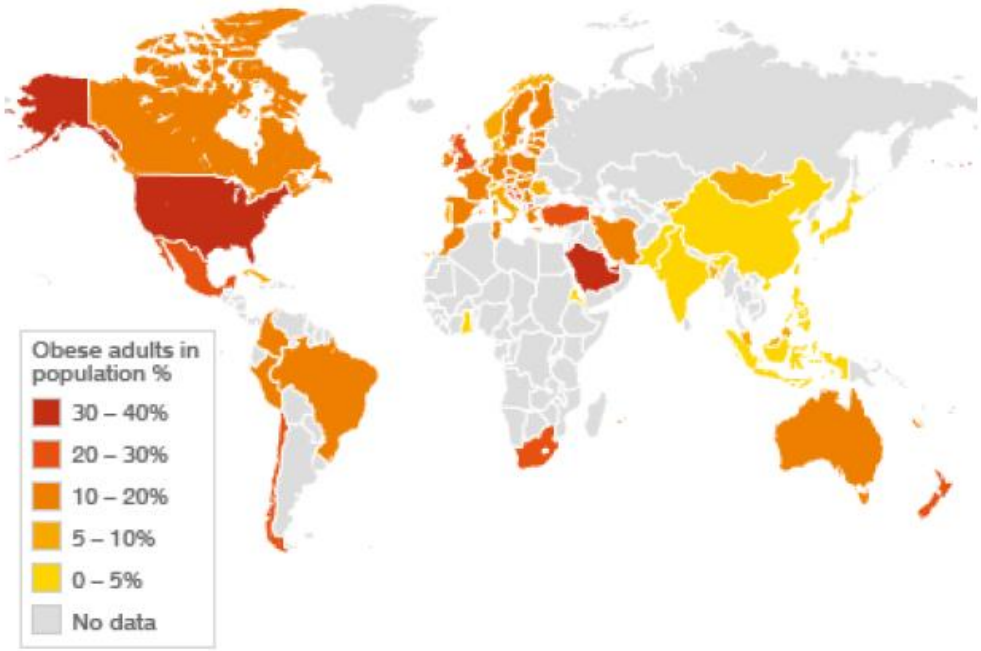

Figure 2 - Obesity as a pandemic.
Global distribution of obesity as defined by a BMI ≥ 30 kg/m^2. From: Global database on Body Mass Index, WHO, 2011, reprinted with the permission of the World Health Organization, see LETTERS OF APPROVAL

Obesity poses an increased risk to health as it elevates the probability of developing various diseases and conditions that are associated with increased mortality. This includes cardiovascular diseases (CVD), chronic kidney disease (CKD), certain types of cancer, depression, hyperlipidemia, hypertension, metabolic syndrome (MetS), nonalcoholic fatty liver disease (NAFLD). obstructive sleep apnea, osteoarthritis and Type 2 diabetes (T2D) (Swinburn et al. 2011). Furthermore, obesity also appears to be a major problem for the health system, as it is estimated that obese people have 30% higher medical costs than people with a normal BMI (WHO Consultation on Obesity 1999).

Several mechanisms are known to lead to obesity (Dubern 2019). One of the main causes of obesity is that significantly more energy is taken in through energy-rich foods than the body can consume. If more energy is taken in than the body needs to meet its energy requirement, the adipose tissue must expand. There are two ways to expand adipose tissue: hypertrophy or hyperplasia (Fig. 3). Hypertrophy describes the increase in size of existing adipocytes, whereas hyperplasia means the formation of new adipocytes from precursors in the process of adipogenesis (Ghaben and Scherer 2019). Hypertrophy is considered the unhealthier of the two mechanisms, since an increase in adipocyte size is correlated with increased systemic insulin resistance (Salans et al. 1968; Krotkiewski, 1983). In contrast to that, decreased susceptibility to developing diabetes is often correlated with small adipocytes (Lönn et al. 2010; Yang et al. 2012).

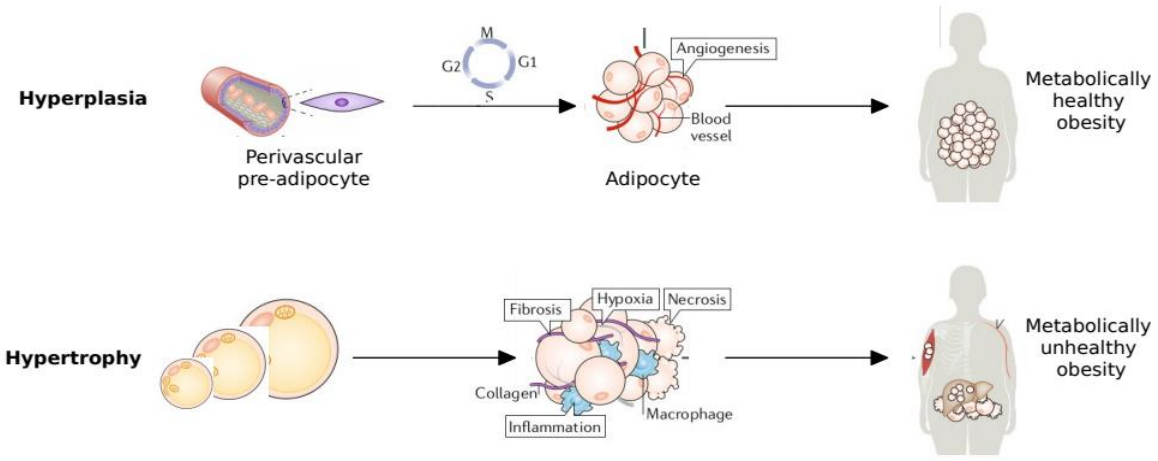

Figure 3 - Mechanisms of adipose tissue expansion.
Adipose tissue can primarily expand in one of two ways: through differentiation of resident tissue precursors to form new adipocytes (hyperplasia) or through enlargement of existing adipocytes (hypertrophy). Hyperplasia of adipose tissue is generally considered healthy and adaptive, because the tissue is able to maintain proper vascularization and levels of the insulin-sensitizing, anti-inflammatory hormone adiponectin and other metabolism-modulatory adipokines. Hypertrophy of adipocytes is associated with an increase in hypoxia experienced by these cells because of their massively expanded size. The hypoxic reaction of the fatty tissue is not sufficient to induce angiogenesis. Hypoxic adipose tissue increases the expression of pro-fibrotic genes and leads to tissue fibrosis. Sometimes, hypoxic adipocytes undergo necrosis, leading to infiltration by immune cells and tissue inflammation. These factors combine to decrease adipose tissue function, leading to persistently elevated levels of nutrients (sugars and lipids) in the blood and contributing to earlier onset of metabolic disease and causing toxic lipid deposition in other tissues, such as muscle and liver. Adapted from: Ghaben and Scherer, 2019

Increased adipocyte size leads to elevated mechanical stress as they are more in contact with neighbouring cells and the extracellular matrix (ECM). If they expand to a size that reaches the limits of oxygen diffusion, they can suffer from hypoxia. Both the mechanical and hypoxic stress can lead to inflammation in adipose tissue (Halberg et al. 2009; Khan et al. 2009). Furthermore, hypoxic stress in large adipocytes stimulate increased rate of collagen synthesis, fibrosis and adipocyte necrosis which leads to an enhancement of pro-inflammatory cytokines and inflammatory infiltration (Halberg et al. 2009; Scherer, 2016). Larger adipocytes may also exhibit different biochemical properties compared to smaller adipocytes including increased inflammatory cytokine secretion, elevated lipolysis and reduced secretion of anti-inflammatory adipokines such as leptin and adiponectin (Bambace et al. 2011; Laurencikiene et al. 2011; Meyer et al. 2013; Skurk et al. 2007). In the process of the metabolic disturbances associated with obesity, the adipocyte does not respond properly to almost all extracellular signals, especially to insulin, resulting in increased plasma glucose and lipid levels (Rosen and Spiegelman, 2014; Stern, Rutkowski and Scherer 2016). Moreover, it could be shown that adipose tissue secretes lipid subtypes which have an influence on insulin sensitivity and can contribute to insulin resistance associated with obesity (Holland et al. 2007; 35 Xia et al. 2015). In contrast, the formation of smaller fat cells by adipogenesis with increased angiogenesis reduces hypoxic stress in the fat depot and subsequent inflammation (Sun et al. 2012). It also prevents the accumulation of toxic lipids (lipotoxicity) in other tissues such as muscle, liver and heart and correlates with the maintenance of metabolic function.

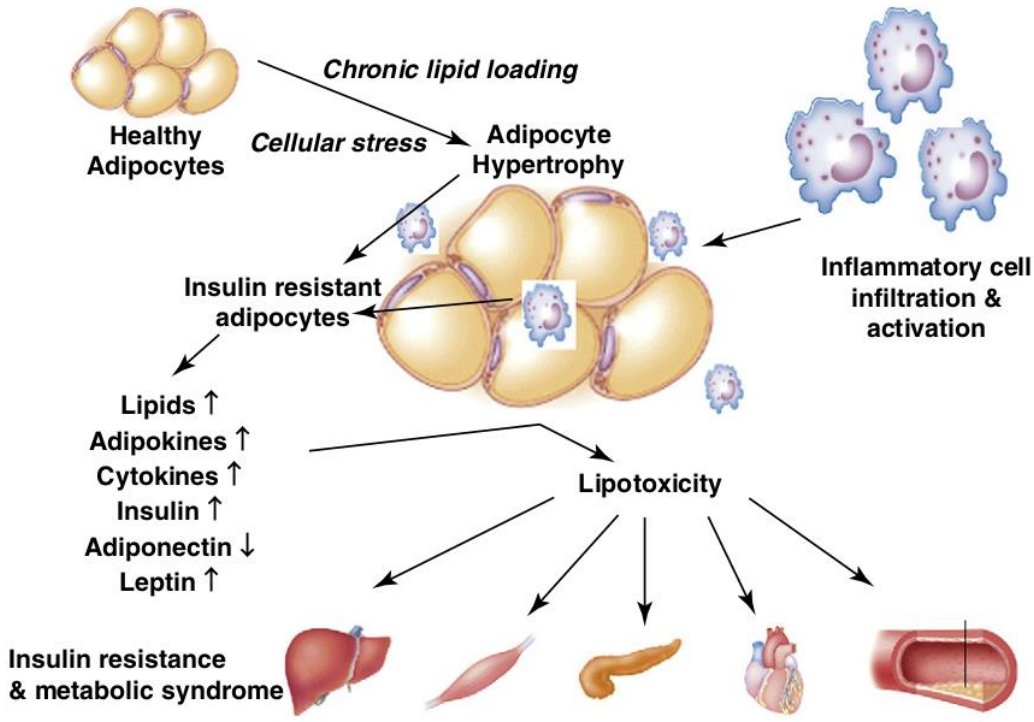

Figure 4 - Adipocyte dysfunction and local inflammation leading to lipotoxicity-induced insulin resistance.
Chronic overloading of adipocytes induces cellular stress such as endoplasmic reticulum stress that also contributes to the chronic inflammatory state in the adipose tissue, further recruiting macrophages and other inflammatory cells into the adipose tissue to feed-forward the release of free fatty acids, adipokines and inflammatory cytokines. Increase in circulating concentrations of free fatty acids, lipid mediators, inflammatory cytokines/adipokines, insulin and leptin, together with reductions in circulating adiponectin, leads to ectopic lipid storage, lipotoxicity and insulin resistance in non-adipose tissues. From: Iyer and Brown, 2010, reprinted with the permission of Elsevier Journal, see LETTERS OF APPROVAL

1.1.4 Marker genes of fat metabolism and obesity

A previous study identified the variant rs6712203, a regulatory site within the non-coding region at the *COBLL1/GRB14* locus (see chapter 3.2) suggesting a link to T2D (Ocvirk (nee Glunk) et al. 2023). To further evaluate these findings the expression of a set of established marker genes of fat metabolism and the metabolome in obese individuals was analyzed in white subcutaneous adipocytes from females (BMI > 38,82) having the non-risk allele TT or the risk allele CC at rs6712203.

1.1.4.1 PPARG

PPARG encodes for the previously mentioned nuclear hormone receptor peroxisome proliferator-activated receptor-γ (PPARγ), which is the master regulator of adipogenesis (Rosen and MacDougald 2006). The *PPARG* gene has separated promoters and 5' exons which results in three different mRNAs (*PPARG1*, *PPARG2* and *PPARG3*) (Janani et al. 2015). *PPARG1* and *PPARG3* mRNAs give rise to identical proteins, whereas the protein translated via *PPARG2* contains an additional NH2-terminal region

composed of 30 amino acids. The PPARG1 isoform is expressed in nearly all cells, while PPARG2 is limited mainly to adipose tissue (Janani et al. 2015). PPARγ is a TF activated by binding to its ligands. After interaction with the specific ligands, nuclear receptors are translocated to the nucleus, where they change their structure and regulate gene transcription (Rogue et al. 2001; Rogue et al. 2010; Willson et al. 2000). PPARγ plays an important role in lipid metabolism by regulating genes which participate in release, transport and storage of fatty acids (FAs) like lipoprotein lipase (LPL) and the FA transporter CD36 (Lehrke and Lazar 2005; Medina-Gomez et al. 2007; Ren et al. 2002). Dysregulation of PPARγ is associated with the development of obesity, type 2 diabetes and atherosclerosis (Lehrke and Lazar 2005). Polyunsaturated FAs and phytanic acid are natural PPARγ agonists in the human diet which increase glucose uptake and insulin sensitivity (Heim et al. 2002). Furthermore, its synthetic ligands such as thiazolidinediones (TZDs), e.g. troglitazone, rosiglitazone and pioglitazone, improve insulin action and glucose parameters and increase whole body insulin sensitivity. Thus, they are potent insulin sensitizers used in the treatment of type 2 diabetes (Mooradian et al. 2002). TZDs stimulate genes which favor storage of triglycerides and thereby lowering circulating free FA concentrations (Moore et al. 2001). Here it is worth mentioning that the development of insulin resistance is associated with increased levels of circulating free FAs and the accumulation of lipids in non-fatty tissues. Thus, PPARγ protects non-fatty tissues from an excessive lipid load (lipotoxicity) and maintains the normal function of organs, especially liver and skeletal muscle. In addition, PPARγ ensures a balanced and adequate secretion of adipokines (adiponectin and leptin) in adipocytes, which are mediators of insulin action in peripheral tissues (Kintscher and Law 2005).

1.1.4.2 *LEP*

LEP encodes for leptin, which was identified in 1994 as the product of the obese gene in mice, a circulating factor whose mutation leads to severe obesity and type 2 diabetes (Zhang et al. 1994). LEP is primarily produced in white adipose tissue, although it is also expressed in several other tissues, including the stomach, lungs, placenta and possibly the brain (Bado et al. 1998; Hoggard et al. 1997, Vernooy et al. 2009; Wiesner et al. 1997; Zhang et al. 1994). It circulates in the blood in protein-bound forms and free, the latter is the biologically active form (Chan et al. 2002). Leptin regulates fat storage in the body and is produced in proportion to the size of fat deposits in the human body, that means when fat cells increase, leptin levels increase proportionally (Harris 2014). It acts on the satiety center in the brain through binding to the leptin receptors (LEP-R) and suppresses food intake and increases energy expenditure (Fasshauer and Blüher 2015; Zhu and Scherer 2019; Park and Ahima 2015; Papathanasiou et al. 2018). Studies demonstrated that the concentration of circulating leptin decreases during fasting or energy restriction, but increases during refeeding, overfeeding, as well as

during surgical stress (Boden et al. 1996; Dubuc et al. 1998; Kolaczynski et al. 1996; Hernandez et al. 2000). Moreover, leptin plays a vital role in reproductive functioning, fetal growth, proinflammatory immune responses, angiogenesis, and lipolysis (Farr et al. 2015). It also directly promotes adipogenesis of bone marrow mesenchymal precursors and inhibits osteogenic differentiation (Yue et a. 2016). Leptin resistance is characterized by reduced satiety, over- consumption of nutrients, and increased total body mass, which often leads to obesity (Obradovic et al. 2021). This reduces the effectiveness of using exogenous leptin as a therapeutic agent, but combining it with leptin sensitizers could help overcome leptin resistance and possibly obesity.

1.1.4.3 *IRS2*

IRS2 encodes the insulin receptor substrate 2 which ia an essential adaptor that mediates signaling downstream of the insulin receptor and other receptor tyrosine kinases (Guo 2014). The IRS2 protein contains an NH2-terminal pleckstrin homology (PH) domain which mediates cell membrane interactions, a phosphotyrosine binding (PTB) domain which binds to the phosphorylated NPXpY-motif of the activated insulin receptor and a COOH-terminal tail that contains numerous tyrosine and serine/threonine phosphorylation sites that act as on/off switches to transduce insulin action, recruiting downstream signaling proteins, including PI3K subunit, phosphotyrosine phosphatase SHP-2, and adaptor molecules such as Grb-2, suppressor of cytokine signalling 3 (SOCS3), Nck, Crk, SH2B and others (Copps and White 2012; Sun and Liu 2009; White 2003). The insulin receptor (IR) and insulin-like growth factor-1 receptor (IGF1R) are receptor tyrosine kinases that control metabolism, differentiation and growth. After ligand binding at the cell surface, the activated IR or IGF1R undergo conformational changes that allow them to autophosphorylate tyrosine residues on their cytoplasmic subunits (Haeusler et al. 2017). This facilitates the recruitment and phosphorylation of IRS2, which serves as scaffold for the initiation of downstream signalling pathways (Copps and White 2012). There are two major pathways that are stimulated by IRS2, the PI3K-AKT and Ras-Raf-MAPK pathways (Haeusler et al. 2017). In skeletal muscle cells, IRS2 is required for lipid uptake and metabolism (Bouzakri et al. 2006; Long et al. 2011). Interestingly, IRS2 knockout mice reveals a failure in β cells which results in diabetes (Lavin et al. 2016). Inhibition of IRS2 inactivates PI3K and interferes with nutrient homeostasis. It prolongs activation of MAP kinases (ERK1/2, p38, & JNK) which promotes mitogenesis and overgrowth resulting in obesity (Guo 2014).

1.1.4.4 *PIK3CA*

PIK3CA encodes the α-isoform of the 110 kDa catalytic subunit of phosphatidylinositol-4,5-bisphosphate 3-kinase (PI3Kα) and is ubiquitously expressed (Keppler-Noreuil et al. 2016). In human cells, there are three main classes of PI3Ks, which are categorised based on their structure and

substrate preference (Fruman et al. 2017; Goncalves et al. 2018; Liu et al. 2009). PI3Ks of class I comprise a catalytic subunit (p110) and a regulatory subunit (Fruman et al. 2017). There are four isoforms of the p110 catalytic subunit found in mammals (p110α, β, γ and δ) (Keppler-Noreuil et al. 2016; Fruman et al. 2017). Class II PI3Ks and Class III PI3Ks each contain 3 enzymes (PI3K-C2α, β, γ) and one enzyme (hVPS34) (Fruman et al. 2017). Class I PI3Ks are activated downstream of growth factor receptors such as the PDGF receptor, epidermal growth factor receptor (EGFR), insulin-like growth factor receptor (IGFR) and insulin receptor (IR) (Fruman et al. 2017). Class I PI3Ks catalyse the phosphorylation of phosphatidylinositol 4,5-bisphosphate (PIP2) to form phosphatidylinositol 3,4,5-trisphosphate (PIP3), which recruits effector proteins such as the AKT subfamily of AGC-serine/threonine kinases (Keppler-Noreuil et al. 2016; Fruman et al. 2017). AKT activates mTOR, a serine/threonine kinase, indirectly, which is part of the cellular mTORC1 and mTORC2 complexes (Keppler-Noreuil et al. 2016). Furthermore, the components of the PI3K/AKT/mTOR pathway interact with other pathways such as RAS/RAF/MEK/MAPK. The PI3K signalling pathway is involved in many cellular processes, for example proliferation, angiogenesis, survival and metabolism (Adams and Ricci 2019; Hennessy et al. 2005; Hillmann and Fabbro 2019; Keppler-Noreuil et al. 2016; Nguyen et al. 2017). Phosphorylation of PI3K is mainly responsible for insulin-stimulated glucose uptake by Solute carrier family 2, facilitated glucose transporter member 4 (GLUT4), which is responsible for peripheral glucose disposition in muscle and adipose tissue. Interestingly, mice lacking either the PI3K catalytic subunit or Akt2 show insulin resistance and type 2 diabetes (Brachmann, et al. 2005; Cho, et al. 2001).

1.1.4.5 *PLIN1*

PLIN1 encodes the protein perilipin-1, which is one of the major lipid droplet binding proteins (Sohn et al. 2018). It is highly expressed in adipocytes where it coats lipid droplets and participates in droplet formation, triglyceride storage and lipolysis (Patel et al. 2022). In the initial state, PLIN1 envelops lipid droplets and inhibits lipolysis in adipocytes (Tansey et al. 2001). Furthermore, it binds to Comparative Gene Identification-58 (CGI-58), a co-activator of adipose triglyceride lipase (ATGL). However, in the stimulated state, PLIN1 releases CGI-58 to induce lipolysis upon activation of protein kinase A (Granneman et al. 2009). Catecholamines induce translocation of hormone-sensitive lipase (HSL) into lipid droplets, which also promotes lipolysis (Brasaemle et al. 2000; Miyoshi et al. 2006). Moreover, PLIN1 plays a role in unilocular lipid droplet formation by activation of Fsp27 in adipocytes (Sun et al. 2013). Plin1 deficient mice are lean and exhibit glucose intolerance and insulin resistance in the absence of any metabolic stress (Tansey et al. 2001). Interestingly, people with frameshift mutations in the *PLIN1* gene have been shown to develop partial lipodystrophy, severe dyslipidaemia and insulin-resistant diabetes with small subcutaneous adipocytes, macrophage infiltration and fibrosis (Gandotra et al. 2011).

1.1.4.6 ITGAM

ITGAM encodes for the integrin CD11b (alphaM), which combines with the integrin CD18 to form the functional integrin Mac-1 also called alphaMbeta2 or CR3 (Fagerholm et al 2013). Mac-1 is predominantly expressed on the surface of myeloid cells such as macrophages, neutrophils and dendritic cells (DCs) (Fagerholm et al 2013). There are a variety of Mac-1 ligands, such as members of the ICAM family, the complement protein iC3b and fibrinogen. It helps leukocytes reach sites of inflammation by binding ICAM ligands to the endothelium of blood vessels, thereby assisting neutrophils to creep up the endothelium before extravasation occurs (Fagerholm et al. 2006; Phillipson et al. 2006). In addition, Mac-1 mediates phagocytosis of particles that are marked with iC3b such as apoptotic cells (Morelli et al. 2003). Mac-1 has also been associated with the attenuation of macrophage responses through the induction of signalling inhibitors such as SOCS3 and protein A20, and interleukin (IL) 10 (Wang et al. 2010). An important factor in the pathogenesis of insulin resistance is chronic, low-grade inflammation (Kwon and Pessin 2013; Olefsky and Glass 2010). Macrophages secrete a variety of chemokines and cytokines and thus play an important role in regulating inflammation. In humans with obesity, for example, macrophages are recruited to adipose tissue and show pro-inflammatory properties compared to resident adipose tissue macrophages (ATMs) (Lumeng et al. 2017). Elevated fatty acids in the blood, as found in patients with obesity, are a potential trigger for macrophage activation (Suganami et al. 2007). Saturated fatty acids stimulate Toll-like receptor (TLR) 4 on the surface of ATMs, leading to the activation of inflammatory signalling cascades mediated by NF-κB (Suganami et al. 2007).

1.2 The hallmarks of diabetes

According to the WHO, diabetes is a chronic metabolic disease characterised by high blood sugar levels (hyperglycaemia). It is one of the most common diseases worldwide and its prevalence is continuously increasing at an alarming rate. The number of people with diabetes was estimated at 451 million in 2017 and predicted to rise to 693 million by 2045 (Cho et al. 2018). Diabetes is associated with premature death from coronary heart disease, stroke and heart failure, bowel, liver and lung cancer, chronic obstructive pulmonary disease, and liver and kidney disease (Baena-Díez et al. 2016). It is thus a global public health problem (Nolan, Damm and Prentki 2011). For prognosis and treatment, individuals with diabetes are usually divided into type 1 diabetes (T1D), type 2 diabetes (T2D), specific types of diabetes due to other causes and gestational diabetes mellitus (American Diabetes Association 2014).

1.2.1 Type 1 diabetes (T1D)

T1D represents 5-10% of all people with diabetics and was previously termed “insulin-dependent, juvenile or childhood-onset diabetes” (American Diabetes Association 2014). It is the result of cell-mediated autoimmune destruction of the β-cells of the pancreas leading to a deficient insulin production. Insulin is the hormone that is essential for regulating glucose levels in the body. T1D requires continuous administration of insulin. Symptoms of hyperglycaemia include excessive excretion of urine (polyuria), thirst (polydipsia), weight loss, sometimes constant hunger (polyphagia) and blurred vision (American Diabetes Association 2014). These symptoms can also occur suddenly. Furthermore, T1D patients are also prone to other autoimmune disorders such as Hashimoto’s thyroiditis, vitiligo, celiac sprue and others (American Diabetes Association 2014).

1.2.2 Type 2 diabetes (T2D)

T2D has the highest proportion among people with diabetes (90 to 95 %) and was previously referred as non-insulin dependent or adult-onset diabetes (American Diabetes Association 2014). There are probably many different causes of this form of diabetes which all result in a disturbed glucose homeostasis. The inability to assimilate glucose can be caused by defects in insulin secretion, the response to insulin or a combination of both. Most T2D patients are obese, and obesity itself causes some degree of insulin resistance (American Diabetes Association 2014). There is an increasing prevalence of T2D, which can be partly attributed to the increase in overweight and obesity in the general population due to high calorie intake coupled with low physical activity (McAllister et al. 2009). In addition to an increasing T2D prevalence, these lifestyle changes also lead to earlier onset and more severe diabetic complications, including limb-threatening neuropathy, vasculopathy, retinopathy, renal failure, cardiovascular disease, stroke, myocardial infarction and sudden death (D'Adamo & Caprio 2011; Hannon 2005). This suggests that T2D is one of the biggest threats to global healthcare systems (Groop & Pociot 2014).

1.2.3 Epidemiology, causes and treatment

According to WHO, 8.5% of all adults aged 18 and older had diabetes in 2014. In high-income countries, prevalence has increased less than in low- and middle-income countries. In 2019, diabetes led to 1.5 million deaths, indicating that diabetes is a major problem for health systems. The age-standardised mortality rate due to diabetes increased by 3% between 2000 and 2019. Furthermore, the mortality rate due to diabetes increased by 13% in low- to middle-income countries (WHO (diabetes), 2023).

Diabetes can lead to blindness (retinopathy), kidney failure (nephropathy), vascular problems and heart attack, stroke and lower limb amputation. In the transition between normality and diabetes, impaired glucose tolerance (IGT) and impaired fasting glycaemia (IFG) are evident. Therefore, people with IGT or IFG are at high risk of developing T2D, even if it can still be prevented. There are several ways to prevent or delay the onset of T2D. These include a healthy diet with less sugar and highly processed foods, regular physical activity, maintaining a normal body weight and avoiding tobacco to reduce the risk of cardiovascular disease. Accordingly, simple lifestyle measures are effective to avoid or delay the onset of T2D (WHO, 2022).

Diabetes can damage the heart, blood vessels, eyes, kidneys and nerves over time. Adults with diabetes have a two- to three-fold increased risk of heart attacks and strokes (Emerging Risk Factors Collaboration 2010). Neuropathy (nerve damage) in the feet, combined with reduced blood flow, increases the risk of foot ulcers, infections and eventually the need for limb amputation. Due to long-term damage to the small blood vessels in the retina, diabetic retinopathy may cause blindness. Diabetes led to blindness in almost 1 million people (GBD 2019 Blindness and Vision Impairment Collaborators 2021). Furthermore, diabetes is one of the most common causes of kidney failure (Saran et al. 2015).

Early diagnosis is pivotal and can be accomplished through relatively inexpensive testing of blood sugar. Controlling blood glucose levels, especially in T1D is a cost-saving intervention that is feasible even in low- and middle-income countries. People with T1D will always need insulin, while people with T2D may be treated with oral medication.

1.2.4 Association of obesity with T2D development

Age, BMI and sex are important predictors of T2D risk. The prevalence is clearly higher in people with a BMI > 30 and increases across all age groups from 1.1 to 6.1 with increasing BMI (Tab. 1). People with a high BMI and older than 70 years are particularly affected (Tab. 1). Nevertheless, even after adjusting for age, BMI and sex, population-based differences can still be found. Other environmental and genetic factors account for these differences (Prasad & Groop 2015). At first, family- and twin-based studies established the heritability of T2D risk (Meigs et al. 2000; Newman et al. 1987). The subsequent establishment of genome-wide association studies (GWAS) enabled the identification of genetic variations associated with risk for T2D and related traits (Welter et al. 2014). Most of these sites of variation have not yet been mechanistically or functionally characterised.

Table 1 – Number and proportion of people with type 2 diabetes (T2D) per age and weight group in the Health Survey for England 2003.
Age is displayed in years and BMI in kg/m^2. Adapted from: Gough et al. 2009

Age		BMI < 25	BMI 25.0-29.9	BMI ≥ 30
	All, n	1390	568	266
16–29	With T2D, n	2	0	3
	Proportion with T2D, %	0.1	0.0	1.1
	All, n	1780	1765	1084
30–49	With T2D, n	6	14	29
	Proportion with T2D, %	0.3	0.8	2.7
	All, n	1071	1674	1073
50–69	With T2D, n	23	56	108
	Proportion with T2D, %	2.1	3.3	10.1
	All, n	456	661	400
70+	With T2D, n	23	62	47
	Proportion with T2D, %	5.0	9.4	11.8
	All, n	4697	4668	2823
All	With T2D, n	54	132	187
	Proportion with T2D, %	1.1	2.8	6.6

1.3 Genome-wide association studies (GWAS)

The genome-wide association study (GWAS) is an experimental design applied to detect associations between genetic variants and traits in samples from populations (Visscher et al. 2017). GWASs focused on detecting associations between common single nucleotide polymorphisms (SNPs) and common diseases such as heart disease, diabetes, autoimmune diseases and psychiatric disorders (Visscher et al. 2012). The major objective of GWAS is a better understanding of the biology of diseases, assuming that a better knowledge will lead to novel approaches to the diagnosis, prevention, treatment, and monitoring of disease.

The principle on which GWAS is based is the linkage disequilibrium (LD) at the level of the population. LD is the non-random association between alleles at different loci and arises from evolutionary forces

such as mutation, drift and selection and is degraded by recombination (Hartl and Clark 1997). The LD structure was investigated as part of the HapMap project. The result was a list of tag SNPs that maps most of the common genomic variation in a number of human populations (International HapMap Consortium 2005). The first results from GWASs were reported in 2005 and 2006 on age-related macula degeneration (Dewan et al. 2006; Klein et al. 2005). In 2007, the Wellcome Trust Case Control Consortium (WTCCC) conducted the first large, well-designed GWAS for complex diseases, using a SNP chip that had good genome coverage (Wellcome Trust Case Control Consortium 2007). Since then, about 10,000 strong associations between genetic variants and one or more complex traits have been identified (Welter et al., 2014). For most traits and diseases studied, the mutation target in the genome appears to be high so that polymorphisms in many genes contribute to genetic variation in the population (Visscher et al. 2017). The majority of GWAS-identified risk alleles are non-coding variants. For the interpretation of these non-coding variants, the maps of regulatory annotations such as deoxyribonucleic acid (DNA) accessibility, DNA methylation, histone modification and RNA expression levels and connections in disease-relevant tissues produced by projects such as ENCODE, Epigenome RoadMap, 69 and GTEx, 70 are crucial (ENCODE Project Consortium 2012; Roadmap Epigenomics Consortium 2015; GTEx Consortium 2013).

1.3.1 GWAS in T2D

GWAS approaches have identified over 400 genes associated with T2D (Srinivasan et al. 2021; Chen et al. 2019). The challenges in deciphering GWAS are to identify causal variants, long genomic regulations, relevant cell types, regulators, target genes and their biological role. To this end, Claussnitzer and colleagues have developed the comparative genomics approach Phylogenetic Module Complexity Analysis (PMCA), which, in combination with state-of-the-art experimental validation, has identified a non-coding functional variant rs4684847 in the PPARG locus associated with T2D (Claussnitzer et al. 2014). It was found that the homeobox factor PRRX1 bind to the rs4684847 risk allele within the PPARG locus, which leads to repression of the PPARG isoform PPARG2 in adipose cells. This repression leads to adverse effects on lipid metabolism and systemic insulin sensitivity. This study demonstrated the isoform-specific cis-regulatory role of a non-coding intronic variant in an adipocyte-specific manner (Claussnitzer et al. 2014). Another study examined the biological role of the FTO locus, which has the strongest genetic association with obesity Claussnitzer et al. 2015. Therefore, an adapted version of PMCA was used integrated with large-scale epigenomic profiling in 127 cell types and tissues. This approach identified a long-range regulatory super-enhancer in the FTO locus that is specifically active in adipocyte progenitor cells from carriers of the risk allele. The rs1421085 T-to-C variant disrupts a conserved motif for the ARID5B repressor. This leads to an overexpression of IRX3 and IRX5 during early adipocyte differentiation. As a result, there is a cell-autonomous

developmental shift from energy-releasing beige (brite) adipocytes to energy-storing white adipocytes, with a 5-fold reduction in mitochondrial thermogenesis and an increase in lipid storage (Claussnitzer et al. 2015). Another interesting locus for which GWAS has shown several non-coding T2D risk variants is the GBR14/COBLL1 locus, which is discussed in detail in the next chapter.

1.3.2 Importance of the intergenic variant rs6712203 at the *GRB14/COBLL1* locus for T2D risk

The *GRB14/COBLL1* locus is located in an intergenic region between *COBLL1* and *GRB14* (Fig. 5). The association region stretches from the intergenic region between *GRB14* and *COBLL1*, clustering around the 3'-UTR and the fifth 3'-intron of *COBLL1*.

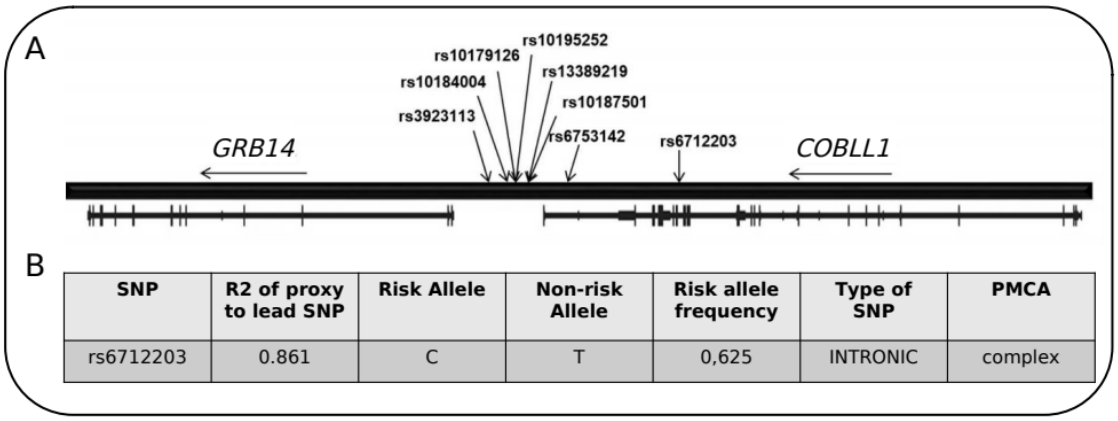

SNP	R2 of proxy to lead SNP	Risk Allele	Non-risk Allele	Risk allele frequency	Type of SNP	PMCA
rs6712203	0.861	C	T	0,625	INTRONIC	complex

Figure 5 - Variants at the T2D risk locus GRB14/COBLL1.
Panel A shows the *COBLL1 /GRB14* locus and the annotated risk variants. In Panel B, characteristics of the variant rs6712203 are shown. SNP: single nucleotide polymorphism; PMCA: Phylogenetic Module Complexity Analysis. Adapted from: Ocvirk (nee Glunk) et al. 2023.

At first, the rs3923113 variant was associated with T2D and insulin sensitivity in a population of South Asian ancestry and later verified in a transethnic meta-analysis (Kooner et al. 2011; DIAbetes Genetics Replication And Meta-analysis (DIAGRAM) Consortium et al. 2014). Another variant rs13389219 in the same haplotype was also associated with T2D and insulin resistance in a European Metabochip study (DIAbetes Genetics Replication And Meta-analysis (DIAGRAM) Consortium et al. 2012). The exonic COBLL1 variant rs7607980, which is a missense mutation in the third COBLL1 3' exon, has been associated with T2D and lower fasting insulin and HOMA-IR levels (Albrechtsen et al. 2013; Mancina et al. 2013). It is unlikely that this exonic variant fully underlies the non-coding GRB14/COBLL1 T2D association signal, as it is in partial LD with rs3923113 and rs13389219. Additionally, GWAS studies reported non-coding variants at the GRB14/COBLL1 locus with waist-to-hip ratio (WHR), HDL cholesterol and triglyceride levels besides association with T2D and insulin resistance (Heid et al. 2010; Desmarchelier et al. 2014; Teslovich et al. 2010; Randall et al. 2013). Furthermore, pleiotropic studies linked GRB14/COBLL1 to metabolic syndrome, inflammation, endometriosis, WHR (adjusted for BMI),

body fat percentage and cardiovascular events (Kraja et al. 2014; Lu et al. 2016; Rahmioglu et al. 2015). A sexual dimorphism has been shown for the association with WHR and BMI, with stronger effects found in women (Heid et al. 2010; Randall et al. 2013; Morris 2011). Interestingly, GWAS analyses at the GRB14/COBLL1 locus also showed sex- and BMI-specific associations with insulin resistance and T2D (DIAbetes Genetics Replication And Meta-analysis (DIAGRAM) Consortium et al. 2012; DIAbetes Genetics Replication And Meta-analysis (DIAGRAM) Consortium 2014; Kooner et al. 2011; Heid et al. 2010; Manning et al. 2012).

Both *GRB14* and *COBLL1* are convincing target genes for the underlying mechanisms of the *GRB14*/*COBLL1* locus variants for T2D risk. *GRB14* encodes for the cytoplasmic adaptor protein GRB14, which binds to a number of activated receptor tyrosine kinases such as the fibroblast growth factor receptor (FGFR), PDGFR, IR and the tunica endothelial kinase (Tek/Tie2) receptor (Scharf et al., 2004). GPR14 can act as negative regulator of the insulin receptor. In human visceral adipose tissue, the expression of GRB14 has been shown to be increased in obese and type 2 diabetic subjects (Schleinitz et al. 2014). So far, however, it has not been convincingly demonstrated that GRB14 is the target gene of T2D association.

The *COBLL1* gene encodes for the COBLL1 protein. Unfortunately, the functional role of COBLL1 in metabolic diseases in humans is poorly understood. Until recently, expression analysis linking COBLL1 to T2D disease signalling was also not comprehensive and could not elucidate the regulatory circuit (Heid et al. 2010; Morris 2011; Albrechtsen et al. 2013; Schleinitz et al. 2014). In a recent study, Ocvirk (nee Glunk) and colleagues investigated the regulatory mechanisms of the rs6712203 variant of the *GPR14/COBLL1* locus (Ocvirk (nee Glunk) et al., 2023). The first question that arose was which tissue might play a role in the rs6712203 variant. For this purpose, information on the epigenetic marks for primary cells and tissues was used from the NIH Roadmap Epigenomics Consortium and an adipocyte-specific enhancer region surrounding the intronic *COBLL1* variant rs6712203 was found (Roadmap Epigenomics Consortium et al. 2015). Next, a TF motif analysis was performed and a rs6712203-T non-risk allele specific POU2F2 binding site was identified (Fig. 6). CRISPR/Cas9 experiments were used to investigate the effect of POU2F2 on *COBLL1* expression. It was shown that POU2F2 binding at the adipocyte-specific enhancer leads to increased *COBLL1* expression, which was completely abolished by both POU2F2 knockdown and disruption of the binding site in carriers of the rs6712203-C risk allele. Finally, it was shown that impaired *COBLL1* expression leads to impaired actin remodelling during adipogenesis, followed by reduced insulin-stimulated glucose uptake, diminished triglyceride storage and decreased stimulated lipolysis. The cellular phenotypes observed in the study are relevant to type 2 diabetes and are consistent with the association of the *GRB14*/*COBLL1* locus with type 2 diabetes in

different populations, which may be due to peripheral insulin resistance with dysfunctional energy regulation in adipose tissue.

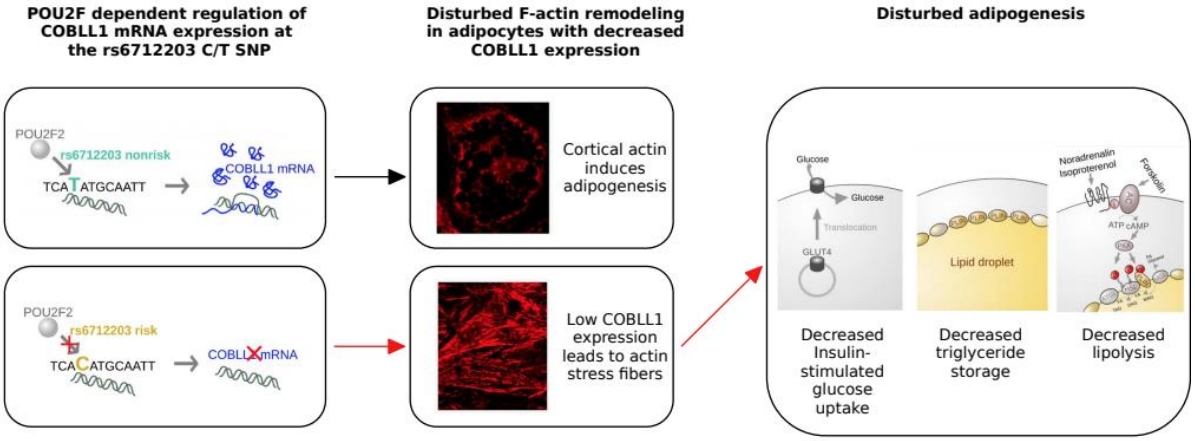

Figure 6 - Mechanistic model of the POU2F2 dependent up-regulation of COBLL1 expression in rs6712203-T non-risk allele carriers.
In rs6712203-T non-risk human adipocytes, the expression of COBLL1 is POU2F2 dependent upregulated. In rs6712203-C risk adipocytes, the POU2F2 motif is partially disrupted, which prevents the up-regulation of COBLL1. COBLL1 perturbation in human adipocytes, leads to a disturbed remodeling of F-actin fibers from stress fibers to cortical actin, which is essential for adipogenesis and for the adaptation to changes in the microenvironment of the cell. Lower cortical actin structures cause disturbances during adipogenesis and result in a decreased insulin-stimulated glucose uptake, lipolysis and triglyceride storage. Adapted from: Glunk et al., 2023).

1.4 Metabolomics

The word "metabolism" originates from the Greek and means change. In all living organisms, various types of biological transformations take place that characterise metabolism. Metabolites are the end products of cellular regulatory systems, so changes in metabolites reflect the responses of biological systems to intrinsic and extrinsic regulators such as pathological changes in metabolism (Patti et al. 2012). Metabolomics is the comprehensive and quantitative detection and identification of all metabolites of an organism or a biofluid (Fiehn 2002; Raamsdonk et al. 2001; Wilson et al. 2005). Metabotype is described as a metabolic profil that determines a phenotype related to the genetic variation of the organism (Gavaghan et al. 2000). It is the result of interaction with environmental factors such as gender, age, lifestyle, diet, stress level and gut microbiota and within this interaction, disease risk may arise (Daviglus et al. 2004; Li et al. 2008; Nicholson et al. 2002). Metabolic profiling requires the analysis of various metabolites in biofluids such as plasma, serum, urine or exhaled breath condensate (Nicholson et al. 2002; Holmes et al. 2008). There are endogenous metabolites, which are under the control of the host genome and depend on cell function, or exogenous metabolites, which are introduced by environmental influences or via diet and drugs (Nicholson and Wilson 2003). The updated version of the Human Metabolome Database (HMDB) contains 40,335 metabocard entries

(Wishart et al. 2009). The mass of metabolites ranges from 50 Da to 1500 Da and from low picomolar concentration (e.g. hormones) to molar concentration (e.g. albumin, urea). Their chemical and physical properties can be strongly polar as well as strongly apolar. Furthermore, the stereochemistry of metabolites leads to different biological functions (Chen et al. 2008). The detection of this diversity of metabolites in a biological sample requires the integration of different analytical platforms to enable the highest level of analyte detection and identification through high sensitivity, selectivity and resolution (Lenz et al. 2004; Wishart et al. 2007; Wishart et al. 2008).

The two main metabolomic techniques are mass spectrometry (MS) and nuclear magnetic resonance (NMR) spectroscopy (Dettmer et al. 2007; Emwas, et al. 2019; Monge et al. 2019; Nicholson et al. 2008; Patti et al. 2012). MS-based metabolomics has much higher sensitivity and selectivity compared to NMR-based metabolomics (Emwas 2015; Griffin et al. 2011; Han et al. 2012). Direct injection (DI) coupled with Fourier transform ion cyclotron resonance mass spectrometry (FT-ICR/MS) is able to cover a wide range of metabolites in a short measurement time, even with complex sample matrices without prior chromatographic separation. Furthermore, it has an extremely high resolution compared to various liquid chromatography coupled with mass spectrometry analysis techniques and a very high sensitivity compared to NMR (Aharoni et al. 2002; Witting et al. 2015; Zhu et al. 2021).

Another technique used in targeted metabolomic studies is solid phase extraction (SPE). It is used to quantitatively isolate certain classes of compounds of interest. The advantages of SPE are the minimisation of ion suppression and possible automation. To integrate this technique into non-targeted metabolomics analysis, a suitable absorption material must be selected.

1.4.1 The mode of operation of Fourier-Transform Ion Cyclotron Resonance Mass Spectrometers (FT-ICR/MS)

Fourier-Transform Ion Cyclotron Resonance Mass Spectrometry (FT-ICR/MS) is currently the state-of-the-art mass spectrometric technology with the highest resolution and accuracy. Mass detection is based on the circular oscillation that charged ions exhibit when introduced into a homogeneous magnetic field. The equation (1) shows the relationship of the (Lorentz) force (f) with the mass (m), the charge (z), the velocity (v) and the strength of the magnetic field (B) in Tesla.

$$\frac{zB}{Wc} \quad (1)$$

A conversion of this equation gives the relations (2) and (3), where W_c is the cyclotron frequency of mass m for a given charge z and magnetic field strength B (Marshall et al. 1998).

$$W_c = \frac{zB}{m} \quad (2)$$

$$m = \frac{zB}{Wc} \quad (3)$$

From this relationship, it can be deduced that a particle with a certain mass has its specific ion cyclotron frequency. In a typical ICR cell, all ions of a sample oscillate with their specific frequencies W_c around the z-axis of the cell. By superimposing the cyclotron frequency of a specific molecule on an oscillating RF (resonance frequency) field of the same frequency, this specific molecule is moved to a trajectory more distant from the z-axis. Detector plates are located there to detect the frequency and presence of this molecule in this this post-excitational orbit (Fig. 7).

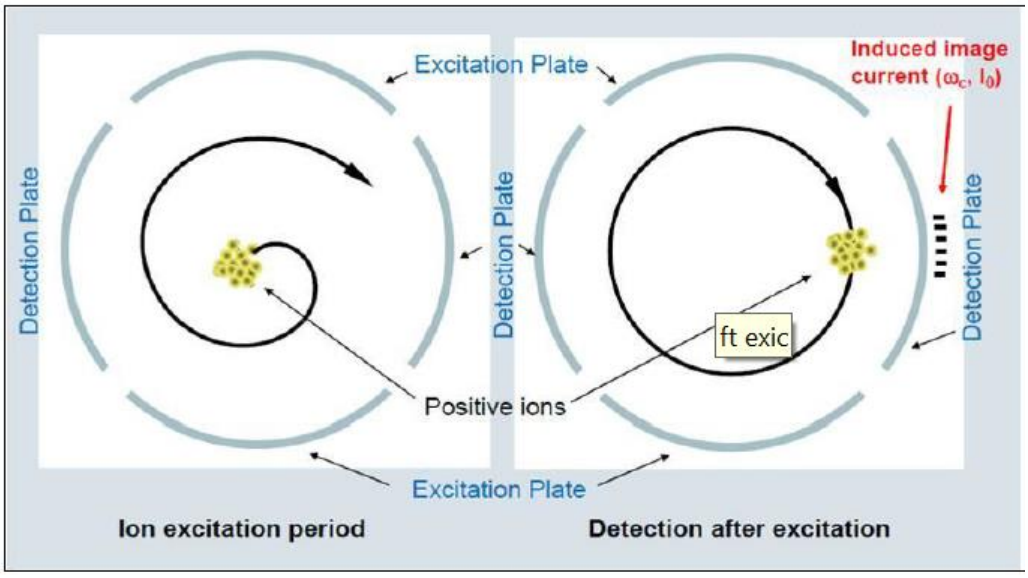

Figure 7 - Schematic representation of the ICR process.
Ions introduced into the ICR cell begin to oscillate at mass-specific frequencies in the centre of the cell. The superposition with the RF resonance frequency leads to an excitation near the detector plates. The ion cyclotron frequency now becomes measurable as an image stream is Fourier-transformed into mass spectra. Reprinted with permission from Bruker solariX FTMS User Manual, see LETTERS OF APPROVAL

From equation (3) it can be concluded that the higher the magnetic field strength, the more prominent the frequency difference between two masses. Consequently, the resolution, mass accuracy and scanning speed increase with increasing magnetic field strength (Chernushevich et al. 2001). Molecules with a mass between 150 and 1000 Da, have frequencies between kHz and MHz. Typically, sampling times of between 1s and 2s are required to detect each mass frequency over a sufficient period of time. In general, the sensitivity per scan of FT-ICR/MS mass spectrometers is relatively low (Li X et al. 2009). It is likely that this observation is due to the fact that all ions generated from a sample coexist in a spatially confined orbit around the z-axis of the ICR cell, resulting in interactions of like-charged ions. Ions with the same charge repel each other, which leads to different thermal states of the ions and consequently to off-resonance excitations. This makes it difficult to be detected by this noise, especially for ions with relatively low abundance. For this reason, successive

FT-ICR/MS scans are usually superimposed. In this way, the repeated occurrence of certain masses enhances peak formation, while noise signals cancel each other out.

Coupling the FT-ICR/MS with liquid chromatography (LC) is not practical due to the long scan times required for high resolution. Furthermore, developments in LC-MS have focused on higher peak capacity, shorter gradient times and consequently shorter chromatographic peaks. In general, at least 15 data points per peak width are required to obtain a chromatographic peak with good mass spectrometric resolution (Rainville 2010). For this reason, FT-ICR/MS is best carried out with direct injection electrospray ionisation. This technique generates a constant ion flux, optimising the sensitivity and accuracy of FT-ICR/MS. These advantages of FT-ICR/MS minimise the lack of chromatographic resolution in the differentiation of isobaric masses, which is a major disadvantage of other spectrometers.

1.4.2 Prediabetes Lifestyle Intervention Study (PLIS)

The Prediabetes Lifestyle Intervention Study (PLIS) currently ongoing at 7 cooperating institutes across Germany (Berlin, Dresden, Düsseldorf, Heidelberg, Munich, Potsdam, Tübingen) investigates to what extent lifestyle changes such as a balanced diet and increased exercise are able to reduce the risk of T2D. The local subproject "Genotype-driven deep metabotyping and *de novo* Type 2 Diabetes biomarker identification" is currently ongoing as well in Munich, Freising-Weihenstephan and Neuherberg.

Early metabolic changes may occur many years before the clinical manifestation of a metabolic disease and before the actual onset of the disease. This is also true for T2D. Moreover, because T2D is highly heterogeneous in terms of its symptoms and pathophysiology, it is of great importance to identify specific and stable biomarkers indicative of such early metabolic changes. The blood glucose level by itself does not meet the requirements. A better comprehension of the pathophysiology of T2D, i.e. its genetic background and typical early abnormal metabolism, will improve early risk prediction and preventive measures. While through GWAS, numerous genetic T2D risk loci have already been successfully identified, but the mechanisms behind these associations remain to be discovered.

Associated SNPs may just follow the neighbouring SNPs actually driving a phenotypic association. So far, the predictive power of existing risk scores is only slightly increased by adding GWAS association information. Revealing their biological function and metabolic causalities and consequences, and by successfully integrating this genetic information will be invaluable for disease prediction strategies.

Recent approaches, novel bioinformatics technologies and a comprehensive biological validation framework, offer a powerful new tool for understanding how causal non-coding genetic variants and T2D traits are associated (Claussnitzer et al, 2014). After it demonstrated its power in the context of the FTO

obesity association locus (Claussnitzer et al. 2015), this unique computational technology is now used to shed light on the molecular mechanisms of relevant T2D loci (*GCK*, *TCF7L2, MTNR1B, GRB14-COBLL1*, *TLE1*) including comprehensive non-targeted metabolic profiling for identification of metabolic profiles in circulating plasma clearly reflecting the metabolic disturbances caused by the relevant genetic variation.

Based on ultra-high resolution and mass spectrometry data from Fourier Transform Ion Cyclotron Resonance/ Mass Spectrometry (FT-ICR/MS) high confidence chemical sum formula annotations become available, and enable the identification of known and as yet unknown metabolites and their respective pathways, allowing a deeper understanding of disease pathophysiology, possibly even in very early stages.

Certain genetic variants (SNPs) are assumed to contribute to an increased risk for T2D and result in alterations in specific pathways causing specific metabolite profiles. Such "metabotypes" may help discriminate between risk allele carriers vs. non-risk allele carriers, i.e. there are metabolite profiles specific for certain disease phenotypes and can be applied as predictive biomarkers.

This subproject of the PLIS study, therefore, aimed to evaluate how diabetes risk SNPs determine the individual "metabotype" by interconnecting functional SNP data (including *GCK, TCF7L2, MTNR1B, GRB14/COBLL1, TLE1* and *FTO*) and metabolomics data.

1 Identification of metabolite profiles/metabolic fingerprints discriminative for risk allele vs. non-risk allele carriers of type 2 diabetes risk genes that clearly reflect the genotype dependent changes in metabolism.

2 Identification and validation of single biomarker/ set of biomarkers that is/ are specific as biomarkers for early metabolic dysfunction in individuals at risk of type 2 diabetes.

For analysis of the genotype-specific metabolic phenotype/metabotype this subproject of the PLIS study involves a phenotyping/genotyping part complemented by non-targeted metabolomics via ultra-high-resolution mass spectrometry. Correlations between genes and metabolites are then mapped using statistic bioinformatics tools (Faith et al. 2007).

For the purpose of phenotyping and genotyping of individuals at elevated risk for type 2 diabetes phenotype data from the PLIS oral glucose tolerance test (OGTT) were used, including anthropometric data, medical history, standard clinical parameters and diabetes-related parameters. Biological material collected during an OGTT will be used for genotyping and metabolomics.

Participants were genotyped for 5 diabetes-relevant risk loci (MTNR1B, GCK, GRB14-COBLL1, TCF7L2, and TLE1) together with the obesity and type 2 diabetes-associated FTO locus.

Non-targeted metabolomics measurements of blood plasma were performed via DI-FT-ICR/MS analysis with ultra-high resolution and high mass accuracy at the collaborating Research Unit Analytical Biogeochemistry (BGC) at the Helmholtz Zentrum Munich in compliance with established protocols (Forcisi et al. 2013; Forcisi et al. 2015; Moritz et al. 2015). This part also includes further application of MS/MS techniques and high-resolution chromatographic techniques for the validation and quantification of candidate biomarkers (Forcisi et al. 2015; Walker et al. 2014).

1.5 Aim of thesis

The aim of this thesis was to determine and confirm whether there is a link between the *COBLL1* intronic variant SNP rs6712203 and type 2 diabetes using patient-derived cell culture studies. In the work of Glunk et al., 2023 the TF POU2F2 was found to bind to the *COBLL1* enhancer in the region of the rs6712203 variant in carriers of the non-risk allele and promote *COBLL1* expression. However, in the risk allele carriers, *COBLL1* expression is reduced, and actin remodelling is impaired. The changes in *COBLL1* expression have clear implications for cell physiology: It reduces insulin-stimulated glucose uptake, triglyceride storage and lipolytic stimulation. A further study of the Hauner laboratory investigated the effect of ablated *COBLL1* expression in the serum of patients with rs6712203 risk and non-risk alleles and a pattern was observed by metabolomic analysis that pointed to the genes *PLIN5*, *ILK* (integrity linked kinase) and *PPARG* (Al Sadat et al. 2022/unpublished data). In the present work, *in vitro* adipocyte differentiation of subcutaneous adipose tissue isolated from eleven obese rs6712203 risk and non-risk female patients, marker gene expression analysis and metabolomic studies using FT-ICR/MS were performed to determine which metabolic pathways are affected by COBLL1 directly in human adipocytes.

2 MATERIALS AND METHODS

2.1 Chemicals and media

Chemicals and reagents used for cell culture and cell sample processing are presented in Table 2.

Table 2 – Chemical agents and components used

Chemical	Company	Storage	Order Number
(+)D-Biotin	Roth	4 °C	3822.1
5X MyTaq Reaction Buffer	Bioline	-20 °C	BIO-21106
10X RT Buffer, High-Capacity cDNA (complementary deoxyribonucleic acid) Reverse Transcription Kit	Applied Biosystems	-20 °C	4368814
10X RT Random Primers, High-Capacity cDNA Reverse Transcription Kit	Applied Biosystems	-20 °C	4368814
25X dNTP (deoxyribonucleotide triphosphate) Mix (100 mM), High-Capacity cDNA Reverse Transcription Kit	Applied Biosystems	-20 °C	4368814
Acid phenol: chlorophorm 5:1	Ambion	RT	AM9720
apo-Transferrin, human	Sigma	4° C	T2252
BCA (bicinchoninic acid) Reagent A, Pierce Microplate BCA Protein Assay Kit	Thermo Scientific	RT	23252
BCA Reagent B, Pierce Microplate BCA Protein Assay Kit	Thermo Scientific	RT	23252
BSA (bovine serum albumin)	Sigma	4 °C	A 7906-500G
BSA solution 10 % in DPBS (Dulbecco's phosphate buffered saline)	Sigma	4 °C	A1595
Compatibility Reagent, Pierce Microplate BCA Protein Assay Kit	Thermo Scientific	RT	23252
Chloroform	Rothe	RT (under hood)	3313.1
Complete Mini	Roche	-20 °C	11836153001
Deoxycholate	Sigma	RE	D6750
Dexamethasone	Sigma	4 °C	D4902
DMSO (dimethyl sulfoxide)	Merck	RT	102.931
EDTA (ethylenediamine tetraacetic acid)	Merck	RT	108.417
EGF (epidermal growth factor)	R&D Systems	-20 °C	236-EG
Elution solution, Invitrogen mirVana miRNA (micro ribonucleic acid) and mRNA (messenger ribonucleic acid) Isolation Kit	Thermo Scientific	any T	AM1560
EtOH (ethanol) abs.	VWR	RT	20.821.330
EtOH abs. analytical reagent grade	Fisher Scientific	RT	E/0650DF/C17
FCS (fetal calf serum)	Sigma	-20 °C	F7524

FGF (fibroblast growth factor)	R & D Systems	-20 °C	233-FB
Formaldehyde solution 37 %	Roth	RT	4979.1
Gibco™ DMEM/F-12, No Phenol Red	Fisher Scientific	4 °C	11580546
Histofix	Roth	RT	P087
Honeywell Riedel-de Haen™Methanol, LC-MS CHROMASOLV™, Honeywell Riedel-de Haen™	Fisher Scientific	-20 °C	15614740
Hydrocortisone	Sigma	4° C	H4001
Insulin, human	Sigma	4° C	19278
Isopropanol = Propan2-ol	Thermo Scientific	RT (under hood)	P/7500/PC17
IBMX (3-isobutyl-1-methylxanthine)	SERVA	RT	26445
LightSNip rs6712203 COBLL1	TIB MOLBIOL	4° C	-
Lysis buffer, Invitrogen mirVana miRNA and mRNA Isolation Kit	Thermo Scientific	4° C	AM1560
Maxima SYBR Green/ROX qPCR Master Mix (2X)	Thermo Scientific	-20 °C	K0223
MultiScribe Reverse Transcriptase (50 U/µL), High-Capacity cDNA Reverse Transcription Kit Capacity cDNA Reverse Transcription Kit	Applied Biosystems	-20 °C	4368814
MyTaq DNA Polymerase	Bioline	-20 °C	BIO-21106
NaCl (sodium chloride)	Merck	RT	6404
NADH (nicotinamide adenine dinucleotide hydride)	Applichem	-20 °C	A-1393
NP-40	Fluka	RT	74385
NucBlue™ Live ReadyProbes Reagent (Hoechst 33342)	Thermo Scientific	RT	R37605
Oil Red O	Sigma	RT	O0625
Pantothenate (D-pantothenic acid hemicalcium salt)	Sigma	4 °C	P5155
PBS (phosphate-buffered saline) w/o Ca2+/Mg2+	Merck	RT	L182-50
PCR grade water, provided by ultrapure water system	Elga Veolia Purelab flex	RT	-
PhosphoStop	Roche	-20 °C	4906837001
PMSF	Sigma	RT (poison cupboard)	P7626
qPCR Primer	Eurofins/Sigma	-20 °C	-
RLT buffer, RNeasy Kit Qiagen RT	Qiagen	RT	1015762
RNaseZAP	Sigma	RT	R2020
Rosiglitazone	Sigma	4 °C	R2408
SDS	Omnilab	RT	2.700.131
T3 (3,3'-5-triiodo-L-thyronin sodium salt)	Sigma	-20 °C	T-6397
Triethanolamine-HCl (hydrochloric acid)	Sigma	RT	T1502
Tris-HCl	Sigma	RT	T3253

Trizol Reagent	Ambion/ Qiagen	RT (under hood)	-
Trypan Blue solution 0.4 %	Sigma	RT	T8154
Trypsin/EDTA	Sigma	-20 °C	T3924
Ultrapure RNase free H_2O	Qiagen/Roth	water device with ultrapure filter	
96-well plates	Brand	-	-
96-well plates sealing foils	Brand	-	-

Compositions, preparation and storage instructions for solutions and buffers used in cell culture and cell sample processing are given in Table 3.

Table 3 – Composition, preparation and storage of solutions and buffers

Solution/buffer	Composition and Preparation	C_{final}
Biotin/Pantothenate solution	400 mg Biotin 200 mg Pantothenate dissolve in 500 ml DMEM-F12, sterile filter 0.2 µm, store at -20°C	3.3 mM 1.7 mM
BSA solution in PBS	0.1 g BSA, dissolve in 100 ml PBS, sterile filter 0.2 µm, store at 4°C	0.1 %
BSA solution in H_2O	20 g BSA, dissolve in 100 ml H_2O (double distilled water), store at 4°C	200 mg/ml
Dexamethasone solution	Dissolve 9.81 mg Dexamethasone in 1 ml EtOH 95 % (stock), dilute 1:1000 in 50% EtOH. (15 µl plus 14985 µl EtOH 50 %), sterile filter 0.2 µm, store at -20 °C	25 mM
EGF solution	200 µg EGF (lyophilized), dissolve in 4 ml BSA solution in PBS (stock), dilute 1:10, (500 µl in 4.5 ml BSA solution in PBS), store at -20 °C	5 µg/ml
FGF solution	25 µg FGF lyophilized, dissolve in 5 ml BSA solution in PBS (stock), dilute 1:10 (500 µl in 4.5 ml BSA solution in PBS), store at -20 °C	0.5 µg/ml
Formaldehyde fixation solution	Formaldehyde solution 37 %, dilute 1:10 in H_2O (20 ml formaldehyde 37 % + 180 ml H_2O)	3.7 %
Hydrocortisone solution	3.625 mg Hydrocortisone, dissolve in 1 ml EtOH abs. (stock), dilute 1:100 in EtOH 50 % (500 µl in 49.5 ml EtOH 50 %), sterile filter 0.2 µm, store at -20 °C	100 µM
IBMX solution	220 mg IBMX, dissolve in 50 ml ddH2O plus 1 tip of a spatula Na2CO3, sterile filter, 0.2 µm, store at 4 °C	20 mM
NADH buffer	8.51 mg NADH, dissolve in 1 ml TRAM buffer, prepare fresh	12 mM
RNA (ribonucleic acid) harvesting solution	140 µl ß-Mercaptoethanol, dissolve in 14 ml RLT buffer, store dark at RT	1%
Rosiglitazone solution	10 mg Rosiglitazone, dissolve in 2.797 ml DMSO (stock), dilute 1:5 (1 ml in 4 ml DMSO), sterile filter 0.2 µm, store at -20 °C	2 mM
T3 solution	5 mg T3, dissolve in 7.4 ml EtOH abs. plus 2 drops 1 M NaOH, dilute 1:20 (500 µl in 9.5 ml EtOH abs.) (stock), dilute 1:25 in EtOH 50 % (500 µl) in 12 ml EtOH 50 %), sterile filter 0.2 µm, store at -20 °C	2 µM
TRAM buffer	18.57 g Triethanolamine-HCl 0.931 g EDTA dissolve in 80 ml ddH2O, pH 7.4, fill up to 100 ml, store dark at 4 °C	1 M 1 mM
Transferrin solution	100 mg apo-Transferrin, dissolve in 100 ml ddH2O, sterile filter 0.2 µm, store at -20 °C	1 mg/ml

The composition of the proliferation medium with FCS is given in Table 4.

Table 4 – Composition of proliferation medium with FCS

	250 ml	500 ml	Working solution	C_{final}
DMEM/F12	240.23 ml	480.46 ml		-
Biotin/Pantothenate solution	2.5 ml	5 ml		1%
FCS	6.25 ml	12.5 ml	-	2.5%
Insulin	19.2 µl	38.4 µl	1.722 mM	0.000131954 mM
EGF solution	500 µl	1000 µl	5 µg/ml	0.01 µg/ml
FGF solution	500 µl	1000 µl	0.5 µgml	0.001 µg/ml

The composition of the proliferation medium without (w/o) FCS is specified in Table 5.

Table 5 – Composition of proliferation medium without (w/o) FCS

	250 ml	500 ml	Working solution	C_{final}
DMEM/F12	246.48 ml	492.96 ml	-	-
Biotin/Pantothenate solution	2.5 ml	5 ml	-	1%
Insulin	19.2 µl	38.4 µl	1.722 mM	0.000131954 mM
EGF solution	500 µl	1000 µl	5 µg/ml	0.01 µg/ml
FGF solution	500 µl	1000 µl	0.5 µgml	0.001 µg/ml

The composition of the differentiation medium is indicated in table 6.

Table 6 – Composition of differentiation medium.

	250 ml	500 ml	Working solution	C_{final}
DMEM/F12	244.5 ml	489 ml	-	-
Biotin/Pantothenate solution	2.5 ml	5 ml	-	1%
Transferrin solution	2.5 ml	5 ml	1 mg/ml	0.01 mg/ml
Insulin	125 µl	250 µl	1.722 mM	0.861 µM
T3 solution	125 µl	250 µl	2 µM	1 nM
Hydrocortisone solution	250 µl	500 µl	100 µM	0.1µM

The composition of the induction medium is provided in Table 7.

Table 7 – Composition of induction medium.

	Total volume			
	250 ml	500 ml	Working solution	C_{final}
Differentiation medium	246.5 ml	493 ml	-	-
Rosiglitazone solution	125 µl	250 µl	2 mM	1 µM
Dexamethasone solution	250 µl	500 µl	25 µM	25 nM
IBMX solution	312.5 µl	625 µl	20 mM	0.25 mM

Compositions, preparation and storage instructions for solutions and buffers used in protein isolation are listed in Table 8.

Table 8 – Solutions for protein isolation

Solutions/ Buffers	Composition and Preparation	C_{final}
1 M TRIS-HCl, pH 8.0	15.76 g TRIS, dissolve in 80 ml H_2O solution, adjust to pH 8.0 with HCl, fill up to 100 ml, autoclave	1 M
PBS buffer	10x PBS stock, dilute in H_20, autoclave	137 mM NaCl, 2.7 mM KCl, 4.3 mM $Na_2HPO_4x2H_2O$1.4 mM KH_2PO_4
NaCl stock solution	2.34 g NaCl, dissolve in 20 ml H_2O, autoclave	2 M
SDS stock solution	10 g SDS, dissolve in 100 ml H_2O	10% (w/v)
NP-40 solution	20 g of 100% NP-40, dilute in 100 ml H_2O	20% (w/v)
PMSF solution	0.875 g PMSF, dissolve in 10 ml H_2O, aliquot a 0.5 ml, store at -20°C	0.5M
RIPA stock solution (100 ml)	5 ml of 1 M TRIS HCl pH 8.0 7.5 ml of 2 M NaCl 2 ml of 10% SDS solution 5 ml of 20% NP-40 solution 0.5 g Sodium-Deoxycholate add H_2O ad 100 ml, store at 4°C	50 mM 150 mM 0.2% 1% 0.5 % (w/v)
RIPA harvesting solution	20 µl 0.5 M PMSF Solution, dilute in 10 ml RIPA storage solution, freshly prepared	-
BSA dilution buffer	mix 22 parts of H_2O and 3 parts of RIPA harvesting solution	-
BSA stock solution	20 mg BSA, dissolve in 10 ml H_2O, prepare standard dilution series	2 mg/ml
BSA standards	500 µl BSA stock solution, diluted in 500 µl BSA dilution buffer, preparation of a BSA standard series with 1:2 dilutions	1.0 mg/ml 0.5 mg/ml 0.25 mg/ml 0.125 mg/ml 0.0625 mg/ml 0.03125 mg/ml
BCA working solution	mix 50 parts of BCA reagent A and 1 part of BCA reagent B (provided in the kit), freshly prepared	

Compositions, preparation and storage instructions for solutions and buffers used in RNA isolation are listed in Table 9.

Table 9 – Solutions used in RNA Isolation

Solution/Buffer	Composition and Preparation	C_{final}
NaOH	Dilute 500 µl of 1 M NaOH with 49.5 ml H_2O	10 mM
70% ETOH	Mix 35 ml ETOH abs. with 15 ml Ultrapur4 RNase free H_2O	50 ml

The materials and chemicals used for the metabolome analysis are provided in Table 10.

Table 10 – Materials and chemicals used in metabolomic analysis

Material/ Chemical	Company	Storage	Order Number
Methanol	Honeywell/Fluka	RT	348060-2.5L
2% Formic acid	Honeywell/Fluka	RT	94318-50mL
85% Ortho-phosphoric acid(H3PO4)	Merck	RT	1.00552.0250
Bead Tubes	Machery & Nagel	-	740786.50
LCMS Certified Clear Glass 12 x 32 mm Screw Neck Max Recovery Vial, with Cap and Preslit PTFE/Silicone Septum, 2 mL Volume, 100/pk	Waters	-	600000670CV

2.2 Primary cell material

We obtained Human primary adipose-derived mesenchymal stem cells (hAMSCs) from subcutaneous tissue extracted from patients during a variety of abdominal laparoscopic surgeries (sleeve gastrectomy, fundoplication or appendectomy). This subcutaneous adipose tissue was obtained from beneath the skin at the site of surgical incision. Additionally, human liposuction material was obtained from a collaborating private plastic surgery clinic, Med aesthetic Privat Klinik Hoffmann & Hoffmann in Munich, Germany.

Each participant gave written informed consent before inclusion, and the study protocol was approved by the ethics committee of the Technical University of Munich (Study No. 5716/13; 1946/07, 409/14s).

In the department of Nutritional Medicine at the Technical University Munich (TUM) subcutaneous adipose tissue from severely or morbidly obese patients who have received abdominal laparoscopic surgery is collected and subsequently stored in the Munich Obesity Biobank (MOBB). From these tissue samples, subcutaneous pre-adipocyte cells (PAC) have been isolated and cryopreserved. For this thesis, cellular material from eleven different patients of the MOBB was used who fulfilled the

following criteria: female, overweight, between 18 and 65 years of age (mean BMI 48.41 kg/m²). This is detailed below (see Table 11).

Table 11 – Patient Characteristics

Patient ID	Rs6712203	Age	Height (m)	Weight (kg)	BMI (kg/m^2)	T2D	HbA1C
1	CC	35	1.58	104	41.66	N	5.8
2	CC	34	1.65	161	59.14	Y	6.0
3	CC	59	1.64	135	50.19	N	N/A
4	CC	36	1.62	136	51.82	N	5.6
5	TT	37	1.70	142	49.13	N	N/A
6	CC	45	1.83	130	38.82	Y	5.9
7	TT	52	1.66	155	56.25	N	N/A
8	TT	25	1.65	120	44.08	Y	5.4
9	CC	21	1.73	135	45.11	N	5.5
10	TT	45	1.71	161	55.06	N	5.6
11	TT	44	1.64	111	41.27	N	5.6

Adipose tissue is collected at various clinics in the operating theatre and transported to the Freising laboratory to expand the MOBB. At the Chair for Nutritional Medicine, blood samples and tissue samples are prepared and frozen for later analyses of DNA, ribonucleic acid (RNA) and various histological evaluations, including biopsies of fat, muscle and liver tissue.

The majority of the fat tissue received was processed in the S2 Cell Culture Lab according to an established protocol in order to produce primary preadipocytes. These are cultivated and grown over a period of about two weeks and then preserved at -80°C; to be thawed on ice later and ready to be used for cell culture. In this way an ever-increasing biobank has been developed, and complemented with medical patient data supplied by the surgical clinics of the supporting hospitals.

2.3 Genotyping

For genotyping of the rs6712203 variant at the *COBLL1* locus Roche SimpleProbes were used. Roche SimpleProbes are molecular hybridisation markers that emit fluorescence by binding to complementary DNA. The probe sequence matched the rs6712203 non-risk allele (TT). In a melting curve analysis, where temperature was increased gradually, the probe dissociated at a higher melting temperature (T_M) when it fully matched the complementary sequence (Fig. 8). If a mismatch/SNP was present, the probe dissociated earlier resulting in a decrease of fluorescent signal at lower T_M. Therefore, each variant resulted in a unique melting curve. The melting curve of the homozygous rs6712203 non-risk allele carriers (TT) showed a peak at 58,7°C and the risk allele carriers (CC) showed

a melting temperature at 53.3°C. Heterozygous melting curves showed two peaks at the respective temperatures.

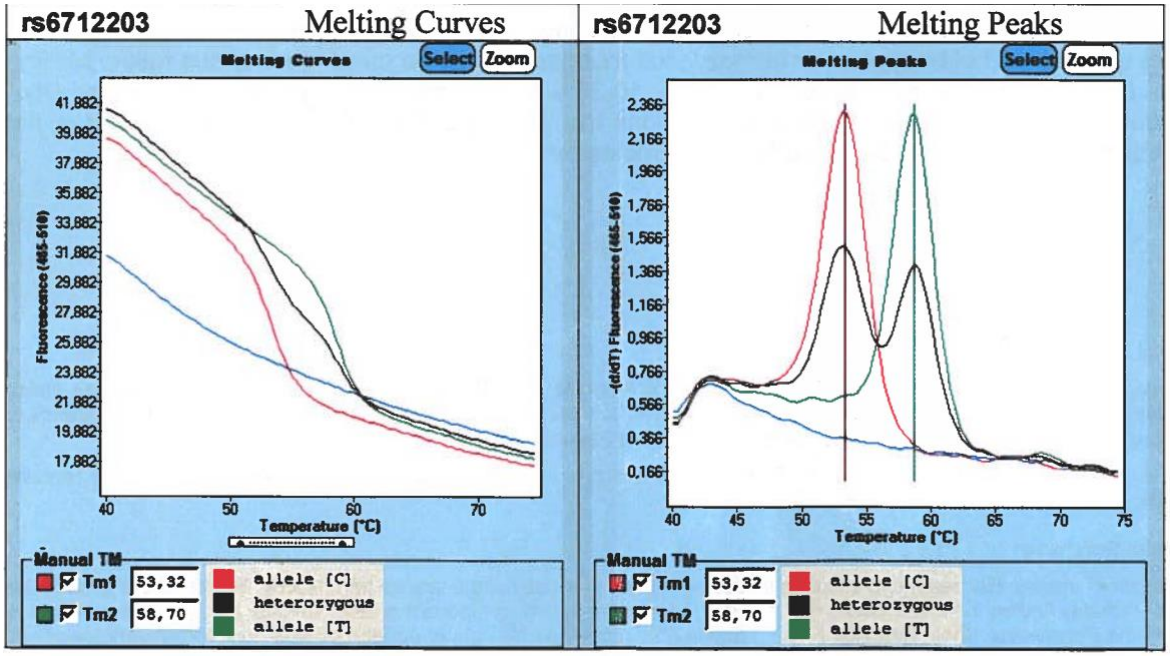

Figure 8 - Melting curves of the rs6712003 variant at the COBBL1 locus.
The probe is designed to match the rs6712003 non-risk allele (TT). Since the sequence completely matches the non-risk allele, the probe dissociates from the template at the highest melting temperature (T_M) of 58,7 °C (green melting curve). For homozygous rs6712003 risk allele (CC) samples, the probe shows mismatches for both non-risk alleles and there is a single peak at the low T_M of 53,3 °C (red melting curve). Since the heterozygous variant has both a non-risk and a risk allele, it shows two peaks with the respective melting temperatures (black melting curve).

For the polymerase-chain-reaction (PCR) reaction a reaction mixture of 10 µl was used composed of the following components: 5 µl PCR grade water, 2 µl 5xMyTAq Reaction Buffer (Bioline, Meridian Bioscience), 0.2 µl MyTAq Polymerase (Bioline, Meridian Bioscience), 0.5 µl Reagent Mix Simple Probe LightSNip rs6712003 COBLL1 (TIB MOLBIOL) and 2 µl of the prepared DNA solution. The analysis was performed in a Roche Lightcycler 480 (Roche) with the following program settings (Table 12).

Table 12 – Program of the rs6712203 genotyping PCR

Parameter	Dena-tura-tion	Cycling			Melting			Cooling
Analysis mode	None	Quantification			Melting Curves			None
Cycles	1	45			1			1
Segment	1	1	2	3	1	2	3	1
Target [°Ĉ]	95	95	60	72	95	40	75	40
Hold [mm:ss]	10:00	00:10	00:10	00:15	00:30	02:00	00:00	00:30
Ramp Rate [°C/s] 384	4.6	4.6	2.4	4.6	4.6	2.0	-	2.0
Ramp Rate [°C/s]96	4.4	4.4	2.2	4.4	4.4	1.5	-	1.5
Acquisition mode	None	None	Single	None	None	None	Continuous	None
Acquisition [per °C]	-	-	-	-	-	-	3	-

2.4 Cell culture

2.4.1 Thawing procedure

Before thawing, proliferation medium with FCS was preheated at 37 °C. One 50 ml tube with 18 ml and one 15 ml tube with one ml prewarmed proliferation medium were prepared under sterile conditions. The cryopreserved vials were thawed in a water bath at 37 °C immediately after removal from the liquid nitrogen tank. Each vial contains $5x10^5$ cells in 1 ml freezing medium. After thawing, the vial was taken under the sterile bench. One ml of the proliferation medium from the prepared 50 ml tube was drawn into a 5 ml serology pipette, and only then was the thawed cell suspension taken up from the cryovial. Finally, one ml of the proliferation medium was carefully drawn up from the 50 ml tube into the pipette without allowing air bubbles to enter the cell layer. The three phases (medium: cell suspension: medium) in the pipette were then carefully transferred into the prepared 50 ml tube. The cryo vial was rinsed with one ml proliferation medium from the 15 ml tube and was then added to the 50 ml tube. The cell suspension was mixed carefully in the 50 ml tube and the total amount of 20 ml was distributed to two T25 Falcon® cell culture flasks. Normally $1.25x10^5$ cells per 10 ml are seeded in a T25 cell culture flask for maintenance. For thawing, twice this amount is used to compensate for the expected loss of cells during this process. The proliferation medium was completely replaced after 24 h to remove dead cells and residual DMSO.

2.4.2 Splitting procedure and cultivation

After thawing, the PACs were grown in T25 cell culture flasks and the proliferation medium with FCS was changed twice a week (Fig. 9). When the cells had reached 95 % confluence, they were split onto

6-well plates (Fig. 9). For this purpose, the medium was discarded, and the cells were washed twice with 10 ml prewarmed PBS. For detachment, cells were incubated with one ml trypsin/EDTA for about 10 min which was confirmed by visual control under the microscope. After the proteolytic activity of trypsin was stopped by adding nine ml of pre-warmed proliferation medium, the cell suspension was transferred to a 50 ml tube. The cell suspension was mixed carefully and an aliquot of 50 µl was collected. After mixing the aliquot with 50 µl trypan blue solution, cells were counted in a Neubauer chamber. The number of cells per ml was determined as follows: cells/ml = $X/8*2*1x10^4$ where X represents the number of cells counted in eight large squares of the Neubauer chamber. The required volume of cell suspension for seeding the cells at a density of $2.5x10^5$ per 6-well plate was calculated as follows: required number of cells divided by the calculated cells/ml. Seven six-well plates were required per patient to perform the experiment.

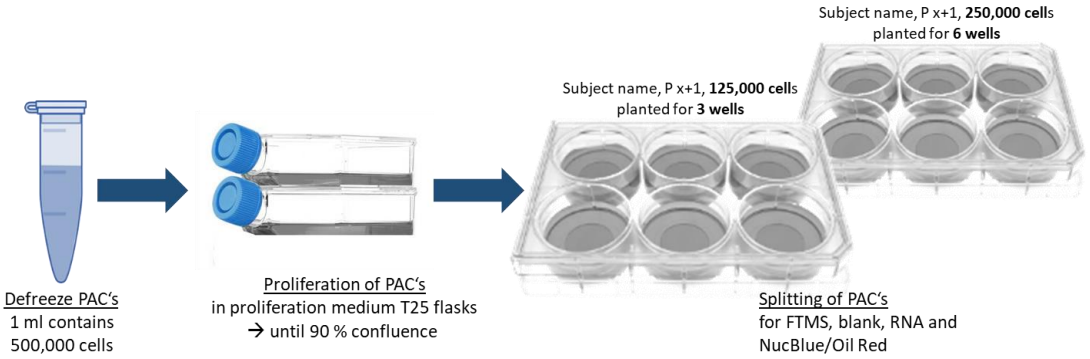

Figure 9 - Workflow of thawing and splitting of Cells.

2.4.3 Adipogenic differentiation

Once the PACs in the 6-well plates reached 90-95 % confluence, adipogenic differentiation was induced. For this purpose, the proliferation medium was replaced by two ml freshly prepared induction medium per well. The induction day was defined as day 0 (d0). Three days after the induction of differentiation (d3), the medium was replaced completely by the required differentiation medium. The differentiating cells were cultured for a total of 14 days (d14), changing the differentiation medium twice a week.

2.4.4 Harvesting procedure

Three harvest time points were selected for subsequent analyses: Three days before induction of differentiation (d0-3), when cells had reached 60 to 70 % confluence, three days (d3) and 14 days (d14) after induction of differentiation.

For time point d0-3, the PACs were prepared 24 hours before collection. The proliferation medium with FCS was removed and the cells were washed twice with two ml proliferation medium without FCS. Finally, one ml of fresh proliferation medium without FCS was added per well. Cells of six wells were harvested and pooled for metabolomic analysis (Fig. 10). Another six wells were harvested and joined as blank controls for metabolomic analysis (Fig. 10). PACs of three wells were combined and harvested for RNA isolation and two wells were combined for protein extraction (Fig. 10). One well was used for NucBlue staining.

For time point d3, 24 hours before sample collection the differentiating PACs were prepared. Therefore, therefore the induction medium was removed and replaced by one ml fresh of induction medium per well. Cells of three wells were harvested and pooled for metabolomic analysis as well as blank controls (Fig. 10). The cell material of two wells were harvested and combined for RNA isolation (Fig. 10) and one well was harvested for protein extraction. From the three remaining wells, the best-looking cells were used for NucBlue staining.

For time point d14, the differentiated adipocytes were prepared 24 hours before harvesting. For this, the differentiation medium was removed and replaced by one ml of fresh differentiation medium per well. For metabolomic analysis, three wells were harvested and pooled as samples as well as three wells as blank controls. Two wells were harvested and joined for RNA isolation, and one well was harvested for protein extraction. From the three remaining wells, the best-looking cells were used for NucBlue and Oil Red O staining.

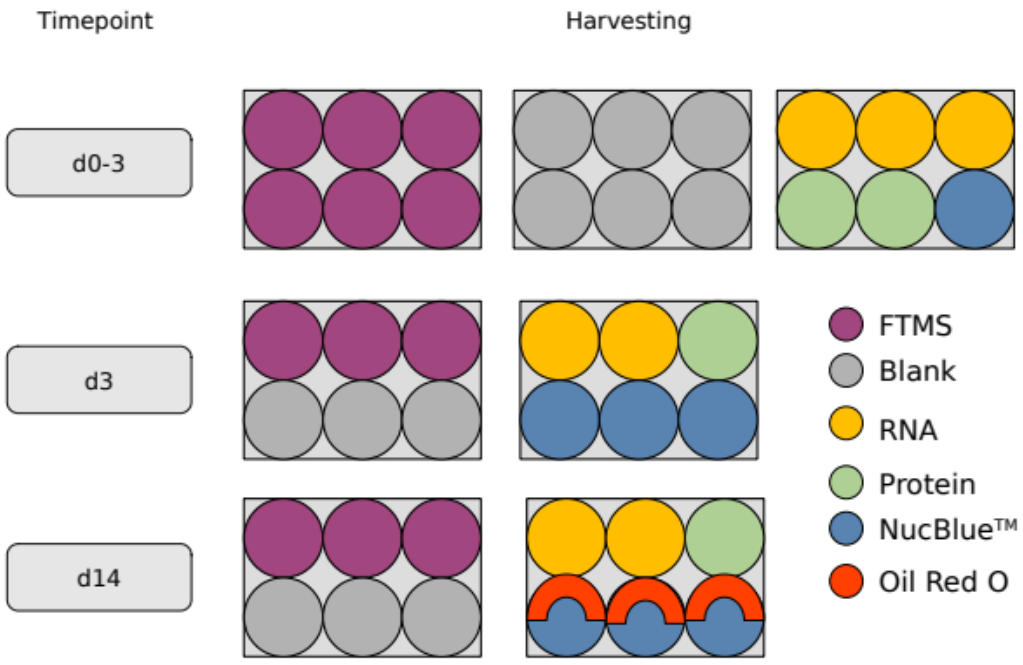

Figure 10 - Overview of cell harvesting for the different subsequent experiments

To isolate RNA, the medium was removed and the cells were washed twice with ice-cold PBS. The cells of the indicated amount of wells (Fig. 10), were resuspended in 350 µl Trizol solution and transferred into a 2.0 ml Eppendorf® DNA LoBind reaction tube. The harvested material was stored on dry ice until the end of the harvest day and then frozen at -80 °C.

To harvest the cells for metabolomic analysis, the medium was removed and the cells and blank controls were washed twice with 2.0 ml MilliQ H2O (4°C). Subsequently, cells from the indicated wells (Fig. 10) were scraped with 500 µl ice-cold (-20°) methanol (MeOH) harvesting solution and transferred to a 2.0 ml Eppendorf® Protein LoBind tube. The harvested material was stored on dry ice until the end of the harvest day and then frozen at -80 °C.

For protein extraction, all steps are performed on ice after removing the cells from the incubator. First, the medium was aspirated and the cells were washed twice with 5 ml cold (4 °C) PBS per well. Then 250 µl Radioimmunoprecipitation assay (RIPA) harvesting solution was added to each of the indicated wells of a 6-well plate and the cells were scraped off with a cell scraper. The cell suspension was transferred into a 1.5 ml reaction tube and was stored at -80 °C.

NucBlue staining was performed as described in chapter 2.5.

For Oil Red O staining, the medium was removed and the cells were washed twice with cold PBS. To fix the cells, 2 ml of Histofix solution was added to the well and incubated for 20 min (d0-3, d3) or 1 h (d14) at room temperature (RT). The Histofix solution was then removed and the Oil Red O staining was performed as described in chapter 2.6.

2.5 NucBlue staining

NucBlue™ staining was performed to determine cell counts. Therefore, 200 µl NucBlue™ Live ReadyProbes Reagent was added per well and incubated for 20 min. The medium was then changed and panoramic brightfield images of five specified areas of the selected well were taken using a KEYENCE© fluorescence microscope (Fig. 11). To determine the number of nuclei, the five images per well were analysed using CellProfiler™ software. To calculate the total number of nuclei per well, the total number of nuclei in the five images was divided by five and then multiplied by a factor of 61,505. Using the sets of five images respectively for each time point, the average number of nuclei per image was calculated, and then extrapolated by the factor 61.505 to obtain the total number of nuclei per well.

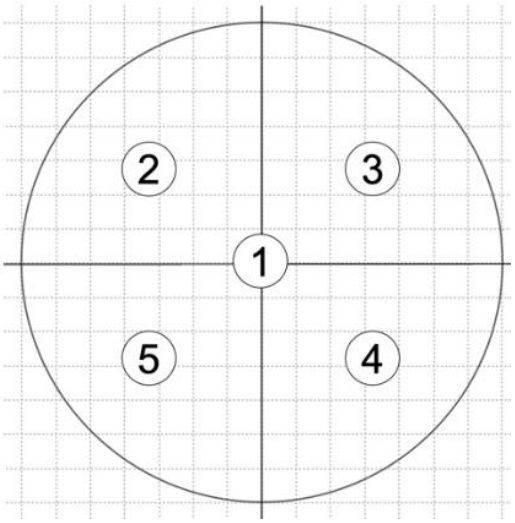

Figure 11 - Defined well regions for imaging of NucBlue™ staining.

Panoramic images were taken of five specified regions, from which the number of nuclei was determined to extrapolate the total number of cells per well.

2.6 Oil Red O lipid staining

After cell fixation, 2 ml of Oil Red O staining solution was added to the relevant well and incubated for one hour. Afterwards, the Oil Red O staining solution was removed, and the cells were washed twice with 2 ml of PBS. Finally, 2 ml of PBS and additional 4 drops of NucBlue™ were added. The plate was wrapped with aluminium foil and incubated for 20 min at RT in the dark. Using a KEYENCE© microscope, images were taken in reflected light and UV light, as well as UV 5x5 stitch images (300x magnification, REC format 1600 x 1200 pixels) with scale bars of 100 µm. The plate was then wrapped in Parafilm, covered and stored in the fridge at 4°C for later analysis. To preserve the effect of light-sensitive NucBlue™, the plate was wrapped in opaque cover.

For quantification of Oil Red O, PBS was removed from the wells and the cells were air dried for 10 minutes. Subsequently, the cells were resuspended with 800 µl isopropanol per well and incubated for 10 to 20 minutes at (RT) in a shaker until the staining had completely resolved. Three aliquots of 75 µl per well were transferred to a 96-well Brand® flat-bottomed plate and the absorbance of the dissolved dye was measured at A = 492 nm using a TECAN™ plate reader. A flash setting of 5 and a settle time of 100 ms were used for the measurement. To determine the intensity per $1x10^5$ cells, the determined optical density (OD) at 492 nm was divided by the number of cells.

2.7 Protein extraction and quantification

The samples were thawed on ice and homogenised three times on ice using an insulin syringe. After centrifugation at 10,000 g/rcf for 1 min at 4°C, the supernatant was then transferred without its upper fat layer to a new 1.5 ml reaction tube.

The Bicinchoninic acid (BCA) assay was used to quantify the protein extracts. The BCA working solution was prepared as indicated in Table 8. If any crystallisation is visible, the BCA working solution can be incubated for 5 min at 37°C and mixed by vortexing. 25 µl of the BSA standards and blank control were pipetted as duplicates per well into a 96-well plate. Per sample, 3 µl of the protein extract was diluted in 22 µl H2O directly in one well of the 96-well plate. The samples were also prepared as duplicates. Then 200 µl of BCA working solution was added per well using a multiple pipette. The plate was covered with sealing foil and placed on the shaker for 30 s for mixing. Subsequently, the plate was incubated for a maximum of 30 min at 37 °C in the dark. Finally, the plate was cooled down to RT for 5 min and the absorbance at A = 562 nm was measured with a TECAN™ 96-well plate reader. A flash setting of 5 and a settle time of 100 ms were used for the measurement.

2.8 Gene expression analysis

In order to determine the expression of the fat metabolism and obesity marker genes, messenger RNA (mRNA) expression levels of *PPARG*, *LEP*, *IRS2*, *PI3KCA*, *PLIN1*, *ITGAM* were examined by RT-PCR. For this purpose, first the total mRNA was isolated from the cells, which was then transcribed into complementary DNA (cDNA) using reverse transcription. The cDNA was then used for the qRT-PCR analysis.

2.8.1 RNA isolation and quantification

RNA was isolated using an in house established method. Before starting the extraction, the centrifuge was cooled down to 4°C and ultra-pure RNase-free H_2O was pre-warmed to 37°C. After the fume hood and RNA pipettes were cleaned with RNAse ZAP, the samples were removed from storage at -80°C and thawed for 5 min on ice. Then 70 µl of chloroform was added to the reaction tubes containing resuspended cells in 350 µl of Trizol reagent and everything was thoroughly mixed by vortexing. After incubation on ice for 10 minutes, samples were centrifuged at 14,000 g/rcf for 10 minutes at 4 °C. In the meantime, new 1.5 ml reaction tubes were prepared, each containing 175 µl isopropanol. After centrifugation, the aqueous phase containing the RNA was carefully pipetted into the prepared reaction tubes. All reaction tubes are carefully inverted until all smears have vanished. The mixture is incubated on ice for 10 minutes and the samples are then centrifuged again at 14,000 g/rcf at 4 °C for 10 minutes. Following centrifugation, the RNA is in the gel-like pellet. The supernatant was carefully removed, and the pellet was washed with 1 ml of 70% ethanol. Samples were again centrifuged at 14,000 g/rcf for 10 minutes at 4°C. The washing procedure was repeated once, the remaining ethanol was removed, and the reaction tubes were placed upside down on a paper towel for min. To allow the

remaining ethanol to evaporate, the reaction tubes were placed with open lids on ice under a fume hood for 5 min. Then the RNA pellets were resuspended in 30 µl high purity RNase-free H_20.

RNA concentration and sample purity were determined photometrically using a Tecan® photometer. For this purpose, 2 µl of each sample was added to a 0.2 ml strip and the optical density was measured at 260 nm. The OD value of OD260 was set to an RNA concentration of 40 ng/µL. The purity of the RNA was determined by the ratio between the A260 and A280 values, for pure RNA the ratio should be about 2.

Furthermore, RNA quality of five randomly selected RNA samples was determined via Bioanalyzer. Total RNA was measured with the Agilent RNA 6000 Nano Kit on an Agilent Technologies 2100 Bioanalyzer, and high-quality RNA was determined by a RIN score > 7.

2.8.2 cDNA synthesis

The extracted RNA was transcribed into cDNA using the High-Capacity cDNA Reverse Transcription Kit following the Applied Biosystems™ protocol. For cDNA synthesis, 500 ng RNA were used in a volume of 10 µl. The master mix for reverse transcription was prepared from the corresponding solutions of the kit and 10 µl were added to each RNA sample (Table 13).

Table 13 – Preparation of master mix according to High-Capacity cDNA Reverse Transcription Kit.

High capacity cDNA RT Kit	Volume per sample
10 x RT Reaction Buffer	2 µl
RNase-Free water	4.2 µl
25 x dNTP Mix (100 mM)	0.8 µl
10 x RT Random Primer	2 µl
Multi-Rev. Transcriptase	1 µl
Total	10 µl

For pipetting mRNA samples, master mix and water in 200 µl strips, a Hamilton© Microlab VANTAGE pipetting robot was used. An Eppendorf® Mastercycler® was used for the synthesis reaction. For this, the samples were first incubated for 10 min at 25 °C, followed by 2 h at 37 °C, and finally 5 min at 85 °C. The negative control for the procedure was pure water in PCR quality. The cDNA samples were stored at -20 °C.

2.8.3 Quantitative real-time PCR (qRT-PCR)

Quantitative real-time PCR (qRT-PCR) was used to quantify relative changes in gene expression during adipogenesis in in carriers of the rs6712203-C risk allele and carriers of the rs6712203-T non-risk allele. The primers used for the qRT-PCR were synthesised by Sigma/Merck©. Primer sequences of fat

metabolism and obesity marker genes as well as of the housekeeping genes glyceraldehyde-3-phosphate dehydrogenase (*GAPDH*) and importin 8 (*IPO8*) are listed in Table 14. An initial primer test run, using a small subset of representative samples, PCR-grade water as negative control and PAC d14 (PPARG2, LEP and PLIN1) and PAC d0 (IRS2, PI3KCA and ITGAM) as positive controls, ensured that all selected primers were working and operating at an annealing temperature of 60°C.

Table 14 – Primer sequences used for qRT-PCR

Target gene	Primer orientation	Primer Sequence
PPARG2	forward	GAA AGC GAT TCC TTC ACT GAT
	reverse	TCA AAG GAG TGG GAG TGG TC
LEP	forward	TTT GGC CCT ATC TTT TCT ATG TCC
	reverse	TGG AGG AGA CTG ACT GCG TG
IRS2	forward	CCTGCCCCCTGCCAACACCT
	reverse	TGTGACATCCTGGTGATAAAGCC
PI3KCA	forward	AGAGCCCCGAGCGTTTC
	reverse	TCACCTGATGATGGTCGTGG
PLIN1	forward	GCGGAATTTGCTGCCAACACTC
	reverse	AGACTTCTGGGCTTGCTGGTGT
ITGAM	forward	GGAACGCCATTGTCTGCTTTCG
	reverse	ATGCTGAGGTCATCCTGGCAGA
GAPDH	forward	GAT CAT CAG CAA TGC CTC CTG C
	reverse	ACA GTC TTC TGG GTG GCA GTG A
IPO8	forward	CGGATTATAGTCTCTGACCATGTG
	reverse	TGTGTCACCATGTTCTTCAGG

All qRT-PCRs were performed as SYBR Green® assays. To prepare the respective master mix, the Maxima™ SYBR™ Green/ROX qPCR Master Mix (2X) (Thermo Scientific™) was used (Table 15).

Table 15 – Composition of the qRT-PCR Master Mix

Component	Volume per sample
Maxima SYBR Green/ROX qPCR Master Mix (2X)	5 µl
Primer forward (10 µM)	0.3 µl
Primer reverse (10 µM)	0.3 µl
Ultrapure RNase free water	2.4 µl
Total	8 µl

Dilutions of the synthesised cDNA samples were prepared with PCR-grade water to obtain a concentration of 5 ng/µl. 8 µl of the respective master mix and 2 µl of cDNA sample (10 ng) were pipetted into a well of a 384-well plate (4titude®). A Hamilton© Microlab VANTAGE pipetting robot was used for pipetting. After pipetting, the 384-well plate was sealed and centrifuged at 1500 rpm for

30 s at RT. Assays were run in a LightCycler®480 (Roche©) by using the Roche© LightCycler® software. The programme used for the qRT-PCRs is shown in Table 16.

Table 16 – Program of the qRT-PCR assay

Para-meter	Pre-treatment	De-natura-tion	Cycling			Melting			
Analysis mode	None	None	Quantification			Melting Curves			
Cycles	1	1	40			1			
Seg-ment	1	1	1	2	3	1	2	3	4
Target [°Ĉ]	50	95	95	60	72	95	60	95	95
Hold [mm:ss]	02:00	10:00	00:15	00:30	00:30	00:10	00:01	-	00:20
Ramp Rate [°C/s]	4.8	1.0	4.8	2.5	4.8	1.0	2.5	0.29	4.8
Acqui-sition mode	None	None	None	None	Single	None	None	Continuous	None
Acqui-sition [per °C]	-	-	-	-	-	-	-	2	-

Gene expression was calculated using the ΔΔCt method. In this calculation, the Cycle threshold (Ct) value of a reference gene for instance an housekeeping gene or a non-regulated gene was subtracted from the value of the target gene (ΔCt). *GAPDH* and *IPO8* were used as housekeeping genes in this thesis. The mean of the calculated ΔCts of the rs6712203-T non-risk allele pre-adipocytes (*PPARG2*; *IRS2*; *PIK3CA*, *ITGAM*) or *in vitro* differentiating pre-adipocytes (*LEP*; *PLIN1*) was subtracted from the respective Δct of the sample (ΔΔCt). The **ΔΔ**Ct value was then log-transformed ($2^{-\Delta\Delta Ct}$) to represent the induction for the gene in interest.

2.9 Metabolomic analysis

Sample collection and storage are critical for metabolomic analysis and standardised protocols are required to avoid contamination or interference with instruments that may lead to metabolite variability or degradation. Long-term stable and robust results when using a non-targeted metabolome platform require important control points ranging from sampling to data analysis. The following section presents and discusses the crucial points in the workflow that ensure reliable results when analysing PACs and cell media.

2.9.1 Cell collection and preparation

Standardized collection methods are essential in order to allow comparison of different samples collected from different laboratories, for preserving quality, for reproducibility and stability in the long term. They have been defined by the International Standards Organization (ISO) with the aim to ensure the capacity of a sample to preserve its properties over a period of time, based on the observation of defined compounds (such compounds assumed as reference to help assess the variability of a sample) when the sample is stored under specified conditions (ISO Guide 30, 1992).

Metabolomics analysis of cultured cells has emerged as an important technology for studying cellular biochemistry, thereby providing a snapshot of ongoing cellular metabolic pathways. The major bottlenecks associated with cell sample preparation metabolomics are efficient sampling, quenching and metabolites extraction in order to preserve the internal metabolite signatures (Kapoore et al. 2017).

Metabolomics analyses have been performed on a broad range of adherent cell numbers, ranging from 1×10^4 up to 4×10^7 cells (Lorenz et al, 2011). Depending on the cells and the technology used to process the cell extraction, the seeding number must be optimized in order to get sufficient signals in MS, to be able to detect small metabolites that are present at low concentration but that still may be important for biological processes, especially when global metabolomics is performed.

Cell density and growth conditions have significant effects on metabolism. For best comparison, all replicate cell cultures need to be grown under identical conditions (i.e. seeding of the same number of cells/mL in the same quantity of medium for the same number of days before performing sample preparation. For rigorous biological replicates, a different passage of cells needs to be used for each replicate.

Due to the nature of mass spectrometry, for accurate results, data must not be normalized post hoc. Therefore, an identical biomass for all samples (e.g. by cell count) is required and any necessary adjustments need to be made already during sample preparation by appropriate dilution (Glasgow Polynomics, 2013).

Independently of any experimental context, the aim of sample preparation is always to extract a compound of interest (the analyte) from the sample or matrix it is embedded in. Any procedures are required to be reproducible, and any remaining analytes should be unaltered by the sample preparation and reflect their quantity in the original sample.

First requirement for sample preparation procedures in biochemical studies is that they must be non-destructive. In performing a metabolomics study, it is necessary to take the composition of the sample

matrix used into account. Independent of the ionization technique used later in the workflow, these compounds may carry a variety of ionizable functionalities or, e.g. in the case of metals, may feature various oxidation states. They are very potent competitors for ionization as they scavenge energy and therefore reduce the energy available for the metabolites of interest. Multiply charged compounds may also complicate mass spectrometry and formula annotation. In instruments with lower resolution their peaks may overlay metabolite peaks and thus interfere with detection. Therefore, sample preparation in metabolomics must aim to remove proteins, polymers, salts and metals, while preserving the relative and, if feasible, absolute concentration of metabolites. The most common techniques for these purposes are solid phase extraction (SPE) and protein precipitation extraction (PPE) (Bruce et al. 2009, Polson et al. 2003).

During the PPE process not only proteins, but salts as well precipitate. They are not effectively separated from the liquid phase by centrifugation and are retained in the supernatant. As a consequence, SPE is the method to be preferred when performing ICR-FT/MS metabolomics.

Typically, SPE is performed using funnel shaped cartridges which are filled with sorbent material. Fluids and aqueous samples are inoculated into the wider, upper end of the cartridge. The respective fluid rests upon the pressed sorbent bed until a force is applied. This can either be performed by application of pressure through the upper end of the cartridge or by creating an underpressure at the lower end of it. The first procedure is faster but possibly more destructive, since pressures up to several bars may occur. The second method is slower and more material-friendly since, given a perfect vacuum, the maximal pressure difference is one bar. SPE procedures based on reversed phase silica sorbents commonly follow these steps:

1) Washing of the cartridge by flushing sorbent material with MeOH

2) Equilibration/activation of the sorbent by flushing with water or water with acidic or basic additives

3) Application/loading of the sample to be prepared

4) Washing off salts and (hopefully) proteins again using the water mixture of step 2)

5) Eluting the analytes using MeOH or any other preferably apolar solvent

According to our experience, these steps alone effectively remove salts and to some extent proteins as well. The reason for contemproary protein removal may be that small metabolites associate with the sorbent more rapidly than proteins do, therefore inhibiting protein-sorbent interactions. (Bruce S.J. et al, 2009). Preparation is a crucial step especially in non-targeted metabolomics studies, and an incisive sample pre-treatment is fundamental. The factors to be considered in choosing the most

reliable method are the number of extracted features, the effectiveness of protein removal and repeatability. In non-targeted metabolomics the principal aim is to extract the widest number of metabolites, and therefore to remove compounds that could interfere with the mass spectrometer (e.g. salts) or with the chromatographic system. A suitable sample preparation is characterized by a minimal number of steps, in order to avoid the degradation of thermo-labile compounds and to minimize contaminations and inter-laboratory errors as well. Additionally, the ideal sample preparation requires the lowest volume of cell and media possible and needs to consider a possible integration with other analytic platforms, enabling a high throughput of sample analyses.

The samples used for this study in hand belong to the Munich Obesity Biobank, which is part of the German Obesity Biobank. The adipocyte samples are preserved at -80C and ready to be used after thawing on ice for cell culture: cultivation, proliferation and splitting (see chapter 2.2). After preparation, the samples were stored at -80° C until sample analysis.

Nevertheless, there are strong concerns about the quality of the samples after such a long time at RT. Based on our experience, already after 8-10 hours at RT fundamental changes can be observed, especially for untreated samples where enzymes are still present. Significant changes in the blood plasma metabolome were detected when blood was exposed to RT for 2, 4, 8 and 24h. (Peiyuan, Yin et al.). Therefore, the samples were stored in -80° C until analysis.

Prior to sending any biological samples for analysis to Helmholtz, it is mandatory to ensure that these samples have tested negative for HIV, HBV, HCV, and SARS-CoV-2 (COVID-19), especially if the samples were collected since January 2020. (For details on the declaration applied see Helmholtz Center Declaration)

2.9.1.1 Pre-Preparation of PAC samples

Before commencing sample preparation, it is crucial to number the samples according to ZipTip Protocol C18 and coding template and to compile a list of samples with acronyms for labelling of corresponding Eppis/vials.

Additionally, ensuring the correct order according to the measurement protocol is essential, initially handling blanks before moving on to actual samples, beginning with day 0-3, then day 3, and finally day 14, while increasing cell numbers per day.

To prepare, a dispenser for LC-MS quality MeOH and water is required as well as clean Eppis, 96-well plates (0.5 mL and 2 mL), reservoirs, and vials with MeOH. Blanks are prepared in advance by filling 2/3 of the vials with MeOH and sealing them with caps.

See below for excerpt from protocol for pre-preparation of PAC samples:

Cleaning and labelling instructions:

Cleaning Instructions:
*Water Bottle (Before Use)**:***
- Clean in the following order:
  1. Three rounds of water
  2. One round of MeOH
  3. Three more rounds of water

*Methanol Bottle (*Before *Use):*
- Clean in the following order:
  1. Three rounds of water
  2. Three rounds of MeOH

96-Well Plate Cleaning:
- For pretreatment and washing, use three rounds of MeOH.
- For elution, use three rounds of MeOH.

Vials Cleaning:
- Clean vials with three rounds of Methanol.
- Use "max recovery vials" or "conical vials."
- Label the vials at both the top and bottom.
- Close them with new magnet FTMS caps.

Labeling for FT Measurements:
- Label vials, Eppis, and cryos with beads with sequential numbers on the bottom. Use 1, 2, 3, and so on for clear identification.

2.9.1.2 Sample (Cell and Media) Preparation of PAC samples

See below for excerpt from protocol for media preparation:

Plate/Reservoir Preparation:
Clean 96 well plates with 3 rounds of MeOH.p
- 1 loading [0.5 mL]
- 3 washings [2 mL]
- 1 elution [0.5 mL]

Clean the reservoirs with 3 rounds of MeOH.
- 1 pretreatment (H3 PO4 2%)
- 1 conditioning (MeOH)
- 1 equilibration (FA 2%)

As the focus of this study is analysis of cells, it will not go into further details regarding media here.

See below for excerpt from protocol for cell sample processing:

1. Sample Warming and Mixing:
- Warm the samples (approximately 1 mL) for about 2 hours.
- Vortex mix the samples for 2 seconds in between to expedite the process.

2. Pre-Treatment:
- Prepare a pre-treatment mixture by combining 50 µL of media with 50 µL of H3 PO4 2%. Ensure this step is performed on ice.

- Distribute the pre-treatment mixture into a 96-well plate.
- Subsequently, pipette 50 µL of H3 PO4 2% from the reservoir into the loading plate (0.5 mL) (Step 1.1).
- Manually add 50 µL of the original media sample to the acid (Step 1.2).
- Mix the contents using the robot after all samples are in the plate.

3. Conditioning:
- Conduct conditioning using MeOH for ten rounds from the reservoir.
- Use a special tip from the green tip box C18.
- Insert the Eppendorf Robot 300 µL Tips Holder into the ZipTip Tips for this process.

4. Equilibration:
- Perform equilibration with FA 2% for ten rounds in a 96 well plate (2 mL).

5. Sample Loading:
- Load the samples 50 times into a 0.5 mL 96 well plate.

6. Washing (FA 2%):
- Wash each well with FA 2% (500 µL per well), repeating this process three times (3 x 10).
- Dispense FA 2% from the reservoir into the 96 well washing plates, initially with 300 µL, followed by 200 µL, as the largest tips available are 300 µL.

7. Elution (MeOH):
- Elute with MeOH by pipetting 100 µL into each well, repeating this process 30 times for a 1:2 dilution.
- Carefully cover the elution plate with a lid.

8. Elution Transfer:
- Transfer the eluted samples from the 96-well elution plate (0.5 mL) into 0.5-mL Eppis on dry ice. Note that the elution process itself cannot be executed on dry ice with the robot.

9. Prepare Dilutions (on Dry Ice):
- When the samples are prepared in Eppis, conduct dilutions on dry ice.
- For samples prepared in vials, dilutions should be performed on ice.
- Ensure that the mother solutions (media eluates) stored at -80°C are kept on dry ice during this process.

Dilution Ratio: 1:20
- Prepare the dilutions by following these steps:
  - Add 300 µL of MeOH.
  - Subtract 30 µL of MeOH.
  - Add 30 µL of the elution sample.
  - Wet the first tip and then discard the MeOH amount.
  - Wet the second tip and pipette the sample.
  - Vortex the dilutions for thorough mixing.

Transfer Dilution Samples:
- Utilize clean Eppis for transferring and storing the dilution samples.
- Label the Eppis with sequential numbers at the bottom (e.g., 1, 2, 3).
- Arrange the order for measurements, starting from low-concentration to high-concentration samples.
- Fill 250 µL of the dilutions from the Eppis or well plate into vials, and securely close them with new magnet caps (labelled as "screw magn").
- Label each vial with numbers according to Sara Forcisis Protocol re. number coding.
- Place the vials (both samples and blanks) in a Styrofoam box filled with ice, and store it in the FTMS room for measuring the samples

- Keep the eluates and dilutions in a freezer at -20°C for a maximum of one day.

Important Notes on Workflow Setup

- Ensure that workflow on the bench is well-organized, with all necessary containers, tubs, and plates readily available. Place tissues underneath to maintain a clean workspace.
- Prior to loading the sample onto the cartridge, the sample is to be pre-treated with 2% acid buffer (2% H3PO4) at the dilution ratio of 1/1. This step is necessary in order to disrupt protein binding. Load, wash and elute fractions were collected in order to assess the information relative to each fraction.
- Work on dry ice for points 7 and 8 if prepared in Eppis.
- For dilutions done in vials, vortex mixing is only necessary once, right after preparing the dilution.
- Labelling of reservoirs and 96-well plates is not required.

2.9.2 DI-FT-ICR/MS Analysis

In order to analyse the metabolites involved in the two differentiation phases in the rs6712203 risk versus non-risk individuals, an untargeted metabolomic analysis was performed using DI-FT-ICR/MS. This part of the experiments was performed at the Helmholtz Zentrum Munich.

2.9.2.1 Sample measurements

Detailed description of DI-FT-ICR-MS measurements:

The extracts underwent thorough analysis in positive electrospray ionization mode (ESI) through direct infusion Fourier transform ion cyclotron resonance mass spectrometry (DI-FT-ICR MS). This analysis was conducted using a state-of-the-art Bruker SolariX instrument, equipped with a powerful 12-Tesla magnet and an Apollo II ESI source, all provided by Bruker Daltonik GmbH in Bremen, Germany.

To ensure the accuracy and precision of the instrument, it was externally calibrated using clusters of arginine (1 mg/mL in methanol/water with an 80/20 ratio). The calibration process resulted in impressively low calibration errors, all measuring below 0.1 parts per million (ppm).

During the analysis, the injection flow rate was set at precisely 120 µL/h, ensuring a consistent and controlled sample introduction. For each spectrum, a total of 300 scans were meticulously acquired and subsequently averaged. These scans covered a specific mass-to-charge (m/z) range, ranging from 147.4 to 1000.0 m/z, and were captured with a time domain of 4 mega words (MWs).

To further optimize the instrument's performance, the capillary voltage was adjusted to 3800 V, and the spray shield voltage was set to -500 V. An ion accumulation time of 200 ms was established, and the time of flight to the detector was calibrated to 1 ms. The nebulizer gas flow rate was maintained at

1 bar, while the drying gas flow rate was carefully controlled at 4 L/min, with the drying gas being heated to a temperature of 250 °C.

This highly sophisticated and precisely controlled DI-FT-ICR-MS method ensured that the mass spectrometry analysis of the extracts was conducted with the utmost accuracy and reliability, providing invaluable insights into the composition and characteristics of the analyzed samples.

2.9.2.2 Data preprocessing and matrix generation

Data preprocessing

The acquired spectra underwent a meticulous data preprocessing phase, employing the robust Data Analysis 4.4 software provided by Bruker Daltonik, GmbH in Bremen, Germany. A peak-picking algorithm was meticulously executed, applying a signal-to-noise ratio (S/N) threshold of 4 and a minimum intensity threshold set at 1.5 × 10^6 counts. These settings ensured that only robust and reliable peaks were considered for further analysis.

Following the peak-picking process, all the spectra were diligently exported as tab-separated ASCII (asc) files. Subsequently, these files were imported into the Kernel Calibrator (Smirnov K.S., et al, 2019), a specialized tool for further data manipulation and calibration.

In the generated data matrix, m/z (mass-to-charge ratio) features that were present in less than 10% of all samples were thoughtfully excluded. This filtering step aimed to retain only the most prevalent and informative features for subsequent analysis.

For molecular formula assignment, a well-established mass difference network approach Tziotis D., et al, 2011) was thoughtfully applied. This sophisticated method allowed for the accurate determination of molecular formulas, contributing to a deeper understanding of the compounds within the analyzed samples.

Matrix Generation:

The peak alignment and generation of data matrices for both cell lysates and media samples were conducted with the aid of a meticulously designed, in-house-written matrix generator algorithm. This algorithm was thoughtfully configured to align peaks within an impressively tight 1-ppm error window, ensuring the accurate alignment of mass peaks across all spectra.

The resulting data matrices served as the foundation for subsequent statistical and computational analyses. This step was crucial in organizing and structuring the data for meaningful interpretation, allowing researchers to draw valuable insights from the mass spectrometry data collected during the study.

2.9.2.3 Over-representation analysis (ORA)

In the context of this study, a detailed analysis was conducted using a process known as Over-Representation Analysis (ORA). This analysis aimed to shed light on the molecular composition of the spectra generated from the cell extracts and to uncover any significant associations with known metabolites and cellular processes. The method involved the following steps:

1) Molecular Formulae Assignment: Initially, the spectra generated from the cell extracts were carefully examined, and molecular formulae were confidently assigned using a specialized method called Mass Difference Network (MDiN) approach (Tziotis et al., 2011). This step involved identifying the molecular formulas that corresponded to the various compounds present in the samples.
2) Matching with HMDB: To further advance the analysis and gain insights into the identity of these compounds, the identified molecular formulae were compared and aligned with the Human Metabolome Database (HMDB) (Wishart, D.S., et al. 2018). The HMDB is a comprehensive resource that contains information about a wide range of metabolites found in humans.
3) Over-representation Analysis (ORA): With the known metabolites identified through HMDB alignment, over-representation analysis (ORA) was performed in the next step. This analysis was performed using the Reactome database (Gillespie M., et. al., 2022). The Reactome database is a valuable resource for understanding biological pathways and processes.

In essence, the ORA process aimed to uncover any significant associations between the compound classes identified and specific biological pathways or cellular processes. By cross-referencing the molecular formulae with known metabolites and applying ORA through the Reactome database, the study sought to provide deeper insights into the metabolic and molecular aspects of the cell extracts, potentially revealing valuable information about the underlying biological mechanisms and pathways at play in the samples under investigation.

2.9.2.4 Mass difference enrichment analysis (MDEA)

Mass Difference Enrichment Analysis (MDEA) is a powerful analytical approach that serves to examine the mass differences observed in mass-to-charge (m/z) signals acquired during mass spectrometry.

This technique allows researchers to monitor biochemical reactions and gain insights into the activity of enzymes. The method involves the following steps:

1) Objective of MDEA: The primary goal of MDEA (Moritz, F. et al., 2017), is to assess whether statistically significant m/z peaks (mass-to-charge ratios of ions) tend to be associated with specific mass differences. These mass differences are indicative of various chemical reactions occurring within the sample. In essence, MDEA is a method for screening and deciphering the building blocks that constitute a metabolome, i.e., the complete set of metabolites present in a biological system.
2) Selection of Mass Differences: One of the crucial steps in MDEA is the selection of such mass differences that allow researchers to draw conclusions or hypotheses about specific biochemical processes. These mass differences may represent the transformations or conversions of metabolites through the activity of enzymes. Enzymes interact with small molecules (metabolites) and directly convert them. Alternatively, proteins interact with their specific ligands, either triggering or inhibiting particular enzymatic activities.
3) Database Comparison: To establish connections between enzymes and the mass differences associated with their activities, the results obtained in the study were compared with a database of chemical reactions known as the Rhea Database (Rhea DB) (Bansal, P., et al, 2022). The Rhea DB is a comprehensive resource that catalogues various chemical reactions and their associated reactants and products.
4) Identifying Mass Differences for Each Enzyme: The analysis involved the collection of pairs of products and substrates, enabling the identification of mass differences characteristic of each enzyme. Typically, these characteristics are represented by the average of Z-scores for each enzyme, providing a quantitative measure of their involvement in specific reactions.
5) Exclusion of Non-Relevant Genes: To ensure precision, genes that do not catalyse a reaction or were not found in the Rhea DB were excluded from the original list of enzymes. This step helps in focusing the analysis on enzymes that play a role in the detected biochemical reactions.

In summary, MDEA is a sophisticated method for unravelling the complex web of biochemical reactions in biological samples, shedding light on the activities of enzymes and their connections to metabolites. This approach is instrumental in deciphering the underlying molecular mechanisms and metabolic processes within a given system, ultimately enhancing our understanding of biological phenomena at the molecular level.

2.10 Statistics

The compiled data was analysed using Microsoft Excel software. Cell counts were presented as bar graphs with means and positive standard deviations (SDs). Fat production was expressed as intensity per $1x10^5$ cells. For illustration purposes, the individual data points were presented as scatter plots, with mean±SD indicated. The evaluation of marker gene expression was conducted with log-transformed data and were depicted as bar graphs with means and SDs. To determine the statistical significance of the experimental results, a student's t-test was performed. Results with a p-value of ≤ 0.05 were considered as statistically significant. A p-value of ≤ 0.05 was indicated with one star (*), a p-value of ≤ 0.01 with two stars (**) and a p-value of ≤ 0.001 with three stars (***) in the Results chapter.

3 RESULTS

To investigate the influence of the SNP variant rs6712003 on the development of T2D, pre-adipocytes were isolated from subcutaneous adipose tissue of eleven severely or morbidly obese female patients undergoing abdominal laparoscopic surgery (see Table 11). These pre-adipocytes were cultured and differentiated *in vitro*. In a large experiment, samples of pre-adipocytes (d 0-3, 60-70% confluence, three days before before reaching 100% confluence), of differentiating pre-adipocytes (three days after inducing differentiation, d3) and of mature adipocytes (14 days after inducing differentiation, d14) were taken for examination (Fig. 12). At each time point, cells were counted, the morphology was examined, RNA was isolated, and samples were taken for DI-FT-ICR/MS measurement for all eleven samples. Adipocytes (d14) were examined for their maturation by Oil Red O lipid staining.

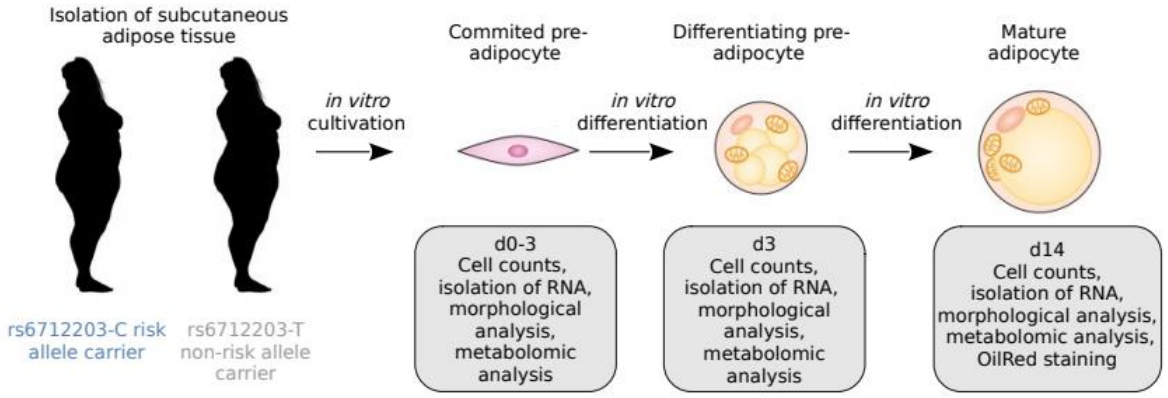

Figure 12 - Experimental setup of the in vitro adipocyte differentiation
Pre-adipocytes were isolated from subcutaneous adipose tissue of six rs6712203-C risk allele carriers and five rs6712203-T non-risk allele obese female patients. Pre-adipocytes (d0-3) were plated into 6-well plates and differentiation was induced by medium change. Indicated samples were collected three days prior (d0-3), three (d3) and 14 (d14) days after induction of adipocyte differentiation.

3.1 Adipocytes of rs6712203-C risk allele carriers reveal no morphological changes

To understand the role of *COBLL1* in adipogenesis, pre-adipocytes isolated from subcutaneous adipose tissue of six rs6712203-C risk allele and five rs6712203-T non-risk allele carriers were differentiated for 14 days *in vitro*. Pre-adipocytes three days before initiation of the differentiation (d0-3) showed a confluency of 60 to 70% and the characteristic flat fibroblast-like morphology in both s6712203-C risk allele and five rs6712203-T non-risk allele carriers (Fig. 13A). Three days after onset of the differentiation (d3), a small amount of cells started to change the shape and form lipid droplets (Fig. 13A). Under the microscope, there appeared to be more tiny fat droplets in this early differentiation stage (d0-3 to d3) in rs6712203-C risk allele carriers compared to rs6712203-T non-risk allele carriers,

although no Oil Red O staining was performed at these time points. After 14 days of differentiation (d14) mature round shaped adipocytes were generated which were filled with lipid droplets in cultures from both genotypes (Fig. 13A).

To investigate the effect of COBLL1 on the proliferation capacity of pre-adipocytes, cell numbers were counted three days before initiation of differentiation (d0-3), three days (d3) and 14 days (d14) after the onset of differentiation. Initially, $4.17x10^4$ pre-adipocytes were seeded per well on a 6-well plate. Three days before initiation of the differentiation (d0-3), $2.68\pm0.41x10^5$ cells in cultures from rs6712203-T non-risk allele pre-adipocytes and $2.44\pm0.55x10^5$ cells in cultures from rs6712203-C risk allele pre-adipocytes were counted (Fig. 13B). Differentiating pre-adipocytes (d3) of rs6712203-T non-risk allele carriers revealed a cell number of $4.91\pm0.64x10^5$ three days after onset of differentiation and rs6712203-C risk allele carriers showed a cell number of $4.60\pm0.80x10^5$ cells per well (Fig. 13B). After 14 days, $3.55\pm0.52x10^5$ mature adipocytes of rs6712203-T non-risk allele carriers and $3.27\pm1.17x10^5$ mature adipocytes of rs6712203-C risk allele carriers were counted (Fig. 13B).

To further understand the effect of COBLL1 on adipocyte maturation, the fat storage capacity in mature adipocytes was examined by Oil Red O lipid staining. Mature adipocytes from both genotypes developed lipid droplets (Fig. 13C). The fat storage capacity of rs6712203-T non-risk adipocytes was 0.08 ± 0.01 per 10^5 cells and 0.09 ± 0.02 per 10^5 cells in rs6712203-C risk adipocytes (Fig. 13D).

In summary, adipocytes from rs6712203-C risk allele carriers reveal no morphological changes and form the same amount of fat compared to adipocytes from rs6712203-T non-risk allele carriers.

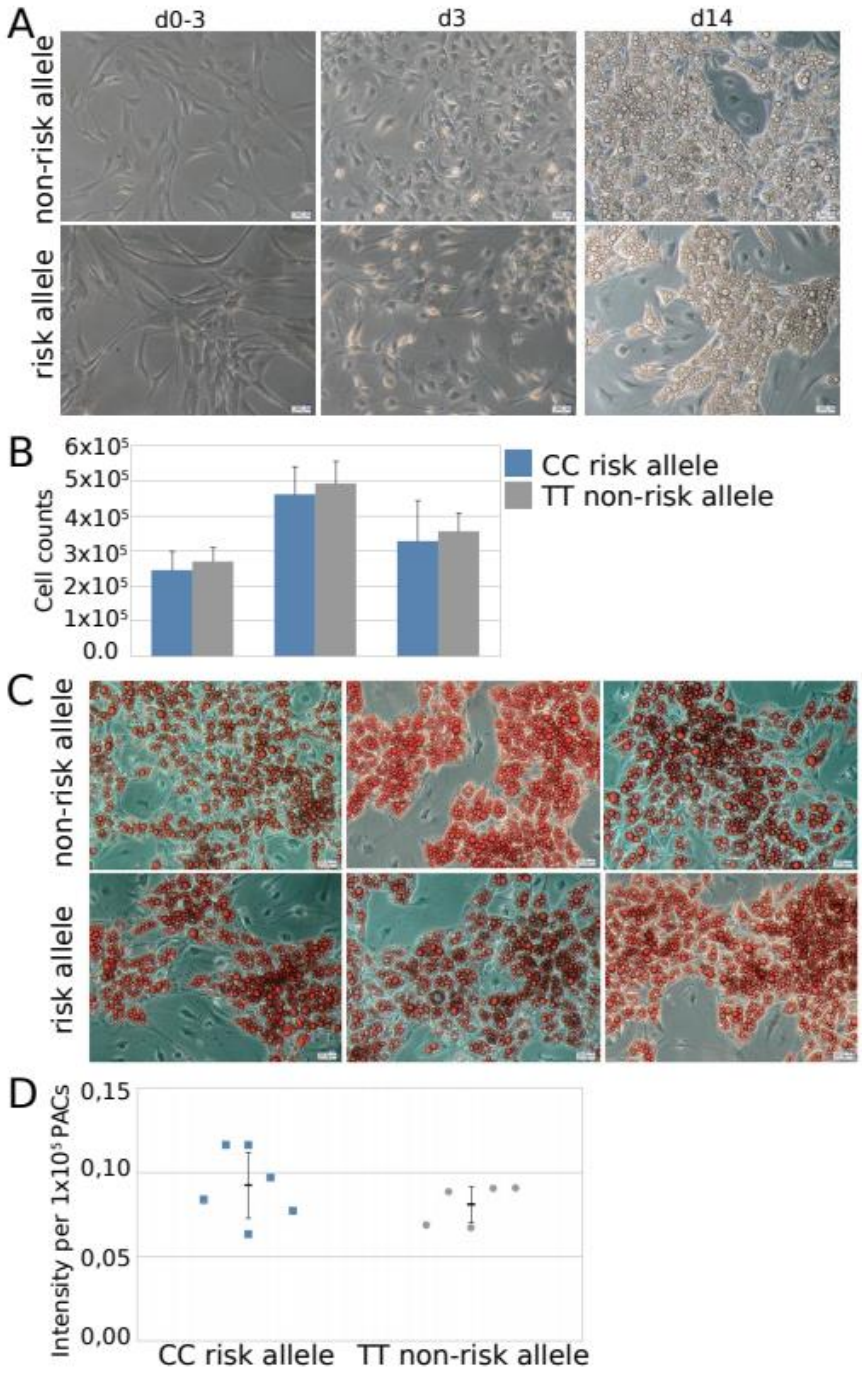

Figure 13 - **Adipocyte differentiation in pre-adipocytes (stromal-vascular cell fraction) from rs6712203-C risk allele and rs6712203-T non-risk allele carriers.**

A Representative microscopic pictures of pre-adipocytes (d0-3), in *vitro* differentiating pre-adipocytes (d3) and *in vitro* derived mature adipocytes (d14) from rs6712203-C risk allele and rs6712203-T non-risk allele carriers. **B** Proliferation capacity as cell counts in pre-adipocytes (d0-3), in *vitro* differentiating pre-adipocytes (d3) and *in vitro* derived mature adipocytes (d14) from rs6712203-C risk allele (blue) and rs6712203-T non-risk allele (grey) carriers. Results were shown as mean plus SD. **C** Representative Oil Red O lipid staining in *in vitro* derived differentiated adipocytes (d14) from rs6712203-C risk allele (CC risk allele, patient 3, 6 and 9) and rs6712203-T non-risk allele (TT non-risk allele, patient 7, 8 and 10) carriers. **D** Fat production was measured by Oil Red O lipid staining and is shown as intensity (OD at 492 nm) per $1x10^5$ cells *in vitro* derived differentiated adipocytes (d14) from rs6712203-C risk allele (CC risk allele) and rs6712203-T non-risk allele (TT non-risk allele) carriers. Results were shown as mean±SD.

3.2 *In vitro* differentiated adipocytes from rs6712203-C risk allele carriers reveal changes in selected fat metabolism and obesity marker genes

As the storage of fat is the primary function of white adipocytes (Rosen and MacDougald, 2006), the question arised whether *in vitro* derived white subcutaneous adipocytes from female persons with severe adiposity (BMI > 38,82 kg/m²) carrying the rs6712203-C risk allele show altered expression of selected fat metabolism and obesity marker genes compared to white adipocytes from rs6712203-T non-risk allele carriers.

First, the expression of *PPARG2* was examined since it encodes for the master regulator of adipogenesis and is crucial for maturation of adipocytes (Rosen and MacDougald 2006). *PPARG2* expression increased during differentiation with a mean expression of 171.69±91.51 in differentiating pre-adipocytes (d3) from CC risk allele carriers and 124.23±61.08 in TT non-risk allele carriers (Fig. 14A). The *PPARG2* expression was highest in mature adipocytes (d14) with a mean expression of 490.50±140.74 in CC risk allele carriers and 560.02±88.03 in TT non-risk allele carriers (Fig. 14A). There were no significant differences between rs6712203-C risk allele carriers and rs6712203-T non-risk allele carriers.

Next, the expression of *LEP* was examined, which encodes for the hormone leptin that signals fat stores to the brain (Harris 2014). *LEP* expression was undetectable in pre-adipocytes (d0-3) and increased during adipogenesis (Fig. 14B). Differentiating pre-adipocytes (d3) revealed a mean expression of 0.17±0.06 in CC risk allele carriers and 1.09±0.40 in TT non-risk allele carriers (Fig. 14B). Mature white adipocytes (d14) revealed a mean *LEP* expression of 1.35±0.16 in CC risk allele carriers and 2.48±0.41 in TT non-risk allele carriers (Fig. 14B). Differentiating pre-adipocytes (p-value=0.7259) and mature adipocytes (p-value=0.03897) of rs6712203-C risk allele carriers revealed a decreased *LEP* expression compared to rs6712203-T non-risk allele carriers, although only the latter was statistically significant.

IRS2 encodes the insulin receptor substrate 2, an essential adaptor mediating downstream signaling of the insulin receptor (Guo 2014). *IRS2* was highest expressed in differentiating pre-adipocytes (d3) with a mean expression of 8.14±2.49 in CC risk allele carriers and 8.12±1.48 in TT non-risk allele carriers (Fig. 14C). In mature white adipocytes (d14), *IRS2* expression slighly decreased with a mean expression of 5.36±0.93 in CC risk allele carriers and 5.25±0.17 in TT non-risk allele carriers (Fig. 14C). There were no significant differences in *IRS2* expression under all three conditions between rs6712203-C risk allele and s6712203-T non-risk allele carriers.

PIK3CA encodes the α-isoform of the catalytic subunit of phosphatidylinositol-4,5-bisphosphate 3-kinase (PI3Kα) and its phosphorylation is responsible for insulin-stimulated glucose uptake by GLUT4 (Keppler-Noreuil et al. 2016). *PIK3CA* showed a similar expression pattern in comparison to *IRS2* (Fig. 14C, D). It was upregulated in differentiating pre-adipocytes (d3) with a mean expression of 10.82±1.98 in CC risk allele carriers and 6.05±0.48 in TT non-risk allele carriers (Fig. 14D). In mature white adipocytes (d14), *PIK3CA* expression slightly decreased witch a mean expression of 2.36±0.49 in CC risk allele carriers and 2.71±0.54 in TT non-risk allele carriers (Fig. 14D). Interestingly, *PIK3CA* expression was significantly higher in differentiating pre-adipocytes from rs6712203-C risk allele (p-value=0.03) compared to rs6712203-T non-risk allele carriers.

Next, the expression of *PLIN1* was investigated. *PLIN1* encodes the protein perilipin-1, which coats lipid droplets and participates in droplet formation, triglyceride storage and lipolysis (Patel et al. 2022). *PLIN1* showed a similar expression pattern compared to *LEP* (Fig. 14B, E). In pre-adipocytes (d0-3) *PLIN1* expression was undetectable and its expression increased during differentiation (Fig. 14E). Differentiating pre-adipocytes (d3) revealed a mean expression of 2.35±0.56 in CC risk allele carriers and 1.00±0.06 in TT non-risk allele carriers (Fig. 14E). Mature white adipocytes (d14) revealed a mean PLIN1 expression of 2.02±0.89 in CC risk allele carriers and 2.55±1.16 in TT non-risk allele carriers (Fig. 14E). Surprisingly, *PLIN1* expression was significantly higher in differentiating pre-adipocytes from rs6712203-C risk allele (p-value=0.02112) compared to rs6712203-T non-risk allele carriers.

Finally, the expression of *ITGAM* was examined, which encodes for the integrin CD11b (alphaM) and is predominantly expressed on the surface of myeloid cells (Fagerholm et al 2013). *ITGAM* showed a similar expression pattern compared to IRS2 and PIK3CA (Fig. 14C, D, F). Pre-adipocytes from CC risk allele carriers revealed a mean expression of 3.90±1.43 and pre-adipocytes from TT non-risk allele carriers showed a mean expression of 1.02±0.19 (Fig. 14F). Interestingly, this upregulation of *ITGAM* in rs6712203-C risk allele compared to rs6712203-T non-risk allele carriers was significant (p-value=0.01755). Differentiating pre-adipocytes (d3) revealed a mean expression of 32.18±6.50 in CC risk allele carriers and 38.27±16.61 in TT non-risk allele carriers (Fig. 14F). Mature white adipocytes (d14) from CC risk allele carriers showed a mean *ITGAM* expression of 5.62±2.23 and mature white adipocytes from TT non-risk allele carriers revealed a mean expression of 3.96±1.58.

In summary, aim of the study was to show if there are any changes between risk-allele (C) and non-risk-allele carriers (T) in comparison in the course of adipogenesis in adipocytes of rs6712203 in *LEP*, *PIK3CA, PLIN1* and *ITGAM, PPARG 2, IRS2*.

Adipocytes of rs6712203-C risk allele carriers exhibited a similar pattern of expression as adipocytes from rs6712203-T non-risk allele carriers with respect to PPARG2 and IRS2. PIK3CA and PLIN1 expression was upregulated in in-vitro differentiating pre-adipocytes of carriers of the rs6712203-C risk allele, as was ITGAM expression in pre-adipocytes of same risk allele carriers. LEP expression however was decreased in in-vitro differentiated adipocytes of those carriers of the rs6712203-C risk allele.

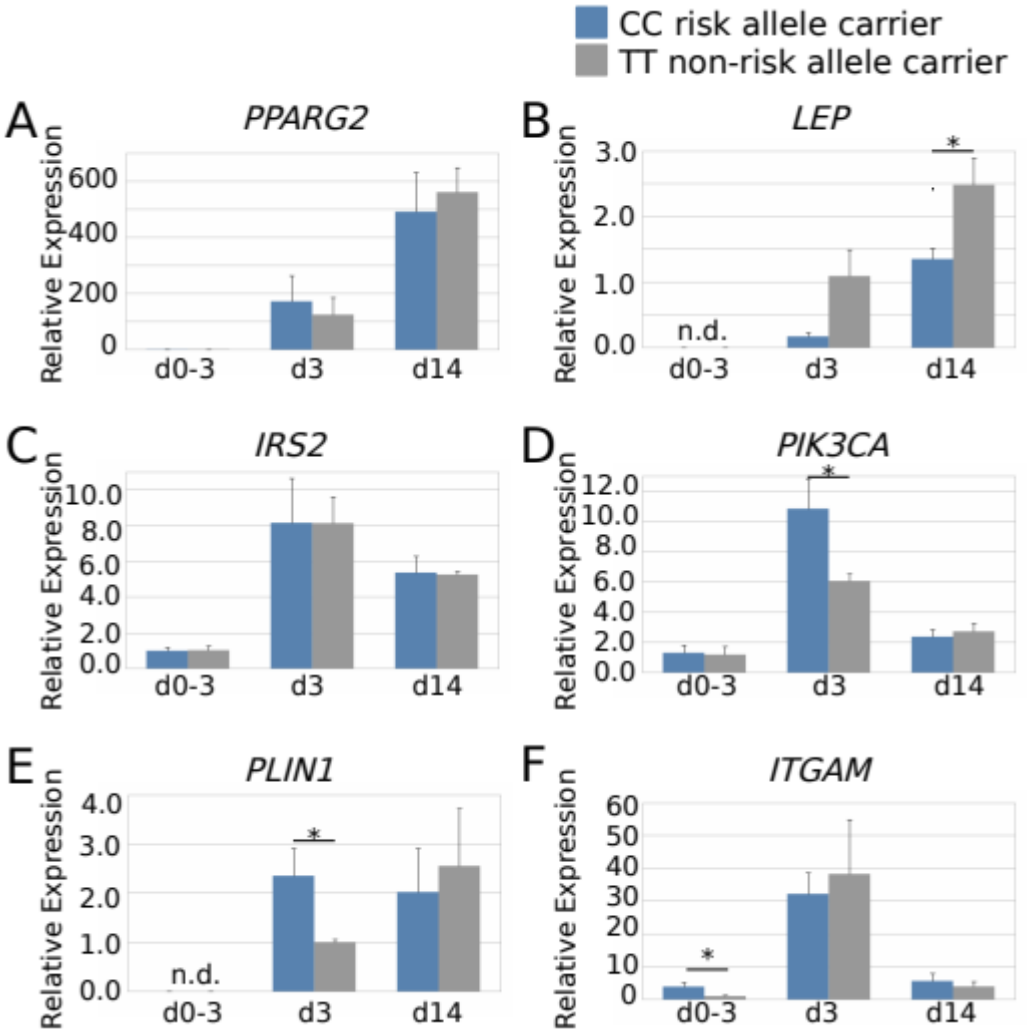

Figure 14 - **Expression of fat metabolism and obesity marker genes in rs6712203-C risk allele and rs6712203-T non-risk allele carriers during adipose differentiation**.
RT-PCR demonstrating expression levels of **A** *PPARG2,* **B** *LEP*, **C** *IRS2,* **D** *PIK3CA,* **E** *PLIN1* and **F** *ITGAM* in pre-adipocytes (d0-3), *in vitro* differentiating pre-adipocytes (d3) and *in vitro* derived mature adipocytes (d14) from rs6712203-C risk allele (blue; n=3-6) and rs6712203-T non-risk allele (grey; n=3-5) carriers. Results were shown as fold over *GAPDH* transcripts (mean±SD) normalized to the expression of rs6712203-T non-risk allele pre-adipocytes (*PPARG2; IRS2; PIK3CA, ITGAM*) or *in vitro* differentiating pre-adipocytes (*LEP; PLIN1*) *: p≤0.05 (t-test).

3.3 Adipocytes of rs6712203-C risk allele carriers reveal metabolomic changes

To elucidate which metabolic pathways are affected by the COBLL1 gene, DI-FT-ICR/MS measurements were performed in cell lysates of pre-adipocytes (d0-3), differentiating pre-adipocytes (d3) and mature adipocytes (d14) from rs6712203-C risk allele carriers and rs6712203-T non-risk allele carriers. To evaluate the results of the metabolomic measurements of the three time points, they were divided into two phases (Fig. 15A). Phase 1 represents early adipogenesis and starts three days before initiation of differentiation (d0-3) and lasts until day three after the induction of differentiation (d3). Phase 2 represents adipocyte maturation and covers the period from three (d3) to 14 days (d14) after the onset of differentiation.

In order to identify the compound classes, the 18.205 metabolic features detected were aligned with the Human Metabolome Database (HMDB). For 13 % of the metabolites a compound class could be annotated. Over-representation analysis (ORA) of compounds in phase 1 revealed a strong increase in steroids and steroid derivates, glycerophospholipids and prenol lipids in rs6712203-C risk allele carriers (Fig. 15B). Steroids are biologically active organic compounds with a core structure of seventeen carbon atoms bound in three cyclohexane rings and one cyclopentane ring. The male sex hormone testosterone, the female sex hormones estradiol and progesterone and the lipid cholesterol are examples of steroids. All steroids are produced in the cells from the sterol lanosterol, which is derived from the cyclisation of the triterpene squalene (Mazein et al. 2013). Since adipose tissue is a large endocrine organ that stores and metabolises steroid hormones, upregulation of these pathways could have immense effects on the entire body (Li et al. 2015).

Furthermore, organooxygen compounds are downregulated in rs6712203-C risk allele adipocytes (Fig. 15B). The oxygen-organic compounds are mainly carbohydrates and carbohydrate conjugates. The results from the ORA in phase 2 cannot be interpreted because these are flavonoids that only occur in plants and their frequency is too low to be statistically reliable. In summary, in differentiating adipocytes (d3) of rs6712203-C risk allele carriers, increased lipid production and less sugars are found compared to adipocytes of rs6712203-T non-risk allele carriers.

Next, mass difference enrichment analysis (MDEA) was performed based on all 18205 metabolites. Here, an upregulation of reaction products of enzymes involved in glycerophospholipid synthesis were observed in early adipogenesis (phase 1) of rs6712203-C risk allele pre-adipocytes including synthesis of PC, synthesis of PE, inositol phosphate metabolism, synthesis of PIPs at the plasma membrane, synthesis of PIPs at the endosome membrane and PI metabolism (Fig. 15C). In addition, overall

metabolism appears to be increased in early adipogenesis in rs6712203-C risk allele carriers. This is indicated by the annotations nucleotide catabolism, metabolism of amino acids and derivatives, glycolysis, fatty acyl-CoA biosynthesis and carnitine synthesis (Fig. 15C). Carnitine is produced in the human body from the amino acid lysine and methionine. Interestingly, it is involved in fatty acid metabolism and mediates the transport of fatty acid chains into the mitochondrial matrix so that adipocytes can burn off fat and obtain energy from the stored fat reserves (Pekala et al. 2011). In phase 2, reaction prodcuts of phospholipid metabolism, sphingolipid metabolism, glycosphingolipid metabolism, peroxisomal lipid metabolism, fatty acid metabolism, glycerophospholipid biosynthesis and acyl chain remodelling of phospholipids indicates were upregulated in Phase (d3 – d14) of risk allale rs6712203-C, which can be summarized as phospholipid metabolism (Fig. 15D). The reaction products of cholesterol biosynthesis, metabolism of steroid hormones and bile acid and bile salt metabolism were also upregulated in phase 2 and can be grouped together as steroid metabolism (Fig. 15D).

These findings collectively imply that risk pre-adipocytes initiate lipid production early during differentiation, while the ability to remodel the cellular skeleton, particularly actin-related processes, is diminished in late differentiation (Phase 2). This suggests a fundamental shift in metabolic priorities and cellular activities as pre-adipocytes progress through differentiation phases, with potential implications for adipocyte function and metabolism.

In conclusion, primary metabolism and glycerophospholipids synthesis are upregulated in early adipogenesis (phase 1) and phospholipid and steroid metabolism is increased in late adipogenesis (phase 2).

Table 17 Comparison of compounds classes enrichment analysis outcomes and Mass- differences in Phase 1 and Phase 2. In Phase 1 indicated a strong increase in lipid metabolism, while in Phase 2, the ORA results were irrelevant. In Phase 1, Up-regulated mass- differences were TCA, Glycolysis and IP metabolism, while in Phase 2, Steroid metabolism and phospholipid metabolism were Up-regulated mass-differences.

Risk Allele Carriers	Compounds(HMDB)	Mass Differences
Phase 1 (d0-3 to d3)	Glucose/ Organooxygen ↓ Prenol lipids ↑ Glycerophosphoilipids ↑ Steroids ↑	TCA↑ Glycolysis ↑ IP metabolism ↑
Phase 2 (d3 to d14)	Resulting from flavonoids Frequency of compound classes too low for statistical reliability	Steroid metabolism↑ Phospholipid metabolism↑

The Mass Difference Enrichment Analysis (MDEA) of enzyme-annotated mass differences on metabolome data reveals intriguing insights into the metabolic changes occurring during different phases of pre-adipocyte differentiation, particularly in relation to risk pre-adipocytes (PACs). In more detail, the findings were as follows:

In Phase 1, several metabolic pathways showed upregulation, including the tricarboxylic acid (TCA) cycle, glycolysis, inositol phosphate (IP) metabolism, and primary metabolism. Conversely, these pathways were downregulated in Phase 2. Notably, IP metabolism is closely linked to the biosynthesis of myotubulin and actin, suggesting increased cellular activity in Phase 1.

On the other hand, steroid metabolism and lipid metabolism exhibited a contrasting pattern. They were downregulated in Phase 1 but upregulated in Phase 2. These results suggest a dynamic shift in metabolic processes during pre-adipocyte differentiation.

Mass Difference Enrichment Analysis clearly showed that in Phase 1 the metabolism of risk pre-adipocytes is characterized by active primary metabolism, faster lipid production, and an intact actin-related metabolism. This suggests that Phase 1 is marked by heightened cellular activity, efficient energy production (TCA and glycolysis), and actin-related processes.

Conversely, in Phase 2, primary metabolism, including TCA and glycolysis, and actin-related processes are downregulated, while the metabolism of lipids and steroids is enhanced. This shift indicates a change from active energy production to a focus on lipid and steroid production, potentially associated with later stages of adipocyte differentiation.

The supplementary tables in the APPENDICES illustrate the over-represented mass-differences associated with the upregulation and downregulation of products in the risk allele carriers. Phase 1(d0-3 - d3) and Phase 2 (d3 - d14).

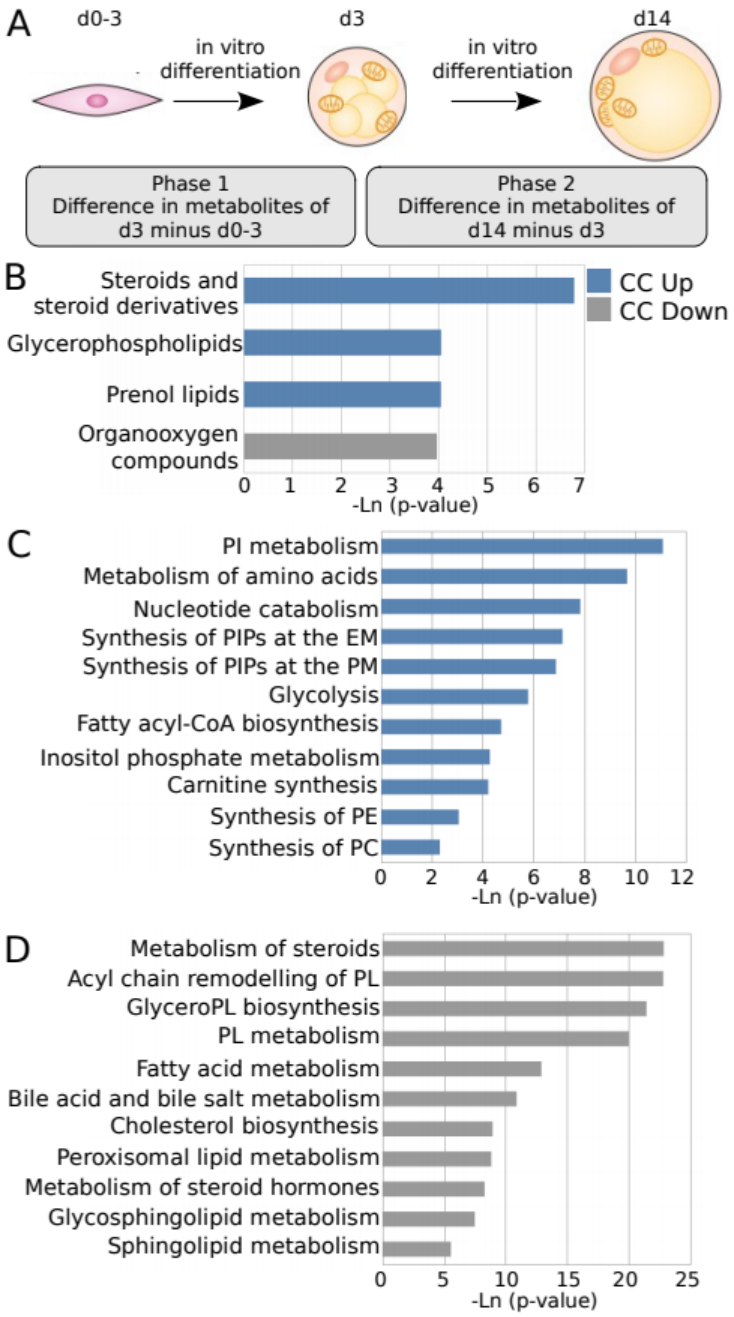

Figure 15 - Metabolomic changes in rs6712203-C risk allele adipocytes.

A Scheme of the used bioinformatical analysis strategy. Adipocyte differentiation was separated in two phases, where phase 1 lasts from d0-3 to d3 and phase 2 from d3 to d14. First, differences of metabolites of differentiating pre-adipocytes (d3) and pre-adipocytes (d0-3) were calculated per genotype for phase 1. For phase 2, differences of metabolites of mature adipocytes (d14) and differentiating pre-adipocytes (d3) were calculated per genotype. B Over-Representation Analysis of HMDB compound classes in phase 1 in rs6712203-C risk allele carriers compared to rs6712203-T non-risk allele carriers. In rs6712203-C risk allele carriers upregulated compound classes are shown in blue and downregulated compound classes are depicted in grey. C-D Mass difference enrichment analysis of phase 1 shows upregulated C and downregulated D reaction products in rs6712203-C risk allele carriers. EM: endosome membrane; PC: Phosphatidylcholin; PE: Phosphatidylethanolamin; PI: phosphatidylinositol; PIP: Phosphoinositide; PL: phospholipid; PM: plasma membrane

4 DISCUSSION

This study delves into an extensive examination of adipocyte differentiation, marker gene expression, and metabolomic profiles, employing in-vitro techniques to scrutinize adipocytes isolated from two distinct groups: obese individuals carrying the rs6712203 risk allele (C) and non-risk allele (T) carriers. The aim was to decipher potential variations in these adipocytes, particularly those with the risk allele, to gain a deeper understanding of their metabolic characteristics.

Remarkably, the morphological aspects and marker-gene expressions within adipocytes obtained from obese women, regardless of their allele type (rs6712203-C risk or rs6712203-T non-risk), exhibited no noticeable distinctions. This observation suggests that at the structural and gene-expression levels, these cells appear quite similar.

However, the metabolomic analyses uncovered striking disparities. During the early stages of adipocyte development (d0-3 to d3), pre-adipocytes of rs6712203-C risk allele displayed a notable reduction in glucose and a simultaneous increase in lipid production, as illustrated in Figure 15B. This finding implies a shift in metabolic priorities towards enhanced lipid production in risk-allele carriers during the early phases of adipogenesis.

Glycerophospholipids increased, and according to MDEA results, there was also glycerophospholipid conjugation with sugars, which are organic oxygen species, leading to their decrease. Sugar-modified glycerophospholipids always have implications for the extracellular matrix, meaning they play a role in signalling as well as cell-cell contact.

Furthermore, these pre-adipocytes carrying the rs6712203-C risk allele exhibited an upregulation of reaction products of enzymes in the early phase, such as TCA (Citrate Cycle), glycolysis, IP (Inositol Phosphate) metabolism, primary metabolism, faster lipid production, and intact actin-related metabolism compared to their rs6712203-T non-risk allele counterparts, as depicted in Figure 15C. This therefore also suggests a more robust metabolic state during early adipocyte differentiation. When the differentiation process reached the late phase (d3 to d14), a notable upregulation in both fat and steroid metabolism was observed in adipocytes carrying the rs6712203-C risk allele, as indicated in Figure 15D. This points to significant alterations in the metabolic pathways associated with fat and steroid metabolism in risk-allele carriers.

In conclusion, this comprehensive analysis highlights the complex interplay of genetic variations and metabolic processes in adipocytes. While morphological and marker-gene expression remained consistent between the two allele groups, the metabolomic data revealed substantial differences,

particularly in early adipogenesis, suggesting that the presence of the rs6712203-C risk allele significantly affects the metabolic characteristics of adipocytes, and may ultimately contribute to our understanding of the metabolic factors associated with obesity, although the detailed picture of the metabolic alterations remains to be elucidated.

4.1 COBLL1 and adipogenesis

The morphological changes from flat fibroblast-like pre-adipocytes to round shaped mature adipocytes during adipogenesis is accompanied by changes in cytoskeletal organization and contacts with the ECM (Kawaguchi et al. 2003). Pre-adipocytes possess long organised filamentous actin (F-actin) stress fibres which are localised at the cell bottom and are in contact with the substratum (Kanzaki & Pessin 2001). In contrast to that, mature adipocytes display a dense layer of F-actin on the cell cortex, which coats the inside of the plasma membrane and is known as cortical actin (Kanzaki & Pessin 2001). In other words, cytoskeletal remodelling from F-actin stress fibres to cortical actin is a necessary step for adipocyte differentiation (Yang, Thein, Wang, et al. 2014; Kanzaki & Pessin 2001). This cytoskeleton remodelling is organized by two independently regulated processes: the degradation of stress fibres and the formation of cortical actin (Yang, Thein, Wang, et al. 2014). Several actin-binding proteins (ABPs) control the linear elongation (polymerization), shortening (depolymerization) and architectural organisation of actin filaments in response to environmental stimuli (Stossel et al. 2006). It could be shown that the disruption of stress fibres is mediated by the actin-severing protein cofilin-1 (Yang, Thein, Wang, et al. 2014). The formation of cortical actin starts with the aggregation of F-actin patches at the cell cortex which is mediated by the actin-related protein 2/3 (Arp2/3) complex (Yang, Thein, Lim et al. 2014). Furthermore, cortical actin assembly is mediated through activation of the small GTPases Rac, Rho and Cdc42 (Jaffe & Hall 2005).

The cytoskeletal remodelling during adipogenesis is important for adipocyte function involving lipid storage in lipid droplets (Orlicky et al. 2013; Smas & Sul 1995) and glucose uptake by GLUT4 translocation through the plasma membrane (Kanzaki & Pessin 2001). Adipocytes from rs6712203-C risk allele carriers reveal no morphological changes examined by microscopy and form the same amount of fat compared to adipocytes from rs6712203-T non-risk allele carriers. In a previous study, COBLL1 knockdown in primary human adipose-derived stromal cells (hASC) revealed the presence of actin stress fibers and the absence of cortical actin in *in vitro* derived mature adipocytes (Glunk et al., 2023). Furthermore, stable repression experiments with shRNAS directed against COBLL1 in the Simpson–Golabi–Behmel syndrome (SGBS) cells, revealed lower amounts of lipids in shCOBLL1 adipocytes compared to control cells. In contrast to these findings with artificial COBLL1 knockdowns,

rs6712203-C risk allele adipocytes revealed no significant differences in lipid production (Fig. 13C, D). Furthermore, metabolites of steroid and fat metabolism were upregulated in mature rs6712203-C risk allele adipocytes (phase 2) and were downregulated in pre-adipocytes (phase 1) (Fig. 15D). Surprisingly, the metabolites in phosphatidylinositol (PI) metabolism were strikingly elevated in rs6712203-C risk allele pre-adipocytes (Fig. 15C). Polyphosinositides are known to promote actin polymerization by removing capping proteins from barbed ends (Stossel et al. 2006). In addition, the interaction of N-WASP with PIP2 together with the activated Rho proteins Cdc42 and TC10 was shown to expose the VCA domain of N-WASP, which subsequently activates the Arp2/3 complex (Kanzaki et al. 2002; Prehoda et al. 2000; Rohatgi et al. 1999). The Arp2/3 complex is responsible for actin nucleation, which is the formation of new actin filaments from actin monomers (Welch & Mullins 2002). The data may suggest that the adipocyte upregulates PI metabolism to compensate for the missing or reduced signals induced by COBLL1. A limitation of the present work is that no qPCR or Western blot was performed to check the expression of COBLL1 (Glunk et al., 2023). Differences in expression may exist between the rs6712203-C risk allele carriers or the reduction of COBLL1 may not be as drastic as in the knockdown studies with SGBS cells. The differences in COBLL1 expression between the carriers of the risk allele in fat production support this assumption. Patient 3 showed low fat production (intensity per $1x10^5$ cells: 0.06), while patients 2 and 4 showed increased fat production (intensity per $1x10^5$ cells: 0.12).

Before the mechanistic studies of Glunk et al. (Glunk et al., 2023), the function of COBLL1 in the context of type 2 diabetes and obesity was widely unknown. The Cordon-bleu protein (COBL), which is a paralog of COBLL1, is able to nucleate (polymerize) and sever (depolymerize) actin filaments and, thereby, to promote the dynamic regulation of the actin cytoskeleton (Husson et al. 2011; Jiao et al. 2014). Both proteins contain one or more Wiskott–Aldrich syndrome protein (WASP)-homology 2 (WH2) domains which are found in many proteins that can alter the cytoskeleton through direct actin binding (Husson et al. 2011). In COBLL1, one or two WH2 domains in combination with a K region are sufficient for actin nucleation, while at least two WH2 domains are required for actin severing (Husson et al. 2011). Furthermore, the COBLL1 WH2 domain can form a complex with monomeric G-actin, thereby inhibiting the F- actin pointed-end growth (Husson et al. 2011). In contrast to that, COBLL1 contains only one WH2 domain and the K-region can not be found. In prostate cancer cells, it could be shown that COBLL1 activate actin filamentation (Takayama et al. 2018). In accordance with this knowledge, COBLL1 localizes in the cytoplasm in proximity to actin filaments in *in vitro* differentiated hASC (Glunk et al., 2023). Furthermore, COBLL1 can be found in complexes with PACSIN's, which interact with N-WASP, an activator of Arp2/3 (Kessels & Qualmann 2004; Stark et al. 2006).

Nevertheless, the exact mechanism by which COBLL1 contributes to actin filamentation remains unclear.

Cortical actin formation is essential for the cellular translocation of GLUT4 (Kanzaki & Pessin 2001). GLUT4 is an insulin-responsive glucose transporter which is stored in intra-cellular vesicles. Upon insulin stimulation GLUT4 is translocated from these intra-cellular vesicles to the plasma membrane and, thereby, mediates glucose uptake in adipocytes (Kanzaki & Pessin 2001). ORA revealed evidence for decreased glucose in rs6712203-C risk allele pre-adipocytes compared to rs6712203-T non-risk allele counterparts (Fig. 15B). This is in line with previous findings, where insulin-stimulated glucose uptake assays with a stable lentiviral knock down of COBLL1 in the SGBS cell line revealed a lower glucose uptake under basal conditions as well as no significantly increased glucose uptake after insulin stimulation in shCOBLL1 adipocytes (Glunk et al. 2023). This indicates that a potential reduction in COBLL1 expression in mature rs6712203-C risk allele adipocytes leads to a reduced glucose uptake and a loss of insulin sensitivity.

4.2 COBLL1 and adipocyte marker gene expression

Adipocytes of rs6712203-C risk allele carriers revealed distinct changes in *LEP, PIK3CA*, *PLIN1* and *ITGAM* expression compared to adipocytes from rs6712203-T non-risk allele carriers (Fig. 14). Whereas *PPARG2 and IRS2* showed a similar expression pattern in both genotypes. *PPARG2* encodes for the adipocyte key TF PPARγ and it was shown that it is upregulated during adipogenesis (Kawaguchi et al. 2003). The missing morphological differences in adipocytes from rs6712203- C risk allele carriers compared to non-carriers (Fig. 13), went along with a normaly upregulated *PPARG2* during adipogenesis (Fig. 14A). In accordance with a study in which cofilin-1 expression was reduced via shRNAs in the murine preadipocyte cell line 3T3-L1, a diminished expression of a ABP had no influence on the expression of *PPARG* (Yang, Thein, Wang, et al. 2014). This is also in line with a study that has shown that it is not the expression patterns of TFs, but rather their target patterns and the resulting regulatory networks that are responsible for the regulation of tissue-specific processes (Sonawane et al. 2017). In contrast to that, in another study knocking down the actin nucleation factor Arp3 in 3T3-L1 cells, revealed a decrease in *PPARG* expression (Yang, Thein, Lim et al. 2014).

LEP and *PLIN1* are marker genes of mature adipocytes (Ghaben and Scherer, 2019). Therefore, it is not surprising that these two genes are not expressed in pre-adipocytes and were upregulated during differentiation (Fig. 14B, E). Interestingly, mature adipocytes of rs6712203-C risk allele carriers revealed a decreased *LEP* expression compared to rs6712203-T non-risk allele carriers (Fig. 14B). This is in accordance with a previous study from our group where COBLL1 expression was reduced via

shRNA in differentiated SGBS cells which also revealed a decreased *LEP* expression (Glunk et al. 2023). The exact mechanism of regulation of *LEP* expression in adipocytes is not yet clear, but it is likely that it is sensitive to hormonal and dietary signals (Zhang & Chua 2017). *LEP* expression is suppressed by growth hormone and catecholamines, which are both involved in the induction of lipolysis (Asada et al 2000; Isozaki et al. 1999; Kosaki et al. 1996; Scriba et al. 2000; Sivitz et al. 1999; Trayhurn et al. 1996). In accordance with that, *LEP* expression is increased by antilipolytic agents such as prostaglandin E2 (PGE2) (Fain et al. 2000a; Fain et al. 2000b). Furthermore, insulin and glucocortioids also stimulate *LEP* expression (Bradley & Cheatham 1999; Russell et al. 1998; Saladin et al. 1995; Slieker et al. 1996; Wabitsch, M & Hauner, H, et al. 1996). Likewise, long chain fatty acids have been shown to inhibit *LEP* expression in 3T3-L1 adipocytes (Rentsch & Chiesi 1996; Shintani et al. 2000). Furthermore, the transcription factor FOSL2 was shown to mediate the adipocyte-specific *LEP* expression which could be a candidate for mediating the effect of adipocyte size on *LEP* expression (Wrann et al. 2012). Since FOSL2 levels are not affected by nutritional changes such as 24-h fasting and refeeding, it is not likely to be involved in the nutritional regulation of *LEP* expression (Wrann et al. 2012).

In contrast to *LEP* expression, *PLIN1* was upregulated in differentiating pre-adipocytes of rs6712203-C risk allele carriers compared to rs6712203-T non-risk allele carriers, whereas its expression was equally in mature adipocytes (Fig. 14E). This is in line with the per eye observation, that differentiating pre-adipocytes of rs6712203-C risk allele carriers produced more lipid droplets in this early differentiation stage (data not obtained via Oil Red O staining), since PLIN1 is involved in the formation of lipid droplets (Patel et al. 2022). In contrast, mature adipocytes derived from in vitro differentiated SGBS cells with COBLL1 knockdown mediated by shRNAs showed reduced levels of PLIN1 protein, which was associated with a reduced capacity for lipolysis (Glunk et al. 2023). Although gene expression does not always mean protein expression, since regulation can also take place at the protein level, for example through ubiquination, there seems to be serious changes in the differentiating pre-adipocytes. Although the overall transcriptional regulation of *PLIN1* is still incompletely defined, it has already been shown that the transcription factors PPARG, NFkappaB and LXRA regulate PLIN1 transcription (Dalen et al. 2004; Laurencikiene et al. 2007; Stenson et al. 2011). Since *PPARG* expression is not affected in adipocytes from rs6712203-C risk allele carriers, one of the other two TFs or another epigenetic modification may be responsible for *PLIN1* upregulation. Epigenetic modifications are all influences on gene expression and chromosome structure that are not mediated by changes in the DNA sequence (Li 2002). There was one study that showed that CpG methylation of the PLIN1 promoter was higher in adipocytes from obese women than in non-obese women (Bialesova et al. 2017). Since higher promoter methylation is associated with low or absent transcription (Suzuki & Bird, 2008), *PLIN1* promoter methylation resulted in a decrease in *PLIN1*

expression and lipolytic activity (Bialesova et al. 2017). Interestingly, external factors such as diet and physical activity have an influence on DNA methylation (Boqué et al. 2013; Rönn et al. 2013; Gillberg et al. 2016).

In a previous study from our group, it could be shown that *COBLL1* is co-expressed with *ITGAM* and *PIK3CA* using genome-wide expression data from primary human AMSCs in a cohort of 12 healthy, non-obese individuals (Glunk et al. 2023). In line with this, *ITGAM* and *PIK3CA* showed a similar expression pattern in adipogenesis. Both genes were upregulated in early adipogenesis and downregulated in mature adipocytes (Fig. 14D, F). Surprisingly, both genes were upregulated in early adipogenesis in pre-adipocytes from CC risk allele carriers compared to rs6712203-T non-risk allele carriers. *ITGAM* encodes for the integrin CD11b, which forms integrin Mac-1 together with the integrin CD18. Since Mac-1 is predominantly expressed on the surface of myeloid cells, not much is known about its role or regulation in adipocytes (Fagerholm et al. 2013). *PIK3CA* encodes the α-isoform of the catalytic subunit of PI3K, which catalyses the phosphorylation of PIP2 to PIP3 and is a master regulator of cell survival and metabolism. Furthermore, the PI3K/AKT pathway has been shown to regulate both the differentiation of adipose progenitor cells and the progression of adipogenesis through the translocation of downstream TFs (Jeffery et al. 2015; Nagai et al. 2018). Since PI3K is involved in mediating gene regulation through TF translocation, the question may arise whether the upregulation of *PIK3CA* in differentiating preadipocytes together with the upregulation of PI metabolism in early adipogenesis, is a mechanism to compensate for missing signals mediated by COBLL1 (Fig. 15C).

In summary, the expression of *PPARG2* and *IRS2* was not affected by COBLL1, but COBLL1 ablation had an effect on the expression of *LEP*, *PIK3CA*, *PLIN1* and *ITGAM*. The question that arises here is whether COBLL1 has a direct effect on gene regulation of these genes or whether its absence has an effect on metabolism, which in turn affects adipocyte expression. In addition to being localised in the cytoplasm, COBLL1 is also found in cell nuclei (Glunk et al. 2023). The presence of actin and actin nucleation factors in the nucleus leads to the assumption that they may be involved in the remodelling of chromatin and the regulation of gene transcription (Weston et al. 2012). In line with this, the monomeric G-actin seems to play a role in adipogenesis. When G-actin is bound to megakaryoblastic leukaemia 1 (MLK1), it can not be translocated to the nucleus and thus *PPARG* expression is increased (Nobusue et al. 2014). In addition, the shuttling of proteins between the nucleus and lipid droplets is a novel and potentially crucial regulatory level that connects transcriptional control and metabolic pathways in white adipocytes (Morigny et al. 2021).

4.3 COBLL1 and adipocyte metabolism

Metabolites are the end products of cellular regulatory systems, thus changes in metabolites reflect the response to intrinsic and extrinsic signals (Patti et al. 2012). White adipocytes are specialised in metabolism, especially in storing chemical energy in the form of triacylglycerol (TAG) and releasing it in the form of FAs (Morigny et al. 2021). Furthermore, they link glucose metabolism pathways to lipid metabolism, particularly through the de novo synthesis of FAs and glycerol. White adipocytes, through their metabolism, control the secretion of proteins and lipids that have local and systemic effects on insulin sensitivity and inflammation (Morigny et al. 2021). Changes in adipocyte metabolism lead to dysfunctions that can affect the whole organism. In accordance with that, it has been shown that hypertrophic adipocytes have defects in glucose metabolism (Czech 1976). The hypertrophic adipocyte phenotype is associated with an adverse cardiometabolic profile (Rutkowski et al. 2015; Tandon et al. 2018); Honecker, J, et al, 2022).

Glycerophospholipids (GPL) and sphingolipids are the two classes of phospholipids (PL), which are both important components of all cell membranes (Reddan et al. 2018). GPLs usually consist of a glycerol backbone which contains three hydroxyl groups (sn-1, sn-2, and sn-3). The phosphate group is esterified at sn-3, whereas the two long-chain FAs are esterfied at sn-1 and sn-2 (Castro-Gómez et al. 2015). Due to their amphiphilic characteristic, they can form lipid bilayers. The phosphate group located at sn-3 forms the hydrophilic head of the GPL molecule, while the FAs attached to sn-1 and sn-2 form the hydrophobic tail (Castro-Gómez et al. 2015). GPLs also serve as anchors for proteins in cell membranes and are involved in cell signalling systems. Known glycerophospholipids are phosphatidic acid (PA), phosphatidylethanolamine (PE), phosphatidylcholine (PC), phosphatidylserine (PS) and phosphoinositides including phosphatidylinositol (PI), phosphatidylinositol phosphate (PIP), phosphatidylinositol bisphosphate (PIP2) and phosphatidylinositol trisphosphate (PIP3). Phosphoinositides act as master regulators of cellular signalling involved in cell growth, metabolism and cell death (Balla et al. 2013). Prenol lipids (PR) or isoprenoids are synthesised from the five carbon precursors isopentenyl diphosphate (IPP) and its isomer dimethylallyldiphosphate (DMAPP), which are mainly generated via the mevalonic acid (MVA) pathway and the methylerythritol phosphate (MEP) pathway (Zhao et al. 2013). PR and their phosphorylated derivatives play an important role in the transport of oligosaccharides through membranes. Polyprenol phosphate sugars and polyprenol diphosphate sugars are involved in extracytoplasmic glycosylation reactions and N-glycosylation of proteins. Interestingly, the C30 isoprenoid squalene is the starting substrate of the cholesterol biosynthesis pathway (Mazein et al. 2013). Squalene epoxidase (SQLE), also called squalene monooxygenase is the enzyme that catalyzes the conversion of squalene into squalene-2,3-epoxide

and the conversion of squalene-2,3-epoxide (2,3-oxidosqualene) into 2,3:22,23-diepoxysqualene (2,3:22,23-dioxidosqualene). Both reactions take place at the membrane of the endoplasmic reticulum, and this is thought to be one of the rate-limiting steps in this metabolic pathway (Nagai et al. 1997). This indicates that SQLE is the slowest enzyme in the pathway and its regulation alone determines how much cholesterol is produced at the end.

This thesis discovered distinct metabolomic changes in adipogenesis of rs6712203-C risk allele carriers (Fig. 15). ORA results revealed a strong increase of steroids and steroid derivates, glycerophospholipids and prenol lipids and a decrease of carbohydrates and carbohydrate conjugates in early adipogenesis of rs6712203-C risk allele carriers (Fig. 15B). MDEA results point to a higher metabolomic activity combined with increased metabolites of GPL synthesis pathways in early adipogenesis of rs6712203-C risk allele carriers (Fig. 15C). In late adipogenesis, MDEA revealed an enrichment of metabolites of phospholipid and steroid metabolism in rs6712203-C risk allele carriers (Fig. 15D). First of all, it is important to mention that for the ORA only the HMDB annotated metabolites were used, which account for only 13 % of all detected metabolites. In both analyses, metabolites of GPL synthesis pathways were enriched. It also makes sense that organooxygen compounds are decreased as they are metabolised by glycolysis and the tricarboxylic acid cycle (TCA). In addition, proteins and lipids can also be modified by the addition of sugars, which is referred to as glycosylation (Reily et al. 2019). Glycosylated haemoglobin (HbA1c), for instance, is a surrogate for average blood glucose levels over the last 3 months and is used to monitor long-term management of diabetes (Cerami et al. 1979). Furthermore, pathogenesis of diabetes is associated with abnormal O-linked N-acetylglucosamine-mediated signalling and increased glycation of several proteins (Reily et al. 2019). What seems to be contradictory at first sight are the results of ORA and MDEA regarding the accumulation of steroid metabolites. ORA showed an enrichment of steroid metabolites, whereas these were decreased in MDEA in early adipogenesis. The HMDB annotation file shows for the enriched steroids mainly versions of steroid hormones mostly sex hormone derivatives. In contrast, the declining steroids are mainly larger conjugates that could also be bile acids (Figure 15D). A uniprot analysis of the steroid enzymes whose products go down in early adipogenesis show that they are located centrally or at the end of the cholesterol biosynthesis pathway including lathosterol oxidase (SC5DL), sterol-4-alpha-carboxylate 3-dehydrogenase, decarboxylating (NSDHL), cholesterol 25-hydroxylase (CH25H), lanosterol 14-alpha demethylase (CYP51A1), cytochrome P450, family 27, subfamily A, polypeptide 1 (CYP27A1), Cytochrome P450, family 7, subfamily A, polypeptide 1 (CYP7A1), methylsterol monooxygenase 1 (MSMO1) and cytochrome P450 46A1 (CYP46A1). As mentioned earlier, SQLE, the first enzyme in this metabolic pathway, is the rate-limiting enzyme (Nagai et al. 1997). If in a pathway the enzymes downstream of the rate-limiting enzyme are upregulated,

then the reaction products downstream of SQLE are reacted away much faster than SQLE can produce squalene-2,3-epoxide and 2,3:22,23-diepoxysqualene. This indicates that all metabolic products that are between squalene-2,3-epoxide and 2,3:22,23-diepoxysqualene and cholesterol are almost immediately converted into cholesterol. Therefore, they hardly appear at all, because they are immediately processed further. In this case, the downregulation of the metabolites implies an upregulation of the metabolic pathway. In pathways where the rate limiting enzyme is at the end, and not at the beginning like SQLE, the metabolites accumulate before the rate limiting enzyme depending on the activity of the enzymes that produce them. In this case, up-regulation of metabolites also implies up-regulation of the respective enzymes. This is the case with GPLs, they are more or less the end points of the pathways which means GPLs are hardly metabolized further and accumulate. Near its role in cell membrane formation, they mediate cellular signalling and cell-cell contacts (Reily et al. 2019). Thus, changes in GPL metabolism can have a huge impact. As discussed earlier, PIs play a role in actin remodelling. PIs interact directly with many actin-binding proteins, control the subcellular localization of larger scaffolding proteins, and regulate proteins which control the activity of Rho family small GTPases (Saarikangas et al. 2010).

Another study examined the effects of ablated COBLL1 expression in serum (Al Sadat, unpublished data). Metabolomic analysis were performed of serum samples taken 0, 60 and 120 minutes after an OGTT of selected patients with rs6712203 risk and non-risk alleles. The results of the metabolomic measurements at the three time points, were divided into two effects with effect 1 describing the metabolic differences between the starting point (0 min) and 60 min and effect 2 the metabolic differences between 60 min and 120 min. Surprisingly, ORA also revealed an upregulation of steroids and steroid derivatives and glycerophospholipids in effect 1 in rs6712203-C risk allele carriers. Furthermore, steroids and steroid derivatives were also upregulated in effect 2 in rs6712203-C risk allele carriers. Interestingly, they performed MDEA mapping the mass differences to a list of eleven COBLL1 co-regulated genes and could detect the mass differences related to *PPARG, PLIN5* and *ILK.* The same approach was performed with the data of this thesis, but there were no relations to these genes. This is not surprising, as adipocyte metabolites were determined in the present study and blood plasma from cohort participants in the former study. One major difference is that people participating in a cohort eat and drink different things and are exposed to many other influences, whereas cell culture allows for the same defined conditions. Furthermore, blood plasma samples would more match cell culture medium rather than cells, if at all, so the results are difficult to correlate. Nevertheless, phospholipids, sphingomyelins and triglycerides in blood or urine samples have been linked to insulin resistance and type 2 diabetes in humans (Wang et al. 2011; Salihovic et al. 2020).

In summary, this work provides exciting insights into the metabolic changes of adipocytes of rs6712203-C risk allele carriers and offers a basis for the search for possible therapeutic approaches.

5 OUTLOOK

Type 2 diabetes (T2D) is a chronic metabolic disease whose prevalence is steadily increasing at an alarming rate. The main priorities in T2D research are to improve risk prediction and identify new molecular therapeutic targets. Identification of currently unknown molecular mechanisms of T2D pathogenesis could act as novel treatment targets. Adipocyte metabolism offers promising targets for the treatment of T2D as well as associated cardiovascular disease and cancer-related disorders.

This thesis provides unprecedented insight into the metabolic changes of adipocytes from s6712203-C risk allele carriers. In early adipogenesis, basic and glycerophospholipid metabolism are upregulated and phospholipid and steroid metabolisms are increased in late adipogenesis of rs6712203-C risk allele carriers. The metabolic data indicate a link between prenol lipid metabolits and cholesterol biosynthesis, which should be further validated. First, expression of cholesterol biosynthesis enzymes with downregulated metabolites (CH25H; CYP27A1; YP46A1; CYP51A1; CYP7A1; MSMO1; NSDHL and SC5DL) can be validated via qPCR and Western Blot. If the results are in line with the metabolic data, cell culture studies with inhibitors of the respective targets could be performed. If the treatment with inhibitors produces results in cell culture, a suitable mouse model could be developed for further studies.

Furthermore, it is essential to investigate COBLL1 expression in individual samples and to increase sample size. F-actin staining may shed light on the unresolved question of why lipid droplet production was possible even though glucose uptake appeared to be impaired in rs6712203-C risk allele adipocytes. Another interesting study would be the Oil Red O staining three days after differentiation, to see if the increased lipid metabolites also have an effect on increased fat droplet production. Since white adipocyte size and turnover determine systemic insulin sensitivity and cardiometabolic risk in humans, it would be interesting to investigate whether there is also a change in size and turnover of rs6712203-C risk allele adipocytes.

To unravel the mysteries of the pathogenesis of various diseases, an approach combining genetics, gene expression (transcriptomics), protein analysis (proteomics) and metabolite analysis (metabolomics) would be desirable. With the development of high-throughput metabolomics technologies over the last decade, this approach may be feasible in the future. Another desirable step would be to transfer these analyses from cell culture models to the human organism. While studies in cultures are very useful, the cells do not grow in their natural environment, where they are additionally surrounded by other cells with which they might interact and be influenced by their metabolites.

6 COLLABORATIONS

PAC Isolation

Subcutaneous PACs were isolated and cryopreserved in the Department of Nutritional Medicine at TUM as described in Chapters 2.3 to 2.8 of this work.

Genotyping

Genotyping of the MOBB samples was partly carried out by Samantha Laber at the Broad Institute of Harvard Medical School and partly by me at the facilities of the Chair of Nutritional Medicine at the TUM using the LightSNIP assay for the analysis of human variation rs6712203. For details see Chapter 2.3.

DI-FT-ICR/MS sample measurements and Bioinformatics

DI-FT-ICR/MS sample measurements and bioinformatic analysis of the DI-FT-ICR/MS data were performed with the help of Dr Sara Forcisi from the laboratory of Analytical Biogeochemistry (BGC) at the Helmholtz Center Munich as described in Chapter 2.9 of this work.

APPENDICES

Supplementary table 1: Enzymes of up-regulated metabolites in phase 1 and down-regulated metabolites in phase 2

Uniprot ID	Gene name(s)	Protein name(s)	Re-weighted M Scores
Q9Y216	MTMR7	Myotubularin-related protein 7 (Inositol 1,3-bisphosphate phosphatase) (EC 3.1.3.-) (Phosphatidylinositol-3-phosphate phosphatase) (EC 3.1.3.64)	-13,93
Q9UNW1	MINPP1 MIPP UNQ900/PRO1917	Multiple inositol polyphosphate phosphatase 1 (EC 3.1.3.62) (2,3-bisphosphoglycerate 3-phosphatase) (2,3-BPG phosphatase) (EC 3.1.3.80) (Inositol (1,3,4,5)-tetrakisphosphate 3-phosphatase) (Ins(1,3,4,5)P(4) 3-phosphatase)	-13,23
Q9NPB8	GPCPD1 GDE5 KIAA1434	Glycerophosphocholine phosphodiesterase GPCPD1 (EC 3.1.4.2) (Glycerophosphodiester phosphodiesterase 5)	-13,21
O95336	PGLS	6-phosphogluconolactonase (6PGL) (EC 3.1.1.31)	-12,94
O43598	DNPH1 C6orf108 RCL	2'-deoxynucleoside 5'-phosphate N-hydrolase 1 (EC 3.2.2.-) (c-Myc-responsive protein RCL)	-12,83
Q8WTR4	GDPD5 GDE2 PP6037 PP9363 UNQ1850/PRO3580	Glycerophosphodiester phosphodiesterase domain-containing protein 5 (Glycerophosphocholine phosphodiesterase GDPD5) (EC 3.1.4.2) (Glycerophosphodiester phosphodiesterase 2) (Phosphoinositide phospholipase C GDPD5) (EC 3.1.4.11)	-12,83
Q9BW91	NUDT9 NUDT10 PSEC0099 UNQ3012/PRO9771	ADP-ribose pyrophosphatase, mitochondrial (EC 3.6.1.13) (ADP-ribose diphosphatase) (ADP-ribose phosphohydrolase) (Adenosine diphosphoribose pyrophosphatase) (ADPR-Ppase) (Nucleoside diphosphate-linked moiety X motif 9) (Nudix motif 9)	-11,43
P04035	HMGCR	3-hydroxy-3-methylglutaryl-coenzyme A reductase (HMG-CoA reductase) (EC 1.1.1.34)	-11,00
Q13615	MTMR3 KIAA0371 ZFYVE10	Myotubularin-related protein 3 (EC 3.1.3.48) (FYVE domain-containing dual specificity protein phosphatase 1) (FYVE-DSP1) (Phosphatidylinositol-3,5-bisphosphate 3-phosphatase) (EC 3.1.3.95) (Phosphatidylinositol-3-phosphate phosphatase) (EC 3.1.3.64) (Zinc finger FYVE domain-containing protein 10)	-10,34
Q13057	COASY PSEC0106	Bifunctional coenzyme A synthase (CoA synthase) (NBP) (POV-2) [Includes: Phosphopantetheine	-10,13

Uniprot ID	Gene name(s)	Protein name(s)	Re-weighted M Scores
		adenylyltransferase (EC 2.7.7.3) (Dephospho-CoA pyrophosphorylase) (Pantetheine-phosphate adenylyltransferase) (PPAT); Dephospho-CoA kinase (DPCK) (EC 2.7.1.24) (Dephosphocoenzyme A kinase) (DPCOAK)]	
Q16222	UAP1 SPAG2	UDP-N-acetylhexosamine pyrophosphorylase (Antigen X) (AGX) (Sperm-associated antigen 2) [Includes: UDP-N-acetylgalactosamine pyrophosphorylase (EC 2.7.7.83) (AGX-1); UDP-N-acetylglucosamine pyrophosphorylase (EC 2.7.7.23) (AGX-2)]	-10,08
Q9HCC8	GDPD2 GDE3 OBDPF UNQ1935/PRO4418	Glycerophosphoinositol inositolphosphodiesterase GDPD2 (EC 3.1.4.43) (Glycerophosphodiester phosphodiesterase 3) (Glycerophosphodiester phosphodiesterase domain-containing protein 2) (Osteoblast differentiation promoting factor)	-9,96
P15309	ACP3 ACPP	Prostatic acid phosphatase (PAP) (EC 3.1.3.2) (5'-nucleotidase) (5'-NT) (EC 3.1.3.5) (Acid phosphatase 3) (Ecto-5'-nucleotidase) (Protein tyrosine phosphatase ACP3) (EC 3.1.3.48) (Thiamine monophosphatase) (TMPase) [Cleaved into: PAPf39]	-9,85
Q13496	MTM1 CG2	Myotubularin (Phosphatidylinositol-3,5-bisphosphate 3-phosphatase) (EC 3.1.3.95) (Phosphatidylinositol-3-phosphate phosphatase) (EC 3.1.3.64)	-9,79
Q13574	DGKZ DAGK6	Diacylglycerol kinase zeta (DAG kinase zeta) (EC 2.7.1.107) (Diglyceride kinase zeta) (DGK-zeta)	-9,43
Q8TCT1	PHOSPHO1	Phosphoethanolamine/phosphocholine phosphatase (EC 3.1.3.75)	-9,27
Q9Y617	PSAT1 PSA	Phosphoserine aminotransferase (EC 2.6.1.52) (Phosphohydroxythreonine aminotransferase) (PSAT)	-8,70
O75356	ENTPD5 CD39L4 PCPH	Ectonucleoside triphosphate diphosphohydrolase 5 (NTPDase 5) (EC 3.6.1.6) (CD39 antigen-like 4) (ER-UDPase) (Guanosine-diphosphatase ENTPD5) (GDPase ENTPD5) (EC 3.6.1.42) (Nucleoside diphosphatase) (Uridine-diphosphatase ENTPD5) (UDPase ENTPD5)	-8,44
Q9NPH0	ACP6 ACPL1 LPAP UNQ205/PRO231	Lysophosphatidic acid phosphatase type 6 (EC 3.1.3.2) (Acid phosphatase 6, lysophosphatidic) (Acid phosphatase-like protein 1) (PACPL1)	-8,34
Q9NR45	NANS SAS	Sialic acid synthase (N-acetylneuraminate synthase) (EC 2.5.1.56) (N-acetylneuraminate-9-phosphate synthase) (EC 2.5.1.57) (N-acetylneuraminic acid phosphate synthase) (N-acetylneuraminic acid synthase)	-8,32

Uniprot ID	Gene name(s)	Protein name(s)	Re-weighted M Scores
Q4G176	ACSF3 PSEC0197	Malonate—CoA ligase ACSF3, mitochondrial (EC 6.2.1.n3) (Acyl-CoA synthetase family member 3)	-7,91
Q6P988	NOTUM OK/SW-CL.30	Palmitoleoyl-protein carboxylesterase NOTUM (EC 3.1.1.98) (hNOTUM)	-7,88
Q86V21	AACS ACSF1	Acetoacetyl-CoA synthetase (EC 6.2.1.16) (Acyl-CoA synthetase family member 1) (Protein sur-5 homolog)	-7,73
Q8TCT0	CERK KIAA1646	Ceramide kinase (hCERK) (EC 2.7.1.138) (Acylsphingosine kinase) (Lipid kinase 4) (LK4)	-7,62
P52758	RIDA HRSP12	2-iminobutanoate/2-iminopropanoate deaminase (EC 3.5.99.10) (14.5 kDa translational inhibitor protein) (hp14.5) (p14.5) (Heat-responsive protein 12) (Reactive intermediate imine deaminase A homolog) (Translation inhibitor L-PSP ribonuclease) (UK114 antigen homolog)	-7,55
Q96CM8	ACSF2 UNQ493/PRO1009	Medium-chain acyl-CoA ligase ACSF2, mitochondrial (EC 6.2.1.2)	-7,34
P54886	ALDH18A1 GSAS P5CS PYCS	Delta-1-pyrroline-5-carboxylate synthase (P5CS) (Aldehyde dehydrogenase family 18 member A1) [Includes: Glutamate 5-kinase (GK) (EC 2.7.2.11) (Gamma-glutamyl kinase); Gamma-glutamyl phosphate reductase (GPR) (EC 1.2.1.41) (Glutamate-5-semialdehyde dehydrogenase) (Glutamyl-gamma-semialdehyde dehydrogenase)]	-7,33
Q13613	MTMR1	Myotubularin-related protein 1 (Phosphatidylinositol-3,5-bisphosphate 3-phosphatase) (EC 3.1.3.95) (Phosphatidylinositol-3-phosphate phosphatase) (EC 3.1.3.64)	-7,09
P46926	GNPDA1 GNPI HLN KIAA0060	Glucosamine-6-phosphate isomerase 1 (EC 3.5.99.6) (Glucosamine-6-phosphate deaminase 1) (GNPDA 1) (GlcN6P deaminase 1) (Oscillin)	-7,05
Q8TDQ7	GNPDA2 GNP2	Glucosamine-6-phosphate isomerase 2 (EC 3.5.99.6) (Glucosamine-6-phosphate deaminase 2) (GNPDA 2) (GlcN6P deaminase 2) (Glucosamine-6-phosphate isomerase SB52)	-7,05
P49189	ALDH9A1 ALDH4 ALDH7 ALDH9	4-trimethylaminobutyraldehyde dehydrogenase (TMABA-DH) (TMABALDH) (EC 1.2.1.47) (Aldehyde dehydrogenase E3 isozyme) (Aldehyde dehydrogenase family 9 member A1) (EC 1.2.1.3) (Gamma-aminobutyraldehyde dehydrogenase) (EC 1.2.1.19) (R-aminobutyraldehyde dehydrogenase) [Cleaved into: 4-trimethylaminobutyraldehyde dehydrogenase, N-terminally processed]	-6,88
P78330	PSPH	Phosphoserine phosphatase (PSP) (PSPase) (EC 3.1.3.3) (L-3-phosphoserine phosphatase) (O-	-6,87

Uniprot ID	Gene name(s)	Protein name(s)	Re-weighted M Scores
		phosphoserine phosphohydrolase)	
P35520	CBS	Cystathionine beta-synthase (EC 4.2.1.22) (Beta-thionase) (Serine sulfhydrase)	-6,75
P04406	GAPDH GAPD CDABP0047 OK/SW-cl.12	Glyceraldehyde-3-phosphate dehydrogenase (GAPDH) (EC 1.2.1.12) (Peptidyl-cysteine S-nitrosylase GAPDH) (EC 2.6.99.-)	-6,61
P0C7M7	ACSM4	Acyl-coenzyme A synthetase ACSM4, mitochondrial (EC 6.2.1.2) (Acyl-CoA synthetase medium-chain family member 4)	-6,51
Q96GR2	ACSBG1 BGM KIAA0631 LPD	Long-chain-fatty-acid—CoA ligase ACSBG1 (EC 6.2.1.3) (Acyl-CoA synthetase bubblegum family member 1) (hBG1) (hsBG) (hsBGM) (Lipidosin)	-6,44
O15327	INPP4B	Inositol polyphosphate 4-phosphatase type II (Type II inositol 3,4-bisphosphate 4-phosphatase) (EC 3.1.3.66)	-6,42
Q96PE3	INPP4A	Inositol polyphosphate-4-phosphatase type I A (Inositol polyphosphate 4-phosphatase type I) (Type I inositol 3,4-bisphosphate 4-phosphatase) (EC 3.1.3.66)	-6,42
Q8WUK0	PTPMT1 MOSP PLIP PNAS-129	Phosphatidylglycerophosphatase and protein-tyrosine phosphatase 1 (EC 3.1.3.27) (PTEN-like phosphatase) (Phosphoinositide lipid phosphatase) (Protein-tyrosine phosphatase mitochondrial 1) (EC 3.1.3.16) (EC 3.1.3.48)	-6,34
P51688	SGSH HSS	N-sulphoglucosamine sulphohydrolase (EC 3.10.1.1) (Sulfoglucosamine sulfamidase) (Sulphamidase)	-6,26
Q6ZVK8	NUDT18 MTH3	8-oxo-dGDP phosphatase NUDT18 (EC 3.6.1.58) (2-hydroxy-dADP phosphatase) (7,8-dihydro-8-oxoguanine phosphatase) (MutT homolog 3) (Nucleoside diphosphate-linked moiety X motif 18) (Nudix motif 18)	-6,1
Q6ZNW5	GDPGP1 C15orf58	GDP-D-glucose phosphorylase 1 (EC 2.7.7.78)	-6,07
P11498	PC	Pyruvate carboxylase, mitochondrial (EC 6.4.1.1) (Pyruvic carboxylase) (PCB)	-6,04
P16930	FAH	Fumarylacetoacetase (FAA) (EC 3.7.1.2) (Beta-diketonase) (Fumarylacetoacetate hydrolase)	-6,04
Q9BVG9	PTDSS2 PSS2	Phosphatidylserine synthase 2 (PSS-2) (PtdSer synthase 2) (EC 2.7.8.29) (Serine-exchange enzyme	-5,92

Uniprot ID	Gene name(s)	Protein name(s)	Re-weighted M Scores
		II)	
Q6YP21	KYAT3 CCBL2 KAT3	Kynurenine—oxoglutarate transaminase 3 (EC 2.6.1.7) (Cysteine-S-conjugate beta-lyase 2) (EC 4.4.1.13) (Kynurenine aminotransferase 3) (Kynurenine aminotransferase III) (KATIII) (Kynurenine—glyoxylate transaminase) (EC 2.6.1.63) (Kynurenine—oxoglutarate transaminase III)	-5,89
P23743	DGKA DAGK DAGK1	Diacylglycerol kinase alpha (DAG kinase alpha) (EC 2.7.1.107) (80 kDa diacylglycerol kinase) (Diglyceride kinase alpha) (DGK-alpha)	-5,88
Q92835	INPP5D SHIP SHIP1	Phosphatidylinositol 3,4,5-trisphosphate 5-phosphatase 1 (EC 3.1.3.86) (Inositol polyphosphate-5-phosphatase D) (EC 3.1.3.56) (Inositol polyphosphate-5-phosphatase of 145 kDa) (SIP-145) (Phosphatidylinositol 4,5-bisphosphate 5-phosphatase) (EC 3.1.3.36) (SH2 domain-containing inositol 5'-phosphatase 1) (SH2 domain-containing inositol phosphatase 1) (SHIP-1) (p150Ship) (hp51CN)	-5,83
P15104	GLUL GLNS	Glutamine synthetase (GS) (EC 6.3.1.2) (Glutamate—ammonia ligase) (Palmitoyltransferase GLUL) (EC 2.3.1.225)	-5,77
P00492	HPRT1 HPRT	Hypoxanthine-guanine phosphoribosyltransferase (HGPRT) (HGPRTase) (EC 2.4.2.8)	-5,65
Q9Y227	ENTPD4 KIAA0392 LALP70 LYSAL1	Ectonucleoside triphosphate diphosphohydrolase 4 (NTPDase 4) (EC 3.6.1.15) (EC 3.6.1.6) (Golgi UDPase) (Lysosomal apyrase-like protein of 70 kDa) (Uridine-diphosphatase) (UDPase) (EC 3.6.1.42)	-5,63
Q9UKK9	NUDT5 NUDIX5 HSPC115	ADP-sugar pyrophosphatase (EC 3.6.1.13) (8-oxo-dGDP phosphatase) (EC 3.6.1.58) (Nuclear ATP-synthesis protein NUDIX5) (EC 2.7.7.96) (Nucleoside diphosphate-linked moiety X motif 5) (Nudix motif 5) (hNUDT5) (YSA1H)	-5,50
Q8NFU5	IPMK IMPK	Inositol polyphosphate multikinase (EC 2.7.1.140) (EC 2.7.1.151) (EC 2.7.1.153) (Inositol 1,3,4,6-tetrakisphosphate 5-kinase)	-5,46
Q9UK39	NOCT CCR4 CCRN4L NOC	Nocturnin (EC 3.1.3.108) (Carbon catabolite repression 4-like protein)	-5,42
Q9UKG9	CROT COT	Peroxisomal carnitine O-octanoyltransferase (COT) (EC 2.3.1.137)	-5,35
P17050	NAGA	Alpha-N-acetylgalactosaminidase (EC 3.2.1.49) (Alpha-galactosidase B)	-5,22

Uniprot ID	Gene name(s)	Protein name(s)	Re-weighted M Scores
Q96J66	ABCC11 MRP8	ATP-binding cassette sub-family C member 11 (EC 7.6.2.2) (EC 7.6.2.3) (Multidrug resistance-associated protein 8)	-5,10
Q8IVS8	GLYCTK HBEBP4 LP5910	Glycerate kinase (EC 2.7.1.31) (HbeAg-binding protein 4)	-4,99
P22234	PAICS ADE2 AIRC PAIS	Multifunctional protein ADE2 [Includes: Phosphoribosylaminoimidazole-succinocarboxamide synthase (EC 6.3.2.6) (SAICAR synthetase); Phosphoribosylaminoimidazole carboxylase (EC 4.1.1.21) (AIR carboxylase) (AIRC)]	-4,97
Q03426	MVK	Mevalonate kinase (MK) (EC 2.7.1.36)	-4,96
Q08AH1	ACSM1 BUCS1 LAE MACS1	Acyl-coenzyme A synthetase ACSM1, mitochondrial (EC 6.2.1.2) (Acyl-CoA synthetase medium-chain family member 1) (Benzoate—CoA ligase) (EC 6.2.1.25) (Butyrate—CoA ligase 1) (Butyryl-coenzyme A synthetase 1) (Lipoate-activating enzyme) (Middle-chain acyl-CoA synthetase 1) (Xenobiotic/medium-chain fatty acid-CoA ligase HXM-B)	-4,93
Q9UHJ6	SHPK CARKL	Sedoheptulokinase (SHK) (EC 2.7.1.14) (Carbohydrate kinase-like protein)	-4,81
O15438	ABCC3 CMOAT2 MLP2 MRP3	ATP-binding cassette sub-family C member 3 (EC 7.6.2.-) (EC 7.6.2.2) (EC 7.6.2.3) (Canalicular multispecific organic anion transporter 2) (Multi-specific organic anion transporter D) (MOAT-D) (Multidrug resistance-associated protein 3)	-4,74
Q8N0W3	FCSK FUK	L-fucose kinase (Fucokinase) (EC 2.7.1.52)	-4,73
O14734	ACOT8 ACTEIII PTE1	Acyl-coenzyme A thioesterase 8 (Acyl-CoA thioesterase 8) (EC 3.1.2.1) (EC 3.1.2.11) (EC 3.1.2.2) (EC 3.1.2.3) (EC 3.1.2.5) (Choloyl-coenzyme A thioesterase) (EC 3.1.2.27) (HIV-Nef-associated acyl-CoA thioesterase) (Peroxisomal acyl-CoA thioesterase 2) (PTE-2) (Peroxisomal acyl-coenzyme A thioester hydrolase 1) (PTE-1) (Peroxisomal long-chain acyl-CoA thioesterase 1) (Thioesterase II) (hACTE-III) (hACTEIII) (I)	-4,72
Q9ULI2	RIMKLB FAM80B KIAA1238	Beta-citrylglutamate synthase B (EC 6.3.1.17) (N-acetyl-aspartylglutamate synthetase B) (NAAG synthetase B) (NAAGS) (EC 6.3.2.41) (Ribosomal protein S6 modification-like protein B)	-4,61
Q13614	MTMR2 KIAA1073	Myotubularin-related protein 2 (Phosphatidylinositol-3,5-bisphosphate 3-phosphatase) (EC 3.1.3.95) (Phosphatidylinositol-3-phosphate phosphatase) (EC 3.1.3.64)	-4,57
Q9Y217	MTMR6	Myotubularin-related protein 6 (Phosphatidylinositol-3,5-bisphosphate 3-phosphatase) (EC	-4,57

Uniprot ID	Gene name(s)	Protein name(s)	Re-weighted M Scores
		3.1.3.95) (Phosphatidylinositol-3-phosphate phosphatase) (EC 3.1.3.64)	
O95477	ABCA1 ABC1 CERP	Phospholipid-transporting ATPase ABCA1 (EC 7.6.2.1) (ATP-binding cassette sub-family A member 1) (ATP-binding cassette transporter 1) (ABC-1) (ATP-binding cassette 1) (Cholesterol efflux regulatory protein)	-4,54
Q9HBH1	PDF PDF1A	Peptide deformylase, mitochondrial (EC 3.5.1.88) (Polypeptide deformylase)	-4,53
P53597	SUCLG1	Succin—e--CoA ligase [ADP/GDP-forming] subunit alpha, mitochondrial (EC 6.2.1.4) (EC 6.2.1.5) (Succinyl-CoA synthetase subunit alpha) (SCS-alpha)	-4,52
Q9NPJ3	ACOT13 THEM2 HT012 PNAS-27	Acyl-coenzyme A thioesterase 13 (Acyl-CoA thioesterase 13) (EC 3.1.2.-) (Hotdog-fold thioesterase superfamily member 2) (Palmitoyl-CoA hydrolase) (EC 3.1.2.2) (Thioesterase superfamily member 2) (THEM2) [Cleaved into: Acyl-coenzyme A thioesterase 13, N-terminally processed]	-4,32
P49619	DGKG DAGK3	Diacylglycerol kinase gamma (DAG kinase gamma) (EC 2.7.1.107) (Diglyceride kinase gamma) (DGK-gamma)	-4,31
Q9Y6T7	DGKB DAGK2 KIAA0718	Diacylglycerol kinase beta (DAG kinase beta) (EC 2.7.1.107) (90 kDa diacylglycerol kinase) (Diglyceride kinase beta) (DGK-beta)	-4,31
Q8N9L9	ACOT4 PTE2B PTEIB	Peroxisomal succinyl-coenzyme A thioesterase (EC 3.1.2.3) (Acyl-coenzyme A thioesterase 4) (Acyl-CoA thioesterase 4) (EC 3.1.2.2) (PTE-2b) (Peroxisomal acyl coenzyme A thioester hydrolase Ib) (Peroxisomal long-chain acyl-CoA thioesterase Ib) (PTE-Ib)	-4,23
Q7Z2E3	APTX AXA1	Aprataxin (EC 3.6.1.71) (EC 3.6.1.72) (Forkhead-associated domain histidine triad-like protein) (FHA-HIT)	-4,15
Q8IY17	PNPLA6 NTE	Patatin-like phospholipase domain-containing protein 6 (EC 3.1.1.5) (Neuropathy target esterase)	-4,08
A0A024B7W1	0	Genome polyprotein [Cleaved into: Capsid protein C (Capsid protein) (Core protein); Protein prM (Precursor membrane protein); Peptide pr (Peptide precursor); Small envelope protein M (Matrix protein); Envelope protein E; Non-structural protein 1 (NS1); Non-structural protein 2A (NS2A); Serine protease subunit NS2B (Flavivirin protease NS2B regulatory subunit) (Non-structural protein 2B); Serine protease NS3 (EC 3.4.21.91) (EC 3.6.1.15) (EC 3.6.4.13) (Flavivirin protease NS3 catalytic subunit) (Non-structural protein 3); Non-structural protein 4A (NS4A); Peptide 2k; Non-	-3,97

Uniprot ID	Gene name(s)	Protein name(s)	Re-weighted M Scores
		structural protein 4B (NS4B); RNA-directed RNA polymerase NS5 (EC 2.1.1.56) (EC 2.1.1.57) (EC 2.7.7.48) (NS5)]	
A0A142I5B9	0	Genome polyprotein [Cleaved into: Capsid protein C (Capsid protein) (Core protein); Protein prM (Precursor membrane protein); Peptide pr (Peptide precursor); Small envelope protein M (Matrix protein); Envelope protein E; Non-structural protein 1 (NS1); Non-structural protein 2A (NS2A); Serine protease subunit NS2B (Flavivirin protease NS2B regulatory subunit) (Non-structural protein 2B); Serine protease NS3 (EC 3.4.21.91) (EC 3.6.1.15) (EC 3.6.4.13) (Flavivirin protease NS3 catalytic subunit) (Non-structural protein 3); Non-structural protein 4A (NS4A); Peptide 2k; Non-structural protein 4B (NS4B); RNA-directed RNA polymerase NS5 (EC 2.1.1.56) (EC 2.1.1.57) (EC 2.7.7.48) (NS5)]	-3,97
Q5T6J7	IDNK C9orf103	Probable gluconokinase (EC 2.7.1.12) (Gluconate kinase)	-3,87
Q16851	UGP2 UGP1	—P--glucose-1-phosphate uridylyltransferase (EC 2.7.7.9) (UDP-glucose pyrophosphorylase) (UDPGP) (UGPase)	-3,82
Q5T1C6	THEM4 CTMP	Acyl-coenzyme A thioesterase THEM4 (Acyl-CoA thioesterase THEM4) (EC 3.1.2.2) (Carboxyl-terminal modulator protein) (Thioesterase superfamily member 4)	-3,81
Q9UNQ0	ABCG2 ABCP BCRP BCRP1 MXR	Broad substrate specificity ATP-binding cassette transporter ABCG2 (EC 7.6.2.2) (ATP-binding cassette sub-family G member 2) (Breast cancer resistance protein) (CDw338) (Mitoxantrone resistance-associated protein) (Placenta-specific ATP-binding cassette transporter) (Urate exporter) (CD antigen CD338)	-3,78
P80108	GPLD1 PIGPLD1	Phosphatidylinositol-glycan-specific phospholipase D (PI-G PLD) (EC 3.1.4.50) (Glycoprotein phospholipase D) (Glycosyl-phosphatidylinositol-specific phospholipase D) (GPI-PLD) (GPI-specific phospholipase D)	-3,74
O00757	FBP2	Fructose-1,6-bisphosphatase isozyme 2 (FBPase 2) (EC 3.1.3.11) (D-fructose-1,6-bisphosphate 1-phosphohydrolase 2) (Muscle FBPase)	-3,50
P09467	FBP1 FBP	Fructose-1,6-bisphosphatase 1 (FBPase 1) (EC 3.1.3.11) (D-fructose-1,6-bisphosphate 1-phosphohydrolase 1) (Liver FBPase)	-3,50
P49441	INPP1	Inositol polyphosphate 1-phosphatase (IPP) (IPPase) (EC 3.1.3.57)	-3,50

Uniprot ID	Gene name(s)	Protein name(s)	Re-weighted M Scores
Q9NQ88	TIGAR C12orf5	Fructose-2,6-bisphosphatase TIGAR (EC 3.1.3.46) (TP53-induced glycolysis and apoptosis regulator) (TP53-induced glycolysis regulatory phosphatase)	-3,50
A6NDG6	PGP	Glycerol-3-phosphate phosphatase (G3PP) (EC 3.1.3.21) (Aspartate-based ubiquitous Mg(2+)-dependent phosphatase) (AUM) (EC 3.1.3.48) (Phosphoglycolate phosphatase) (PGP)	-3,49
P06865	HEXA	Beta-hexosaminidase subunit alpha (EC 3.2.1.52) (Beta-N-acetylhexosaminidase subunit alpha) (Hexosaminidase subunit A) (N-acetyl-beta-glucosaminidase subunit alpha)	-3,46
P07686	HEXB HCC7	Beta-hexosaminidase subunit beta (EC 3.2.1.52) (Beta-N-acetylhexosaminidase subunit beta) (Hexosaminidase subunit B) (Cervical cancer proto-oncogene 7 protein) (HCC-7) (N-acetyl-beta-glucosaminidase subunit beta) [Cleaved into: Beta-hexosaminidase subunit beta chain B; Beta-hexosaminidase subunit beta chain A]	-3,46
P33527	ABCC1 MRP MRP1	Multidrug resistance-associated protein 1 (EC 7.6.2.2) (ATP-binding cassette sub-family C member 1) (Glutathione-S-conjugate-translocating ATPase ABCC1) (EC 7.6.2.3) (Leukotriene C(4) transporter) (LTC4 transporter)	-3,41
Q9Y6X5	ENPP4 KIAA0879 NPP4	Bi’(5'-adenosyl)-triphosphatase ENPP4 (EC 3.6.1.29) (AP3A hydrolase) (AP3Aase) (Ectonucleotide pyrophosphatase/phosphodiesterase family member 4) (E-NPP 4) (NPP-4)	-3,38
Q99497	PARK7	Parkinson disease protein 7 (Maillard deglycase) (Oncogene DJ1) (Parkinsonism-associated deglycase) (Protein DJ-1) (DJ-1) (Protein/nucleic acid deglycase DJ-1) (EC 3.1.2.-) (EC 3.5.1.-) (EC 3.5.1.124)	-3,18
P19367	HK1	Hexokinase-1 (EC 2.7.1.1) (Brain form hexokinase) (Hexokinase type I) (HK I) (Hexokinase-A)	-3,11
Q9Y3R4	NEU2	Sialidase-2 (EC 3.2.1.18) (Cytosolic sialidase) (N-acetyl-alpha-neuraminidase 2)	-3,11
Q8NDL9	AGBL5 CCP5	Cytosolic carboxypeptidase-like protein 5 (EC 3.4.17.-) (EC 3.4.17.24) (ATP/GTP-binding protein-like 5) (Protein deglutamylase CCP5)	-3,04
O14772	FPGT GFPP	Fucose-1-phosphate guanylyltransferase (EC 2.7.7.30) (GDP-L-fucose diphosphorylase) (GDP-L-fucose pyrophosphorylase)	-2,95
Q9Y5P6	GMPPB	Mannose-1-phosphate guanyltransferase beta (EC 2.7.7.13) (GDP-mannose pyrophosphorylase B) (GTP-mannose-1-phosphate guanylyltransferase beta)	-2,95

Uniprot ID	Gene name(s)	Protein name(s)	Re-weighted M Scores
P14618	PKM OIP3 PK2 PK3 PKM2	Pyruvate kinase PKM (EC 2.7.1.40) (Cytosolic thyroid hormone-binding protein) (CTHBP) (Opa-interacting protein 3) (OIP-3) (Pyruvate kinase 2/3) (Pyruvate kinase muscle isozyme) (Thyroid hormone-binding protein 1) (THBP1) (Tumor M2-PK) (p58)	-2,91
P30613	PKLR PK1 PKL	Pyruvate kinase PKLR (EC 2.7.1.40) (Pyruvate kinase 1) (Pyruvate kinase isozymes L/R) (R-type/L-type pyruvate kinase) (Red cell/liver pyruvate kinase)	-2,91
Q9H993	ARMT1 C6orf211	Damage-control phosphatase ARMT1 (EC 3.1.3.-) (Acidic residue methyltransferase 1) (Protein-glutamate O-methyltransferase) (EC 2.1.1.-) (Sugar phosphate phosphatase ARMT1)	-2,44
Q01415	GALK2 GK2	N-acetylgalactosamine kinase (EC 2.7.1.157) (GalNAc kinase) (Galactokinase 2)	-1,69
Q9UJ70	NAGK	N-acetyl-D-glucosamine kinase (N-acetylglucosamine kinase) (EC 2.7.1.59) (GlcNAc kinase)	-1,69
Q96C11	FGGY	FGGY carbohydrate kinase domain-containing protein (D-ribulokinase FGGY) (EC 2.7.1.47)	-1,65
Q8TE04	PANK1 PANK	Pantothenate kinase 1 (hPanK) (hPanK1) (EC 2.7.1.33) (Pantothenic acid kinase 1)	-1,57
Q9BZ23	PANK2 C20orf48	Pantothenate kinase 2, mitochondrial (hPanK2) (EC 2.7.1.33) (Pantothenic acid kinase 2) [Cleaved into: Pantothenate kinase 2, mitochondrial intermediate form (iPanK2); Pantothenate kinase 2, mitochondrial mature form (mPanK2)]	-1,57
Q9H999	PANK3	Pantothenate kinase 3 (hPanK3) (EC 2.7.1.33) (Pantothenic acid kinase 3)	-1,57
O60825	PFKFB2	6-phosphofructo-2-kinase/fructose-2,6-bisphosphatase 2 (6PF-2-K/Fru-2,6-P2ase 2) (PFK/FBPase 2) (6PF-2-K/Fru-2,6-P2ase heart-type isozyme) [Includes: 6-phosphofructo-2-kinase (EC 2.7.1.105); Fructose-2,6-bisphosphatase (EC 3.1.3.46)]	-1,44
P16118	PFKFB1 F6PK PFRX	6-phosphofructo-2-kinase/fructose-2,6-bisphosphatase 1 (6PF-2-K/Fru-2,6-P2ase 1) (PFK/FBPase 1) (6PF-2-K/Fru-2,6-P2ase liver isozyme) [Includes: 6-phosphofructo-2-kinase (EC 2.7.1.105); Fructose-2,6-bisphosphatase (EC 3.1.3.46)]	-1,44
Q16875	PFKFB3	6-phosphofructo-2-kinase/fructose-2,6-bisphosphatase 3 (6PF-2-K/Fru-2,6-P2ase 3) (PFK/FBPase 3) (6PF-2-K/Fru-2,6-P2ase brain/placenta-type isozyme) (Renal carcinoma antigen NY-REN-56) (iPFK-2) [Includes: 6-phosphofructo-2-kinase (EC 2.7.1.105); Fructose-2,6-bisphosphatase (EC 3.1.3.46)]	-1,44

Uniprot ID	Gene name(s)	Protein name(s)	Re-weighted M Scores
Q16877	PFKFB4	6-phosphofructo-2-kinase/fructose-2,6-bisphosphatase 4 (6PF-2-K/Fru-2,6-P2ase 4) (PFK/FBPase 4) (6PF-2-K/Fru-2,6-P2ase testis-type isozyme) [Includes: 6-phosphofructo-2-kinase (EC 2.7.1.105); Fructose-2,6-bisphosphatase (EC 3.1.3.46)]	-1,44
P05165	PCCA	Propionyl-CoA carboxylase alpha chain, mitochondrial (PCCase subunit alpha) (EC 6.4.1.3) (Propanoyl-CoA:carbon dioxide ligase subunit alpha)	-1,43
P05166	PCCB	Propionyl-CoA carboxylase beta chain, mitochondrial (PCCase subunit beta) (EC 6.4.1.3) (Propanoyl-CoA:carbon dioxide ligase subunit beta)	-1,43
P19174	PLCG1 PLC1	1-phosphatidylinositol 4,5-bisphosphate phosphodiesterase gamma-1 (EC 3.1.4.11) (PLC-148) (Phosphoinositide phospholipase C-gamma-1) (Phospholipase C-II) (PLC-II) (Phospholipase C-gamma-1) (PLC-gamma-1)	-1,34
P51178	PLCD1	1-phosphatidylinositol 4,5-bisphosphate phosphodiesterase delta-1 (EC 3.1.4.11) (Phosphoinositide phospholipase C-delta-1) (Phospholipase C-III) (PLC-III) (Phospholipase C-delta-1) (PLC-delta-1)	-1,34
Q00722	PLCB2	1-phosphatidylinositol 4,5-bisphosphate phosphodiesterase beta-2 (EC 3.1.4.11) (Phosphoinositide phospholipase C-beta-2) (Phospholipase C-beta-2) (PLC-beta-2)	-1,34
Q01970	PLCB3	1-phosphatidylinositol 4,5-bisphosphate phosphodiesterase beta-3 (EC 3.1.4.11) (Phosphoinositide phospholipase C-beta-3) (Phospholipase C-beta-3) (PLC-beta-3)	-1,34
Q15147	PLCB4	1-phosphatidylinositol 4,5-bisphosphate phosphodiesterase beta-4 (EC 3.1.4.11) (Phosphoinositide phospholipase C-beta-4) (Phospholipase C-beta-4) (PLC-beta-4)	-1,34
Q9BRC7	PLCD4	1-phosphatidylinositol 4,5-bisphosphate phosphodiesterase delta-4 (hPLCD4) (EC 3.1.4.11) (Phosphoinositide phospholipase C-delta-4) (Phospholipase C-delta-4) (PLC-delta-4)	-1,34
Q9NQ66	PLCB1 KIAA0581	1-phosphatidylinositol 4,5-bisphosphate phosphodiesterase beta-1 (EC 3.1.4.11) (PLC-154) (Phosphoinositide phospholipase C-beta-1) (Phospholipase C-I) (PLC-I) (Phospholipase C-beta-1) (PLC-beta-1)	-1,34
Q9UQ49	NEU3	Sialidase-3 (EC 3.2.1.18) (Ganglioside sialidasedis) (Membrane sialidase) (N-acetyl-alpha-neuraminidase 3)	-1,14

Uniprot ID	Gene name(s)	Protein name(s)	Re-weighted M Scores
O95861	BPNT’	3’(2’’,5'-bisphosphate nucleotidase 1 (EC 3.1.3.7) (Bisphosphat’ 3'-nucleotidase 1) (PAP-inositol 1,4-phosphatase) (PIP)	-1,04
P49903	SEPHS1 SELD SPS SPS1	Selenide, water dikinase 1 (EC 2.7.9.3) (Selenium donor protein 1) (Selenophosphate synthase 1)	-1,04
Q99611	SEPHS2 SPS2	Selenide, water dikinase 2 (EC 2.7.9.3) (Selenium donor protein 2) (Selenophosphate synthase 2)	-1,04
Q9NX62	BPNT2 IMPA3 IMPAD1	Golgi-resident adenosin’ 3’,5'-bisphosphat’ 3'-phosphatase (Golgi-resident PAP phosphatase) (gPAPP) (EC 3.1.3.7)’(3’(2')’ 5'-bisphosphate nucleotidase 2) (Inositol monophosphatase domain-containing protein 1) (Myo-inositol monophosphatase A3) (Phosphoadenosine phosphat’ 3'-nucleotidase)	-1,04
P32189	GK	Glycerol kinase (GK) (Glycerokinase) (EC 2.7.1.30) (ATP:glycerol 3-phosphotransferase)	-0,93
Q14409	GK3P GKP3 GKTB	Glycerol kinase 3 (GK 3) (Glycerokinase 3) (EC 2.7.1.30) (ATP:glycerol 3-phosphotransferase 3) (Glycerol kinase 3 pseudogene) (Glycerol kinase, testis specific 1)	-0,93
Q14410	GK2 GKP2 GKTA	Glycerol kinase 2 (GK 2) (Glycerokinase 2) (EC 2.7.1.30) (ATP:glycerol 3-phosphotransferase 2) (Glycerol kinase, testis specific 2)	-0,93
Q6ZS86	GK5	Putative glycerol kinase 5 (GK 5) (Glycerokinase 5) (EC 2.7.1.30) (ATP:glycerol 3-phosphotransferase 5)	-0,93
Q9BVA6	FICD HIP13 HYPE UNQ3041/PRO9857	Protein adenylyltransferase FICD (EC 2.7.7.n1) (AMPylator FICD) (De-AMPylase FICD) (EC 3.1.4.-) (FIC domain-containing protein) (Huntingtin yeast partner E) (Huntingtin-interacting protein 13) (HIP-13) (Huntingtin-interacting protein E)	-0,70
Q6EMB2	TTLL5 KIAA0998 STAMP	Tubulin polyglutamylase TTLL5 (EC 6.3.2.-) (SRC1 and TIF2-associated modulatory protein) (STAMP protein) (Tubu—n--tyrosine ligase-like protein 5)	-0,67
Q6ZT98	TTLL7	Tubulin polyglutamylase TTLL7 (EC 6.3.2.-) (Testis development protein NYD-SP30) (Tubu—n--tyrosine ligase-like protein 7)	-0,67
Q8N841	TTLL6 TTL.6	Tubulin polyglutamylase TTLL6 (EC 6.3.2.-) (Protein polyglutamylase TTLL6) (Tubu—n--tyrosine ligase-like protein 6)	-0,67
Q8NHH1	TTLL11 C9orf20	Tubulin polyglutamylase TTLL11 (EC 6.3.2.-) (Tubu—n--tyrosine ligase-like protein 11)	-0,67

Uniprot ID	Gene name(s)	Protein name(s)	Re-weighted M Scores
P30215	HE 2b	Hemagglutinin-esterase (HE protein) (EC 3.1.1.53) (E3 glycoprotein)	-0,60
Q0ZME8	HE 2	Hemagglutinin-esterase (HE protein) (EC 3.1.1.53) (E3 glycoprotein)	-0,60
Q14EB1	HE 2	Hemagglutinin-esterase (HE protein) (EC 3.1.1.53) (E3 glycoprotein)	-0,60
Q5MQD1	HE 2	Hemagglutinin-esterase (HE protein) (EC 3.1.1.53) (E3 glycoprotein)	-0,60
Q9HAT2	SIAE YSG2	Sialate O-acetylesterase (EC 3.1.1.53) (H-Lse) (Sialic acid-specific 9-O-acetylesterase)	-0,60
Q9Q9G3	HE	Hemagglutinin-esterase (HE protein) (EC 3.1.1.53) (E3 glycoprotein)	-0,60
O76074	PDE5A PDE5	cGMP-specifi’ 3’,5'-cyclic phosphodiesterase (EC 3.1.4.35) (cGMP-binding cGMP-specific phosphodiesterase) (CGB-PDE)	-0,49
O76083	PDE9A	High affinity cGMP-specifi’ 3’,5'-cyclic phosphodiesterase 9A (EC 3.1.4.35)	-0,49
P16499	PDE6A PDEA	Rod cGMP-specifi’ 3’,5'-cyclic phosphodiesterase subunit alpha (GMP-PDE alpha) (EC 3.1.4.35) (PDE V-B1)	-0,49
P18545	PDE6G PDEG	Retinal rod rhodopsin-sensitive cGM’ 3’,5'-cyclic phosphodiesterase subunit gamma (GMP-PDE gamma) (EC 3.1.4.35)	-0,49
P35913	PDE6B PDEB	Rod cGMP-specifi’ 3’,5'-cyclic phosphodiesterase subunit beta (GMP-PDE beta) (EC 3.1.4.35)	-0,49
P51160	PDE6C PDEA2	Cone cGMP-specifi’ 3’,5'-cyclic phosphodiesterase subunit al’ha' (EC 3.1.4.35) (cGMP phosphodiesterase 6C)	-0,49
Q13956	PDE6H	Retinal cone rhodopsin-sensitive cGM’ 3’,5'-cyclic phosphodiesterase subunit gamma (GMP-PDE gamma) (EC 3.1.4.35)	-0,49
Q99755	PIP5K1A	Phosphatidylinositol 4-phosphate 5-kinase type-1 alpha (PIP5K1-alpha) (PtdIns(4)P-5-kinase 1 alpha) (EC 2.7.1.68) (68 kDa type I phosphatidylinositol 4-phosphate 5-kinase alpha) (Phosphatidylinositol 4-phosphate 5-kinase type I alpha) (PIp5KIalpha)	-0,33
P52429	DGKE DAGK5	Diacylglycerol kinase epsilon (DAG kinase epsilon) (EC 2.7.1.107) (Diglyceride kinase epsilon) (DGK-epsilon)	-0,33
Q9NP58	ABCB6 MTABC3 PRP	ATP-binding cassette sub-family B member 6 (ABC-type heme transporter ABCB6) (EC 7.6.2.5)	-0,24

Uniprot ID	Gene name(s)	Protein name(s)	Re-weighted M Scores
	UMAT	(Mitochondrial ABC transporter 3) (Mt-ABC transporter 3) (P-glycoprotein-related protein) (Ubiquitously-expressed mammalian ABC half transporter)	

Supplementary table 2: Enzymes of down-regulated metabolites in phase 1 and 2

Uniprot ID	Gene name(s)	Protein name(s)	Re-weighted M Scores
P22310	UGT1A4 GNT1 UGT1	UDP-glucuronosyltransferase 1A4 (UGT1A4) (EC 2.4.1.17) (Bilirubin-specific UDPGT isozyme 2) (hUG-BR2) (UDP-glucuronosyltransferase 1-4) (UDPGT 1-4) (UGT1*4) (UGT1-04) (UGT1.4) (UDP-glucuronosyltransferase 1-D) (UGT-1D) (UGT1D)	-8,63
Q9NQR4	NIT2 CUA002	Omega-amidase NIT2 (EC 3.5.1.3) (Nitrilase homolog 2)	-7,91
Q99489	DDO	D-aspartate oxidase (DASOX) (DDO) (EC 1.4.3.1)	-7,27
Q8N0X4	CLYBL CLB	Citramalyl-CoA lyase, mitochondrial (EC 4.1.3.25) ((3S)-malyl-CoA thioesterase) (EC 3.1.2.30) (Beta-methylmalate synthase) (EC 2.3.3.-) (Citrate lyase subunit beta-like protein) (Citrate lyase beta-like) (Malate synthase) (EC 2.3.3.9)	-7,02
Q6NVY1	HIBCH	3-hydroxyisobutyryl-CoA hydrolase, mitochondrial (EC 3.1.2.4) (3-hydroxyisobutyryl-coenzyme A hydrolase) (HIB-CoA hydrolase) (HIBYL-CoA-H)	-5,60
O43772	SLC25A20 CAC CACT	Mitochondrial carnitine/acylcarnitine carrier protein (Carnitine/acylcarnitine translocase) (CAC) (Solute carrier family 25 member 20)	-5,16
P54803	GALC	Galactocerebrosidase (GALCERase) (EC 3.2.1.46) (Galactocerebroside beta-galactosidase) (Galactosylceramidase) (Galactosylceramide beta-galactosidase)	-4,72
O00154	ACOT7 BACH	Cytosolic acyl coenzyme A thioester hydrolase (EC 3.1.2.2) (Acyl-CoA thioesterase 7) (Brain acyl-CoA hydrolase) (BACH) (hBACH) (CTE-IIa) (CTE-II) (Long chain acyl-CoA thioester hydrolase)	-4,47

Uniprot ID	Gene name(s)	Protein name(s)	Re-weighted M Scores
Q86VF5	MOGAT3 DC7 DGAT2L7 UNQ9383/PRO34208	2-acylglycerol O-acyltransferase 3 (EC 2.3.1.20) (EC 2.3.1.22) (Acyl-CoA:monoacylglycerol acyltransferase 3) (MGAT3) (Diacylglycerol O-acyltransferase candidate 7) (hDC7) (Diacylglycerol acyltransferase 2-like protein 7) (Monoacylglycerol O-acyltransferase 3)	-4,45
P54317	PNLIPRP2 PLRP2	Pancreatic lipase-related protein 2 (PL-RP2) (Cytotoxic T lymphocyte lipase) (Galactolipase) (EC 3.1.1.26) (Triacylglycerol lipase) (EC 3.1.1.3)	-4,28
P00367	GLUD1 GLUD	Glutamate dehydrogenase 1, mitochondrial (GDH 1) (EC 1.4.1.3)	-4,21
P49448	GLUD2 GLUDP1	Glutamate dehydrogenase 2, mitochondrial (GDH 2) (EC 1.4.1.3)	-4,21
P11509	CYP2A6 CYP2A3	Cytochrome P450 2A6 (EC 1.14.14.-) (1,4-cineole 2-exo-monooxygenase) (CYPIIA6) (Coumarin 7-hydroxylase) (Cytochrome P450 IIA3) (Cytochrome P450(I))	-4,15
P54868	HMGCS2	Hydroxymethylglutaryl-CoA synthase, mitochondrial (HMG-CoA synthase) (EC 2.3.3.10) (3-hydroxy-3-methylglutaryl coenzyme A synthase)	-4,00
Q01581	HMGCS1 HMGCS	Hydroxymethylglutaryl-CoA synthase, cytoplasmic (HMG-CoA synthase) (EC 2.3.3.10) (3-hydroxy-3-methylglutaryl coenzyme A synthase)	-4,00
Q15493	RGN SMP30	Regucalcin (RC) (Gluconolactonase) (GNL) (EC 3.1.1.17) (Senescence marker protein 30) (SMP-30)	-3,92
A6ND91	ASPDH	Putative L-aspartate dehydrogenase (EC 1.4.1.21) (Aspartate dehydrogenase domain-containing protein)	-3,92
Q9NVV5	AIG1 CGI-103	Androgen-induced gene 1 protein (AIG-1) (Fatty acid esters of hydroxy fatty acids hydrolase AIG1) (FAHFA hydrolase AIG1) (EC 3.1.-.-)	-3,86
Q8WXI4	ACOT11 BFIT KIAA0707 THEA	Acyl-coenzyme A thioesterase 11 (Acyl-CoA thioesterase 11) (EC 3.1.2.-) (Acyl-CoA thioester hydrolase 11) (Adipose-associated thioesterase) (Brown fat-inducible thioesterase) (BFIT) (Palmitoyl-coenzyme A thioesterase) (EC 3.1.2.2)	-3,81
O75390	CS	Citrate synthase, mitochondrial (EC 2.3.3.1) (Citrate (Si)-synthase)	-3,75
Q53FZ2	ACSM3 SAH	Acyl-coenzyme A synthetase ACSM3, mitochondrial (EC 6.2.1.2) (Acyl-CoA synthetase medium-chain family member 3) (Butyrate--CoA ligase 3) (Butyryl-coenzyme A synthetase 3) (Middle-chain acyl-CoA synthetase 3) (Propionate--CoA ligase) (EC 6.2.1.17) (Protein SA homolog)	-3,61

Uniprot ID	Gene name(s)	Protein name(s)	Re-weighted M Scores
Q68D91	MBLAC2	Acyl-coenzyme A thioesterase MBLAC2 (Acyl-CoA thioesterase MBLAC2) (EC 3.1.2.2) (Beta-lactamase MBLAC2) (EC 3.5.2.6) (Metallo-beta-lactamase domain-containing protein 2) (Palmitoyl-coenzyme A thioesterase MBLAC2)	-3,56
P08910	ABHD2 LABH2	Monoacylglycerol lipase ABHD2 (EC 3.1.1.23) (2-arachidonoylglycerol hydrolase) (Abhydrolase domain-containing protein 2) (Acetylesterase) (EC 3.1.1.6) (Lung alpha/beta hydrolase 2) (Progesterone-sensitive lipase) (EC 3.1.1.79) (Protein PHPS1-2)	-3,53
Q8WYK0	ACOT12 CACH CACH1 STARD15	Acetyl-coenzyme A thioesterase (EC 3.1.2.1) (Acyl-CoA thioester hydrolase 12) (Acyl-coenzyme A thioesterase 12) (Acyl-CoA thioesterase 12) (Cytoplasmic acetyl-CoA hydrolase 1) (CACH-1) (hCACH-1) (START domain-containing protein 15) (StARD15)	-3,44
P42765	ACAA2	3-ketoacyl-CoA thiolase, mitochondrial (EC 2.3.1.16) (Acetyl-CoA acetyltransferase) (EC 2.3.1.9) (Acetyl-CoA acyltransferase) (Acyl-CoA hydrolase, mitochondrial) (EC 3.1.2.-) (EC 3.1.2.1) (EC 3.1.2.2) (Beta-ketothiolase) (Mitochondrial 3-oxoacyl-CoA thiolase) (T1)	-3,21
O95237	LRAT	Lecithin retinol acyltransferase (EC 2.3.1.135) (Phosphatidylcholine--retinol O-acyltransferase)	-2,64
P21217	FUT3 FT3B LE	3-galactosyl-N-acetylglucosaminide 4-alpha-L-fucosyltransferase FUT3 (EC 2.4.1.65) (Alpha-3-fucosyltransferase FUT3) (EC 2.4.1.-) (Blood group Lewis alpha-4-fucosyltransferase) (Lewis FT) (Fucosyltransferase 3) (Fucosyltransferase III) (FucT-III)	-1,96
Q16880	UGT8 CGT UGT4	2-hydroxyacylsphingosine 1-beta-galactosyltransferase (EC 2.4.1.47) (Ceramide UDP-galactosyltransferase) (Cerebroside synthase) (UDP-galactose-ceramide galactosyltransferase)	-1,46
O43175	PHGDH PGDH3	D-3-phosphoglycerate dehydrogenase (3-PGDH) (EC 1.1.1.95) (2-oxoglutarate reductase) (EC 1.1.1.399) (Malate dehydrogenase) (EC 1.1.1.37)	3,03

Supplementary table 3: Enzymes of up-regulated metabolites in phase 1 and 2

Uniprot ID	Gene name(s)	Protein name(s)	Re-weighted M Scores
P35558	PCK1 PEPCK1	Phosphoenolpyruvate carboxykinase, cytosolic [GTP] (PEPCK-C) (EC 4.1.1.32) (Serine-protein kinase PCK1) (EC 2.7.11.-)	-6,16
P31327	CPS1	Carbamoyl-phosphate synthase [ammonia], mitochondrial (EC 6.3.4.16) (Carbamoyl-phosphate synthetase I) (CPSase I)	-5,29
Q9BT40	INPP5K PPS SKIP	Inositol polyphosphate 5-phosphatase K (EC 3.1.3.56) (Phosphatidylinositol-3,4,5-trisphosphate 5-phosphatase) (EC 3.1.3.86) (Phosphatidylinositol-4,5-bisphosphate 5-phosphatase) (EC 3.1.3.36) (Skeletal muscle and kidney-enriched inositol phosphatase)	-4,93
Q15392	DHCR24 KIAA0018	Delta(24)-sterol reductase (EC 1.3.1.72) (24-dehydrocholesterol reductase) (3-beta-hydroxysterol Delta-24-reductase) (Diminuto/dwarf1 homolog) (Seladin-1)	-4,26
Q9UBM7	DHCR7 D7SR	7-dehydrocholesterol reductase (7-DHC reductase) (EC 1.3.1.21) (Delta7-sterol reductase) (Sterol Delta(7)-reductase) (Sterol reductase SR-2)	-3,34
O76062	TM7SF2 ANG1	Delta(14)-sterol reductase TM7SF2 (Delta-14-SR) (EC 1.3.1.70) (3-beta-hydroxysterol Delta (14)-reductase) (Another new gene 1 protein) (C-14 sterol reductase) (C14SR) (Putative sterol reductase SR-1) (Sterol C14-reductase) (Transmembrane 7 superfamily member 2)	-1,94
Q14739	LBR	Delta(14)-sterol reductase LBR (Delta-14-SR) (EC 1.3.1.70) (3-beta-hydroxysterol Delta (14)-reductase) (C-14 sterol reductase) (C14SR) (Integral nuclear envelope inner membrane protein) (LMN2R) (Lamin-B receptor) (Sterol C14-reductase)	-1,94
P11908	PRPS2	Ribose-phosphate pyrophosphokinase 2 (EC 2.7.6.1) (PPRibP) (Phosphoribosyl pyrophosphate synthase II) (PRS-II)	-1,12
P21108	PRPS1L1 PRPS3 PRPSL	Ribose-phosphate pyrophosphokinase 3 (EC 2.7.6.1) (Phosphoribosyl pyrophosphate synthase 1-like 1) (PRPS1-like 1) (Phosphoribosyl pyrophosphate synthase III) (PRS-III)	-1,12

Uniprot ID	Gene name(s)	Protein name(s)	Re-weighted M Scores
P60891	PRPS1	Ribose-phosphate pyrophosphokinase 1 (EC 2.7.6.1) (PPRibP) (Phosphoribosyl pyrophosphate synthase I) (PRS-I)	-1,12
A4ZCW6	-	Protein VP3 [Includes: 2',5'-phosphodiesterase (EC 3.1.4.-); mRNA guanylyltransferase (EC 2.7.7.50); mRNA (guanine-N(7))-methyltransferase (EC 2.1.1.56)]	0,29
A7J392	-	Protein VP3 [Includes: 2',5'-phosphodiesterase (EC 3.1.4.-); mRNA guanylyltransferase (EC 2.7.7.50); mRNA (guanine-N(7))-methyltransferase (EC 2.1.1.56)]	0,29
A7J3A4	-	Protein VP3 [Includes: 2',5'-phosphodiesterase (EC 3.1.4.-); mRNA guanylyltransferase (EC 2.7.7.50); mRNA (guanine-N(7))-methyltransferase (EC 2.1.1.56)]	0,29
B1NKR1	-	Protein VP3 [Includes: 2',5'-phosphodiesterase (EC 3.1.4.-); mRNA guanylyltransferase (EC 2.7.7.50); mRNA (guanine-N(7))-methyltransferase (EC 2.1.1.56)]	0,29
B1NKR5	-	Protein VP3 [Includes: 2',5'-phosphodiesterase (EC 3.1.4.-); mRNA guanylyltransferase (EC 2.7.7.50); mRNA (guanine-N(7))-methyltransferase (EC 2.1.1.56)]	0,29
B1NKS7	-	Protein VP3 [Includes: 2',5'-phosphodiesterase (EC 3.1.4.-); mRNA guanylyltransferase (EC 2.7.7.50); mRNA (guanine-N(7))-methyltransferase (EC 2.1.1.56)]	0,29
B1NKT1	-	Protein VP3 [Includes: 2',5'-phosphodiesterase (EC 3.1.4.-); mRNA guanylyltransferase (EC 2.7.7.50); mRNA (guanine-N(7))-methyltransferase (EC 2.1.1.56)]	0,29
B1NKT9	-	Protein VP3 [Includes: 2',5'-phosphodiesterase (EC 3.1.4.-); mRNA guanylyltransferase (EC 2.7.7.50); mRNA (guanine-N(7))-methyltransferase (EC 2.1.1.56)]	0,29
B1NKU3	-	Protein VP3 [Includes: 2',5'-phosphodiesterase (EC 3.1.4.-); mRNA guanylyltransferase (EC 2.7.7.50); mRNA (guanine-N(7))-methyltransferase (EC 2.1.1.56)]	0,29
Q3ZK57	-	Protein VP3 [Includes: 2',5'-phosphodiesterase (EC 3.1.4.-); mRNA guanylyltransferase (EC 2.7.7.50); mRNA (guanine-N(7))-methyltransferase (EC 2.1.1.56)]	0,29
Q6WNW3	-	Protein VP3 [Includes: 2',5'-phosphodiesterase (EC 3.1.4.-); mRNA guanylyltransferase (EC 2.7.7.50); mRNA (guanine-N(7))-methyltransferase (EC 2.1.1.56)]	0,29
Q6WNW5	-	Protein VP3 [Includes: 2',5'-phosphodiesterase (EC 3.1.4.-); mRNA guanylyltransferase (EC	0,29

Uniprot ID	Gene name(s)	Protein name(s)	Re-weighted M Scores
		2.7.7.50); mRNA (guanine-N(7))-methyltransferase (EC 2.1.1.56)]	
Q6WVH5	-	Protein VP3 [Includes: 2',5'-phosphodiesterase (EC 3.1.4.-); mRNA guanylyltransferase (EC 2.7.7.50); mRNA (guanine-N(7))-methyltransferase (EC 2.1.1.56)]	0,29
Q91HJ9	-	Protein VP3 [Includes: 2',5'-phosphodiesterase (EC 3.1.4.-); mRNA guanylyltransferase (EC 2.7.7.50); mRNA (guanine-N(7))-methyltransferase (EC 2.1.1.56)]	0,29
Q9QNB1	-	Protein VP3 [Includes: 2',5'-phosphodiesterase (EC 3.1.4.-); mRNA guanylyltransferase (EC 2.7.7.50); mRNA (guanine-N(7))-methyltransferase (EC 2.1.1.56)]	0,29
P22102	GART PGFT PRGS	Trifunctional purine biosynthetic protein adenosine-3 [Includes: Phosphoribosylamine--glycine ligase (EC 6.3.4.13) (Glycinamide ribonucleotide synthetase) (GARS) (Phosphoribosylglycinamide synthetase); Phosphoribosylformylglycinamidine cyclo-ligase (EC 6.3.3.1) (AIR synthase) (AIRS) (Phosphoribosyl-aminoimidazole synthetase); Phosphoribosylglycinamide formyltransferase (EC 2.1.2.2) (5'-phosphoribosylglycinamide transformylase) (GAR transformylase) (GART)]	3,55
P08684	CYP3A4 CYP3A3	Cytochrome P450 3A4 (EC 1.14.14.1) (1,4-cineole 2-exo-monooxygenase) (1,8-cineole 2-exo-monooxygenase) (EC 1.14.14.56) (Albendazole monooxygenase (sulfoxide-forming)) (EC 1.14.14.73) (Albendazole sulfoxidase) (CYPIIIA3) (CYPIIIA4) (Cholesterol 25-hydroxylase) (Cytochrome P450 3A3) (Cytochrome P450 HLp) (Cytochrome P450 NF-25) (Cytochrome P450-PCN1) (Nifedipine oxidase) (Quinine 3-monooxygenase) (EC 1.14.14.55)	3,82
O15528	CYP27B1 CYP1ALPHA CYP27B	25-hydroxyvitamin D-1 alpha hydroxylase, mitochondrial (EC 1.14.15.18) (25-OHD-1 alpha-hydroxylase) (25-hydroxyvitamin D(3) 1-alpha-hydroxylase) (VD3 1A hydroxylase) (Calcidiol 1-monooxygenase) (Cytochrome P450 subfamily XXVIIB polypeptide 1) (Cytochrome P450C1 alpha) (Cytochrome P450VD1-alpha) (Cytochrome p450 27B1)	3,97
P05093	CYP17A1 CYP17 S17AH	Steroid 17-alpha-hydroxylase/17,20 lyase (EC 1.14.14.19) (17-alpha-hydroxyprogesterone aldolase) (EC 1.14.14.32) (CYPXVII) (Cytochrome P450 17A1) (Cytochrome P450-C17) (Cytochrome P450c17) (Steroid 17-alpha-monooxygenase)	4,01
Q07973	CYP24A1 CYP24	1,25-dihydroxyvitamin D(3) 24-hydroxylase, mitochondrial (24-OHase) (Vitamin D(3) 24-hydroxylase) (EC 1.14.15.16) (Cytochrome P450 24A1) (Cytochrome P450-CC24)	4,34
P24462	CYP3A7	Cytochrome P450 3A7 (EC 1.14.14.1) (CYPIIIA7) (Cytochrome P450-HFLA) (P450HLp2)	4,38

Uniprot ID	Gene name(s)	Protein name(s)	Re-weighted M Scores
P23141	CES1 CES2 SES1	Liver carboxylesterase 1 (Acyl-coenzyme A:cholesterol acyltransferase) (ACAT) (Brain carboxylesterase hBr1) (Carboxylesterase 1) (CE-1) (hCE-1) (EC 3.1.1.1) (Cholesteryl ester hydrolase) (CEH) (EC 3.1.1.13) (Cocaine carboxylesterase) (Egasyn) (HMSE) (Methylumbelliferyl-acetate deacetylase 1) (EC 3.1.1.56) (Monocyte/macrophage serine esterase) (Retinyl ester hydrolase) (REH) (Serine esterase 1) (Triacylglycerol hydrolase) (TGH)	4,48
P50583	NUDT2 APAH1	Bis(5'-nucleosyl)-tetraphosphatase [asymmetrical] (EC 3.6.1.17) (Diadenosine 5',5'''-P1,P4-tetraphosphate asymmetrical hydrolase) (Ap4A hydrolase) (Ap4Aase) (Diadenosine tetraphosphatase) (Nucleoside diphosphate-linked moiety X motif 2) (Nudix motif 2)	5,12
P11086	PNMT PENT	Phenylethanolamine N-methyltransferase (PNMTase) (EC 2.1.1.28) (Noradrenaline N-methyltransferase)	6,43
P40261	NNMT	Nicotinamide N-methyltransferase (EC 2.1.1.1)	8,59

Supplementary table 4: Enzymes of down-regulated metabolites in phase 1 and up-regulated metabolites in phase 2

Uniprot ID	Gene name(s)	Protein name(s)	Re-weighted M Scores
Q15067	ACOX1 ACOX	Peroxisomal acyl-coenzyme A oxidase 1 (AOX) (EC 1.3.3.6) (Palmitoyl-CoA oxidase) (Straight-chain acyl-CoA oxidase) (SCOX) [Cleaved into: Peroxisomal acyl-CoA oxidase 1, A chain; Peroxisomal acyl-CoA oxidase 1, B chain; Peroxisomal acyl-CoA oxidase 1, C chain]	1,20
P28300	LOX	Protein-lysine 6-oxidase (EC 1.4.3.13) (Lysyl oxidase) [Cleaved into: Protein-lysine 6-oxidase, long form; Protein-lysine 6-oxidase, short form]	1,51
Q9Y4K0	LOXL2	Lysyl oxidase homolog 2 (EC 1.4.3.13) (Lysyl oxidase-like protein 2) (Lysyl oxidase-related protein 2) (Lysyl oxidase-related protein WS9-14)	1,51
O75106	AOC2	Retina-specific copper amine oxidase (RAO) (EC 1.4.3.21) (Amine oxidase [copper-containing]) (Semicarbazide-sensitive amine oxidase) (SSAO)	1,51

Uniprot ID	Gene name(s)	Protein name(s)	Re-weighted M Scores
P14920	DAO DAMOX	D-amino-acid oxidase (DAAO) (DAMOX) (DAO) (EC 1.4.3.3)	1,51
P21397	MAOA	Amine oxidase [flavin-containing] A (EC 1.4.3.4) (Monoamine oxidase type A) (MAO-A)	1,51
P27338	MAOB	Amine oxidase [flavin-containing] B (EC 1.4.3.4) (Monoamine oxidase type B) (MAO-B)	1,51
Q16853	AOC3 VAP1	Membrane primary amine oxidase (EC 1.4.3.21) (Copper amine oxidase) (HPAO) (Semicarbazide-sensitive amine oxidase) (SSAO) (Vascular adhesion protein 1) (VAP-1)	1,51
Q9H2A2	ALDH8A1 ALDH12	2-aminomuconic semialdehyde dehydrogenase (EC 1.2.1.32) (Aldehyde dehydrogenase 12) (Aldehyde dehydrogenase family 8 member A1)	1,51
P23109	AMPD1	AMP deaminase 1 (EC 3.5.4.6) (AMP deaminase isoform M) (Myoadenylate deaminase)	1,76
Q01432	AMPD3	AMP deaminase 3 (EC 3.5.4.6) (AMP deaminase isoform E) (Erythrocyte AMP deaminase)	1,76
Q01433	AMPD2	AMP deaminase 2 (EC 3.5.4.6) (AMP deaminase isoform L)	1,76
Q7L8W6	DPH6 ATPBD4	Diphthine--ammonia ligase (EC 6.3.1.14) (ATP-binding domain-containing protein 4) (Diphthamide synthase) (Diphthamide synthetase) (Protein DPH6 homolog)	1,76
P15291	B4GALT1 GGTB2	Beta-1,4-galactosyltransferase 1 (Beta-1,4-GalTase 1) (Beta4Gal-T1) (b4Gal-T1) (EC 2.4.1.-) (Beta-N-acetylglucosaminyl-glycolipid beta-1,4-galactosyltransferase) (Beta-N-acetylglucosaminylglycopeptide beta-1,4-galactosyltransferase) (EC 2.4.1.38) (Lactose synthase A protein) (EC 2.4.1.22) (N-acetyllactosamine synthase) (EC 2.4.1.90) (Nal synthase) (Neolactotriaosylceramide beta-1,4-galactosyltransferase) (EC 2.4.1.275) (UDP-Gal:beta-GlcNAc beta-1,4-galactosyltransferase 1) (UDP-galactose:beta-N-acetylglucosamine beta-1,4-galactosyltransferase 1) [Cleaved into: Processed beta-1,4-galactosyltransferase 1]	2,20
P04181	OAT	Ornithine aminotransferase, mitochondrial (EC 2.6.1.13) (Ornithine delta-aminotransferase) (Ornithine--oxo-acid aminotransferase) [Cleaved into: Ornithine aminotransferase, hepatic form; Ornithine aminotransferase, renal form]	2,26
P49588	AARS1 AARS	Alanine--tRNA ligase, cytoplasmic (EC 6.1.1.7) (Alanyl-tRNA synthetase) (AlaRS) (Renal carcinoma antigen NY-REN-42)	2,42
Q5JTZ9	AARS2 AARSL KIAA1270	Alanine--tRNA ligase, mitochondrial (EC 6.1.1.7) (Alanyl-tRNA synthetase) (AlaRS)	2,42

Uniprot ID	Gene name(s)	Protein name(s)	Re-weighted M Scores
O95340	PAPSS2 ATPSK2	Bifunctional 3'-phosphoadenosine 5'-phosphosulfate synthase 2 (PAPS synthase 2) (PAPSS 2) (Sulfurylase kinase 2) (SK 2) (SK2) [Includes: Sulfate adenylyltransferase (EC 2.7.7.4) (ATP-sulfurylase) (Sulfate adenylate transferase) (SAT); Adenylyl-sulfate kinase (EC 2.7.1.25) (3'-phosphoadenosine-5'-phosphosulfate synthase) (APS kinase) (Adenosine-5'-phosphosulfate 3'-phosphotransferase) (Adenylylsulfate 3'-phosphotransferase)]	2,77
Q00796	SORD	Sorbitol dehydrogenase (SDH) (EC 1.1.1.-) ((R,R)-butanediol dehydrogenase) (EC 1.1.1.4) (L-iditol 2-dehydrogenase) (EC 1.1.1.14) (Polyol dehydrogenase) (Ribitol dehydrogenase) (RDH) (EC 1.1.1.56) (Xylitol dehydrogenase) (XDH) (EC 1.1.1.9)	3,02
Q9H4A9	DPEP2 UNQ284/PRO323	Dipeptidase 2 (EC 3.4.13.19)	3,05
Q8TDN7	ACER1 ASAH3	Alkaline ceramidase 1 (AlkCDase 1) (Alkaline CDase 1) (EC 3.5.1.-) (EC 3.5.1.23) (Acylsphingosine deacylase 3) (N-acylsphingosine amidohydrolase 3)	3,20
Q9NWW9	PLAAT2 HRASLS2	Phospholipase A and acyltransferase 2 (EC 2.3.1.-) (EC 3.1.1.32) (EC 3.1.1.4) (HRAS-like suppressor 2)	3,23
P09211	GSTP1 FAEES3 GST3	Glutathione S-transferase P (EC 2.5.1.18) (GST class-pi) (GSTP1-1)	3,29
Q6PIU2	NCEH1 AADACL1 KIAA1363	Neutral cholesterol ester hydrolase 1 (NCEH) (EC 3.1.1.-) (Arylacetamide deacetylase-like 1)	3,30
P09488	GSTM1 GST1	Glutathione S-transferase Mu 1 (EC 2.5.1.18) (GST HB subunit 4) (GST class-mu 1) (GSTM1-1) (GSTM1a-1a) (GSTM1b-1b) (GTH4)	3,31
P33897	ABCD1 ALD	ATP-binding cassette sub-family D member 1 (EC 3.1.2.-) (EC 7.6.2.-) (Adrenoleukodystrophy protein) (ALDP)	3,31
P15289	ARSA	Arylsulfatase A (ASA) (EC 3.1.6.8) (Cerebroside-sulfatase) [Cleaved into: Arylsulfatase A component B; Arylsulfatase A component C]	3,52
P36959	GMPR GMPR1	GMP reductase 1 (GMPR 1) (EC 1.7.1.7) (Guanosine 5'-monophosphate oxidoreductase 1) (Guanosine monophosphate reductase 1)	3,54
Q9P2T1	GMPR2	GMP reductase 2 (GMPR 2) (EC 1.7.1.7) (Guanosine 5'-monophosphate oxidoreductase 2) (Guanosine monophosphate reductase 2)	3,54

Uniprot ID	Gene name(s)	Protein name(s)	Re-weighted M Scores
P48448	ALDH3B2 ALDH8	Aldehyde dehydrogenase family 3 member B2 (EC 1.2.1.3) (Aldehyde dehydrogenase 8)	3,54
P43353	ALDH3B1 ALDH7	Aldehyde dehydrogenase family 3 member B1 (EC 1.2.1.28) (EC 1.2.1.5) (EC 1.2.1.7) (Aldehyde dehydrogenase 7)	3,86
Q9HBI6	CYP4F11	Cytochrome P450 4F11 (CYPIVF11) (EC 1.14.14.1) (3-hydroxy fatty acids omega-hydroxylase CYP4F11) (Docosahexaenoic acid omega-hydroxylase) (EC 1.14.14.79) (Long-chain fatty acid omega-monooxygenase) (EC 1.14.14.80) (Phylloquinone omega-hydroxylase CYP4F11) (EC 1.14.14.78)	3,91
Q9H221	ABCG8	ATP-binding cassette sub-family G member 8 (EC 7.6.2.-) (Sterolin-2)	3,92
Q9H222	ABCG5	ATP-binding cassette sub-family G member 5 (EC 7.6.2.-) (Sterolin-1)	3,92
P35354	PTGS2 COX2	Prostaglandin G/H synthase 2 (EC 1.14.99.1) (Cyclooxygenase-2) (COX-2) (PHS II) (Prostaglandin H2 synthase 2) (PGH synthase 2) (PGHS-2) (Prostaglandin-endoperoxide synthase 2)	3,97
P31153	MAT2A AMS2 MATA2	S-adenosylmethionine synthase isoform type-2 (AdoMet synthase 2) (EC 2.5.1.6) (Methionine adenosyltransferase 2) (MAT 2) (Methionine adenosyltransferase II) (MAT-II)	4,07
Q00266	MAT1A AMS1 MATA1	S-adenosylmethionine synthase isoform type-1 (AdoMet synthase 1) (EC 2.5.1.6) (Methionine adenosyltransferase 1) (MAT 1) (Methionine adenosyltransferase I/III) (MAT-I/III)	4,07
P34913	EPHX2	Bifunctional epoxide hydrolase 2 [Includes: Cytosolic epoxide hydrolase 2 (CEH) (EC 3.3.2.10) (Epoxide hydratase) (Soluble epoxide hydrolase) (SEH); Lipid-phosphate phosphatase (EC 3.1.3.76)]	4,07
Q08477	CYP4F3 LTB4H	Cytochrome P450 4F3 (EC 1.14.14.1) (20-hydroxyeicosatetraenoic acid synthase) (20-HETE synthase) (CYPIVF3) (Cytochrome P450-LTB-omega) (Docosahexaenoic acid omega-hydroxylase CYP4F3) (EC 1.14.14.79) (Leukotriene-B(4) 20-monooxygenase 2) (Leukotriene-B(4) omega-hydroxylase 2) (EC 1.14.14.94)	4,10
Q96LT4	SAMD8	Sphingomyelin synthase-related protein 1 (SMSr) (EC 2.7.8.-) (Ceramide phosphoethanolamine synthase) (CPE synthase) (Sterile alpha motif domain-containing protein 8) (SAM domain-containing protein 8)	4,15
Q9NV35	NUDT15 MTH2	Nucleotide triphosphate diphosphatase NUDT15 (EC 3.6.1.9) (MutT homolog 2) (MTH2)	4,21

Uniprot ID	Gene name(s)	Protein name(s)	Re-weighted M Scores
		(Nucleoside diphosphate-linked moiety X motif 15) (Nudix motif 15) (Nucleoside diphosphate-linked to another moiety X hydrolase 15) (Nudix hydrolase 15)	
Q9Y2S2	CRYL1 CRY	Lambda-crystallin homolog (EC 1.1.1.45) (L-gulonate 3-dehydrogenase) (Gul3DH)	4,39
P52209	PGD PGDH	6-phosphogluconate dehydrogenase, decarboxylating (EC 1.1.1.44)	4,44
Q9BQG2	NUDT12	NAD-capped RNA hydrolase NUDT12 (DeNADding enzyme NUDT12) (EC 3.6.1.-) (NADH pyrophosphatase NUDT12) (EC 3.6.1.22) (Nucleoside diphosphate-linked moiety X motif 12) (Nudix motif 12)	4,44
Q9Y4D2	DAGLA C11orf11 KIAA0659 NSDDR	Diacylglycerol lipase-alpha (DAGL-alpha) (DGL-alpha) (EC 3.1.1.116) (Neural stem cell-derived dendrite regulator) (Sn1-specific diacylglycerol lipase alpha)	4,44
P19021	PAM	Peptidyl-glycine alpha-amidating monooxygenase (PAM) [Includes: Peptidylglycine alpha-hydroxylating monooxygenase (PHM) (EC 1.14.17.3); Peptidyl-alpha-hydroxyglycine alpha-amidating lyase (EC 4.3.2.5) (Peptidylamidoglycolate lyase) (PAL)]	4,47
P11413	G6PD	Glucose-6-phosphate 1-dehydrogenase (G6PD) (EC 1.1.1.49)	4,52
P50135	HNMT	Histamine N-methyltransferase (HMT) (EC 2.1.1.8)	4,63
Q6P1J6	PLB1 PLB	Phospholipase B1, membrane-associated (Phospholipase B) (hPLB) (Lysophospholipase) (EC 3.1.1.5) (Phospholipase A2) (EC 3.1.1.4) (Phospholipase B/lipase) (PLB/LIP) (Triacylglycerol lipase) (EC 3.1.1.3)	4,63
Q86X67	NUDT13	NAD(P)H pyrophosphatase NUDT13, mitochondrial (EC 3.6.1.22) (Nucleoside diphosphate-linked moiety X motif 13) (Nudix motif 13) (Protein KiSS-16)	4,66
O75881	CYP7B1	Cytochrome P450 7B1 (24-hydroxycholesterol 7-alpha-hydroxylase) (EC 1.14.14.26) (25/26-hydroxycholesterol 7-alpha-hydroxylase) (EC 1.14.14.29) (3-hydroxysteroid 7-alpha hydroxylase) (Oxysterol 7-alpha-hydroxylase)	4,67
Q969G6	RFK	Riboflavin kinase (EC 2.7.1.26) (ATP:riboflavin 5'-phosphotransferase) (Flavokinase)	4,68
Q02928	CYP4A11 CYP4A2	Cytochrome P450 4A11 (EC 1.14.14.1) (20-hydroxyeicosatetraenoic acid synthase) (20-HETE synthase) (CYP4AII) (CYPIVA11) (Cytochrome P-450HK-omega) (Cytochrome P450HL-omega)	4,71

Uniprot ID	Gene name(s)	Protein name(s)	Re-weighted M Scores
		(Fatty acid omega-hydroxylase) (Lauric acid omega-hydroxylase) (Long-chain fatty acid omega-monooxygenase) (EC 1.14.14.80)	
Q9NUN7	ACER3 APHC PHCA	Alkaline ceramidase 3 (AlkCDase 3) (Alkaline CDase 3) (EC 3.5.1.-) (EC 3.5.1.23) (Alkaline dihydroceramidase SB89) (Alkaline phytoceramidase) (aPHC)	4,74
Q6XZB0	LIPI LPDL PRED5	Lipase member I (LIPI) (EC 3.1.1.-) (Cancer/testis antigen 17) (CT17) (LPD lipase) (Membrane-associated phosphatidic acid-selective phospholipase A1-beta) (mPA-PLA1 beta)	4,74
Q8WWY8	LIPH LPDLR MPAPLA1 PLA1B	Lipase member H (LIPH) (EC 3.1.1.-) (LPD lipase-related protein) (Membrane-associated phosphatidic acid-selective phospholipase A1-alpha) (mPA-PLA1 alpha) (Phospholipase A1 member B)	4,74
P14555	PLA2G2A PLA2B PLA2L RASF-A	Phospholipase A2, membrane associated (EC 3.1.1.4) (GIIC sPLA2) (Group IIA phospholipase A2) (Non-pancreatic secretory phospholipase A2) (NPS-PLA2) (Phosphatidylcholine 2-acylhydrolase 2A)	4,79
O60218	AKR1B10 AKR1B11	Aldo-keto reductase family 1 member B10 (EC 1.1.1.300) (EC 1.1.1.54) (ARL-1) (Aldose reductase-like) (Aldose reductase-related protein) (ARP) (hARP) (Small intestine reductase) (SI reductase)	4,80
P38571	LIPA	Lysosomal acid lipase/cholesteryl ester hydrolase (Acid cholesteryl ester hydrolase) (LAL) (EC 3.1.1.13) (Cholesteryl esterase) (Lipase A) (Sterol esterase)	4,86
Q04828	AKR1C1 DDH DDH1	Aldo-keto reductase family 1 member C1 (EC 1.1.1.-) (EC 1.1.1.112) (EC 1.1.1.209) (EC 1.1.1.210) (EC 1.1.1.357) (EC 1.1.1.51) (EC 1.1.1.53) (EC 1.1.1.62) (EC 1.3.1.20) (20-alpha-hydroxysteroid dehydrogenase) (20-alpha-HSD) (EC 1.1.1.149) (Chlordecone reductase homolog HAKRC) (Dihydrodiol dehydrogenase 1) (DD1) (High-affinity hepatic bile acid-binding protein) (HBAB)	4,94
P78329	CYP4F2	Cytochrome P450 4F2 (EC 1.14.14.1) (20-hydroxyeicosatetraenoic acid synthase) (20-HETE synthase) (Arachidonic acid omega-hydroxylase) (CYPIVF2) (Cytochrome P450-LTB-omega) (Docosahexaenoic acid omega-hydroxylase) (EC 1.14.14.79) (Leukotriene-B(4) 20-monooxygenase 1) (Leukotriene-B(4) omega-hydroxylase 1) (EC 1.14.14.94) (Phylloquinone omega-hydroxylase CYP4F2) (EC 1.14.14.78)	4,94
P51589	CYP2J2	Cytochrome P450 2J2 (EC 1.14.14.-) (Albendazole monooxygenase (hydroxylating)) (EC 1.14.14.74) (Albendazole monooxygenase (sulfoxide-forming)) (EC 1.14.14.73) (Arachidonic acid	5,00

Uniprot ID	Gene name(s)	Protein name(s)	Re-weighted M Scores
		epoxygenase) (CYPIIJ2) (Hydroperoxy icosatetraenoate isomerase) (EC 5.4.4.7)	
Q9NYL5	CYP39A1	24-hydroxycholesterol 7-alpha-hydroxylase (EC 1.14.14.26) (Cytochrome P450 39A1) (hCYP39A1) (Oxysterol 7-alpha-hydroxylase)	5,14
Q96DE0	NUDT16	U8 snoRNA-decapping enzyme (EC 3.6.1.62) (IDP phosphatase) (IDPase) (EC 3.6.1.64) (Inosine diphosphate phosphatase) (Nucleoside diphosphate-linked moiety X motif 16) (Nudix motif 16) (Nudix hydrolase 16) (U8 snoRNA-binding protein H29K) (m7GpppN-mRNA hydrolase)	5,17
P14550	AKR1A1 ALDR1 ALR	Aldo-keto reductase family 1 member A1 (EC 1.1.1.2) (EC 1.1.1.372) (EC 1.1.1.54) (Alcohol dehydrogenase [NADP(+)]) (Aldehyde reductase) (Glucuronate reductase) (EC 1.1.1.19) (Glucuronolactone reductase) (EC 1.1.1.20)	5,31
P08319	ADH4	All-trans-retinol dehydrogenase [NAD(+)] ADH4 (EC 1.1.1.105) (Alcohol dehydrogenase 4) (Alcohol dehydrogenase class II pi chain)	5,48
Q9Y6A2	CYP46A1 CYP46	Cholesterol 24-hydroxylase (CH24H) (EC 1.14.14.25) (Cholesterol 24-monooxygenase) (Cholesterol 24S-hydroxylase) (Cytochrome P450 46A1)	5,60
P28907	CD38	ADP-ribosyl cyclase/cyclic ADP-ribose hydrolase 1 (EC 3.2.2.6) (2'-phospho-ADP-ribosyl cyclase) (2'-phospho-ADP-ribosyl cyclase/2'-phospho-cyclic-ADP-ribose transferase) (EC 2.4.99.20) (2'-phospho-cyclic-ADP-ribose transferase) (ADP-ribosyl cyclase 1) (ADPRC 1) (Cyclic ADP-ribose hydrolase 1) (cADPr hydrolase 1) (T10) (CD antigen CD38)	5,64
P13995	MTHFD2 NMDMC	Bifunctional methylenetetrahydrofolate dehydrogenase/cyclohydrolase, mitochondrial [Includes: NAD-dependent methylenetetrahydrofolate dehydrogenase (EC 1.5.1.15); Methenyltetrahydrofolate cyclohydrolase (EC 3.5.4.9)]	5,64
Q9H903	MTHFD2L	Probable bifunctional methylenetetrahydrofolate dehydrogenase/cyclohydrolase 2 (NADP-dependent methylenetetrahydrofolate dehydrogenase 2-like protein) (MTHFD2-like) [Includes: NAD-dependent methylenetetrahydrofolate dehydrogenase (EC 1.5.1.15); Methenyltetrahydrofolate cyclohydrolase (EC 3.5.4.9)]	5,64
Q6VVX0	CYP2R1	Vitamin D 25-hydroxylase (EC 1.14.14.24) (Cytochrome P450 2R1)	5,66
Q53H76	PLA1A NMD PSPLA1	Phospholipase A1 member A (EC 3.1.1.111) (Phosphatidylserine-specific phospholipase A1) (PS-	5,67

Uniprot ID	Gene name(s)	Protein name(s)	Re-weighted M Scores
		PLA1)	
Q9UNK4	PLA2G2D SPLASH	Group IID secretory phospholipase A2 (GIID sPLA2) (sPLA2-IID) (EC 3.1.1.4) (PLA2IID) (Phosphatidylcholine 2-acylhydrolase 2D) (Secretory-type PLA, stroma-associated homolog)	5,70
Q8TBG4	ETNPPL AGXT2L1	Ethanolamine-phosphate phospho-lyase (EC 4.2.3.2) (Alanine--glyoxylate aminotransferase 2-like 1)	5,76
Q9NP80	PNPLA8 IPLA22 IPLA2G BM-043	Calcium-independent phospholipase A2-gamma (EC 3.1.1.-) (EC 3.1.1.5) (Intracellular membrane-associated calcium-independent phospholipase A2 gamma) (iPLA2-gamma) (PNPLA-gamma) (Patatin-like phospholipase domain-containing protein 8) (iPLA2-2)	5,80
Q96NR8	RDH12 SDR7C2	Retinol dehydrogenase 12 (EC 1.1.1.300) (All-trans and 9-cis retinol dehydrogenase) (Short chain dehydrogenase/reductase family 7C member 2)	5,83
Q6SZW1	SARM1 KIAA0524 SAMD2 SARM	NAD(+) hydrolase SARM1 (NADase SARM1) (hSARM1) (EC 3.2.2.6) (NADP(+) hydrolase SARM1) (EC 3.2.2.-) (Sterile alpha and Armadillo repeat protein) (Sterile alpha and TIR motif-containing protein 1) (Sterile alpha motif domain-containing protein 2) (MyD88-5) (SAM domain-containing protein 2) (Tir-1 homolog) (HsTIR)	5,85
O15067	PFAS KIAA0361	Phosphoribosylformylglycinamidine synthase (FGAM synthase) (FGAMS) (EC 6.3.5.3) (Formylglycinamide ribonucleotide amidotransferase) (FGAR amidotransferase) (FGAR-AT) (Formylglycinamide ribotide amidotransferase)	5,88
Q6NUM6	TYW1B RSAFD2	S-adenosyl-L-methionine-dependent tRNA 4-demethylwyosine synthase TYW1B (EC 4.1.3.44) (Radical S-adenosyl methionine and flavodoxin domain-containing protein 2) (tRNA wybutosine-synthesizing protein 1 homolog B)	5,90
Q9NV66	TYW1 RSAFD1	S-adenosyl-L-methionine-dependent tRNA 4-demethylwyosine synthase TYW1 (EC 4.1.3.44) (Radical S-adenosyl methionine and flavodoxin domain-containing protein 1) (tRNA wybutosine-synthesizing protein 1 homolog) (tRNA-yW-synthesizing protein)	5,90
Q9UL19	PLAAT4 RARRES3 RIG1 TIG3	Phospholipase A and acyltransferase 4 (EC 2.3.1.-) (EC 3.1.1.32) (EC 3.1.1.4) (HRAS-like suppressor 4) (HRSL4) (RAR-responsive protein TIG3) (Retinoic acid receptor responder protein 3) (Retinoid-inducible gene 1 protein) (Tazarotene-induced gene 3 protein)	5,96

Uniprot ID	Gene name(s)	Protein name(s)	Re-weighted M Scores
P11586	MTHFD1 MTHFC MTHFD	C-1-tetrahydrofolate synthase, cytoplasmic (C1-THF synthase) (Epididymis secretory sperm binding protein) [Cleaved into: C-1-tetrahydrofolate synthase, cytoplasmic, N-terminally processed] [Includes: Methylenetetrahydrofolate dehydrogenase (EC 1.5.1.5); Methenyltetrahydrofolate cyclohydrolase (EC 3.5.4.9); Formyltetrahydrofolate synthetase (EC 6.3.4.3)]	6,00
P15121	AKR1B1 ALDR1 ALR2	Aldo-keto reductase family 1 member B1 (EC 1.1.1.300) (EC 1.1.1.372) (EC 1.1.1.54) (Aldehyde reductase) (Aldose reductase) (AR) (EC 1.1.1.21)	6,02
Q8IWX5	SGPP2	Sphingosine-1-phosphate phosphatase 2 (SPPase2) (Spp2) (hSPP2) (EC 3.1.3.-) (Sphingosine-1-phosphatase 2)	6,06
Q8WU67	ABHD3	Phospholipase ABHD3 (EC 3.1.1.32) (EC 3.1.1.4) (Abhydrolase domain-containing protein 3)	6,10
P07902	GALT	Galactose-1-phosphate uridylyltransferase (Gal-1-P uridylyltransferase) (EC 2.7.7.12) (UDP-glucose--hexose-1-phosphate uridylyltransferase)	6,12
Q9H773	DCTPP1 XTP3TPA CDA03	dCTP pyrophosphatase 1 (EC 3.6.1.12) (Deoxycytidine-triphosphatase 1) (dCTPase 1) (RS21C6) (XTP3-transactivated gene A protein)	6,22
Q9NZK7	PLA2G2E	Group IIE secretory phospholipase A2 (GIIE sPLA2) (sPLA2-IIE) (EC 3.1.1.4) (Phosphatidylcholine 2-acylhydrolase 2E)	6,25
P80365	HSD11B2 HSD11K SDR9C3	Corticosteroid 11-beta-dehydrogenase isozyme 2 (EC 1.1.1.-) (11-beta-hydroxysteroid dehydrogenase type 2) (11-DH2) (11-beta-HSD2) (11-beta-hydroxysteroid dehydrogenase type II) (11-HSD type II) (11-beta-HSD type II) (NAD-dependent 11-beta-hydroxysteroid dehydrogenase) (11-beta-HSD) (Short chain dehydrogenase/reductase family 9C member 3)	6,30
Q9UBK8	MTRR	Methionine synthase reductase (MSR) (EC 1.16.1.8) (Aquacobalamin reductase) (AqCbl reductase)	6,46
O60733	PLA2G6 PLPLA9	85/88 kDa calcium-independent phospholipase A2 (CaI-PLA2) (EC 3.1.1.4) (2-lysophosphatidylcholine acylhydrolase) (EC 3.1.1.5) (Group VI phospholipase A2) (GVI PLA2) (Intracellular membrane-associated calcium-independent phospholipase A2 beta) (iPLA2-beta) (Palmitoyl-CoA hydrolase) (EC 3.1.2.2) (Patatin-like phospholipase domain-containing protein 9) (PNPLA9)	6,50

Uniprot ID	Gene name(s)	Protein name(s)	Re-weighted M Scores
Q06278	AOX1 AO	Aldehyde oxidase (EC 1.2.3.1) (Aldehyde oxidase 1) (Azaheterocycle hydroxylase) (EC 1.17.3.-)	6,52
Q9BX95	SGPP1 SPP1	Sphingosine-1-phosphate phosphatase 1 (SPPase1) (Spp1) (hSPP1) (hSPPase1) (EC 3.1.3.-) (Sphingosine-1-phosphatase 1) (Sphingosine-1-phosphate phosphohydrolase 1) (SPP-1)	6,57
Q16773	KYAT1 CCBL1	Kynurenine--oxoglutarate transaminase 1 (EC 2.6.1.7) (Cysteine-S-conjugate beta-lyase) (EC 4.4.1.13) (Glutamine transaminase K) (GTK) (Glutamine--phenylpyruvate transaminase) (EC 2.6.1.64) (Kynurenine aminotransferase 1) (Kynurenine aminotransferase I) (KATI) (Kynurenine--oxoglutarate transaminase I)	6,64
P28845	HSD11B1 HSD11 HSD11L SDR26C1	Corticosteroid 11-beta-dehydrogenase isozyme 1 (EC 1.1.1.146) (11-beta-hydroxysteroid dehydrogenase 1) (11-DH) (11-beta-HSD1) (Short chain dehydrogenase/reductase family 26C member 1)	6,66
Q13822	ENPP2 ATX PDNP2	Ectonucleotide pyrophosphatase/phosphodiesterase family member 2 (E-NPP 2) (EC 3.1.4.39) (Autotaxin) (Extracellular lysophospholipase D) (LysoPLD)	6,72
Q15800	MSMO1 DESP4 ERG25 SC4MOL	Methylsterol monooxygenase 1 (EC 1.14.18.9) (C-4 methylsterol oxidase) (Sterol-C4-methyl oxidase)	6,74
P49326	FMO5	Flavin-containing monooxygenase 5 (FMO 5) (Baeyer-Villiger monooxygenase 1) (hBVMO1) (EC 1.14.13.-) (Dimethylaniline monooxygenase [N-oxide-forming] 5) (EC 1.14.13.8) (Dimethylaniline oxidase 5) (NAPDH oxidase) (EC 1.6.3.1)	6,78
Q9HDD0	PLAAT1 HRASLS	Phospholipase A and acyltransferase 1 (EC 2.3.1.-) (EC 3.1.1.32) (EC 3.1.1.4) (HRAS-like suppressor 1) (HRSL1) (Phospholipid-metabolizing enzyme A-C1)	6,81
Q6DHV7	ADAL ADAL1	Adenosine deaminase-like protein (EC 3.5.4.-) (Adenosine deaminase-like protein isoform 1) (N6-mAMP deaminase) (HsMAPDA) (N6-methyl-AMP aminohydrolase)	6,84
O95870	ABHD16A BAT5 G5 NG26 PP199	Phosphatidylserine lipase ABHD16A (EC 3.1.-.-) (Alpha/beta hydrolase domain-containing protein 16A) (Abhydrolase domain-containing protein 16A) (HLA-B-associated transcript 5) (hBAT5) (Monoacylglycerol lipase ABHD16A) (EC 3.1.1.23) (Protein G5)	6,85
P43251	BTD	Biotinidase (Biotinase) (EC 3.5.1.12)	6,95
Q9Y4U1	MMACHC	Cyanocobalamin reductase / alkylcobalamin dealkylase (Alkylcobalamin:glutathione S-	6,97

Uniprot ID	Gene name(s)	Protein name(s)	Re-weighted M Scores
		alkyltransferase) (EC 2.5.1.151) (CblC) (Cyanocobalamin reductase (cyanide-eliminating)) (EC 1.16.1.6) (Methylmalonic aciduria and homocystinuria type C protein) (MMACHC)	
P22680	CYP7A1 CYP7	Cytochrome P450 7A1 (24-hydroxycholesterol 7-alpha-hydroxylase) (EC 1.14.14.26) (CYPVII) (Cholesterol 7-alpha-hydroxylase) (Cholesterol 7-alpha-monooxygenase) (EC 1.14.14.23)	7,05
P05108	CYP11A1 CYP11A	Cholesterol side-chain cleavage enzyme, mitochondrial (EC 1.14.15.6) (CYPXIA1) (Cholesterol desmolase) (Cytochrome P450 11A1) (Cytochrome P450(scc))	7,06
O95671	ASMTL	Probable bifunctional dTTP/UTP pyrophosphatase/methyltransferase protein [Includes: dTTP/UTP pyrophosphatase (dTTPase/UTPase) (EC 3.6.1.9) (Nucleoside triphosphate pyrophosphatase) (Nucleotide pyrophosphatase) (Nucleotide PPase); N-acetylserotonin O-methyltransferase-like protein (ASMTL) (EC 2.1.1.-)]	7,07
Q16878	CDO1	Cysteine dioxygenase type 1 (EC 1.13.11.20) (Cysteine dioxygenase type I) (CDO) (CDO-I)	7,10
Q9UBM1	PEMT PEMPT PNMT	Phosphatidylethanolamine N-methyltransferase (PEAMT) (PEMT) (EC 2.1.1.17) (EC 2.1.1.71) (PEMT2) (Phospholipid methyltransferase) (PLMT)	7,14
Q02318	CYP27A1 CYP27	Sterol 26-hydroxylase, mitochondrial (EC 1.14.15.15) (5-beta-cholestane-3-alpha,7-alpha,12-alpha-triol 26-hydroxylase) (Cytochrome P-450C27/25) (Cytochrome P450 27) (Sterol 27-hydroxylase) (Vitamin D(3) 25-hydroxylase)	7,16
Q5VYX0	RNLS C10orf59	Renalase (EC 1.6.3.5) (Monoamine oxidase-C) (MAO-C)	7,19
Q9Y6N5	SQOR SQRDL CGI-44	Sulfide:quinone oxidoreductase, mitochondrial (SQOR) (EC 1.8.5.8) (Sulfide dehydrogenase-like) (Sulfide quinone oxidoreductase)	7,34
P33261	CYP2C19	Cytochrome P450 2C19 (EC 1.14.14.1) ((R)-limonene 6-monooxygenase) (EC 1.14.14.53) ((S)-limonene 6-monooxygenase) (EC 1.14.14.51) ((S)-limonene 7-monooxygenase) (EC 1.14.14.52) (CYPIIC17) (CYPIIC19) (Cytochrome P450-11A) (Cytochrome P450-254C) (Fenbendazole monooxygenase (4'-hydroxylating)) (EC 1.14.14.75) (Mephenytoin 4-hydroxylase)	7,47
Q6ZWL3	CYP4V2	Cytochrome P450 4V2 (Docosahexaenoic acid omega-hydroxylase CYP4V2) (EC 1.14.14.79) (Long-chain fatty acid omega-monooxygenase) (EC 1.14.14.80)	7,47
Q8NBK3	SUMF1 PSEC0152	Formylglycine-generating enzyme (FGE) (EC 1.8.3.7) (C-alpha-formylglycine-generating enzyme 1)	7,85

Uniprot ID	Gene name(s)	Protein name(s)	Re-weighted M Scores
	UNQ3037/PRO9852	(Sulfatase-modifying factor 1)	
Q13228	SELENBP1 SBP	Methanethiol oxidase (MTO) (EC 1.8.3.4) (56 kDa selenium-binding protein) (SBP56) (SP56) (Selenium-binding protein 1)	7,95
P30043	BLVRB FLR	Flavin reductase (NADPH) (FR) (EC 1.5.1.30) (Biliverdin reductase B) (BVR-B) (EC 1.3.1.24) (Biliverdin-IX beta-reductase) (Green heme-binding protein) (GHBP) (NADPH-dependent diaphorase) (NADPH-flavin reductase) (FLR)	7,97
P47712	PLA2G4A CPLA2 PLA2G4	Cytosolic phospholipase A2 (cPLA2) (Phospholipase A2 group IVA) [Includes: Phospholipase A2 (EC 3.1.1.4) (Phosphatidylcholine 2-acylhydrolase); Lysophospholipase (EC 3.1.1.5)]	7,98
P26439	HSD3B2 HSDB3B	3 beta-hydroxysteroid dehydrogenase/Delta 5-->4-isomerase type 2 (3 beta-hydroxysteroid dehydrogenase/Delta 5-->4-isomerase type II) (3-beta-HSD II) (3-beta-HSD adrenal and gonadal type) [Includes: 3-beta-hydroxy-Delta(5)-steroid dehydrogenase (EC 1.1.1.145) (3-beta-hydroxy-5-ene steroid dehydrogenase) (Progesterone reductase); Steroid Delta-isomerase (EC 5.3.3.1) (Delta-5-3-ketosteroid isomerase)]	7,99
P07099	EPHX1 EPHX EPOX	Epoxide hydrolase 1 (EC 3.3.2.9) (Epoxide hydratase) (Microsomal epoxide hydrolase) (mEH)	8,21
P10635	CYP2D6 CYP2DL1	Cytochrome P450 2D6 (EC 1.14.14.-) (CYPIID6) (Cholesterol 25-hydroxylase) (Cytochrome P450-DB1) (Debrisoquine 4-hydroxylase)	8,37
Q5T2R2	PDSS1 DPS1 TPRT	All trans-polyprenyl-diphosphate synthase PDSS1 (All-trans-decaprenyl-diphosphate synthase subunit 1) (EC 2.5.1.91) (Decaprenyl pyrophosphate synthase subunit 1) (Decaprenyl-diphosphate synthase subunit 1) (Solanesyl-diphosphate synthase subunit 1) (Trans-prenyltransferase 1) (TPT 1)	8,44
Q86YH6	PDSS2 C6orf210 DLP1	All trans-polyprenyl-diphosphate synthase PDSS2 (All-trans-decaprenyl-diphosphate synthase subunit 2) (EC 2.5.1.91) (Candidate tumor suppressor protein) (Decaprenyl pyrophosphate synthase subunit 2) (Decaprenyl-diphosphate synthase subunit 2) (Solanesyl-diphosphate synthase subunit 2)	8,44
Q9HAB8	PPCS COAB	Phosphopantothenate--cysteine ligase (EC 6.3.2.51) (Phosphopantothenoylcysteine synthetase) (PPC synthetase)	8,45

Uniprot ID	Gene name(s)	Protein name(s)	Re-weighted M Scores
Q9BV57	ADI1 MTCBP1 HMFT1638	1,2-dihydroxy-3-keto-5-methylthiopentene dioxygenase (EC 1.13.11.54) (Acireductone dioxygenase (Fe(2+)-requiring)) (ARD) (Fe-ARD) (Membrane-type 1 matrix metalloproteinase cytoplasmic tail-binding protein 1) (MTCBP-1) (Submergence-induced protein-like factor) (Sip-L)	8,48
Q9UHG3	PCYOX1 KIAA0908 PCL1 UNQ597/PRO1183	Prenylcysteine oxidase 1 (EC 1.8.3.5) (Prenylcysteine lyase)	8,54
Q8N9F7	GDPD1 GDE4	Lysophospholipase D GDPD1 (EC 3.1.4.-) (Glycerophosphodiester phosphodiesterase 4) (Glycerophosphodiester phosphodiesterase domain-containing protein 1)	8,59
P15085	CPA1 CPA	Carboxypeptidase A1 (EC 3.4.17.1)	8,60
P31513	FMO3	Dimethylaniline monooxygenase [N-oxide-forming] 3 (EC 1.14.13.8) (EC 1.14.14.73) (Dimethylaniline oxidase 3) (FMO II) (FMO form 2) (Hepatic flavin-containing monooxygenase 3) (FMO 3) (Trimethylamine monooxygenase) (EC 1.14.13.148)	8,69
P15428	HPGD PGDH1 SDR36C1	15-hydroxyprostaglandin dehydrogenase [NAD(+)] (15-PGDH) (EC 1.1.1.141) (Prostaglandin dehydrogenase 1) (Short chain dehydrogenase/reductase family 36C member 1)	8,72
O94830	DDHD2 KIAA0725 SAMWD1	Phospholipase DDHD2 (EC 3.1.1.-) (DDHD domain-containing protein 2) (KIAA0725p) (SAM, WWE and DDHD domain-containing protein 1)	8,74
Q93088	BHMT	Betaine--homocysteine S-methyltransferase 1 (EC 2.1.1.5)	8,77
Q13093	PLA2G7 PAFAH	Platelet-activating factor acetylhydrolase (PAF acetylhydrolase) (EC 3.1.1.47) (1-alkyl-2-acetylglycerophosphocholine esterase) (2-acetyl-1-alkylglycerophosphocholine esterase) (Group-VIIA phospholipase A2) (gVIIA-PLA2) (LDL-associated phospholipase A2) (LDL-PLA(2)) (PAF 2-acylhydrolase)	8,91
O95992	CH25H	Cholesterol 25-hydroxylase (EC 1.14.99.38) (Cholesterol 25-monooxygenase) (h25OH)	8,98
Q7L5A8	FA2H FAAH FAXDC1	Fatty acid 2-hydroxylase (EC 1.14.18.-) (Fatty acid alpha-hydroxylase) (Fatty acid hydroxylase domain-containing protein 1)	9,03
Q9UNU6	CYP8B1 CYP12	7-alpha-hydroxycholest-4-en-3-one 12-alpha-hydroxylase (EC 1.14.14.139) (7-alpha-hydroxy-4-cholesten-3-one 12-alpha-hydroxylase) (CYPVIIIB1) (Cytochrome P450 8B1) (Sterol 12-alpha-hydroxylase)	9,11

Uniprot ID	Gene name(s)	Protein name(s)	Re-weighted M Scores
P52895	AKR1C2 DDH2	Aldo-keto reductase family 1 member C2 (EC 1.-.-.-) (EC 1.1.1.112) (EC 1.1.1.209) (EC 1.1.1.53) (EC 1.1.1.62) (EC 1.3.1.20) (3-alpha-HSD3) (Chlordecone reductase homolog HAKRD) (Dihydrodiol dehydrogenase 2) (DD-2) (DD2) (Dihydrodiol dehydrogenase/bile acid-binding protein) (DD/BABP) (Type III 3-alpha-hydroxysteroid dehydrogenase) (EC 1.1.1.357)	9,46
C9JRZ8	AKR1B15	Aldo-keto reductase family 1 member B15 (EC 1.1.1.-) (EC 1.1.1.300) (EC 1.1.1.54) (Estradiol 17-beta-dehydrogenase AKR1B15) (Farnesol dehydrogenase) (EC 1.1.1.216) (Testosterone 17beta-dehydrogenase) (EC 1.1.1.64)	9,48
P51659	HSD17B4 EDH17B4 SDR8C1	Peroxisomal multifunctional enzyme type 2 (MFE-2) (17-beta-hydroxysteroid dehydrogenase 4) (17-beta-HSD 4) (D-bifunctional protein) (DBP) (Multifunctional protein 2) (MFP-2) (Short chain dehydrogenase/reductase family 8C member 1) [Cleaved into: (3R)-hydroxyacyl-CoA dehydrogenase (EC 1.1.1.n12); Enoyl-CoA hydratase 2 (EC 4.2.1.107) (EC 4.2.1.119) (3-alpha,7-alpha,12-alpha-trihydroxy-5-beta-cholest-24-enoyl-CoA hydratase)]	9,62
Q9H227	GBA3 CBG CBGL1	Cytosolic beta-glucosidase (EC 3.2.1.21) (Cytosolic beta-glucosidase-like protein 1) (Cytosolic glycosylceramidase) (Cytosolic GCase) (Glucosidase beta acid 3) (Glucosylceramidase beta 3) (Klotho-related protein) (KLrP)	9,67
Q7L5L3	GDPD3 GDE7	Lysophospholipase D GDPD3 (EC 3.1.4.-) (Glycerophosphodiester phosphodiesterase 7) (Glycerophosphodiester phosphodiesterase domain-containing protein 3)	9,73
Q08426	EHHADH ECHD	Peroxisomal bifunctional enzyme (PBE) (PBFE) (L-bifunctional protein) (LBP) (Multifunctional enzyme 1) (MFE1) [Includes: Enoyl-CoA hydratase/3,2-trans-enoyl-CoA isomerase (EC 4.2.1.17) (EC 5.3.3.8); 3-hydroxyacyl-CoA dehydrogenase (EC 1.1.1.35)]	9,77
P40394	ADH7	All-trans-retinol dehydrogenase [NAD(+)] ADH7 (EC 1.1.1.105) (Alcohol dehydrogenase class 4 mu/sigma chain) (EC 1.1.1.1) (Alcohol dehydrogenase class IV mu/sigma chain) (Gastric alcohol dehydrogenase) (Omega-hydroxydecanoate dehydrogenase ADH7) (EC 1.1.1.66) (Retinol dehydrogenase)	9,79
Q15102	PAFAH1B3 PAFAHG	Platelet-activating factor acetylhydrolase IB subunit alpha1 (EC 3.1.1.47) (PAF acetylhydrolase 29 kDa subunit) (PAF-AH 29 kDa subunit) (PAF-AH subunit gamma) (PAFAH subunit gamma)	9,82
P53816	PLAAT3 HRASLS3	Phospholipase A and acyltransferase 3 (EC 2.3.1.-) (EC 3.1.1.32) (EC 3.1.1.4) (Adipose-specific	9,86

Uniprot ID	Gene name(s)	Protein name(s)	Re-weighted M Scores
	HREV107 PLA2G16	phospholipase A2) (AdPLA) (Group XVI phospholipase A1/A2) (H-rev 107 protein homolog) (H-REV107) (HREV107-1) (HRAS-like suppressor 1) (HRAS-like suppressor 3) (HRSL3) (HREV107-3) (Renal carcinoma antigen NY-REN-65)	
Q8TB40	ABHD4	(Lyso)-N-acylphosphatidylethanolamine lipase (EC 3.1.1.-) (Alpha/beta hydrolase domain-containing protein 4) (Abhydrolase domain-containing protein 4) (Alpha/beta-hydrolase 4)	9,91
Q96SZ5	ADO C10orf22	2-aminoethanethiol dioxygenase (EC 1.13.11.19) (Cysteamine dioxygenase)	9,93
O15496	PLA2G10	Group 10 secretory phospholipase A2 (EC 3.1.1.4) (Group X secretory phospholipase A2) (GX sPLA2) (sPLA2-X) (Phosphatidylcholine 2-acylhydrolase 10)	10,03
P51687	SUOX	Sulfite oxidase, mitochondrial (EC 1.8.3.1)	10,06
P42330	AKR1C3 DDH1 HSD17B5 KIAA0119 PGFS	Aldo-keto reductase family 1 member C3 (EC 1.1.1.-) (EC 1.1.1.210) (EC 1.1.1.53) (EC 1.1.1.62) (17-beta-hydroxysteroid dehydrogenase type 5) (17-beta-HSD 5) (3-alpha-HSD type II, brain) (3-alpha-hydroxysteroid dehydrogenase type 2) (3-alpha-HSD type 2) (EC 1.1.1.357) (Chlordecone reductase homolog HAKRb) (Dihydrodiol dehydrogenase 3) (DD-3) (DD3) (Dihydrodiol dehydrogenase type I) (HA1753) (Prostaglandin F synthase) (PGFS) (EC 1.1.1.188) (Testosterone 17-beta-dehydrogenase 5) (EC 1.1.1.239) (EC 1.1.1.64)	10,07
Q8NEL9	DDHD1 KIAA1705	Phospholipase DDHD1 (EC 3.1.1.-) (DDHD domain-containing protein 1) (Phosphatidic acid-preferring phospholipase A1 homolog) (PA-PLA1)	10,16
P17516	AKR1C4 CHDR	Aldo-keto reductase family 1 member C4 (EC 1.1.1.-) (EC 1.1.1.209) (EC 1.1.1.210) (EC 1.1.1.51) (EC 1.1.1.53) (EC 1.1.1.62) (3-alpha-hydroxysteroid dehydrogenase type I) (3-alpha-HSD1) (EC 1.1.1.357) (3alpha-hydroxysteroid 3-dehydrogenase) (Chlordecone reductase) (CDR) (EC 1.1.1.225) (Dihydrodiol dehydrogenase 4) (DD-4) (DD4) (HAKRA)	10,47
Q9BZM2	PLA2G2F	Group IIF secretory phospholipase A2 (GIIF sPLA2) (sPLA2-IIF) (EC 3.1.1.4) (Phosphatidylcholine 2-acylhydrolase 2F)	10,50
Q14914	PTGR1 LTB4DH	Prostaglandin reductase 1 (PRG-1) (15-oxoprostaglandin 13-reductase) (EC 1.3.1.48) (Dithiolethione-inducible gene 1 protein) (D3T-inducible gene 1 protein) (DIG-1) (Leukotriene B4 12-hydroxydehydrogenase) (NAD(P)H-dependent alkenal/one oxidoreductase) (EC 1.3.1.74)	10,59

Uniprot ID	Gene name(s)	Protein name(s)	Re-weighted M Scores
Q14749	GNMT	Glycine N-methyltransferase (EC 2.1.1.20)	10,82
Q7Z449	CYP2U1	Cytochrome P450 2U1 (Long-chain fatty acid omega-monooxygenase) (EC 1.14.14.80)	10,88
Q16850	CYP51A1 CYP51	Lanosterol 14-alpha demethylase (LDM) (EC 1.14.14.154) (CYPLI) (Cytochrome P450 51A1) (Cytochrome P450-14DM) (Cytochrome P45014DM) (Cytochrome P450LI) (Sterol 14-alpha demethylase)	10,88
P37059	HSD17B2 EDH17B2 SDR9C2	17-beta-hydroxysteroid dehydrogenase type 2 (17-beta-HSD 2) (20 alpha-hydroxysteroid dehydrogenase) (20-alpha-HSD) (E2DH) (Estradiol 17-beta-dehydrogenase 2) (EC 1.1.1.62) (Microsomal 17-beta-hydroxysteroid dehydrogenase) (Short chain dehydrogenase/reductase family 9C member 2) (Testosterone 17-beta-dehydrogenase) (EC 1.1.1.239)	10,98
P14060	HSD3B1 3BH HSDB3A	3 beta-hydroxysteroid dehydrogenase/Delta 5-->4-isomerase type 1 (3 beta-hydroxysteroid dehydrogenase/Delta 5-->4-isomerase type I) (3-beta-HSD I) (3-beta-hydroxy-5-ene steroid dehydrogenase) (3-beta-hydroxy-Delta(5)-steroid dehydrogenase) (EC 1.1.1.145) (3-beta-hydroxysteroid 3-dehydrogenase) (EC 1.1.1.270) (Delta-5-3-ketosteroid isomerase) (Dihydrotestosterone oxidoreductase) (EC 1.1.1.210) (Steroid Delta-isomerase) (EC 5.3.3.1) (Trophoblast antigen FDO161G)	11,03
P16152	CBR1 CBR CRN SDR21C1	Carbonyl reductase [NADPH] 1 (EC 1.1.1.184) (15-hydroxyprostaglandin dehydrogenase [NADP(+)]) (EC 1.1.1.196) (EC 1.1.1.197) (20-beta-hydroxysteroid dehydrogenase) (NADPH-dependent carbonyl reductase 1) (Prostaglandin 9-ketoreductase) (PG-9-KR) (Prostaglandin-E(2) 9-reductase) (EC 1.1.1.189) (Short chain dehydrogenase/reductase family 21C member 1)	11,18
Q86W10	CYP4Z1 UNQ3060/PRO9882	Cytochrome P450 4Z1 (EC 1.14.14.1) (CYPIVZ1) (Laurate 7-monooxygenase) (EC 1.14.14.130)	11,20
Q15738	NSDHL H105E3	Sterol-4-alpha-carboxylate 3-dehydrogenase, decarboxylating (EC 1.1.1.170) (Protein H105e3)	11,33
O75845	SC5D SC5DL	Lathosterol oxidase (EC 1.14.19.20) (C-5 sterol desaturase) (Delta(7)-sterol 5-desaturase) (Delta(7)-sterol C5(6)-desaturase) (Lathosterol 5-desaturase) (Sterol-C5-desaturase)	11,39
P17405	SMPD1 ASM	Sphingomyelin phosphodiesterase (EC 3.1.4.12) (Acid sphingomyelinase) (aSMase)	11,46
P40925	MDH1 MDHA	Malate dehydrogenase, cytoplasmic (EC 1.1.1.37) (Cytosolic malate dehydrogenase)	11,56

Uniprot ID	Gene name(s)	Protein name(s)	Re-weighted M Scores
		(Diiodophenylpyruvate reductase) (EC 1.1.1.96)	
O14756	HSD17B6 RODH SDR9C6	17-beta-hydroxysteroid dehydrogenase type 6 (17-beta-HSD 6) (17-beta-HSD6) (EC 1.1.1.105) (EC 1.1.1.209) (EC 1.1.1.239) (EC 1.1.1.53) (EC 1.1.1.62) (3-alpha->beta-hydroxysteroid epimerase) (3-alpha->beta-HSE) (Oxidative 3-alpha hydroxysteroid dehydrogenase) (Short chain dehydrogenase/reductase family 9C member 6)	11,63
P0C869	PLA2G4B	Cytosolic phospholipase A2 beta (cPLA2-beta) (EC 3.1.1.4) (Lysophospholipase A1 group IVB) (EC 3.1.1.5) (Phospholipase A2 group IVB)	11,80
Q99424	ACOX2	Peroxisomal acyl-coenzyme A oxidase 2 (EC 1.17.99.3) (3-alpha,7-alpha,12-alpha-trihydroxy-5-beta-cholestanoyl-CoA 24-hydroxylase) (3-alpha,7-alpha,12-alpha-trihydroxy-5-beta-cholestanoyl-CoA oxidase) (Trihydroxycoprostanoyl-CoA oxidase) (THCA-CoA oxidase) (THCCox)	12,03
Q9NY59	SMPD3	Sphingomyelin phosphodiesterase 3 (EC 3.1.4.12) (Neutral sphingomyelinase 2) (nSMase-2) (nSMase2) (Neutral sphingomyelinase II)	12,11
Q99487	PAFAH2	Platelet-activating factor acetylhydrolase 2, cytoplasmic (EC 3.1.1.47) (PAF:lysophospholipid transacetylase) (PAF:sphingosine transacetylase) (Platelet-activating factor acetyltransferase PAFAH2) (EC 2.3.1.149) (Serine-dependent phospholipase A2) (SD-PLA2) (hSD-PLA2)	12,11
P68402	PAFAH1B2 PAFAHB	Platelet-activating factor acetylhydrolase IB subunit alpha2 (EC 3.1.1.47) (PAF acetylhydrolase 30 kDa subunit) (PAF-AH 30 kDa subunit) (PAF-AH subunit beta) (PAFAH subunit beta)	12,13
Q9NZ20	PLA2G3	Group 3 secretory phospholipase A2 (EC 3.1.1.4) (Group III secretory phospholipase A2) (GIII sPLA2) (sPLA2-III) (Phosphatidylcholine 2-acylhydrolase 3)	12,22
Q86XP0	PLA2G4D	Cytosolic phospholipase A2 delta (cPLA2-delta) (EC 3.1.1.4) (Phospholipase A2 group IVD)	12,33
P11766	ADH5 ADHX FDH	Alcohol dehydrogenase class-3 (EC 1.1.1.1) (Alcohol dehydrogenase 5) (Alcohol dehydrogenase class chi chain) (Alcohol dehydrogenase class-III) (Glutathione-dependent formaldehyde dehydrogenase) (FALDH) (FDH) (GSH-FDH) (EC 1.1.1.-) (S-(hydroxymethyl)glutathione dehydrogenase) (EC 1.1.1.284)	12,46
Q96F10	SAT2 SSAT2	Thialysine N-epsilon-acetyltransferase (EC 2.3.1.-) (Diamine acetyltransferase 2) (EC 2.3.1.57) (Spermidine/spermine N(1)-acetyltransferase 2) (SSAT-2)	13,55

Uniprot ID	Gene name(s)	Protein name(s)	Re-weighted M Scores
Q68DD2	PLA2G4F	Cytosolic phospholipase A2 zeta (cPLA2-zeta) (EC 3.1.1.4) (Phospholipase A2 group IVF)	14,56
Q8TAV3	CYP2W1	Cytochrome P450 2W1 (EC 1.14.14.-) (CYPIIW1)	17,14

Helmholtz Center Declaration of no-objection of sample material

Declaration of no-objection of sample material

11.05.2021

To:
Helmholtz Zentrum München – Deutsches Forschungszentrum für Gesundheit und Umwelt GmbH
Research Unit Analytical BioGeoChemistry / Prof. Dr. Philippe Schmitt-Kopplin
Ingolstaedter Landstr. 1
D-85764 Neuherberg

From:
Else Kröner-Fresenius-Zentrum für Ernährungsmedizin der TU München
Wissenschaftszentrum Weihenstephan
Lehrstuhl für Ernährungsmedizin
ZIEL - Institute for Food & Health

Address:
Gregor-Mendel-Str. 2
85354 Freising, Germany

Contact person:
Sonia Erfanian
Tel.: 08161/712397
E-Mail: sonia.erfanian@tum.de

Title of the project:
Investigation of COBLL1 mechanism and its impact on the metabolomics signature (Metabolomic analysis of cells and cell media)

Information on sample material to be analyzed:
No. of samples: 11
Sample matrix: cells and cell media

We hereby confirm that samples send for analysis have been negatively tested against HIV, HBV, HCV and SARS-CoV-2 (COVID19; if samples were collected since January 2020). Copies of certificates are attached.

NOTICE: Non-tested or positively tested sample material or sample material without respective certificates may not be analyzed according to safety regulations.

11.5.21

Signature principal investigatorCompany

Prof. Dr. H. Hauner
Direktor des Else Kröner-Fresenius-Zentrums für Ernährungsmedizin d. TU München
Wissenschaftszentrum Weihenstephan
Lehrstuhl für Ernährungsmedizin
ZIEL - Institute for Food & Health
Gregor-Mendel-Str. 2
85354 Freising, Germany

stamp

LETTERS OF APPROVAL

WHO Letter of Approval, March 2023

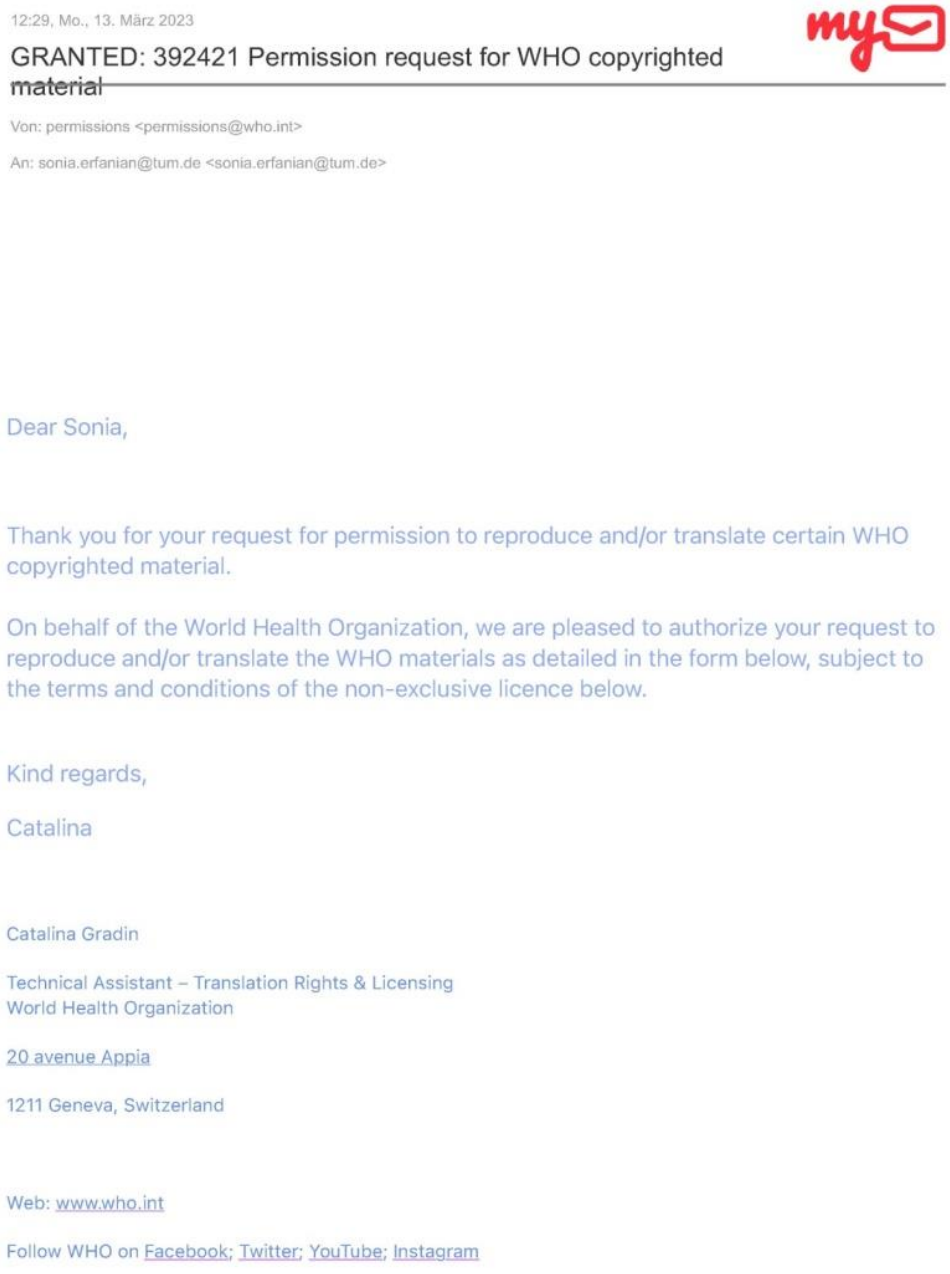

12:29, Mo., 13. März 2023

GRANTED: 392421 Permission request for WHO copyrighted material

Von: permissions <permissions@who.int>

An: sonia.erfanian@tum.de <sonia.erfanian@tum.de>

Dear Sonia,

Thank you for your request for permission to reproduce and/or translate certain WHO copyrighted material.

On behalf of the World Health Organization, we are pleased to authorize your request to reproduce and/or translate the WHO materials as detailed in the form below, subject to the terms and conditions of the non-exclusive licence below.

Kind regards,

Catalina

Catalina Gradin

Technical Assistant – Translation Rights & Licensing
World Health Organization

20 avenue Appia

1211 Geneva, Switzerland

Web: www.who.int

Follow WHO on Facebook; Twitter; YouTube; Instagram

[...]

Elsevier Letter of Approval, April 2023

ELSEVIER LICENSE
TERMS AND CONDITIONS

Apr 10, 2023

This Agreement between TUM Munich -- Sonia Erfanian ("You") and Elsevier ("Elsevier") consists of your license details and the terms and conditions provided by Elsevier and Copyright Clearance Center.

License Number	5519270650666
License date	Mar 31, 2023
Licensed Content Publisher	Elsevier
Licensed Content Publication	Drug Discovery Today: Disease Mechanisms
Licensed Content Title	Lipid mediators and inflammation in glucose intolerance and insulin resistance
Licensed Content Author	Abishek Iyer,Lindsay Brown
Licensed Content Date	Winter 2010
Licensed Content Volume	7
Licensed Content Issue	3-4
Licensed Content Pages	7
Start Page	e191
End Page	e197
Type of Use	reuse in a thesis/dissertation

[...]

Brucker Letter of Approval, April 2023

21:32, Do., 13. April 2023

RE: BRKR-0956208: Request for Permission to Reprint [ref:_00Dd0fwhj._5006Nb7LCd:ref]

Von: Service BDAL DE <service.bdal.de@bruker.com>

An: soniaerfanian@hotmail.de <soniaerfanian@hotmail.de>

Hallo Frau Erfanian,

Sie können die Abbildung gerne verwenden mit dem Verweis, dass sie von Bruker ist (Trainingsmaterial).

Mit freundlichen Grüßen / Best regards,

i. A. Dr. Matthias Witt
Customer Support MRMS Application

Bruker Daltonik GmbH
Fahrenheitstr. 4
28359 Bremen, Germany
Phone: +49 421 2205-268
mrms.appl.support.emea@bruker.com
www.bruker.com

Besucher- und Lieferadresse / Visitor and Shipping address:
Bruker Daltonik GmbH
Wiener Straße 6
28359 Bremen, Germany

[...]

LITERATURE

Adams DM, Ricci KW. Vascular Anomalies: Diagnosis of Complicated Anomalies and New Medical Treatment Options. Hematol Oncol Clin North Am. 2019 Jun;33(3):455-470. doi: 10.1016/j.hoc.2019.01.011. PMID: 31030813.

Aharoni A, Ric de Vos CH, Verhoeven HA, Maliepaard CA, Kruppa G, Bino R, Goodenowe DB. Nontargeted metabolome analysis by use of Fourier Transform Ion Cyclotron Mass Spectrometry. OMICS. 2002;6(3):217-34. doi: 10.1089/15362310260256882. PMID: 12427274.

American Diabetes Association. Diagnosis and classification of diabetes mellitus. Diabetes Care. 2013 Jan;36 Suppl 1(Suppl 1):S67-74. doi: 10.2337/dc13-S067. PMID: 23264425; PMCID: PMC3537273.

American Diabetes Association. 2. Classification and Diagnosis of Diabetes: Standards of Medical Care in Diabetes-2021. Diabetes Care. 2021 Jan;44(Suppl 1):S15-S33. doi: 10.2337/dc21-S002. Erratum in: Diabetes Care. 2021 Sep;44(9):2182. PMID: 33298413.

Asada N, Takahashi Y, Honjo M. Effects of 22K or 20K human growth hormone on lipolysis, leptin production in adipocytes in the presence and absence of human growth hormone binding protein. Horm Res. 2000;54(4):203-7. doi: 10.1159/000053260. PMID: 11416239.

Ataey A, Jafarvand E, Adham D, Moradi-Asl E. The Relationship Between Obesity, Overweight, and the Human Development Index in World Health Organization Eastern Mediterranean Region Countries. J Prev Med Public Health. 2020 Mar;53(2):98-105. doi: 10.3961/jpmph.19.100. Epub 2020 Mar 31. PMID: 32268464; PMCID: PMC7142010.

Baena-Díez JM, Peñafiel J, Subirana I, Ramos R, Elosua R, Marín-Ibañez A, Guembe MJ, Rigo F, Tormo-Díaz MJ, Moreno-Iribas C et al. Risk of Cause-Specific Death in Individuals With Diabetes: A Competing Risks Analysis. Diabetes Care. 2016 Nov;39(11):1987-1995. doi: 10.2337/dc16-0614. Epub 2016 Aug 4. PMID: 27493134.

Bado A, Levasseur S, Attoub S, Kermorgant S, Laigneau JP, Bortoluzzi MN, Moizo L, Lehy T, Guerre-Millo M, Le Marchand-Brustel Y, Lewin MJ. The stomach is a source of leptin. Nature. 1998 Aug 20;394(6695):790-3. doi: 10.1038/29547. PMID: 9723619.

Balla T. Phosphoinositides: tiny lipids with giant impact on cell regulation. Physiol Rev. 2013 Jul;93(3):1019-137. doi: 10.1152/physrev.00028.2012. PMID: 23899561; PMCID: PMC3962547.

Bambace C, Telesca M, Zoico E, Sepe A, Olioso D, Rossi A, Corzato F, Di Francesco V, Mazzucco A, Santini F, Zamboni M. Adiponectin gene expression and adipocyte diameter: a comparison between epicardial and subcutaneous adipose tissue in men. Cardiovasc Pathol. 2011 Sep-Oct;20(5):e153-6. doi: 10.1016/j.carpath.2010.07.005. Epub 2010 Sep 9. PMID: 20829073.

Banerji J, Rusconi S, Schaffner W. Expression of a beta-globin gene is enhanced by remote SV40 DNA sequences. Cell. 1981 Dec;27(2 Pt 1):299-308. doi: 10.1016/0092-8674(81)90413-x. PMID: 6277502.

Bannister AJ, Kouzarides T. Regulation of chromatin by histone modifications. Cell Res. 2011 Mar;21(3):381-95. doi: 10.1038/cr.2011.22. Epub 2011 Feb 15. PMID: 21321607; PMCID: PMC3193420.

Bansal P, Morgat A, Axelsen KB, Muthukrishnan V, Coudert E, Aimo L, Hyka-Nouspikel N, Gasteiger E, Kerhornou A, Neto TB, et al. Rhea, the reaction knowledgebase in 2022. Nucleic Acids Res. 2022 Jan 7;50(D1):D693-D700. doi: 10.1093/nar/gkab1016. PMID: 34755880; PMCID: PMC8728268.

Barak Y, Nelson MC, Ong ES, Jones YZ, Ruiz-Lozano P, Chien KR, Koder A, Evans RM. PPAR gamma is required for placental, cardiac, and adipose tissue development. Mol Cell. 1999 Oct;4(4):585-95. doi: 10.1016/s1097-2765(00)80209-9. PMID: 10549290.

Barozzi I, Simonatto M, Bonifacio S, Yang L, Rohs R, Ghisletti S, Natoli G. Coregulation of transcription factor binding and nucleosome occupancy through DNA features of mammalian enhancers. Mol Cell. 2014 Jun 5;54(5):844-857. doi: 10.1016/j.molcel.2014.04.006. Epub 2014 May 8. PMID: 24813947; PMCID: PMC4048654.

Bernstein BE, Meissner A, Lander ES. The mammalian epigenome. Cell. 2007 Feb 23;128(4):669-81. doi: 10.1016/j.cell.2007.01.033. PMID: 17320505.

Bialesova L, Kulyté A, Petrus P, Sinha I, Laurencikiene J, Zhao C, Wright KD, Arner P, Dahlman I. Epigenetic Regulation of PLIN 1 in Obese Women and its Relation to Lipolysis. Sci Rep. 2017 Aug 31;7(1):10152. doi: 10.1038/s41598-017-09232-y. PMID: 28860604; PMCID: PMC5578955.

Boden G, Chen X, Mozzoli M, Ryan I. Effect of fasting on serum leptin in normal human subjects. J Clin Endocrinol Metab. 1996 Sep;81(9):3419-23. doi: 10.1210/jcem.81.9.8784108. PMID: 8784108.

Boqué N, de la Iglesia R, de la Garza AL, Milagro FI, Olivares M, Bañuelos O, Soria AC, Rodríguez-Sánchez S, Martínez JA, Campión J. Prevention of diet-induced obesity by apple polyphenols in Wistar rats through regulation of adipocyte gene expression and DNA methylation patterns. Mol Nutr Food Res. 2013 Aug;57(8):1473-8. doi: 10.1002/mnfr.201200686. Epub 2013 Mar 25. PMID: 23529981.

Bouzakri K, Zachrisson A, Al-Khalili L, Zhang BB, Koistinen HA, Krook A, Zierath JR. siRNA-based gene silencing reveals specialized roles of IRS-1/Akt2 and IRS-2/Akt1 in glucose and lipid metabolism in human skeletal muscle. Cell Metab. 2006 Jul;4(1):89-96. doi: 10.1016/j.cmet.2006.04.008. PMID: 16814735.

Bowers RR, Kim JW, Otto TC, Lane MD. Stable stem cell commitment to the adipocyte lineage by inhibition of DNA methylation: role of the BMP-4 gene. Proc Natl Acad Sci U S A. 2006 Aug 29;103(35):13022-7. doi: 10.1073/pnas.0605789103. Epub 2006 Aug 17. PMID: 16916928; PMCID: PMC1559746.

Brachmann SM, Ueki K, Engelman JA, Kahn RC, Cantley LC. Phosphoinositide 3-kinase catalytic subunit deletion and regulatory subunit deletion have opposite effects on insulin sensitivity in mice. Mol Cell Biol. 2005 Mar;25(5):1596-607. doi: 10.1128/MCB.25.5.1596-1607.2005. PMID: 15713620; PMCID: PMC549361.

Bradley RL, Cheatham B. Regulation of ob gene expression and leptin secretion by insulin and dexamethasone in rat adipocytes. Diabetes. 1999 Feb;48(2):272-8. doi: 10.2337/diabetes.48.2.272. PMID: 10334301.

Brasaemle DL, Levin DM, Adler-Wailes DC, Londos C. The lipolytic stimulation of 3T3-L1 adipocytes promotes the translocation of hormone-sensitive lipase to the surfaces of lipid storage droplets. Biochim Biophys Acta. 2000 Jan 17;1483(2):251-62. doi: 10.1016/s1388-1981(99)00179-1. PMID: 10634941.

Bruce SJ, Tavazzi I, Parisod V, Rezzi S, Kochhar S, Guy PA. Investigation of human blood plasma sample preparation for performing metabolomics using ultrahigh performance liquid chromatography/mass spectrometry. Anal Chem. 2009 May 1;81(9):3285-96. doi: 10.1021/ac8024569. PMID: 19323527.

Cao Z, Umek RM, McKnight SL. Regulated expression of three C/EBP isoforms during adipose conversion of 3T3-L1 cells. Genes Dev. 1991 Sep;5(9):1538-52. doi: 10.1101/gad.5.9.1538. PMID: 1840554.

Castro-Gómez P, Garcia-Serrano A, Visioli F, Fontecha J. Relevance of dietary glycerophospholipids and sphingolipids to human health. Prostaglandins Leukot Essent Fatty Acids. 2015 Oct;101:41-51. doi: 10.1016/j.plefa.2015.07.004. Epub 2015 Jul 26. PMID: 26242691.

Cerami A, Stevens VJ, Monnier VM. Role of nonenzymatic glycosylation in the development of the sequelae of diabetes mellitus. Metabolism. 1979 Apr;28(4 Suppl 1):431-7. doi: 10.1016/0026-0495(79)90051-9. PMID: 122296.

Chan JL, Blüher S, Yiannakouris N, Suchard MA, Kratzsch J, Mantzoros CS. Regulation of circulating soluble leptin receptor levels by gender, adiposity, sex steroids, and leptin: observational and interventional studies in humans. Diabetes. 2002 Jul;51(7):2105-12. doi: 10.2337/diabetes.51.7.2105. PMID: 12086939.

Chen J, Zhao X, Fritsche J, Yin P, Schmitt-Kopplin P, Wang W, Lu X, Häring HU, Schleicher ED, Lehmann R, Xu G. Practical approach for the identification and isomer elucidation of biomarkers detected in a metabonomic study for the discovery of individuals at risk for diabetes by integrating the chromatographic and mass spectrometric information. Anal Chem. 2008 Feb 15;80(4):1280-9. doi: 10.1021/ac702089h. Epub 2008 Jan 15. PMID: 18193893.

Chen J, Sun M, Adeyemo A, Pirie F, Carstensen T, Pomilla C, Doumatey AP, Chen G, Young EH, Sandhu M, Morris AP, Barroso I, McCarthy MI, Mahajan A, Wheeler E, Rotimi CN, Motala AA. Genome-wide association study of type 2 diabetes in Africa. Diabetologia. 2019 Jul;62(7):1204-1211. doi: 10.1007/s00125-019-4880-7. Epub 2019 May 2. PMID: 31049640; PMCID: PMC6560001.

Chernushevich IV, Loboda AV, Thomson BA. An introduction to quadrupole-time-of-flight mass spectrometry. J Mass Spectrom. 2001 Aug;36(8):849-65. doi: 10.1002/jms.207. PMID: 11523084.

Cho H, Mu J, Kim JK, Thorvaldsen JL, Chu Q, Crenshaw EB 3rd, Kaestner KH, Bartolomei MS, Shulman GI, Birnbaum MJ. Insulin resistance and a diabetes mellitus-like syndrome in mice lacking the protein kinase Akt2 (PKB beta). Science. 2001 Jun 1;292(5522):1728-31. doi: 10.1126/science.292.5522.1728. PMID: 11387480.

Clapier CR, Cairns BR. The biology of chromatin remodeling complexes. Annu Rev Biochem. 2009;78:273-304. doi: 10.1146/annurev.biochem.77.062706.153223. PMID: 19355820.

Claussnitzer M, Dankel SN, Klocke B, Grallert H, Glunk V, Berulava T, Lee H, Oskolkov N, Fadista J, Ehlers K, Wahl S, Hoffmann C, Qian K, Rönn T, Riess H, Müller-Nurasyid M, Bretschneider N, Schroeder T, Skurk T, Horsthemke B; DIAGRAM+Consortium, Spieler D, Klingenspor M, Seifert M, Kern MJ, Mejhert N, Dahlman I, Hansson O, Hauck SM, Blüher M, Arner P, Groop L, Illig T, Suhre K, Hsu YH, Mellgren G, Hauner H, Laumen H. Leveraging cross-species transcription factor binding site patterns: from diabetes risk loci to disease mechanisms. Cell. 2014 Jan 16;156(1-2):343-58. doi: 10.1016/j.cell.2013.10.058. PMID: 24439387; PMCID: PMC7116609.

Claussnitzer M, Dankel SN, Kim KH, Quon G, Meuleman W, Haugen C, Glunk V, Sousa IS, Beaudry JL, Puviindran V, Abdennur NA, Liu J, Svensson PA, Hsu YH, Drucker DJ, Mellgren G, Hui CC, Hauner H, Kellis M. FTO Obesity Variant Circuitry and Adipocyte Browning in Humans. N Engl J Med. 2015 Sep 3;373(10):895-907. doi: 10.1056/NEJMoa1502214. Epub 2015 Aug 19. PMID: 26287746; PMCID: PMC4959911.

Copps KD, White MF. Regulation of insulin sensitivity by serine/threonine phosphorylation of insulin receptor substrate proteins IRS1 and IRS2. Diabetologia. 2012 Oct;55(10):2565-2582. doi: 10.1007/s00125-012-2644-8. Epub 2012 Aug 8. PMID: 22869320; PMCID: PMC4011499.

Creyghton MP, Cheng AW, Welstead GG, Kooistra T, Carey BW, Steine EJ, Hanna J, Lodato MA, Frampton GM, Sharp PA, Boyer LA, Young RA, Jaenisch R. Histone H3K27ac separates active from poised enhancers and predicts developmental state. Proc Natl Acad Sci U S A. 2010 Dec 14;107(50):21931-6. doi: 10.1073/pnas.1016071107. Epub 2010 Nov 24. PMID: 21106759; PMCID: PMC3003124.

Cristancho AG, Lazar MA. Forming functional fat: a growing understanding of adipocyte differentiation. Nat Rev Mol Cell Biol. 2011 Sep 28;12(11):722-34. doi: 10.1038/nrm3198. PMID: 21952300; PMCID: PMC7171550.

Cypess AM, Kahn CR. Brown fat as a therapy for obesity and diabetes. Curr Opin Endocrinol Diabetes Obes. 2010 Apr;17(2):143-9. doi: 10.1097/MED.0b013e328337a81f. PMID: 20160646; PMCID: PMC3593105.

Czech MP. Cellular basis of insulin insensitivity in large rat adipocytes. J Clin Invest. 1976 Jun;57(6):1523-32. doi: 10.1172/JCI108422. PMID: 932192; PMCID: PMC436811.

D'Adamo E, Caprio S. Type 2 diabetes in youth: epidemiology and pathophysiology. Diabetes Care. 2011 May;34 Suppl 2(Suppl 2):S161-5. doi: 10.2337/dc11-s212. PMID: 21525449; PMCID: PMC3632155.

Dalen KT, Schoonjans K, Ulven SM, Weedon-Fekjaer MS, Bentzen TG, Koutnikova H, Auwerx J, Nebb HI. Adipose tissue expression of the lipid droplet-associating proteins S3-12 and perilipin is controlled by peroxisome proliferator-activated receptor-gamma. Diabetes. 2004 May;53(5):1243-52. doi: 10.2337/diabetes.53.5.1243. PMID: 15111493.

Daviglus ML, Stamler J, Pirzada A, Yan LL, Garside DB, Liu K, Wang R, Dyer AR, Lloyd-Jones DM, Greenland P. Favorable cardiovascular risk profile in young women and long-term risk of cardiovascular and all-cause mortality. JAMA. 2004 Oct 6;292(13):1588-92. doi: 10.1001/jama.292.13.1588. PMID: 15467061.

Desmarchelier C, Martin JC, Planells R, Gastaldi M, Nowicki M, Goncalves A, Valéro R, Lairon D, Borel P. The postprandial chylomicron triacylglycerol response to dietary fat in healthy male adults is significantly explained by a combination of single nucleotide polymorphisms in genes involved in triacylglycerol metabolism. J Clin Endocrinol Metab. 2014 Mar;99(3):E484-8. doi: 10.1210/jc.2013-3962. Epub 2014 Jan 13. PMID: 24423365.

Dettmer K, Aronov PA, Hammock BD. Mass spectrometry-based metabolomics. Mass Spectrom Rev. 2007 Jan-Feb;26(1):51-78. doi: 10.1002/mas.20108. PMID: 16921475; PMCID: PMC1904337.

Dewan A, Liu M, Hartman S, Zhang SS, Liu DT, Zhao C, Tam PO, Chan WM, Lam DS, Snyder M, Barnstable C, Pang CP, Hoh J. HTRA1 promoter polymorphism in wet age-related macular degeneration. Science. 2006 Nov 10;314(5801):989-92. doi: 10.1126/science.1133807. Epub 2006 Oct 19. PMID: 17053108.

DIAbetes Genetics Replication And Meta-analysis (DIAGRAM) Consortium et al. Large-scale association analysis provides insights into the genetic architecture and pathophysiology of type 2 diabetes. Nat Genet. 2012 Sep;44(9):981-90. doi: 10.1038/ng.2383. Epub 2012 Aug 12. PMID: 22885922; PMCID: PMC3442244.

DIAbetes Genetics Replication And Meta-analysis (DIAGRAM) Consortium; Asian Genetic Epidemiology Network Type 2 Diabetes (AGEN-T2D) Consortium; South Asian Type 2 Diabetes (SAT2D) Consortium; Mexican American Type 2 Diabetes (MAT2D) Consortium; Type 2 Diabetes Genetic Exploration by Nex-generation sequencing in muylti-Ethnic Samples (T2D-GENES) Consortium et al. Genome-wide trans-ancestry meta-analysis provides insight into the genetic architecture of type 2 diabetes susceptibility. Nat Genet. 2014 Mar;46(3):234-44. doi: 10.1038/ng.2897. Epub 2014 Feb 9. PMID: 24509480; PMCID: PMC3969612.

Dubern B. Génétique et épigénétique de l'obésité : les pistes pour comprendre [Genetics and epigenetics of obesity: keys to understand]. Rev Prat. 2019 Nov;69(9):1016-1019. French. PMID: 32237628.

Dubuc GR, Phinney SD, Stern JS, Havel PJ. Changes of serum leptin and endocrine and metabolic parameters after 7 days of energy restriction in men and women. Metabolism. 1998 Apr;47(4):429-34. doi: 10.1016/s0026-0495(98)90055-5. PMID: 9550541.

Emerging Risk Factors Collaboration, Sarwar N, Gao P, Seshasai SR, Gobin R, Kaptoge S, Di Angelantonio E, Ingelsson E, Lawlor DA, Selvin E, Stampfer M, et al. Diabetes mellitus, fasting blood glucose concentration, and risk of vascular disease: a collaborative meta-analysis of 102 prospective studies. Lancet. 2010 Jun 26;375(9733):2215-22. doi: 10.1016/S0140-6736(10)60484-9. Erratum in: Lancet. 2010 Sep 18;376(9745):958. Hillage, H L [corrected to Hillege, H L]. PMID: 20609967; PMCID: PMC2904878.

Emwas AH. The strengths and weaknesses of NMR spectroscopy and mass spectrometry with particular focus on metabolomics research. Methods Mol Biol. 2015;1277:161-93. doi: 10.1007/978-1-4939-2377-9_13. PMID: 25677154.

Emwas AH, Roy R, McKay RT, Tenori L, Saccenti E, Gowda GAN, Raftery D, Alahmari F, Jaremko L, Jaremko M, Wishart DS. NMR Spectroscopy for Metabolomics Research. Metabolites. 2019 Jun 27;9(7):123. doi: 10.3390/metabo9070123. PMID: 31252628; PMCID: PMC6680826.

ENCODE Project Consortium. An integrated encyclopedia of DNA elements in the human genome. Nature. 2012 Sep 6;489(7414):57-74. doi: 10.1038/nature11247. PMID: 22955616; PMCID: PMC3439153.

Fagerholm SC, Varis M, Stefanidakis M, Hilden TJ, Gahmberg CG. alpha-Chain phosphorylation of the human leukocyte CD11b/CD18 (Mac-1) integrin is pivotal for integrin activation to bind ICAMs and leukocyte extravasation. Blood. 2006 Nov 15;108(10):3379-86. doi: 10.1182/blood-2006-03-013557. Epub 2006 Jul 20. PMID: 16857989.

Fagerholm SC, MacPherson M, James MJ, Sevier-Guy C, Lau CS. The CD11b-integrin (ITGAM) and systemic lupus erythematosus. Lupus. 2013 Jun;22(7):657-63. doi: 10.1177/0961203313491851. PMID: 23753600.

Fain JN, Leffler CW, Bahouth SW. Eicosanoids as endogenous regulators of leptin release and lipolysis by mouse adipose tissue in primary culture. J Lipid Res. 2000a Oct;41(10):1689-94. PMID: 11013312.

Fain JN, Leffler CW, Bahouth SW, Rice AM, Rivkees SA. Regulation of leptin release and lipolysis by PGE2 in rat adipose tissue. Prostaglandins Other Lipid Mediat. 2000b Oct;62(4):343-50. doi: 10.1016/s0090-6980(00)00088-5. PMID: 11060898.

Faith JJ, Hayete B, Thaden JT, Mogno I, Wierzbowski J, Cottarel G, Kasif S, Collins JJ, Gardner TS. Large-scale mapping and validation of Escherichia coli transcriptional regulation from a compendium of expression profiles. PLoS Biol. 2007 Jan;5(1):e8. doi: 10.1371/journal.pbio.0050008. PMID: 17214507; PMCID: PMC1764438.

Farmer SR. Transcriptional control of adipocyte formation. Cell Metab. 2006 Oct;4(4):263-73. doi: 10.1016/j.cmet.2006.07.001. PMID: 17011499; PMCID: PMC1958996.

Farr OM, Gavrieli A, Mantzoros CS. Leptin applications in 2015: what have we learned about leptin and obesity? Curr Opin Endocrinol Diabetes Obes. 2015 Oct;22(5):353-9. doi: 10.1097/MED.0000000000000184. PMID: 26313897; PMCID: PMC4610373.

Fasshauer M, Blüher M. Adipokines in health and disease. Trends Pharmacol Sci. 2015 Jul;36(7):461-70. doi: 10.1016/j.tips.2015.04.014. Epub 2015 May 25. PMID: 26022934.

Fiehn O. Metabolomics--the link between genotypes and phenotypes. Plant Mol Biol. 2002 Jan;48(1-2):155-71. PMID: 11860207.

Forcisi S, Moritz F, Kanawati B, Tziotis D, Lehmann R, Schmitt-Kopplin P. Liquid chromatography-mass spectrometry in metabolomics research: mass analyzers in ultra high-pressure liquid chromatography coupling. J Chromatogr A. 2013 May 31; 1292:51-65. doi: 10.1016/j.chroma.2013.04.017. Epub 2013 Apr 11. PMID: 23631876.

Forcisi S, Moritz F, Lucio M, Lehmann R, Stefan N, Schmitt-Kopplin P. Solutions for low and high accuracy mass spectrometric data matching: a data-driven annotation strategy in nontargeted metabolomics. Anal Chem. 2015 Sep 1;87(17):8917-24. doi: 10.1021/acs.analchem.5b02049. Epub 2015 Aug 12. PMID: 26197019.

Freytag SO, Paielli DL, Gilbert JD. Ectopic expression of the CCAAT/enhancer-binding protein alpha promotes the adipogenic program in a variety of mouse fibroblastic cells. Genes Dev. 1994 Jul 15;8(14):1654-63. doi: 10.1101/gad.8.14.1654. PMID: 7958846.

Frontini A, Cinti S. Distribution and development of brown adipocytes in the murine and human adipose organ. Cell Metab. 2010 Apr 7;11(4):253-6. doi: 10.1016/j.cmet.2010.03.004. PMID: 20374956.

Fruman DA, Chiu H, Hopkins BD, Bagrodia S, Cantley LC, Abraham RT. The PI3K Pathway in Human Disease. Cell. 2017 Aug 10;170(4):605-635. doi: 10.1016/j.cell.2017.07.029. PMID: 28802037; PMCID: PMC5726441.

Gandotra S, Le Dour C, Bottomley W, Cervera P, Giral P, Reznik Y, Charpentier G, Auclair M, Delépine M, Barroso I, et al. Perilipin deficiency and autosomal dominant partial lipodystrophy. N Engl J Med. 2011 Feb 24;364(8):740-8. doi: 10.1056/NEJMoa1007487. PMID: 21345103; PMCID: PMC3773916.

Gavaghan CL, Holmes E, Lenz E, Wilson ID, Nicholson JK. An NMR-based metabonomic approach to investigate the biochemical consequences of genetic strain differences: application to the C57BL10J and Alpk:ApfCD mouse. FEBS Lett. 2000 Nov 10;484(3):169-74. doi: 10.1016/s0014-5793(00)02147-5. PMID: 11078872.

GBD 2019 Blindness and Vision Impairment Collaborators; Vision Loss Expert Group of the Global Burden of Disease Study. Causes of blindness and vision impairment in 2020 and trends over 30 years, and prevalence of avoidable blindness in relation to VISION 2020: the Right to Sight: an analysis for the Global Burden of Disease Study. Lancet Glob Health. 2021 Feb;9(2): e144-e160. doi: 10.1016/S2214-109X(20)30489-7. Epub 2020 Dec 1. Erratum in: Lancet Glob Health. 2021 Apr;9(4): e408. PMID: 33275949; PMCID: PMC7820391.

Ghaben AL, Scherer PE. Adipogenesis and metabolic health. Nat Rev Mol Cell Biol. 2019 Apr;20(4):242-258. doi: 10.1038/s41580-018-0093-z. PMID: 30610207.

Gillberg L, Perfilyev A, Brøns C, Thomasen M, Grunnet LG, Volkov P, Rosqvist F, Iggman D, Dahlman I, Risérus U, Rönn T, Nilsson E, Vaag A, Ling C. Adipose tissue transcriptomics and epigenomics in low birthweight men and controls: role of high-fat overfeeding. Diabetologia. 2016 Apr;59(4):799-812. doi: 10.1007/s00125-015-3852-9. Epub 2016 Jan 11. PMID: 26750116.

Gillespie M, Jassal B, Stephan R, Milacic M, Rothfels K, Senff-Ribeiro A, Griss J, Sevilla C, Matthews L, Gong C, et al. The reactome pathway knowledgebase 2022. Nucleic Acids Res. 2022 Jan 7;50(D1):D687-D692. doi: 10.1093/nar/gkab1028. PMID: 34788843; PMCID: PMC8689983.

Glunk V., Laber S., Strobel S., Kubitz P., Nemati Moud B., Honecker J., Skurk T., Hauner H., Claussnitzer M., et al., A non-coding variant linked to metabolic obesity with normal weight affects actin remodelling in subcutaneous adipocytes, 2023, Nat Metab. 5 2023 May;5(5):861-879. doi: 10.1038/s42255-023-00807-w. Epub 2023 May 30.

Goncalves MD, Hopkins BD, Cantley LC. Phosphatidylinositol 3-Kinase, Growth Disorders, and Cancer. N Engl J Med. 2018 Nov 22;379(21):2052-2062. doi: 10.1056/NEJMra1704560. PMID: 30462943.

Gough SC, Kragh N, Ploug UJ, Hammer M. Impact of obesity and type 2 diabetes on health-related quality of life in the general population in England. Diabetes Metab Syndr Obes. 2009 Nov 3;2:179-84. doi: 10.2147/dmsott.s7088. PMID: 21437132; PMCID: PMC3048007.

Granneman JG, Moore HP, Krishnamoorthy R, Rathod M. Perilipin controls lipolysis by regulating the interactions of AB-hydrolase containing 5 (Abhd5) and adipose triglyceride lipase (Atgl). J Biol Chem. 2009 Dec 11;284(50):34538-44. doi: 10.1074/jbc.M109.068478. Epub 2009 Oct 22. PMID: 19850935; PMCID: PMC2787315.

Greenberg AS, Coleman RA, Kraemer FB, McManaman JL, Obin MS, Puri V, Yan QW, Miyoshi H, Mashek DG. The role of lipid droplets in metabolic disease in rodents and humans. J Clin Invest. 2011 Jun;121(6):2102-10. doi: 10.1172/JCI46069. Epub 2011 Jun 1. PMID: 21633178; PMCID: PMC3104768.

Griffin JL, Atherton H, Shockcor J, Atzori L. Metabolomics as a tool for cardiac research. Nat Rev Cardiol. 2011 Sep 20;8(11):630-43. doi: 10.1038/nrcardio.2011.138. PMID: 21931361.

Groop L, Pociot F. Genetics of diabetes--are we missing the genes or the disease? Mol Cell Endocrinol. 2014 Jan 25;382(1):726-739. doi: 10.1016/j.mce.2013.04.002. Epub 2013 Apr 13. PMID: 23587769.

GTEx Consortium. The Genotype-Tissue Expression (GTEx) project. Nat Genet. 2013 Jun;45(6):580-5. doi: 10.1038/ng.2653. PMID: 23715323; PMCID: PMC4010069.

Guo S. Insulin signaling, resistance, and the metabolic syndrome: insights from mouse models into disease mechanisms. J Endocrinol. 2014 Jan 8;220(2):T1-T23. doi: 10.1530/JOE-13-0327. PMID: 24281010; PMCID: PMC4087161.

Gupta RK, Arany Z, Seale P, Mepani RJ, Ye L, Conroe HM, Roby YA, Kulaga H, Reed RR, Spiegelman BM. Transcriptional control of preadipocyte determination by Zfp423. Nature. 2010 Mar 25;464(7288):619-23. doi: 10.1038/nature08816. Epub 2010 Mar 3. PMID: 20200519; PMCID: PMC2845731.

Gupta RK, Mepani RJ, Kleiner S, Lo JC, Khandekar MJ, Cohen P, Frontini A, Bhowmick DC, Ye L, Cinti S, Spiegelman BM. Zfp423 expression identifies committed preadipocytes and localizes to adipose endothelial and perivascular cells. Cell Metab. 2012 Feb 8;15(2):230-9. doi: 10.1016/j.cmet.2012.01.010. PMID: 22326224; PMCID: PMC3366493.

Haeusler RA, McGraw TE, Accili D. Biochemical and cellular properties of insulin receptor signalling. Nat Rev Mol Cell Biol. 2018 Jan;19(1):31-44. doi: 10.1038/nrm.2017.89. Epub 2017 Oct 4. PMID: 28974775; PMCID: PMC5894887.

Halberg N, Khan T, Trujillo ME, Wernstedt-Asterholm I, Attie AD, Sherwani S, Wang ZV, Landskroner-Eiger S, Dineen S, Magalang UJ, Brekken RA, Scherer PE. Hypoxia-inducible factor 1alpha induces fibrosis and insulin resistance in white adipose tissue. Mol Cell Biol. 2009 Aug;29(16):4467-83. doi: 10.1128/MCB.00192-09. Epub 2009 Jun 22. PMID: 19546236; PMCID: PMC2725728.

Han X, Yang K, Gross RW. Multi-dimensional mass spectrometry-based shotgun lipidomics and novel strategies for lipidomic analyses. Mass Spectrom Rev. 2012 Jan-Feb;31(1):134-78. doi: 10.1002/mas.20342. Epub 2011 Jul 13. PMID: 21755525; PMCID: PMC3259006.

Hannon TS, Rao G, Arslanian SA. Childhood obesity and type 2 diabetes mellitus. Pediatrics. 2005 Aug;116(2):473-80. doi: 10.1542/peds.2004-2536. PMID: 16061606.

Harms M, Seale P. Brown and beige fat: development, function and therapeutic potential. Nat Med. 2013 Oct;19(10):1252-63. doi: 10.1038/nm.3361. Epub 2013 Sep 29. PMID: 24100998.

Harris RB. Direct and indirect effects of leptin on adipocyte metabolism. Biochim Biophys Acta. 2014 Mar;1842(3):414-23. doi: 10.1016/j.bbadis.2013.05.009. Epub 2013 May 17. PMID: 23685313; PMCID: PMC3838442.

Hartl, D.L. and Clark, A.G. Principles of Population Genetics. 3rd Edition, Sinauer Associates, Inc. Publishers, Sunderland. 1997

Heaton JM. The distribution of brown adipose tissue in the human. J Anat. 1972 May;112(Pt 1):35-9. PMID: 5086212; PMCID: PMC1271341.

Heid IM, Jackson AU, Randall JC, Winkler TW, Qi L, Steinthorsdottir V, Thorleifsson G, Zillikens MC, Speliotes EK, Mägi R, et al. Meta-analysis identifies 13 new loci associated with waist-hip ratio and reveals sexual dimorphism in the genetic basis of fat distribution. Nat Genet. 2010 Nov;42(11):949-60. doi: 10.1038/ng.685. Epub 2010 Oct 10. Erratum in: Nat Genet. 2011 Nov;43(11):1164. PMID: 20935629; PMCID: PMC3000924.

Heim M, Johnson J, Boess F, Bendik I, Weber P, Hunziker W, Fluhmann B. Phytanic acid, a natural peroxisome proliferator-activated receptor (PPAR) agonist, regulates glucose metabolism in rat primary hepatocytes. FASEB J. 2002 May;16(7):718-20. doi: 10.1096/fj.01-0816fje. Epub 2002 Mar 26. PMID: 11923221.

Hennessy BT, Smith DL, Ram PT, Lu Y, Mills GB. Exploiting the PI3K/AKT pathway for cancer drug discovery. Nat Rev Drug Discov. 2005 Dec;4(12):988-1004. doi: 10.1038/nrd1902. PMID: 16341064.

Hernández C, Simó R, Chacón P, Sabin P, Baena JA, Castellanos JM, Planas M. Influence of surgical stress and parenteral nutrition on serum leptin concentration. Clin Nutr. 2000 Feb;19(1):61-4. doi: 10.1054/clnu.1999.0075. PMID: 10700536.

Hershko A, Ciechanover A. The ubiquitin system. Annu Rev Biochem. 1998; 67: 425-79. doi: 10.1146/annurev.biochem.67.1.425. PMID: 9759494.

Hillmann P, Fabbro D. PI3K/mTOR Pathway Inhibition: Opportunities in Oncology and Rare Genetic Diseases. Int J Mol Sci. 2019 Nov 18;20(22):5792. doi: 10.3390/ijms20225792. PMID: 31752127; PMCID: PMC6888641.

Hoggard N, Hunter L, Duncan JS, Williams LM, Trayhurn P, Mercer JG. Leptin and leptin receptor mRNA and protein expression in the murine fetus and placenta. Proc Natl Acad Sci U S A. 1997 Sep 30;94(20):11073-8. doi: 10.1073/pnas.94.20.11073. PMID: 9380761; PMCID: PMC23608.

Holland WL, Brozinick JT, Wang LP, Hawkins ED, Sargent KM, Liu Y, Narra K, Hoehn KL, Knotts TA, Siesky A, Nelson DH, Karathanasis SK, Fontenot GK, Birnbaum MJ, Summers SA. Inhibition of ceramide synthesis ameliorates glucocorticoid-, saturated-fat-, and obesity-induced insulin resistance. Cell Metab. 2007 Mar;5(3):167-79. doi: 10.1016/j.cmet.2007.01.002. PMID: 17339025.

Holmes E, Wilson ID, Nicholson JK. Metabolic phenotyping in health and disease. Cell. 2008 Sep 5;134(5):714-7. doi: 10.1016/j.cell.2008.08.026. PMID: 18775301.

Honecker J, Ruschke S, Seeliger C, Laber S, Strobel S, Pröll P, et al. Transcriptome and fatty-acid signatures of adipocyte hypertrophy and its non-invasive MR-based characterization in human adipose tissue. April 28, 2022, DOI:https://doi.org/10.1016/j.ebiom.2022.104020

Huang H, Song TJ, Li X, Hu L, He Q, Liu M, Lane MD, Tang QQ. BMP signaling pathway is required for commitment of C3H10T1/2 pluripotent stem cells to the adipocyte lineage. Proc Natl Acad Sci U S A. 2009 Aug 4;106(31):12670-5. doi: 10.1073/pnas.0906266106. Epub 2009 Jul 20. PMID: 19620713; PMCID: PMC2722335.

Hunter AJ, Ottoson N, Boerth N, Koretzky GA, Shimizu Y. Cutting edge: a novel function for the SLAP-130/FYB adapter protein in beta 1 integrin signaling and T lymphocyte migration. J Immunol. 2000 Feb 1;164(3):1143-7. doi: 10.4049/jimmunol.164.3.1143. PMID: 10640723.

Husson C, Renault L, Didry D, Pantaloni D, Carlier MF. Cordon-Bleu uses WH2 domains as multifunctional dynamizers of actin filament assembly. Mol Cell. 2011 Aug 5;43(3):464-77. doi: 10.1016/j.molcel.2011.07.010. PMID: 21816349.

Imai T, Takakuwa R, Marchand S, Dentz E, Bornert JM, Messaddeq N, Wendling O, Mark M, Desvergne B, Wahli W, Chambon P, Metzger D. Peroxisome proliferator-activated receptor gamma is required in mature white and brown adipocytes for their survival in the mouse. Proc Natl Acad Sci U S A. 2004 Mar 30;101(13):4543-7. doi: 10.1073/pnas.0400356101. Epub 2004 Mar 16. PMID: 15070754; PMCID: PMC384783.

International HapMap Consortium. A haplotype map of the human genome. Nature. 2005 Oct 27;437(7063):1299-320. doi: 10.1038/nature04226. PMID: 16255080; PMCID: PMC1880871.

Isozaki O, Tsushima T, Miyakawa M, Nozoe Y, Demura H, Seki H. Growth hormone directly inhibits leptin gene expression in visceral fat tissue in fatty Zucker rats. J Endocrinol. 1999 Jun;161(3):511-6. doi: 10.1677/joe.0.1610511. PMID: 10333553.

Iyer, A., Brown, L. (2010). Lipid mediators and inflammation in glucose intolerance and insulin resistance. Drug Discovery Today: Disease Mechanisms, Vot 7, Issues 3-4, p. e191-e197.

Jaffe AB, Hall A. Rho GTPases: biochemistry and biology. Annu Rev Cell Dev Biol. 2005; 21:247-69. doi:10.1146/annurev.cellbio.21.020604.150721. PMID: 16212495.

Janani C, Ranjitha Kumari BD. PPAR gamma gene--a review. Diabetes Metab Syndr. 2015 Jan-Mar;9(1):46-50. doi: 10.1016/j.dsx.2014.09.015. Epub 2014 Oct 13. PMID: 25450819.

Jeffery E, Church CD, Holtrup B, Colman L, Rodeheffer MS. Rapid depot-specific activation of adipocyte precursor cells at the onset of obesity. Nat Cell Biol. 2015 Apr;17(4):376-85. doi: 10.1038/ncb3122. Epub 2015 Mar 2. PMID: 25730471; PMCID: PMC4380653.

Jiao Y, Walker M, Trinick J, Pernier J, Montaville P, Carlier MF. Mutagenetic and electron microscopy analysis of actin filament severing by Cordon-Bleu, a WH2 domain protein. Cytoskeleton (Hoboken). 2014 Mar;71(3):170-83. doi: 10.1002/cm.21161. Epub 2014 Mar 12. PMID: 24415668.

Kadonaga JT. Perspectives on the RNA polymerase II core promoter. Wiley Interdiscip Rev Dev Biol. 2012 Jan-Feb;1(1):40-51. doi: 10.1002/wdev.21. Epub 2011 Dec 6. PMID: 23801666; PMCID: PMC3695423.

Kanzaki M, Pessin JE. Insulin-stimulated GLUT4 translocation in adipocytes is dependent upon cortical actin remodeling. J Biol Chem. 2001 Nov 9;276(45):42436-44. doi: 10.1074/jbc.M108297200. Epub 2001 Sep 6. PMID: 11546823.

Kanzaki M, Watson RT, Hou JC, Stamnes M, Saltiel AR, Pessin JE. Small GTP-binding protein TC10 differentially regulates two distinct populations of filamentous actin in 3T3L1 adipocytes. Mol Biol Cell. 2002 Jul;13(7):2334-46. doi: 10.1091/mbc.01-10-0490. PMID: 12134073; PMCID: PMC117317.

Kanzaki M, Furukawa M, Raab W, Pessin JE. Phosphatidylinositol 4,5-bisphosphate regulates adipocyte actin dynamics and GLUT4 vesicle recycling. J Biol Chem. 2004 Jul 16;279(29):30622-33. doi: 10.1074/jbc.M401443200. Epub 2004 Apr 28. PMID: 15123724.

Kapoore RV, Coyle R, Staton CA, Brown NJ, Vaidyanathan S. Influence of washing and quenching in profiling the metabolome of adherent mammalian cells: a case study with the metastatic breast cancer cell line MDA-MB-231. Analyst. 2017 Jun 7;142(11):2038-2049. doi: 10.1039/c7an00207f. Epub 2017 May 12. PMID: 28497155.

Kawaguchi N, Sundberg C, Kveiborg M, Moghadaszadeh B, Asmar M, Dietrich N, Thodeti CK, Nielsen FC, Möller P, Mercurio AM, Albrechtsen R, Wewer UM. ADAM12 induces actin cytoskeleton and extracellular matrix reorganization during early adipocyte differentiation by regulating beta1 integrin function. J Cell Sci. 2003 Oct 1;116(Pt 19):3893-904. doi: 10.1242/jcs.00699. Epub 2003 Aug 12. PMID: 12915587.

Keppler-Noreuil KM, Parker VE, Darling TN, Martinez-Agosto JA. Somatic overgrowth disorders of the PI3K/AKT/mTOR pathway & therapeutic strategies. Am J Med Genet C Semin Med Genet. 2016

Dec;172(4):402-421. doi: 10.1002/ajmg.c.31531. Epub 2016 Nov 18. PMID: 27860216; PMCID: PMC5592089.

Kessels MM, Qualmann B. The syndapin protein family: linking membrane trafficking with the cytoskeleton. J Cell Sci. 2004 Jul 1;117(Pt 15):3077-86. doi: 10.1242/jcs.01290. PMID: 15226389.

Khan T, Muise ES, Iyengar P, Wang ZV, Chandalia M, Abate N, Zhang BB, Bonaldo P, Chua S, Scherer PE. Metabolic dysregulation and adipose tissue fibrosis: role of collagen VI. Mol Cell Biol. 2009 Mar;29(6):1575-91. doi: 10.1128/MCB.01300-08. Epub 2008 Dec 29. PMID: 19114551; PMCID: PMC2648231.

Kintscher U, Law RE. PPARgamma-mediated insulin sensitization: the importance of fat versus muscle. Am J Physiol Endocrinol Metab. 2005 Feb;288(2):E287-91. doi: 10.1152/ajpendo.00440.2004. PMID: 15637349.

Klein RJ, Zeiss C, Chew EY, Tsai JY, Sackler RS, Haynes C, Henning AK, SanGiovanni JP, Mane SM, Mayne ST, Bracken MB, Ferris FL, Ott J, Barnstable C, Hoh J. Complement factor H polymorphism in age-related macular degeneration. Science. 2005 Apr 15;308(5720):385-9. doi: 10.1126/science.1109557. Epub 2005 Mar 10. PMID: 15761122; PMCID: PMC1512523.

Kolaczynski JW, Considine RV, Ohannesian J, Marco C, Opentanova I, Nyce MR, Myint M, Caro JF. Responses of leptin to short-term fasting and refeeding in humans: a link with ketogenesis but not ketones themselves. Diabetes. 1996 Nov;45(11):1511-5. doi: 10.2337/diab.45.11.1511. PMID: 8866554.

Kolaczynski JW, Ohannesian JP, Considine RV, Marco CC, Caro JF. Response of leptin to short-term and prolonged overfeeding in humans. J Clin Endocrinol Metab. 1996 Nov;81(11):4162-5. doi: 10.1210/jcem.81.11.8923877. PMID: 8923877.

Kooner JS, Saleheen D, Sim X, Sehmi J, Zhang W, Frossard P, Been LF, Chia KS, Dimas AS, Hassanali N et al. Genome-wide association study in individuals of South Asian ancestry identifies six new type 2 diabetes susceptibility loci. Nat Genet. 2011 Aug 28;43(10):984-9. doi: 10.1038/ng.921. PMID: 21874001; PMCID: PMC3773920.

Kosaki A, Yamada K, Kuzuya H. Reduced expression of the leptin gene (ob) by catecholamine through a G(S) protein-coupled pathway in 3T3-L1 adipocytes. Diabetes. 1996 Dec;45(12):1744-9. doi: 10.2337/diab.45.12.1744. PMID: 8922360.

Kouzarides T. Chromatin modifications and their function. Cell. 2007 Feb 23;128(4):693-705. doi: 10.1016/j.cell.2007.02.005. PMID: 17320507.

Kraja AT, Chasman DI, North KE, Reiner AP, Yanek LR, Kilpeläinen TO, Smith JA, Dehghan A, Dupuis J, Johnson AD et al. Pleiotropic genes for metabolic syndrome and inflammation. Mol Genet Metab. 2014 Aug;112(4):317-38. doi: 10.1016/j.ymgme.2014.04.007. Epub 2014 May 9. PMID: 24981077; PMCID: PMC4122618.

Krotkiewski M, Björntorp P, Sjöström L, Smith U. Impact of obesity on metabolism in men and women. Importance of regional adipose tissue distribution. J Clin Invest. 1983 Sep;72(3):1150-62. doi: 10.1172/JCI111040. PMID: 6350364; PMCID: PMC1129283.

Kwok KH, Lam KS, Xu A. Heterogeneity of white adipose tissue: molecular basis and clinical implications. Exp Mol Med. 2016 Mar 11;48(3):e215. doi: 10.1038/emm.2016.5. PMID: 26964831; PMCID: PMC4892883.

Kwon H, Pessin JE. Adipokines mediate inflammation and insulin resistance. Front Endocrinol (Lausanne). 2013 Jun 12;4:71. doi: 10.3389/fendo.2013.00071. PMID: 23781214; PMCID: PMC3679475.

Laurencikiene J, van Harmelen V, Arvidsson Nordström E, Dicker A, Blomqvist L, Näslund E, Langin D, Arner P, Rydén M. NF-kappaB is important for TNF-alpha-induced lipolysis in human adipocytes. J Lipid Res. 2007 May;48(5):1069-77. doi: 10.1194/jlr.M600471-JLR200. Epub 2007 Feb 1. PMID: 17272828.

Laurencikiene J, Skurk T, Kulyté A, Hedén P, Aström G, Sjölin E, Rydén M, Hauner H, Arner P. Regulation of lipolysis in small and large fat cells of the same subject. J Clin Endocrinol Metab. 2011 Dec;96(12):E2045-9. doi: 10.1210/jc.2011-1702. Epub 2011 Oct 12. PMID: 21994963.

Lavin DP, White MF, Brazil DP. IRS proteins and diabetic complications. Diabetologia. 2016 Nov;59(11):2280-2291. doi: 10.1007/s00125-016-4072-7. Epub 2016 Aug 11. PMID: 27514532; PMCID: PMC5506098.

Lee JE, Ge K. Transcriptional and epigenetic regulation of PPARγ expression during adipogenesis. Cell Biosci. 2014 May 29; 4:29. doi: 10.1186/2045-3701-4-29. PMID: 24904744; PMCID: PMC4046494.

Lefterova MI, Zhang Y, Steger DJ, Schupp M, Schug J, Cristancho A, Feng D, Zhuo D, Stoeckert CJ Jr, Liu XS, Lazar MA. PPARgamma and C/EBP factors orchestrate adipocyte biology via adjacent binding on a genome-wide scale. Genes Dev. 2008 Nov 1;22(21):2941-52. doi: 10.1101/gad.1709008. PMID: 18981473; PMCID: PMC2577797.

Lefterova MI, Haakonsson AK, Lazar MA, Mandrup S. PPARγ and the global map of adipogenesis and beyond. Trends Endocrinol Metab. 2014 Jun;25(6):293-302. doi: 10.1016/j.tem.2014.04.001. Epub 2014 Apr 29. PMID: 24793638; PMCID: PMC4104504.

Lehrke M, Lazar MA. The many faces of PPARgamma. Cell. 2005 Dec 16;123(6):993-9. doi: 10.1016/j.cell.2005.11.026. PMID: 16360030.

Lenz EM, Bright J, Knight R, Wilson ID, Major H. A metabonomic investigation of the biochemical effects of mercuric chloride in the rat using 1H NMR and HPLC-TOF/MS: time dependent changes in the urinary profile of endogenous metabolites as a result of nephrotoxicity. Analyst. 2004 Jun;129(6):535-41. doi: 10.1039/b400159c. Epub 2004 Apr 21. PMID: 15152332.

Lepper C, Fan CM. Inducible lineage tracing of Pax7-descendant cells reveals embryonic origin of adult satellite cells. Genesis. 2010 Jul;48(7):424-36. doi: 10.1002/dvg.20630. PMID: 20641127; PMCID: PMC3113517.

Li E. Chromatin modification and epigenetic reprogramming in mammalian development. Nat Rev Genet. 2002 Sep;3(9):662-73. doi: 10.1038/nrg887. PMID: 12209141.

Li X, Fekete A, Englmann M, Frommberger M, Lv S, Chen G, Schmitt-Kopplin P. At-line coupling of UPLC to chip-electrospray-FTICR-MS. Anal Bioanal Chem. 2007 Nov;389(5):1439-46. doi: 10.1007/s00216-007-1524-4. Epub 2007 Sep 5. PMID: 17849105.

Li M, Wang B, Zhang M, Rantalainen M, Wang S, Zhou H, Zhang Y, Shen J, Pang X, Zhang M, Wei H, et al. Symbiotic gut microbes modulate human metabolic phenotypes. Proc Natl Acad Sci U S A. 2008 Feb 12;105(6):2117-22. doi: 10.1073/pnas.0712038105. Epub 2008 Feb 5. PMID: 18252821; PMCID: PMC2538887.

Li J, Papadopoulos V, Vihma V. Steroid biosynthesis in adipose tissue. Steroids. 2015 Nov; 103:89-104. doi: 10.1016/j.steroids.2015.03.016. Epub 2015 Apr 3. PMID: 25846979.

Lidell ME, Betz MJ, Dahlqvist Leinhard O, Heglind M, Elander L, Slawik M, Mussack T, Nilsson D, Romu T, et al. Evidence for two types of brown adipose tissue in humans. Nat Med. 2013 May;19(5):631-4. doi: 10.1038/nm.3017. Epub 2013 Apr 21. PMID: 23603813.

Lin FT, Lane MD. Antisense CCAAT/enhancer-binding protein RNA suppresses coordinate gene expression and triglyceride accumulation during differentiation of 3T3-L1 preadipocytes. Genes Dev. 1992 Apr;6(4):533-44. doi: 10.1101/gad.6.4.533. PMID: 1373117.

Linhart HG, Ishimura-Oka K, DeMayo F, Kibe T, Repka D, Poindexter B, Bick RJ, Darlington GJ. C/EBPalpha is required for differentiation of white, but not brown, adipose tissue. Proc Natl Acad Sci U S A. 2001 Oct 23;98(22):12532-7. doi: 10.1073/pnas.211416898. Epub 2001 Oct 16. PMID: 11606718; PMCID: PMC60088.

Liu P, Cheng H, Roberts TM, Zhao JJ. Targeting the phosphoinositide 3-kinase pathway in cancer. Nat Rev Drug Discov. 2009 Aug;8(8):627-44. doi: 10.1038/nrd2926. PMID: 19644473; PMCID: PMC3142564.

Long YC, Cheng Z, Copps KD, White MF. Insulin receptor substrates Irs1 and Irs2 coordinate skeletal muscle growth and metabolism via the Akt and AMPK pathways. Mol Cell Biol. 2011 Feb;31(3):430-41. doi: 10.1128/MCB.00983-10. Epub 2010 Dec 6. Erratum in: Mol Cell Biol. 2017 Jul 14;37(15): PMID: 21135130; PMCID: PMC3028618.

Lönn M, Mehlig K, Bengtsson C, Lissner L. Adipocyte size predicts incidence of type 2 diabetes in women. FASEB J. 2010 Jan;24(1):326-31. doi: 10.1096/fj.09-133058. Epub 2009 Sep 9. PMID: 19741173.

Lorenz MA, Burant CF, Kennedy RT. Reducing time and increasing sensitivity in sample preparation for adherent mammalian cell metabolomics. Anal Chem. 2011 May 1;83(9):3406-14. doi: 10.1021/ac103313x. Epub 2011 Apr 1. PMID: 21456517; PMCID: PMC3094105.

Lu Y, Day FR, Gustafsson S, Buchkovich ML, Na J, Bataille V, Cousminer DL, Dastani Z, Drong AW, Esko T et al. New loci for body fat percentage reveal link between adiposity and cardiometabolic disease risk. Nat Commun. 2016 Feb 1; 7:10495. doi: 10.1038/ncomms10495. PMID: 26833246; PMCID: PMC4740398.

Luger K, Mäder AW, Richmond RK, Sargent DF, Richmond TJ. Crystal structure of the nucleosome core particle at 2.8 A resolution. Nature. 1997 Sep 18;389(6648):251-60. doi: 10.1038/38444. PMID: 9305837.

Lumeng CN, Deyoung SM, Bodzin JL, Saltiel AR. Increased inflammatory properties of adipose tissue macrophages recruited during diet-induced obesity. Diabetes. 2007 Jan;56(1):16-23. doi: 10.2337/db06-1076. PMID: 17192460.

Manning AK, Hivert MF, Scott RA, Grimsby JL, Bouatia-Naji N, Chen H, Rybin D, Liu CT, Bielak LF, Prokopenko I et al. A genome-wide approach accounting for body mass index identifies genetic variants influencing fasting glycemic traits and insulin resistance. Nat Genet. 2012 May 13;44(6):659-69. doi: 10.1038/ng.2274. PMID: 22581228; PMCID: PMC3613127.

Marshall AG, Hendrickson CL, Jackson GS. Fourier transform ion cyclotron resonance mass spectrometry: a primer. Mass Spectrom Rev. 1998 Jan-Feb;17(1):1-35. doi: 10.1002/(SICI)1098-2787(1998)17:1<1::AID-MAS1>3.0.CO;2-K. PMID: 9768511.

Mazein A, Watterson S, Hsieh WY, Griffiths WJ, Ghazal P. A comprehensive machine-readable view of the mammalian cholesterol biosynthesis pathway. Biochem Pharmacol. 2013 Jul 1;86(1):56-66. doi: 10.1016/j.bcp.2013.03.021. Epub 2013 Apr 10. PMID: 23583456; PMCID: PMC3912678.

McAllister EJ, Dhurandhar NV, Keith SW, Aronne LJ, Barger J, Baskin M, Benca RM, Biggio J, Boggiano MM, Eisenmann JC, Elobeid M, Fontaine KR, Gluckman P, Hanlon EC, Katzmarzyk P, Pietrobelli A, Redden DT, Ruden DM, Wang C, Waterland RA, Wright SM, Allison DB. Ten putative contributors to the obesity epidemic. Crit Rev Food Sci Nutr. 2009 Nov;49(10):868-913. doi: 10.1080/10408390903372599. PMID: 19960394; PMCID: PMC2932668.

Medina-Gomez G, Gray S, Vidal-Puig A. Adipogenesis and lipotoxicity: role of peroxisome proliferator-activated receptor gamma (PPARgamma) and PPARgammacoactivator-1 (PGC1). Public Health Nutr. 2007 Oct;10(10A):1132-7. doi: 10.1017/S1368980007000614. PMID: 17903321.

Meigs JB, Cupples LA, Wilson PW. Parental transmission of type 2 diabetes: the Framingham Offspring Study. Diabetes. 2000 Dec;49(12):2201-7. doi: 10.2337/diabetes.49.12.2201. PMID: 11118026.

Meyer LK, Ciaraldi TP, Henry RR, Wittgrove AC, Phillips SA. Adipose tissue depot and cell size dependency of adiponectin synthesis and secretion in human obesity. Adipocyte. 2013 Oct 1;2(4):217-26. doi: 10.4161/adip.24953. Epub 2013 May 7. PMID: 24052897; PMCID: PMC3774697.

Miyoshi H, Souza SC, Zhang HH, Strissel KJ, Christoffolete MA, Kovsan J, Rudich A, Kraemer FB, Bianco AC, Obin MS, Greenberg AS. Perilipin promotes hormone-sensitive lipase-mediated adipocyte lipolysis via phosphorylation-dependent and -independent mechanisms. J Biol Chem. 2006 Jun 9;281(23):15837-44. doi: 10.1074/jbc.M601097200. Epub 2006 Apr 4. PMID: 16595669.

Monge ME, Dodds JN, Baker ES, Edison AS, Fernández FM. Challenges in Identifying the Dark Molecules of Life. Annu Rev Anal Chem (Palo Alto Calif). 2019 Jun 12;12(1):177-199. doi: 10.1146/annurev-anchem-061318-114959. Epub 2019 Mar 18. PMID: 30883183; PMCID: PMC6716371.

Mooradian AD, Chehade J, Thurman JE. The role of thiazolidinediones in the treatment of patients with type 2 diabetes mellitus. Treat Endocrinol. 2002;1(1):13-20. doi: 10.2165/00024677-200201010-00002. PMID: 15765617.

Moore GB, Chapman H, Holder JC, Lister CA, Piercy V, Smith SA, Clapham JC. Differential regulation of adipocytokine mRNAs by rosiglitazone in db/db mice. Biochem Biophys Res Commun. 2001 Aug 31;286(4):735-41. doi: 10.1006/bbrc.2001.5460. PMID: 11520059.

Morelli AE, Larregina AT, Shufesky WJ, Zahorchak AF, Logar AJ, Papworth GD, Wang Z, Watkins SC, Falo LD Jr, Thomson AW. Internalization of circulating apoptotic cells by splenic marginal zone dendritic cells: dependence on complement receptors and effect on cytokine production. Blood. 2003 Jan 15;101(2):611-20. doi: 10.1182/blood-2002-06-1769. Epub 2002 Sep 5. PMID: 12393562.

Morigny P, Boucher J, Arner P, Langin D. Lipid and glucose metabolism in white adipocytes: pathways, dysfunction and therapeutics. Nat Rev Endocrinol. 2021 May;17(5):276-295. doi: 10.1038/s41574-021-00471-8. Epub 2021 Feb 24. PMID: 33627836.

Moritz F, Janicka M, Zygler A, Forcisi S, Kot-Wasik A, Kot J, Gebefügi I, Namiesnik J, Schmitt-Kopplin P. The compositional space of exhaled breath condensate and its link to the human breath volatilome. J Breath Res. 2015 May 6;9(2):027105. doi: 10.1088/1752-7155/9/2/027105. PMID: 25944811.

Moritz F, Kaling M, Schnitzler JP, Schmitt-Kopplin P. Characterization of poplar metabotypes via mass difference enrichment analysis. Plant Cell Environ. 2017 Jul;40(7):1057-1073. doi: 10.1111/pce.12878. Epub 2017 Apr 6. PMID: 27943315.

Morris AP. Transethnic meta-analysis of genomewide association studies. Genet Epidemiol. 2011 Dec;35(8):809-22. doi: 10.1002/gepi.20630. PMID: 22125221; PMCID: PMC3460225.

Nagai M, Sakakibara J, Wakui K, Fukushima Y, Igarashi S, Tsuji S, Arakawa M, Ono T. Localization of the squalene epoxidase gene (SQLE) to human chromosome region 8q24.1. Genomics. 1997 Aug 15;44(1):141-3. doi: 10.1006/geno.1997.4825. PMID: 9286711.

Nagai S, Matsumoto C, Shibano M, Fujimori K. Suppression of Fatty Acid and Triglyceride Synthesis by the Flavonoid Orientin through Decrease of C/EBPδ Expression and Inhibition of PI3K/Akt-FOXO1 Signaling in Adipocytes. Nutrients. 2018 Jan 26;10(2):130. doi: 10.3390/nu10020130. PMID: 29373533; PMCID: PMC5852706.

Nedergaard J, Bengtsson T, Cannon B. Unexpected evidence for active brown adipose tissue in adult humans. Am J Physiol Endocrinol Metab. 2007 Aug;293(2):E444-52. doi: 10.1152/ajpendo.00691.2006. Epub 2007 May 1. PMID: 17473055.

Newman B, Selby JV, King MC, Slemenda C, Fabsitz R, Friedman GD. Concordance for type 2 (non-insulin-dependent) diabetes mellitus in male twins. Diabetologia. 1987 Oct;30(10):763-8. doi: 10.1007/BF00275741. PMID: 3428496.

Nguyen HL, Boon LM, Vikkula M. Vascular Anomalies Caused by Abnormal Signaling within Endothelial Cells: Targets for Novel Therapies. Semin Intervent Radiol. 2017 Sep;34(3):233-238. doi: 10.1055/s-0037-1604296. Epub 2017 Sep 11. PMID: 28955112; PMCID: PMC5615384.

Nicholson JK, Connelly J, Lindon JC, Holmes E. Metabonomics: a platform for studying drug toxicity and gene function. Nat Rev Drug Discov. 2002 Feb;1(2):153-61. doi: 10.1038/nrd728. PMID: 12120097.

Nicholson JK, Wilson ID. Opinion: understanding 'global' systems biology: metabonomics and the continuum of metabolism. Nat Rev Drug Discov. 2003 Aug;2(8):668-76. doi: 10.1038/nrd1157. PMID: 12904817.

Nicholson JK, Lindon JC. Systems biology: Metabonomics. Nature. 2008 Oct 23;455(7216):1054-6. doi: 10.1038/4551054a. PMID: 18948945.

Nielsen R, Pedersen TA, Hagenbeek D, Moulos P, Siersbaek R, Megens E, Denissov S, Børgesen M, Francoijs KJ, Mandrup S, Stunnenberg HG. Genome-wide profiling of PPARgamma:RXR and RNA polymerase II occupancy reveals temporal activation of distinct metabolic pathways and changes in RXR dimer composition during adipogenesis. Genes Dev. 2008 Nov 1;22(21):2953-67. doi: 10.1101/gad.501108. PMID: 18981474; PMCID: PMC2577787.

Nobusue H, Onishi N, Shimizu T, Sugihara E, Oki Y, Sumikawa Y, Chiyoda T, Akashi K, Saya H, Kano K. Regulation of MKL1 via actin cytoskeleton dynamics drives adipocyte differentiation. Nat Commun. 2014 Feb 26; 5:3368. doi: 10.1038/ncomms4368. PMID: 24569594.

Nolan CJ, Damm P, Prentki M. Type 2 diabetes across generations: from pathophysiology to prevention and management. Lancet. 2011 Jul 9;378(9786):169-81. doi: 10.1016/S0140-6736(11)60614-4. Epub 2011 Jun 24. PMID: 21705072.

Obradovic M, Sudar-Milovanovic E, Soskic S, Essack M, Arya S, Stewart AJ, Gojobori T, Isenovic ER. Leptin and Obesity: Role and Clinical Implication. Front Endocrinol (Lausanne). 2021 May 18; 12:585887. doi: 10.3389/fendo.2021.585887. PMID: 34084149; PMCID: PMC8167040.

Olefsky JM, Glass CK. Macrophages, inflammation, and insulin resistance. Annu Rev Physiol. 2010; 72:219-46. doi: 10.1146/annurev-physiol-021909-135846. PMID: 20148674.

Orlicky DJ, Monks J, Stefanski AL, McManaman JL. Dynamics and molecular determinants of cytoplasmic lipid droplet clustering and dispersion. PLoS One. 2013 Jun 25;8(6): e66837. doi: 10.1371/journal.pone.0066837. PMID: 23825572; PMCID: PMC3692517.

Orphanides G, Lagrange T, Reinberg D. The general transcription factors of RNA polymerase II. Genes Dev. 1996 Nov 1;10(21):2657-83. doi: 10.1101/gad.10.21.2657. PMID: 8946909.

Papathanasiou AE, Nolen-Doerr E, Farr OM, Mantzoros CS. GEOFFREY HARRIS PRIZE LECTURE 2018: Novel pathways regulating neuroendocrine function, energy homeostasis and metabolism in humans. Eur J Endocrinol. 2019 Feb 1;180(2):R59-R71. doi: 10.1530/EJE-18-0847. PMID: 30475221; PMCID: PMC6378110.

Park HK, Ahima RS. Physiology of leptin: energy homeostasis, neuroendocrine function and metabolism. Metabolism. 2015 Jan;64(1):24-34. doi: 10.1016/j.metabol.2014.08.004. Epub 2014 Aug 15. PMID: 25199978; PMCID: PMC4267898.

Patel KA, Burman S, Laver TW, Hattersley AT, Frayling TM, Weedon MN. PLIN1 Haploinsufficiency Causes a Favorable Metabolic Profile. J Clin Endocrinol Metab. 2022 May 17;107(6):e2318-e2323. doi: 10.1210/clinem/dgac104. PMID: 35235652; PMCID: PMC9113801.

Patti GJ, Yanes O, Siuzdak G. Innovation: Metabolomics: the apogee of the omics trilogy. Nat Rev Mol Cell Biol. 2012 Mar 22;13(4):263-9. doi: 10.1038/nrm3314. PMID: 22436749; PMCID: PMC3682684.

Pekala J, Patkowska-Sokoła B, Bodkowski R, Jamroz D, Nowakowski P, Lochyński S, Librowski T. L-carnitine--metabolic functions and meaning in humans life. Curr Drug Metab. 2011 Sep;12(7):667-78. doi: 10.2174/138920011796504536. PMID: 21561431.

Pfaffl MW. A new mathematical model for relative quantification in real-time RT-PCR. Nucleic Acids Res. 2001 May 1;29(9):e45. doi: 10.1093/nar/29.9.e45. PMID: 11328886; PMCID: PMC55695.

Phillipson M, Heit B, Colarusso P, Liu L, Ballantyne CM, Kubes P. Intraluminal crawling of neutrophils to emigration sites: a molecularly distinct process from adhesion in the recruitment cascade. J Exp Med. 2006 Nov 27;203(12):2569-75. doi: 10.1084/jem.20060925. Epub 2006 Nov 20. PMID: 17116736; PMCID: PMC2118150.

PLIS Subproject “Genotype-driven deep metabotyping and de novo Type 2 Diabetes biomarker identification”, TUM Study Protocol to be submitted to Ethics Commission 10/5/2015

Polson C, Sarkar P, Incledon B, Raguvaran V, Grant R. Optimization of protein precipitation based upon effectiveness of protein removal and ionization effect in liquid chromatography-tandem mass spectrometry. J Chromatogr B Analyt Technol Biomed Life Sci. 2003 Mar 5;785(2):263-75. doi: 10.1016/s1570-0232(02)00914-5. PMID: 12554139.

Prasad RB, Groop L. Genetics of type 2 diabetes-pitfalls and possibilities. Genes (Basel). 2015 Mar 12;6(1):87-123. doi: 10.3390/genes6010087. PMID: 25774817; PMCID: PMC4377835.

Prehoda KE, Scott JA, Mullins RD, Lim WA. Integration of multiple signals through cooperative regulation of the N-WASP-Arp2/3 complex. Science. 2000 Oct 27;290(5492):801-6. doi: 10.1126/science.290.5492.801. PMID: 11052943.

Raamsdonk LM, Teusink B, Broadhurst D, Zhang N, Hayes A, Walsh MC, Berden JA, Brindle KM, Kell DB, Rowland JJ, Westerhoff HV, van Dam K, Oliver SG. A functional genomics strategy that uses metabolome data to reveal the phenotype of silent mutations. Nat Biotechnol. 2001 Jan;19(1):45-50. doi: 10.1038/83496. PMID: 11135551.

Rahmioglu N, Macgregor S, Drong AW, Hedman ÅK, Harris HR, Randall JC, Prokopenko I; International Endogene Consortium (IEC), The GIANT Consortium, Nyholt DR, Morris AP, Montgomery GW, Missmer SA, Lindgren CM, Zondervan KT. Genome-wide enrichment analysis between endometriosis and obesity-related traits reveals novel susceptibility loci. Hum Mol Genet. 2015 Feb 15;24(4):1185-99. doi: 10.1093/hmg/ddu516. Epub 2014 Oct 8. PMID: 25296917; PMCID: PMC4576730.

Randall JC, Winkler TW, Kutalik Z, Berndt SI, Jackson AU, Monda KL, Kilpeläinen TO, Esko T, Mägi R, Li S, Workalemahu T, et al. Sex-stratified genome-wide association studies including 270,000 individuals show sexual dimorphism in genetic loci for anthropometric traits. PLoS Genet. 2013 Jun;9(6):e1003500. doi: 10.1371/journal.pgen.1003500. Epub 2013 Jun 6. PMID: 23754948; PMCID: PMC3674993.

Reddan JM, White DJ, Macpherson H, Scholey A, Pipingas A. Glycerophospholipid Supplementation as a Potential Intervention for Supporting Cerebral Structure in Older Adults. Front Aging Neurosci. 2018 Mar 7; 10:49. doi: 10.3389/fnagi.2018.00049. PMID: 29563868; PMCID: PMC5845902.

Reily C, Stewart TJ, Renfrow MB, Novak J. Glycosylation in health and disease. Nat Rev Nephrol. 2019 Jun;15(6):346-366. doi: 10.1038/s41581-019-0129-4. PMID: 30858582; PMCID: PMC6590709.

Ren D, Collingwood TN, Rebar EJ, Wolffe AP, Camp HS. PPARgamma knockdown by engineered transcription factors: exogenous PPARgamma2 but not PPARgamma1 reactivates adipogenesis. Genes Dev. 2002 Jan 1;16(1):27-32. doi: 10.1101/gad.953802. PMID: 11782442; PMCID: PMC155307.

Ren S, Hinzman AA, Kang E, Szczesniak RD, Lu LJ. Computational and statistical analysis of metabolomics data. Metabolomics 11, 1, 492–1513 (2015). doi: 10.1007/s11306-015-0823-6

Rentsch J, Chiesi M. Regulation of ob gene mRNA levels in cultured adipocytes. FEBS Lett. 1996 Jan 22;379(1):55-9. doi: 10.1016/0014-5793(95)01485-3. PMID: 8566229.

Richmond TJ, Davey CA. The structure of DNA in the nucleosome core. Nature. 2003 May 8;423(6936):145-50. doi: 10.1038/nature01595. PMID: 12736678.

Ricquier D. Uncoupling protein 1 of brown adipocytes, the only uncoupler: a historical perspective. Front Endocrinol (Lausanne). 2011 Dec 28 ;2:85. doi: 10.3389/fendo.2011.00085. PMID: 22649389; PMCID: PMC3355862.

Roadmap Epigenomics Consortium et al. Integrative analysis of 111 reference human epigenomes. Nature. 2015 Feb 19;518(7539):317-30. doi: 10.1038/nature14248. PMID: 25693563; PMCID: PMC4530010.

Rogue A, Spire C, Brun M, Claude N, Guillouzo A. Gene Expression Changes Induced by PPAR Gamma Agonists in Animal and Human Liver. PPAR Res. 2010; 2010:325183. doi: 10.1155/2010/325183. Epub 2010 Oct 19. PMID: 20981297; PMCID: PMC2963138.

Rogue A, Lambert C, Jossé R, Antherieu S, Spire C, Claude N, Guillouzo A. Comparative gene expression profiles induced by PPARγ and PPARα/γ agonists in human hepatocytes. PLoS One. 2011 Apr 18;6(4):e18816. doi: 10.1371/journal.pone.0018816. PMID: 21533120; PMCID: PMC3078935.

Rohatgi R, Ma L, Miki H, Lopez M, Kirchhausen T, Takenawa T, Kirschner MW. The interaction between N-WASP and the Arp2/3 complex links Cdc42-dependent signals to actin assembly. Cell. 1999 Apr 16;97(2):221-31. doi: 10.1016/s0092-8674(00)80732-1. PMID: 10219243.

Rönn T, Volkov P, Davegårdh C, Dayeh T, Hall E, Olsson AH, Nilsson E, Tornberg A, Dekker Nitert M, Eriksson KF, Jones HA, Groop L, Ling C. A six months exercise intervention influences the genome-wide DNA methylation pattern in human adipose tissue. PLoS Genet. 2013 Jun;9(6): e1003572. doi: 10.1371/journal.pgen.1003572. Epub 2013 Jun 27. PMID: 23825961; PMCID: PMC3694844.

Rosen ED, Sarraf P, Troy AE, Bradwin G, Moore K, Milstone DS, Spiegelman BM, Mortensen RM. PPAR gamma is required for the differentiation of adipose tissue in vivo and in vitro. Mol Cell. 1999 Oct;4(4):611-7. doi: 10.1016/s1097-2765(00)80211-7. PMID: 10549292.

Rosen ED, Walkey CJ, Puigserver P, Spiegelman BM. Transcriptional regulation of adipogenesis. Genes Dev. 2000 Jun 1;14(11):1293-307. PMID: 10837022.

Rosen ED, MacDougald OA. Adipocyte differentiation from the inside out. Nat Rev Mol Cell Biol. 2006 Dec;7(12):885-96. doi: 10.1038/nrm2066. PMID: 17139329.

Rosen ED, Spiegelman BM. What we talk about when we talk about fat. Cell. 2014 Jan 16;156(1-2):20-44. doi: 10.1016/j.cell.2013.12.012. PMID: 24439368; PMCID: PMC3934003.

Russell CD, Petersen RN, Rao SP, Ricci MR, Prasad A, Zhang Y, Brolin RE, Fried SK. Leptin expression in adipose tissue from obese humans: depot-specific regulation by insulin and dexamethasone. Am J Physiol. 1998 Sep;275(3):E507-15. doi: 10.1152/ajpendo.1998.275.3.E507. PMID: 9725819.

Rutkowski JM, Stern JH, Scherer PE. The cell biology of fat expansion. J Cell Biol. 2015 Mar 2;208(5):501-12. doi: 10.1083/jcb.201409063. PMID: 25733711; PMCID: PMC4347644.

Saarikangas J, Zhao H, Lappalainen P. Regulation of the actin cytoskeleton-plasma membrane interplay by phosphoinositides. Physiol Rev. 2010 Jan;90(1):259-89. doi: 10.1152/physrev.00036.2009. PMID: 20086078.

Saito M, Okamatsu-Ogura Y, Matsushita M, Watanabe K, Yoneshiro T, Nio-Kobayashi J, Iwanaga T, Miyagawa M, Kameya T, Nakada K, Kawai Y, Tsujisaki M. High incidence of metabolically active brown adipose tissue in healthy adult humans: effects of cold exposure and adiposity. Diabetes. 2009 Jul;58(7):1526-31. doi: 10.2337/db09-0530. Epub 2009 Apr 28. PMID: 19401428; PMCID: PMC2699872.

Saladin R, De Vos P, Guerre-Millo M, Leturque A, Girard J, Staels B, Auwerx J. Transient increase in obese gene expression after food intake or insulin administration. Nature. 1995 Oct 12;377(6549):527-9. doi: 10.1038/377527a0. PMID: 7566150.

Salans LB, Knittle JL, Hirsch J. The role of adipose cell size and adipose tissue insulin sensitivity in the carbohydrate intolerance of human obesity. J Clin Invest. 1968 Jan;47(1):153-65. doi: 10.1172/JCI105705. PMID: 16695937; PMCID: PMC297156.

Sanchez-Gurmaches J, Hung CM, Sparks CA, Tang Y, Li H, Guertin DA. PTEN loss in the Myf5 lineage redistributes body fat and reveals subsets of white adipocytes that arise from Myf5 precursors. Cell Metab. 2012 Sep 5;16(3):348-62. doi: 10.1016/j.cmet.2012.08.003. PMID: 22940198; PMCID: PMC3488151.

Saran R, Li Y, Robinson B, Ayanian J, Balkrishnan R, Bragg-Gresham J, Chen JT, Cope E, Gipson D, He K, et al. US Renal Data System 2014 Annual Data Report: Epidemiology of Kidney Disease in the United States. Am J Kidney Dis. 2015 Jul;66(1 Suppl 1):Svii, S1-305. doi: 10.1053/j.ajkd.2015.05.001. Erratum in: Am J Kidney Dis. 2015 Sep;66(3):545. Erratum in: Am J Kidney Dis. 2015 Sep;66(3):545. PMID: 26111994; PMCID: PMC6643986.

Scharf PJ, Witney J, Daly R, Lyons BA. Solution structure of the human Grb14-SH2 domain and comparison with the structures of the human Grb7-SH2/erbB2 peptide complex and human Grb10-

SH2 domain. Protein Sci. 2004 Sep;13(9):2541-6. doi: 10.1110/ps.04884704. PMID: 15322292; PMCID: PMC2280013.

Scherer PE. The Multifaceted Roles of Adipose Tissue-Therapeutic Targets for Diabetes and Beyond: The 2015 Banting Lecture. Diabetes. 2016 Jun;65(6):1452-61. doi: 10.2337/db16-0339. PMID: 27222389; PMCID: PMC4878420.

Schleinitz D, Klöting N, Lindgren CM, Breitfeld J, Dietrich A, Schön MR, Lohmann T, Dreßler M, Stumvoll M, McCarthy MI, Blüher M, Kovacs P. Fat depot-specific mRNA expression of novel loci associated with waist-hip ratio. Int J Obes (Lond). 2014 Jan;38(1):120-5. doi: 10.1038/ijo.2013.56. Epub 2013 Apr 19. PMID: 23670221; PMCID: PMC7116610.

Scriba D, Aprath-Husmann I, Blum WF, Hauner H. Catecholamines suppress leptin release from in vitro differentiated subcutaneous human adipocytes in primary culture via beta1- and beta2-adrenergic receptors. Eur J Endocrinol. 2000 Sep;143(3):439-45. doi: 10.1530/eje.0.1430439. PMID: 11022189.

Seale P, Bjork B, Yang W, Kajimura S, Chin S, Kuang S, Scimè A, Devarakonda S, Conroe HM, Erdjument-Bromage H, Tempst P, Rudnicki MA, Beier DR, Spiegelman BM. PRDM16 controls a brown fat/skeletal muscle switch. Nature. 2008 Aug 21;454(7207):961-7. doi: 10.1038/nature07182. PMID: 18719582; PMCID: PMC2583329.

Shao M, Hepler C, Vishvanath L, MacPherson KA, Busbuso NC, Gupta RK. Fetal development of subcutaneous white adipose tissue is dependent on Zfp423. Mol Metab. 2016 Nov 21;6(1):111-124. doi: 10.1016/j.molmet.2016.11.009. PMID: 28123942; PMCID: PMC5220400.

Shintani M, Nishimura H, Yonemitsu S, Masuzaki H, Ogawa Y, Hosoda K, Inoue G, Yoshimasa Y, Nakao K. Downregulation of leptin by free fatty acids in rat adipocytes: effects of triacsin C, palmitate, and 2-bromopalmitate. Metabolism. 2000 Mar;49(3):326-30. doi: 10.1016/s0026-0495(00)90154-9. PMID: 10726909.

Shogren-Knaak M, Ishii H, Sun JM, Pazin MJ, Davie JR, Peterson CL. Histone H4-K16 acetylation controls chromatin structure and protein interactions. Science. 2006 Feb 10;311(5762):844-7. doi: 10.1126/science.1124000. PMID: 16469925.

Shuster A, Patlas M, Pinthus JH, Mourtzakis M. The clinical importance of visceral adiposity: a critical review of methods for visceral adipose tissue analysis. Br J Radiol. 2012 Jan;85(1009):1-10. doi: 10.1259/bjr/38447238. Epub 2011 Sep 21. PMID: 21937614; PMCID: PMC3473928.

Siersbæk R, Mandrup S. Transcriptional networks controlling adipocyte differentiation. Cold Spring Harb Symp Quant Biol. 2011; 76:247-55. doi: 10.1101/sqb.2011.76.010512. Epub 2011 Sep 6. PMID: 21900150.

Siersbæk R, Nielsen R, John S, Sung MH, Baek S, Loft A, Hager GL, Mandrup S. Extensive chromatin remodelling and establishment of transcription factor 'hotspots' during early adipogenesis. EMBO J. 2011 Apr 20;30(8):1459-72. doi: 10.1038/emboj.2011.65. Epub 2011 Mar 22. PMID: 21427703; PMCID: PMC3102274.

Salihovic S, Broeckling CD, Ganna A, Prenni JE, Sundström J, Berne C, Lind L, Ingelsson E, Fall T, Ärnlöv J, Nowak C. Non-targeted urine metabolomics and associations with prevalent and incident type 2 diabetes. Sci Rep. 2020 Oct 5;10(1):16474. doi: 10.1038/s41598-020-72456-y. PMID: 33020500; PMCID: PMC7536211.

Sivitz WI, Fink BD, Morgan DA, Fox JM, Donohoue PA, Haynes WG. Sympathetic inhibition, leptin, and uncoupling protein subtype expression in normal fasting rats. Am J Physiol. 1999 Oct;277(4):E668-77. doi: 10.1152/ajpendo.1999.277.4.E668. PMID: 10516126.

Skurk T, Alberti-Huber C, Herder C, Hauner H. Relationship between adipocyte size and adipokine expression and secretion. J Clin Endocrinol Metab. 2007 Mar;92(3):1023-33. doi: 10.1210/jc.2006-1055. Epub 2006 Dec 12. PMID: 17164304.

Slieker LJ, Sloop KW, Surface PL, Kriauciunas A, LaQuier F, Manetta J, Bue-Valleskey J, Stephens TW. Regulation of expression of ob mRNA and protein by glucocorticoids and cAMP. J Biol Chem. 1996 Mar 8;271(10):5301-4. doi: 10.1074/jbc.271.10.5301. PMID: 8621378.

Smas CM, Sul HS. Control of adipocyte differentiation. Biochem J. 1995 Aug 1;309 (Pt 3)(Pt 3):697-710. doi: 10.1042/bj3090697. PMID: 7639681; PMCID: PMC1135688.

Smirnov KS, Forcisi S, Moritz F, Lucio M, Schmitt-Kopplin P. Mass Difference Maps and Their Application for the Recalibration of Mass Spectrometric Data in Nontargeted Metabolomics. Anal Chem. 2019 Mar 5;91(5):3350-3358. doi: 10.1021/acs.analchem.8b04555. Epub 2019 Feb 15. PMID: 30707557.

Sohn JH, Lee YK, Han JS, Jeon YG, Kim JI, Choe SS, Kim SJ, Yoo HJ, Kim JB. Perilipin 1 (Plin1) deficiency promotes inflammatory responses in lean adipose tissue through lipid dysregulation. J Biol Chem. 2018 Sep 7;293(36):13974-13988. doi: 10.1074/jbc.RA118.003541. Epub 2018 Jul 24. PMID: 30042231; PMCID: PMC6130955.

Sonawane AR, Platig J, Fagny M, Chen CY, Paulson JN, Lopes-Ramos CM, DeMeo DL, Quackenbush J, Glass K, Kuijjer ML. Understanding Tissue-Specific Gene Regulation. Cell Rep. 2017 Oct 24;21(4):1077-1088. doi: 10.1016/j.celrep.2017.10.001. PMID: 29069589; PMCID: PMC5828531.

Srinivasan S, Chen L, Todd J, Divers J, Gidding S, Chernausek S, Gubitosi-Klug RA, Kelsey MM, Shah R, Black MH, Wagenknecht LE, Manning A, Flannick J, Imperatore G, Mercader JM, Dabelea D, Florez JC; ProDiGY Consortium. The First Genome-Wide Association Study for Type 2 Diabetes in Youth: The Progress in Diabetes Genetics in Youth (ProDiGY) Consortium. Diabetes. 2021 Apr;70(4):996-1005. doi: 10.2337/db20-0443. Epub 2021 Jan 21. Erratum in: Diabetes. 2021 Oct 29; PMID: 33479058; PMCID: PMC7980197.

Stark C, Breitkreutz BJ, Reguly T, Boucher L, Breitkreutz A, Tyers M. BioGRID: a general repository for interaction datasets. Nucleic Acids Res. 2006 Jan 1;34(Database issue): D535-9. doi: 10.1093/nar/gkj109. PMID: 16381927; PMCID: PMC1347471.

Steger DJ, Grant GR, Schupp M, Tomaru T, Lefterova MI, Schug J, Manduchi E, Stoeckert CJ Jr, Lazar MA. Propagation of adipogenic signals through an epigenomic transition state. Genes Dev. 2010 May 15;24(10):1035-44. doi: 10.1101/gad.1907110. PMID: 20478996; PMCID: PMC2867208.

Stenson BM, Rydén M, Venteclef N, Dahlman I, Pettersson AM, Mairal A, Ström G, Blomqvist L, Wang V, Jocken JW, Clément K, Langin D, Arner P, Laurencikiene J. Liver X receptor (LXR) regulates human adipocyte lipolysis. J Biol Chem. 2011 Jan 7;286(1):370-9. doi: 10.1074/jbc.M110.179499. Epub 2010 Oct 28. PMID: 21030586; PMCID: PMC3012995.

Stern JH, Rutkowski JM, Scherer PE. Adiponectin, Leptin, and Fatty Acids in the Maintenance of Metabolic Homeostasis through Adipose Tissue Crosstalk. Cell Metab. 2016 May 10;23(5):770-84. doi: 10.1016/j.cmet.2016.04.011. PMID: 27166942; PMCID: PMC4864949.

Stossel TP, Fenteany G, Hartwig JH. Cell surface actin remodeling. J Cell Sci. 2006 Aug 15;119(Pt 16):3261-4. doi: 10.1242/jcs.02994. PMID: 16899816.

Suganami T, Tanimoto-Koyama K, Nishida J, Itoh M, Yuan X, Mizuarai S, Kotani H, Yamaoka S, Miyake K, Aoe S, Kamei Y, Ogawa Y. Role of the Toll-like receptor 4/NF-kappaB pathway in saturated fatty acid-induced inflammatory changes in the interaction between adipocytes and macrophages. Arterioscler Thromb Vasc Biol. 2007 Jan;27(1):84-91. doi: 10.1161/01.ATV.0000251608.09329.9a. Epub 2006 Nov 2. PMID: 17082484.

Sun XJ, Liu F. Phosphorylation of IRS proteins Yin-Yang regulation of insulin signaling. Vitam Horm. 2009; 80:351-87. doi: 10.1016/S0083-6729(08)00613-4. PMID: 19251044.

Sun K, Wernstedt Asterholm I, Kusminski CM, Bueno AC, Wang ZV, Pollard JW, Brekken RA, Scherer PE. Dichotomous effects of VEGF-A on adipose tissue dysfunction. Proc Natl Acad Sci U S A. 2012 Apr 10;109(15):5874-9. doi: 10.1073/pnas.1200447109. Epub 2012 Mar 26. PMID: 22451920; PMCID: PMC3326476.

Sun Z, Gong J, Wu H, Xu W, Wu L, Xu D, Gao J, Wu JW, Yang H, Yang M, Li P. Perilipin1 promotes unilocular lipid droplet formation through the activation of Fsp27 in adipocytes. Nat Commun. 2013; 4:1594. doi: 10.1038/ncomms2581. Erratum in: Nat Commun. 2014; 5:4985. PMID: 23481402; PMCID: PMC3615468.

Suzuki MM, Bird A. DNA methylation landscapes: provocative insights from epigenomics. Nat Rev Genet. 2008 Jun;9(6):465-76. doi: 10.1038/nrg2341. PMID: 18463664.

Swinburn BA, Sacks G, Hall KD, McPherson K, Finegood DT, Moodie ML, Gortmaker SL. The global obesity pandemic: shaped by global drivers and local environments. Lancet. 2011 Aug 27;378(9793):804-14. doi: 10.1016/S0140-6736(11)60813-1. PMID: 21872749.

Takayama KI, Suzuki T, Fujimura T, Takahashi S, Inoue S. COBLL1 modulates cell morphology and facilitates androgen receptor genomic binding in advanced prostate cancer. Proc Natl Acad Sci U S A. 2018 May 8;115(19):4975-4980. doi: 10.1073/pnas.1721957115. Epub 2018 Apr 23. PMID: 29686105; PMCID: PMC5948986.

Tamori Y, Masugi J, Nishino N, Kasuga M. Role of peroxisome proliferator-activated receptor-gamma in maintenance of the characteristics of mature 3T3-L1 adipocytes. Diabetes. 2002 Jul;51(7):2045-55. doi: 10.2337/diabetes.51.7.2045. PMID: 12086932.

Tandon P, Wafer R, Minchin JEN. Adipose morphology and metabolic disease. J Exp Biol. 2018 Mar 7;221(Pt Suppl 1): jeb164970. doi: 10.1242/jeb.164970. PMID: 29514883.

Tang W, Zeve D, Suh JM, Bosnakovski D, Kyba M, Hammer RE, Tallquist MD, Graff JM. White fat progenitor cells reside in the adipose vasculature. Science. 2008 Oct 24;322(5901):583-6. doi: 10.1126/science.1156232. Epub 2008 Sep 18. PMID: 18801968; PMCID: PMC2597101.

Tansey JT, Sztalryd C, Gruia-Gray J, Roush DL, Zee JV, Gavrilova O, Reitman ML, Deng CX, Li C, Kimmel AR, Londos C. Perilipin ablation results in a lean mouse with aberrant adipocyte lipolysis, enhanced leptin production, and resistance to diet-induced obesity. Proc Natl Acad Sci U S A. 2001 May 22;98(11):6494-9. doi: 10.1073/pnas.101042998. PMID: 11371650; PMCID: PMC33496.

Teslovich TM, Musunuru K, Smith AV, Edmondson AC, Stylianou IM, Koseki M, Pirruccello JP, Ripatti S, Chasman DI, Willer CJ, et al. Biological, clinical and population relevance of 95 loci for blood lipids. Nature. 2010 Aug 5;466(7307):707-13. doi: 10.1038/nature09270. PMID: 20686565; PMCID: PMC3039276.

Tontonoz P, Hu E, Spiegelman BM. Stimulation of adipogenesis in fibroblasts by PPAR gamma 2, a lipid-activated transcription factor. Cell. 1994 Dec 30;79(7):1147-56. doi: 10.1016/0092-8674(94)90006-x. Erratum in: Cell 1995 Mar 24;80(6): following 957. PMID: 8001151.

Trayhurn P, Duncan JS, Rayner DV, Hardie LJ. Rapid inhibition of ob gene expression and circulating leptin levels in lean mice by the beta 3-adrenoceptor agonists BRL 35135A and ZD2079. Biochem Biophys Res Commun. 1996 Nov 12;228(2):605-10. doi: 10.1006/bbrc.1996.1704. PMID: 8920957.

Tziotis D, Hertkorn N, Schmitt-Kopplin P. Kendrick-analogous network visualisation of ion cyclotron resonance Fourier transform mass spectra: improved options for the assignment of elemental compositions and the classification of organic molecular complexity. Eur J Mass Spectrom (Chichester). 2011;17(4):415-21. doi: 10.1255/ejms.1135. PMID: 22006638.

van Marken Lichtenbelt WD, Vanhommerig JW, Smulders NM, Drossaerts JM, Kemerink GJ, Bouvy ND, Schrauwen P, Teule GJ. Cold-activated brown adipose tissue in healthy men. N Engl J Med. 2009 Apr 9;360(15):1500-8. doi: 10.1056/NEJMoa0808718. Erratum in: N Engl J Med. 2009 Apr 30;360(18):1917. PMID: 19357405.

Vernooy JH, Drummen NE, van Suylen RJ, Cloots RH, Möller GM, Bracke KR, Zuyderduyn S, Dentener MA, Brusselle GG, Hiemstra PS, Wouters EF. Enhanced pulmonary leptin expression in patients with severe COPD and asymptomatic smokers. Thorax. 2009 Jan;64(1):26-32. doi: 10.1136/thx.2007.085423. Epub 2008 Oct 3. PMID: 18835960.

Virtanen KA, Lidell ME, Orava J, Heglind M, Westergren R, Niemi T, Taittonen M, Laine J, Savisto NJ, Enerbäck S, Nuutila P. Functional brown adipose tissue in healthy adults. N Engl J Med. 2009 Apr 9;360(15):1518-25. doi: 10.1056/NEJMoa0808949. Erratum in: N Engl J Med. 2009 Sep 10;361(11):1123. PMID: 19357407.

Visscher PM, Brown MA, McCarthy MI, Yang J. Five years of GWAS discovery. Am J Hum Genet. 2012 Jan 13;90(1):7-24. doi: 10.1016/j.ajhg.2011.11.029. PMID: 22243964; PMCID: PMC3257326.

Visscher PM, Wray NR, Zhang Q, Sklar P, McCarthy MI, Brown MA, Yang J. 10 Years of GWAS Discovery: Biology, Function, and Translation. Am J Hum Genet. 2017 Jul 6;101(1):5-22. doi: 10.1016/j.ajhg.2017.06.005. PMID: 28686856; PMCID: PMC5501872.

Vitali A, Murano I, Zingaretti MC, Frontini A, Ricquier D, Cinti S. The adipose organ of obesity-prone C57BL/6J mice is composed of mixed white and brown adipocytes. J Lipid Res. 2012 Apr;53(4):619-29. doi: 10.1194/jlr.M018846. Epub 2012 Jan 23. PMID: 22271685; PMCID: PMC3307639.

Wajchenberg BL. Subcutaneous and visceral adipose tissue: their relation to the metabolic syndrome. Endocr Rev. 2000 Dec;21(6):697-738. doi: 10.1210/edrv.21.6.0415. PMID: 11133069.

Walker A, Lucio M, Pfitzner B, Scheerer MF, Neschen S, de Angelis MH, Hartmann A, Schmitt-Kopplin P. Importance of sulfur-containing metabolites in discriminating fecal extracts between normal and type-2 diabetic mice. J Proteome Res. 2014 Oct 3;13(10):4220-31. doi: 10.1021/pr500046b. Epub 2014 Sep 2. PMID: 24991707.

Wang EA, Israel DI, Kelly S, Luxenberg DP. Bone morphogenetic protein-2 causes commitment and differentiation in C3H10T1/2 and 3T3 cells. Growth Factors. 1993; 9(1):57-71. doi: 10.3109/08977199308991582. PMID: 8347351.

Wang L, Gordon RA, Huynh L, Su X, Park Min KH, Han J, Arthur JS, Kalliolias GD, Ivashkiv LB. Indirect inhibition of Toll-like receptor and type I interferon responses by ITAM-coupled receptors and integrins. Immunity. 2010 Apr 23;32(4):518-30. doi: 10.1016/j.immuni.2010.03.014. Epub 2010 Apr 1. PMID: 20362473; PMCID: PMC2862476.

Wang TJ, Larson MG, Vasan RS, Cheng S, Rhee EP, McCabe E, Lewis GD, Fox CS, Jacques PF, Fernandez C et al. Metabolite profiles and the risk of developing diabetes. Nat Med. 2011 Apr;17(4):448-53. doi: 10.1038/nm.2307. Epub 2011 Mar 20. PMID: 21423183; PMCID: PMC3126616

Wang F, Mullican SE, DiSpirito JR, Peed LC, Lazar MA. Lipoatrophy and severe metabolic disturbance in mice with fat-specific deletion of PPARγ. Proc Natl Acad Sci U S A. 2013 Nov 12;110(46):18656-61. doi: 10.1073/pnas.1314863110. Epub 2013 Oct 28. PMID: 24167256; PMCID: PMC3831974.

Wang W, Seale P. Control of brown and beige fat development. Nat Rev Mol Cell Biol. 2016 Nov;17(11):691-702. doi: 10.1038/nrm.2016.96. Epub 2016 Aug 24. PMID: 27552974; PMCID: PMC5627770.

Welch MD, Mullins RD. Cellular control of actin nucleation. Annu Rev Cell Dev Biol. 2002; 18:247-88. doi: 10.1146/annurev.cellbio.18.040202.112133. Epub 2002 Apr 2. PMID: 12142287.

Wellcome Trust Case Control Consortium. Genome-wide association study of 14,000 cases of seven common diseases and 3,000 shared controls. Nature. 2007 Jun 7;447(7145):661-78. doi: 10.1038/nature05911. PMID: 17554300; PMCID: PMC2719288.

Welter D, MacArthur J, Morales J, Burdett T, Hall P, Junkins H, Klemm A, Flicek P, Manolio T, Hindorff L, Parkinson H. The NHGRI GWAS Catalog, a curated resource of SNP-trait associations. Nucleic Acids Res. 2014 Jan;42(Database issue):D1001-6. doi: 10.1093/nar/gkt1229. Epub 2013 Dec 6. PMID: 24316577; PMCID: PMC3965119.

Weston L, Coutts AS, La Thangue NB. Actin nucleators in the nucleus: an emerging theme. J Cell Sci. 2012 Aug 1;125(Pt 15):3519-27. doi: 10.1242/jcs.099523. Epub 2012 Aug 30. PMID: 22935654; PMCID: PMC3445321.

White MF. Insulin signaling in health and disease. Science. 2003 Dec 5;302(5651):1710-1. doi: 10.1126/science.1092952. PMID: 14657487.

WHO Consultation on Obesity. Obesity: preventing and managing the global epidemic. Report of a WHO consultation. World Health Organ Tech Rep Ser. 2000; 894:i-xii, 1-253. PMID: 11234459.

WHO, 2016 https://www.who.int/news-room/fact-sheets/detail/obesity-and-overweight

WHO, 2022 https://www.who.int/news-room/fact-sheets/detail/diabetes

WHO (obesity), 2023 https://www.who.int/health-topics/obesity#tab=tab_1

WHO (diabetes), 2023 https://www.who.int/news-room/fact-sheets/detail/diabetes

Wieder C, Frainay C, Poupin N, Rodríguez-Mier P, Vinson F, Cooke J, Lai RP, Bundy JG, Jourdan F, Ebbels T. Pathway analysis in metabolomics: Recommendations for the use of over-representation analysis. PLoS Comput Biol. 2021 Sep 7;17(9):e1009105. doi: 10.1371/journal.pcbi.1009105. PMID: 34492007; PMCID: PMC8448349.

Wiesner G, Vaz M, Collier G, Seals D, Kaye D, Jennings G, Lambert G, Wilkinson D, Esler M. Leptin is released from the human brain: influence of adiposity and gender. J Clin Endocrinol Metab. 1999 Jul;84(7):2270-4. doi: 10.1210/jcem.84.7.5854. PMID: 10404789.

Willson TM, Brown PJ, Sternbach DD, Henke BR. The PPARs: from orphan receptors to drug discovery. J Med Chem. 2000 Feb 24;43(4):527-50. doi: 10.1021/jm990554g. PMID: 10691680.

Wilson ID, Plumb R, Granger J, Major H, Williams R, Lenz EM. HPLC-MS-based methods for the study of metabonomics. J Chromatogr B Analyt Technol Biomed Life Sci. 2005 Mar 5;817(1):67-76. doi: 10.1016/j.jchromb.2004.07.045. PMID: 15680789.

Wishart DS, Tzur D, Knox C, Eisner R, Guo AC, Young N, Cheng D, Jewell K, Arndt D, Sawhney S, Fung C, et al. HMDB: the Human Metabolome Database. Nucleic Acids Res. 2007 Jan;35(Database issue): D521-6. doi: 10.1093/nar/gkl923. PMID: 17202168; PMCID: PMC1899095.

Wishart DS, Lewis MJ, Morrissey JA, Flegel MD, Jeroncic K, Xiong Y, Cheng D, Eisner R, Gautam B, Tzur D, et al. The human cerebrospinal fluid metabolome. J Chromatogr B Analyt Technol Biomed Life Sci. 2008 Aug 15;871(2):164-73. doi: 10.1016/j.jchromb.2008.05.001. Epub 2008 May 8. PMID: 18502700.

Wishart DS, Knox C, Guo AC, Eisner R, Young N, Gautam B, Hau DD, Psychogios N, Dong E, Bouatra S, et al. HMDB: a knowledgebase for the human metabolome. Nucleic Acids Res. 2009 Jan;37(Database issue):D603-10. doi: 10.1093/nar/gkn810. Epub 2008 Oct 25. PMID: 18953024; PMCID: PMC2686599.

Wishart DS, Feunang YD, Marcu A, Guo AC, Liang K, Vázquez-Fresno R, Sajed T, Johnson D, Li C, Karu N, et al. HMDB 4.0: the human metabolome database for 2018. Nucleic Acids Res. 2018 Jan 4;46(D1): D608-D617. doi: 10.1093/nar/gkx1089. PMID: 29140435; PMCID: PMC5753273.

Witting M, Lucio M, Tziotis D, Wägele B, Suhre K, Voulhoux R, Garvis S, Schmitt-Kopplin P. DI-ICR-FT-MS-based high-throughput deep metabotyping: a case study of the Caenorhabditis elegans-Pseudomonas aeruginosa infection model. Anal Bioanal Chem. 2015 Feb;407(4):1059-73. doi: 10.1007/s00216-014-8331-5. Epub 2014 Nov 27. PMID: 25428456.

Wrann CD, Eguchi J, Bozec A, Xu Z, Mikkelsen T, Gimble J, Nave H, Wagner EF, Ong SE, Rosen ED. FOSL2 promotes leptin gene expression in human and mouse adipocytes. J Clin Invest. 2012 Mar;122(3):1010-21. doi: 10.1172/JCI58431. Epub 2012 Feb 13. PMID: 22326952; PMCID: PMC3322535.

Wu Z, Bucher NL, Farmer SR. Induction of peroxisome proliferator-activated receptor gamma during the conversion of 3T3 fibroblasts into adipocytes is mediated by C/EBPbeta, C/EBPdelta, and glucocorticoids. Mol Cell Biol. 1996 Aug;16(8):4128-36. doi: 10.1128/MCB.16.8.4128. PMID: 8754811; PMCID: PMC231409.

Wu Z, Rosen ED, Brun R, Hauser S, Adelmant G, Troy AE, McKeon C, Darlington GJ, Spiegelman BM. Cross-regulation of C/EBP alpha and PPAR gamma controls the transcriptional pathway of adipogenesis and insulin sensitivity. Mol Cell. 1999 Feb;3(2):151-8. doi: 10.1016/s1097-2765(00)80306-8. PMID: 10078198.

Xia JY, Holland WL, Kusminski CM, Sun K, Sharma AX, Pearson MJ, Sifuentes AJ, McDonald JG, Gordillo R, Scherer PE. Targeted Induction of Ceramide Degradation Leads to Improved Systemic Metabolism and Reduced Hepatic Steatosis. Cell Metab. 2015 Aug 4;22(2):266-278. doi: 10.1016/j.cmet.2015.06.007. Epub 2015 Jul 16. PMID: 26190650; PMCID: PMC4527941.

Yang J, Eliasson B, Smith U, Cushman SW, Sherman AS. The size of large adipose cells is a predictor of insulin resistance in first-degree relatives of type 2 diabetic patients. Obesity (Silver Spring). 2012 May;20(5):932-8. doi: 10.1038/oby.2011.371. Epub 2012 Jan 12. PMID: 22240722; PMCID: PMC3457700.

Yang W, Thein S, Lim CY, Ericksen RE, Sugii S, Xu F, Robinson RC, Kim JB, Han W. Arp2/3 complex regulates adipogenesis by controlling cortical actin remodelling. Biochem J. 2014 Dec 1;464(2):179-92. doi: 10.1042/BJ20140805. PMID: 25220164.

Yang W, Thein S, Wang X, Bi X, Ericksen RE, Xu F, Han W. BSCL2/seipin regulates adipogenesis through actin cytoskeleton remodelling. Hum Mol Genet. 2014 Jan 15;23(2):502-13. doi: 10.1093/hmg/ddt444. Epub 2013 Sep 10. PMID: 24026679.

Yue R, Zhou BO, Shimada IS, Zhao Z, Morrison SJ. Leptin Receptor Promotes Adipogenesis and Reduces Osteogenesis by Regulating Mesenchymal Stromal Cells in Adult Bone Marrow. Cell Stem Cell. 2016 Jun 2;18(6):782-796. doi: 10.1016/j.stem.2016.02.015. Epub 2016 Mar 24. PMID: 27053299.

Zhang Y, Proenca R, Maffei M, Barone M, Leopold L, Friedman JM. Positional cloning of the mouse obese gene and its human homologue. Nature. 1994 Dec 1;372(6505):425-32. doi: 10.1038/372425a0. Erratum in: Nature 1995 Mar 30;374(6521):479. PMID: 7984236.

Zhang F, Harir M, Moritz F, Zhang J, Witting M, Wu Y, Schmitt-Kopplin P, Fekete A, Gaspar A, Hertkorn N. Molecular and structural characterization of dissolved organic matter during and post cyanobacterial bloom in Taihu by combination of NMR spectroscopy and FTICR mass spectrometry. Water Res. 2014 Jun 15;57:280-94. doi: 10.1016/j.watres.2014.02.051. Epub 2014 Mar 20. PMID: 24727497.

Zhang Y, Chua S Jr. Leptin Function and Regulation. Compr Physiol. 2017 Dec 12;8(1):351-369. doi: 10.1002/cphy.c160041. PMID: 29357132.

Zhao L, Chang WC, Xiao Y, Liu HW, Liu P. Methylerythritol phosphate pathway of isoprenoid biosynthesis. Annu Rev Biochem. 2013; 82:497-530. doi: 10.1146/annurev-biochem-052010-100934. PMID: 23746261; PMCID: PMC5031371.

Zhu Q, Scherer PE. Immunologic and endocrine functions of adipose tissue: implications for kidney disease. Nat Rev Nephrol. 2018 Feb;14(2):105-120. doi: 10.1038/nrneph.2017.157. Epub 2017 Dec 4. PMID: 29199276.

Zhu Y, Wancewicz B, Schaid M, Tiambeng TN, Wenger K, Jin Y, Heyman H, Thompson CJ, Barsch A, Cox ED, et al. Ultrahigh-Resolution Mass Spectrometry-Based Platform for Plasma Metabolomics Applied to Type 2 Diabetes Research. J Proteome Res. 2021 Jan 1;20(1):463-473. doi: 10.1021/acs.jproteome.0c00510. Epub 2020 Oct 15. PMID: 33054244; PMCID: PMC7775897.

ACKNOWLEDGEMENTS

- First and foremost, I would like to express my great gratitude to my supervisor Prof. Dr. Johann J. Hauner, who introduced me to the exciting area of metabolic diseases, specifically Type 2 diabetes and obesity., and also Prof. Dr. Melina Claussnitzer, for her trust and confidence in me as a scientist and for always being available for all my questions.

- What is more, I would also like to thank my supervisor Prof. Dr. Johann J. Hauner for suggesting the exciting and innovative subject and approach to the research for my thesis, his continuous support and great interest taken in my work.

  I am very grateful for the many constructive discussions and countless helpful suggestions. Which enabled me to follow through with my project and make this thesis become reality in sometimes challenging times.

- I also want to express my gratitude to Prof. Dr. Philippe Schmitt-Kopplin from the Helholtz Zentrum in Munich, Germany for the opportunity of performing part of my work with the support of your great team.

  Very special thanks to Dr. Sara Forsici and Dr. Franco Moritz for your collaboration in the measuring the samples using DI-FT-ICR/MS and for your invaluable advice in optimizing an approach to the analysis of the data.

- I would like to thank Lab Assistant Manuela Hubersberger for the many productive and fruitful hours spent at the lab together, and for the patience she had in teaching me the skills required for my dissertation. And Dr. Claudine Seeliger who was always available for questions and advice. Thank you all!

- The best English Teacher and now close friend Eva Schätz inspired me, beyond English linguistics and on a non-scientific level, in an important way, and helped me develop and build the basis for this thesis and everything included.

- I would like to thank Julius Honecker and Simone Heisz for being available for innumerable questions and in-depth discussions during my doctoral research. You always made me feel welcome!

- Thank you very much, Josephine Fischer for your excellent support in proofreading for typos, spelling and grammar.

- I would like to thank both reviewers and examiners of this thesis, for Prof. Dr. Johann J. Hauner and Priv.-Doz. Dr. Ph. Schmitt-Kopplin for accepting to examine my work.

- Throughout the years of my project, I have been very fortunate to meet many extraordinary colleagues; unfortunately, I am unable to mention you all here. Each and every one of you is really unique and made the time of my doctoral studies special on many levels.

- My greatest gratitude of all is owed to my family, especially both my parents. For their unwavering belief in me and my abilities, and their continuous and unconditional support. Without which, without you, my studies would not have been possible. I would never have made it without you. Thank you so much!

"I dedicate this thesis to my beloved Parents."

DECLARATION OF AUTHORSHIP

(Eidesstattliche Erklärung)

I herewith declare that the dissertation submitted with the title:

"The Metabolomic Signature Of The RS6712203-C Risk Allele In Human Adipocyte Tissue"

as submitted to the Technische Universität München, Germany and as accepted by the degree-awarding institution TUM School of Life Sciences, Weihenstephan, Germany, prepared under the supervision of Prof. Dr. Johann J. Hauner, was prepared by me independently and using no other than the sources indicated. I also confirm that this thesis has not been submitted in the same or a similar form to any other university.

Munich, Germany, 16 November 2023